Online Adaptive and Intelligent Control Strategies for Multizone VAV Systems

Guang Qu

A Thesis

in

The Department

of

Building, Civil and Environmental Engineering

Presented in Partial Fulfillment of the Requirements

For the Degree of Doctor of Philosophy at

Concordia University

Montreal, Quebec, Canada

December 2009

Your file Votre référence
ISBN: 978-0-494-67354-6
Our file Notre référence
ISBN: 978-0-494-67354-6

CONCORDIA UNIVERSITY

School of Graduate Studies

This is to certify that the thesis prepared

By: Guang Qu

Entitled: Online Adaptive and Intelligent Control Strategies for Multizone VAV systems

and submitted in partial fulfillment of the requirements for the degree of

Doctor of Philosophy

complies with the regulations of the University and meets the accepted standards with respect to originality and quality.

Signed by the final examining committee:

_____	Chair
Dr.	
_____	External Examiner
Dr.	
_____	External to Program
Dr.	
_____	Examiner
Dr.	
_____	Examiner
Dr.	
_____	Thesis Supervisor
Dr. M. Zaheer-uddin	

Approved by: _____

Chair of Department or Graduate Program Director

December 11 2009 _____

Dean of Faculty

ABSTRACT

Online Adaptive and Intelligent Control Strategies for Multizone VAV Systems

Guang Qu, Ph.D.

Concordia University, 2009

Nearly one half of the total energy used in buildings is consumed by HVAC systems. With escalating cost of energy, several energy efficiency strategies have been implemented in buildings. Among these, the use of VAV systems, and improved method of controlling such systems have received greater attention.

This thesis is devoted to design and development of online adaptive control strategies which will be augmented with optimal and intelligent control algorithms. The considered VAV system consists of zone air temperature control, discharge air temperature control, water temperature control and air pressure control loops. Online adaptive control strategies are developed for these control loops.

In order to design reliable online controls a robust RLS identification algorithm for estimating the parameters of the modeled processes is developed. It is shown that this algorithm avoids wrong estimation and requires fewer variables compared with classical RLS techniques. Three different online control strategies were designed. These are: a robust optimal control algorithm (ROCA), a simplified optimal adaptive control (SOAC) for FOPDT systems, and a two-loop adaptive control strategy which improves both temperature and airflow regulations in VAV systems. ROCA is an on-line optimal proportional-integral plus feedforward controller tuning algorithm for SISO thermal

processes in HVAC systems. It was optimized by combining the H_∞ based PI tuning It is shown that the two-loop adaptive control strategy has both stronger robustness to time-varying thermal loads and lower sensitivity to airflow rate changes into other zones. The developed control strategies were tested by simulation and experiments in a VAV laboratory test facility which uses existing energy management control systems used in commercial buildings.

Also, an adaptive neural network controller is developed. The proposed controller was constructed by augmenting the PID control structure with a neural network control algorithm and an adaptive balance parameter. Simulation results show that the proposed controller has stronger robustness, improved regulation and tracking functions for FOPDT type plants compared to classical PID controllers. Experiments were conducted to verify the characteristics of the developed controller on the DAS in a two-zone VAV test facility.

Applications of the developed control strategies to different control loops in VAV system were demonstrated by conducting several experimental tests under realistic operating conditions.

ACKNOWLEDGEMENTS

I would like to express my sincere appreciation to my supervisor Professor Mohammed Zaheer-uddin for his guidance and assistance during this research work.

My thanks also go to the members of staff in Concordia University for their help whenever I needed it. Special thanks go to Mr. S. Drolet, Mr. L. Demers, Mr. J. Hrib and Mr. J. Payer for their helpful maintenance work.

I would like to dedicate this thesis to my friends and my family especially to my wife, Zuojian Tang, for their patience, understanding and support during my whole studies.

TABLE OF CONTENTS

TABLE OF CONTENTS ---------- vi

LIST OF FIGURES ---------- xi

LIST OF TABLES ---------- xvii

LIST OF SYMBOLS ---------- xviii

1. Introduction ---------- 1

1.1 HVAC Systems ---------- 1

1.2 VAV and VAV-VT Systems ---------- 3

1.3 Zone Temperature Controls ---------- 3

1.4 Supervisory Control in HVAC Systems ---------- 4

1.5 Motivation ---------- 5

1.6 Scope and Objectives ---------- 5

1.7 Thesis Outline ---------- 6

2. Literature Review ---------- 8

2.1 Introduction ---------- 8

2.2 Modeling and Simulation of HVAC Systems ---------- 8

2.3 Design of Controllers for HVAC Systems ---------- 13

2.4 PID Controls in HVAC Systems ---------- 18

2.5 Optimal Controls in HVAC Systems ---------- 23

2.6 Intelligent Controls in HVAC Systems ----------25

2.6.1 Adaptive Controls in HVAC Systems----------25

2.6.2 Fuzzy Logic Controls in HVAC Systems----------28

2.6.3 Neural Networks in HVAC Systems ----------30

2.7 EMCS in HVAC&R Systems ----------35

2.8 Experimental Research in HVAC Controls----------38

2.9 Summary and Discussion ----------40

3. Modified RLS Identification Algorithm for FOPDT Systems ----------43

3.1 RLS Algorithm for Online Identification of FOPDT Systems ------43

3.2 Issues in Using the RLS Algorithm for Online Identification-------47

3.3 Matrix-Reset Technique----------49

3.4 Simulation Studies for the Modified RLS Algorithm ----------54

3.5 Experimental Tests with the Modified RLS Algorithm----------61

3.6 Summary ----------63

4. An Adaptive Control Strategy with a Robust Optimal Control Algorithm for FOPDT Systems ----------64

4.1 Introduction ----------64

4.2 The DAS Model----------66

4.2.1 Physical Model ----------66

4.2.2 Temperature Control----------67
4.2.3 The First-order-plus-dead-time (FOPDT) Model----------68
4.2.4 The Closed-Loop DAS Model----------70
4.3 Optimization----------71
4.4 Tuning Algorithm----------75
4.4.1 Optimal Tuning Algorithm----------75
4.4.2 Guideline for Choosing the Control Input Weighting Parameter Q_2 -----77
4.5 Simulation Studies in an Adaptive Control System----------78
4.5.1 Control Input Energy----------80
4.5.2 Index Comparison with Other Methods----------82
4.5.3 Robustness Studies----------84
4.5.4 Disturbance Rejection----------86
4.6 Simplified Optimal Control Algorithm----------88
4.7 Application to a Heating Coil System----------89
4.7.1 The Problem in the Original Heating Coil Control System----------90
4.7.2 Online Adaptive PI Control Strategy for the Heating Coil Control System
----------91
4.7.3 Variables in the Heating Coil Control System----------91
4.7.4 Identification of the Plant----------92
4.7.5 Algorithm for the Heating Coil Control System----------93
4.7.6 Experimental Results of SOAC for the Heating Coil Control System ----95
4.8 Application to the DAS ---------- 100

4.9 Summary ---------- 102

5. Adaptive Neural Network Strategy for DAS---------- 103

5.1 Introduction ---------- 103

5.2 Adaptive Neural Network Control System ---------- 104

5.3 Neural Network Learning Algorithm---------- 106

5.4 Simulation Results ---------- 114

5.5 Experimental Studies ---------- 128

5.6 Summary ---------- 144

6. Online Adaptive Two-loop PI Control Strategy--------- 146

6.1 Introduction ---------- 146

6.2 Typical Airflow Regulation---------- 147

6.2.1 Pressure Independent Zone Temperature Control System---------- 147

6.2.2 Pressure Dependent Zone Temperature Control System---------- 151

6.3 Adaptive Two-Loop PI Control Strategy ---------- 154

6.3.1 Equal Consideration of the Interior Loop for the Exterior Loop--------- 155

6.3.2 Simulation Results for the Adaptive Two-Loop Control System-------- 157

6.4 Selection of the Factor F ---------- 160

6.5 Load Following Property of the Two-Loop Control ---------- 162

6.6 Implementation in a VAV Test Facility---------- 165

6.7 Summary ---------- 173

7. Conclusions and Recommendations ---------- 174

7.1 Conclusions ---------- 174

7.2 Contributions of This Study ---------- 179

7.3 Recommendations ---------- 180

Reference ---------- 181

Appendix ---------- 192

LIST OF FIGURES

Figure 3.1 Block diagram showing the generation of output prediction error----------43

Figure 3.2 Simulation scheme for on-line adaptive control----------54

Figure 3.3 Identification simulation results for process 3.1 under Cases 3.1, 3.2, 3.6 -56

Figure 3.4 Identification simulation results for process 3.2 under Cases 3.1, 3.2, 3.6 -56

Figure 3.5 Identification simulation results for process 3.3 under Cases 3.1, 3.2, 3.6 -57

Figure 3.6 Identification simulation results for process 3.1 under Cases 3.3, 3.4, 3.6 -58

Figure 3.7 Identification simulation results for process 3.2 under Cases 3.3, 3.4, 3.6 -58

Figure 3.8 Identification simulation results for process 3.3 under Cases 3.3, 3.4, 3.6 -59

Figure 3.9 Identification result comparison for Cases 3.7, 3.8, 3.6----------60

Figure 3.10 Identification results of the experimental tests ----------61

Figure 3.11 System PI parameters of the experimental tests----------62

Figure 3.12 Step responses of the experimental tests ----------62

Figure 4.1 Schematic diagram of DAT system----------66

Figure 4.2 Block diagram of DAS system ----------68

Figure 4.3 First-order plus dead-time model----------69

Figure 4.4 Closed-loop diagrams of DAS with a PI controller $K_d(z)$----------70

Figure 4.5 Closed-loop diagram of the optimal PI controller with feedforward action 74

Figure 4.6 Simulation structure for OTA and OTA-VP----------80

Figure 4.7 Responses with the optimal tuning algorithm (Process 4.1; Case 4.1) ------81

Figure 4.8 Index with respect to reduction factor and Q2-down ----------83

Figure 4.9 Response comparisons between OTA-VP, OTA, H_∞ tuning rules and Z-N method ----------83

Figure 4.10 Robustness comparisons in the CPs 4.1 to 4.4 with Case 4.1 ----------84

Figure 4.11 Robustness comparisons in CPs 4.1 and 4.3 with Cases 4.2 and 4.3 --------85

Figure 4.12 Response with disturbance effect for OTA-VP control ----------87

Figure 4.13 Robustness comparisons for different controls ----------89

Figure 4.14 Original heating coil PI control system----------90

Figure 4.15 Bad performance of the original heating coil PI control system ----------90

Figure 4.16 Adaptive PI control system for the heating coil system ----------91

Figure 4.17 Open-loop tests for determination of the heating coil system delay ---------93

Figure 4.18 Flowchart of the SOAC for the heating coil control ----------95

Figure 4.19 Comparison between the original PI and the adaptive PI controls ----------96

Figure 4.20 Experimental result of SOAC with $Q_2 = 1$ ----------96

Figure 4.21 Experimental result of SOAC with $Q_2 = 0.5$----------97

Figure 4.22 Experimental result of SOAC with $Q_2 = 0.6993$ ----------97

Figure 4.23 Step response of the original PI control ----------98

Figure 4.24 Step response for SOAC with $Q_2 = 1$ ----------99

Figure 4.25 Identification result in SOAC with $Q_2 = 1$ ----------99

Figure 4.26 PI parameter evolution of SOAC with $Q_2 = 1$ ---------- 100

Figure 4.27 Step responses of SOAC with $Q_2 = 1.3889$ and 1.6667 ---------- 101

Figure 4.28 PI gains of SOAC with $Q_2 = 1.3889$ and 1.6667 ---------- 101

Figure 4.29 Identification in SOAC with $Q_2 = 1.3889$ and 1.6667---------- 101

Figure 5.1 Adaptive NN control system---------- 104

Figure 5.2 The adaptive neural network controller ---------- 105

Figure 5.3 Selected normal neural network controller---------- 106

Figure 5.4 Index and IndexSet consideration ---------- 112

Figure 5.5 Flow chart of the adaptive tuning algorithm ---------- 113

Figure 5.6 Flow chart of the adaptive neural network algorithm ---------- 114

Figure 5.7 Adaptive neural network control system implementation in Simulink ---- 116

Figure 5.8 Adaptive neural network controller implementation in Simulink ---------- 116

Figure 5.9 Comparison for the adaptive neural network control with $\alpha_v = 0$ and $\alpha_v \neq 0$ ---------- 118

Figure 5.10 Comparison of step responses of CCM-PID and Adaptive NN control for plant sets 21 to 29 ---------- 120

Figure 5.11 Comparison of CCM-PID and Adaptive NN control Index for plant sets 21 to 29 ---------- 121

Figure 5.12 Effect of w_{ii} and $A0$ for Plant Set 26 ---------- 122

Figure 5.13 Effect of w_{05} and IndexTarget for Set 23 ---------- 123

Figure 5.14 Step responses and Index0 on effect of η_0 for Set 23 ---------- 124

Figure 5.15 Step responses and Indexes with poor parameter selection for Set 23 ---- 125

Figure 5.16 Step responses with $w_{44}(0) = 0.1$ and $c_4 = 0.5$ for Set 15 ---------- 126

Figure 5.17 Step responses with $w_{44}(0) = 0.38$ and $c_4 = 0.1$ for Set 15 ---------- 127

Figure 5.18 Schematic diagram of the VAV-HVAC system and its' controls ---------- 128

Figure 5.19 Discharge air temperature control system implementation ---------- 129

Figure 5.20 Open-loop tests for chilled water flow rate to its controls ---------- 130

Figure 5.21 Step responses of the proposed controller under normal load conditions - 131

Figure 5.22 Index evolution during step response ---------- 131

Figure 5.23 Step responses under high load conditions ---------- 133

Figure 5.24 Index evolutions under high load conditions ---------- 133

Figure 5.25 Step responses in training process 1 ---------- 134

Figure 5.26 Indexes in training process 1---------- 134

Figure 5.27 Sample weighting parameters in training process 1 ---------- 135

Figure 5.28 Step response comparisons for changing η_0 and w_{ii}---------- 136

Figure 5.29 Index comparisons for changing η_0 and w_{ii} ---------- 136

Figure 5.30 w_{1j} for changing η_0 and w_{ii} ---------- 137

Figure 5.31 Step responses in training process 2 and for different values of FAN----- 137

Figure 5.32 Indexes in training process 2 and for different values of FAN ---------- 138

Figure 5.33 Air flow change for training process 2 ---------- 138

Figure 5.34 Step response of ANNC to increased heat to zone 2---------- 139

Figure 5.35 Step response of ANNC to decreased heat to zone 2 ---------- 140

Figure 5.36 Comparison of response to dumper control changes for $\alpha_w = 0$ and $\alpha_w = 1$ ---------- 141

Figure 5.37 Indexes for response comparison under $\alpha_w = 0$ and 1 ---------- 142

Figure 5.38 Dumper control changes for response comparison under $\alpha_w = 0$ and 1 --- 142

Figure 5.39 Response comparison of ANNC and PID control to dumper control changes ---------- 143

Figure 6.1 A classical pressure independent control for zones---------- 148

Figure 6.2 Simulation structure for independent pressure control ---------- 149

Figure 6.3 Sensibility to parameter changes in the independent pressure control ---- 149

Figure 6.4 Airflow rate disturbance effect reductions in the independent pressure control system ---------- 150

Figure 6.5 A classical pressure dependent control for zones ---------- 151

Figure 6.6 Simulation structure in Simulink for the pressure dependent control ----- 152

Figure 6.7 Sensibility to parameter changes in the pressure dependent control------- 153

Figure 6.8 Airflow rate disturbance effect reductions in the pressure dependent control ---------- 154

Figure 6.9 Adaptive two-loop control structure for zone temperature controls ------- 155

Figure 6.10 Bode plots of $G_z(z)$, $G_q(z)$ and the interior closed loop transfer function ---------- 156

Figure 6.11 Simulation structure for the adaptive two-loop control system ---------- 158

Figure 6.12 Sensibility to parameter changes in the adaptive two-loop control system 158

Figure 6.13 Airflow rate disturbance rejections in the adaptive two-loop control system ---------- 159

Figure 6.14 Zone temperature response for different F ---------- 161

Figure 6.15 Damper opening for different F ---------- 161

Figure 6.16 Response to the parameter change (load change) in the adaptive two-loop control system ---------- 163

Figure 6.17 Response to parameter change in the pressure independent control system ---------- 164

Figure 6.18 Adaptive two-loop control and pressure dependent control responses to the parameter change (load change)---------- 165

Figure 6.19 Zone temperature response and velocity pressure setpoint for zone 1 ---- 167

Figure 6.20 Zone temperature response and velocity pressure requirement for zone 2 and fan control ---------- 168

Figure 6.21 Velocity pressure response and airflow rate for zone 1 ---------- 169

Figure 6.22 Velocity pressure response and airflow rate for zone 2 ---------- 170

Figure 6.23 Zone temperature response 2 and velocity pressure requirement for zone 1 ---------- 171

Figure 6.24 Velocity pressure response 2 and airflow rate for zone 1 ---------- 172

Figure 6.25 Zone temperature response 2 and velocity pressure requirement for zone 2 ---------- 172

Figure 6.26 Velocity pressure response 2 and airflow rate for zone 2 ---------- 173

LIST OF TABLES

Table 4.1 Plant parameter changes for considered processes ---- 79

Table 4.2 Effect of Q_2 on energy efficiency ---- 81

Table 4.3 Index comparisons between methods for CPs with Case 4.1 ---- 85

Table 4.4 Index comparisons between methods for CPs 4.1 and 4.3 with Case 4.2 ---- 86

Table 4.5 Index comparisons between methods for CPs 4.1 and 4.3 with Case 4.3 ---- 86

Table 4.6 Index comparisons under disturbances and Case 4.1 between methods ---- 87

Table 5.1 Sets 1 to 9 of the plant parameter changes ---- 115

Table 5.2 Sets 11 to 19 of the plant parameter changes ---- 115

Table 5.3 Sets 21 to 29 of the plant parameter changes ---- 115

Table 5.4 Legends for different plant sets (j = 0, 1, 2) ---- 119

Table 5.5 Initial value selection of $w_{ii}(0)$ and $w_{05}(0)$ for fast learning for different plants ---- 125

Table 5.6 Experimental conditions and parameter set 1 ---- 132

Table 5.7 Experimental conditions and parameter set 2 for high load ---- 133

Table 5.8 Performance results of ANNC to increased heat to zone 2 ---- 139

Table 5.9 Performance results of ANNC to decreased heat to zone 2 ---- 140

Table 5.10 Comparisons between ANNC and PID control ---- 143

Table A.1 Specifications and accuracy of the sensors used ---- 192

LIST OF SYMBOLS

a	system pole of FOPDT model in discrete-time domain
$\hat{a}$, $\hat{b}$	elements of $\hat{\theta}$
$\hat{a}_c$, $\hat{b}_c$	variables for computed values of $\hat{a}$ and $\hat{b}$
a_{max} , a_{min}	bounded values of a
a_v	the estimated value of the parameter a in the identification process
A , B , C	matrices of state equation for PI controlled closed-loop FOPDT system
AHU	air handling unit
ANFIS	adaptive neuro-fuzzy inference system
ANN	artificial neural network
ANNC	adaptive neural networks control
AR	autoregressive
ARMA	autoregressive moving average
ATAEC3GLCBS	heating coil control system setpoint
A0	a small positive parameter for calculating Index0
b	system gain of the FOPDT model in discrete-time domain
b_{max} , b_{min}	bounded values of b
b_v	the estimated value of the parameter b in the identification process

c	a constant for computing fan speed control (FAN)	
c_d	a coefficient for calculating input x_3 of the normal neural network controller	
c_i	a constant for calculating input x_2 of the normal neural network controller	
c_1	a coefficient for calculating normal neural network controller output u_{vn}	
c_{10}	a constant for calculating normal neural network controller output u_{vn}	
c_2	a parameter to compute K_i	
c_4 , c_5	coefficients for calculating normal neural network controller inputs	
c_{40} , c_{50}	constants for calculating normal neural network controller inputs	
C	discharge air temperature controller	
CBCGLC470BS	the input (0 to 100%) of the hot water control valve for the heating coil control system	
CC	cooling coil	
CCITS	the entering air temperature of the cooling coil	
CCM	Cohen Coon Method	
CCOTS	discharge air temperature	(^oC)
CCU	cooling coil unit	
CF	fan speed controller	

CFM	cubic feet per minute	
COV	coefficient of variation	
CP	combined process	
CSB-SQP	complete simulation-based sequential quadratic programming	
CV	constant volume	
CWFRG	chilled water flow rate	(GPM)
CWRTS	chilled water return temperature	(^oC)
CWSTS	chilled water supply temperature	(^oC)
C1, C2	damper controllers	
DAMP1	control input (V) of the damper in the duct to zone 1	
DAMP2	control input (V) of the damper in the duct to zone 2	
DAS	discharge air system	
DAT	discharge air temperature	
DDC	direct digital control	
DM1 , DM2	damper motors	
DP	differential pressure	
DPS	total duct supply air pressure	(CFM)
DPS001	duct supply air pressure to room 1	(MA)
DPS002	duct supply air pressure to room 2	(MA)
D1SP	velocity pressure setpoint to room 1	(MA)
D2SP	velocity pressure setpoint to room 2	(MA)
e	the difference between T_{set} and T_a that is $T_{set} - T_a$	

$e(k;\theta)$	the difference between $y(k)$ and $\hat{y}(k)$
EMC	energy management control
EMCS	energy management control system
EP	evolutionary programming
ESP-r	an integrated modelling tool for the simulation of the thermal, visual and acoustic performance of buildings and the assessment of the energy use and gaseous emissions associated with the environmental control systems and constructional materials
E_T	performance index
F	an adjustable factor of the adaptive PI&PI controller
FAN	the control input of the fan (V)
FCH	fan-coil heating
FCU	fan coil unit
FF	feedforward
FFPI	feedforward proportional-integral
FLCs	fuzzy logic controllers
FOPDT	first order plus dead time
FSC	fuzzy satisfactory clustering
FVS	actuator for fan motor
gpm, GPM	gallons per minute
$g_{11}, g_{12}, g_{21}, g_{22}$	mid-parameters for OTA and OTA-VP
GA	genetic algorithms

GPM	gain and phase margin method
GRNN	general regression neural networks
$G(z)$	transfer function
$G_q(z)$	transfer function of airflow damper's dynamics
$G_z(z)$	transfer function of zone temperature dynamics
h_i	ith hidden unit of neural network
$h_{11}, h_{12}, h_{21}, h_{22}$	mid-parameters for OTA and OTA-VP
H	hidden vector
HEAT1	heat generated by heater in room1
HEAT2	heat generated by heater in room2
HVAC	heating, ventilating, and air-conditioning
HVAC&R	heating, ventilating, air conditioning, and refrigeration
HVACSIM+	HVAC SIMulation PLUS other systems
H_∞	Hankel norm used to measure control system properties
IAE	integrated absolute error
INDEX	integral square-error
INDEXabs	integrated absolute error
IndexNoAbs	integrated error
$IndexP_i$	index of the i th process
$IndexT$	total index

*Index*0 , *IndexSet*	indexes for calculating adaptive weight factor α_v
IndexTarget	a reference index to *Index*0 for updating adaptive weight factor α_v
Inf	infinity
ISE	integral square-error criterion
J	performance criterion
k	time in samples
k_a	a coefficient for computing fan speed control FAN
k_e	adjustable scale coefficient for suitable input values of the normal neural network controller
k_p, k_i, k_d	PID gains
k_0, k_{end}	start time and end time in samples
k_1	a scale factor to adjust the learning rate η_0
K	a column matrix of gains K_p and K_i
K_c	system gain of FOPDT system in continuous domain
$K_d(z)$	z transform of a controller in discrete system
K_{FF}	feedforward gain of PI-FF controller
K_i	integral gain of PI controller
K_{id}	integral gain of $K_d(z)$
K_p	proportional gain of PI controller
K_{pd}	proportional gain of $K_d(z)$

K_{PI}	a row matrix of gains of $K_d(z)$
l	dead-time in samples for FOPDT model
L	a 2×1 matrix
LEE	least enthalpy estimator
LowValue	the lower bound of P_{ss}
LPVOP	the largest positive non-zero value of the processor
LQG	linear quadratic Gaussian
LQR	linear quadratic regulator
LVP	linear varying parameter
L_1, L_2	elements of L
m_j	the number of inputs of the normal neural network controller
m_i	the number of the hidden nodes of the normal neural network controller
$m_{11}, m_{12}, m_{21}, m_{22}$	mid-parameters for OTA and OTA-VP
MIMO	Multiple-Input Multiple-Output
MMPC	multiple model predictive control
MTAEC3GLCB	discharge warm air temperature from heating coil
N	sampling size for minimization
NN	neural network
o_1	output node of neural network
OA	outside air
OTA	Optimal Tuning Algorithm

OTA-VP	Optimal Tuning Algorithm with Variable Parameter	
P	proportional	
P	a 2×2 matrix	
PD	proportional derivative	
PDC	parallel distribution compensation	
PI	proportional integral	
PID	proportional integral derivative	
PI-FF	proportional-integral plus feedforward	
PI&PI	two-loop PI control strategy	
PLY_1, PLY_2	scalar parameters for computing P_{21} and P_{22}	
PMAC	pulse modulation adaptive controller	
PMV	predicted mean vote	
PNN	predictive neural network	
PPCL	Powers Process Control Language a programming language used to write field panel control programs for building control and energy management functions	
PRAC	pattern recognition adaptive controller	
$\bar{P}_{ss}$	the sum of the square values of elements in matrix P	
PS1 , PS2	velocity pressure sensors in supply air ducts	
P_{11}, P_{12}, P_{21}, P_{22}	elements of P	
q_{11}	an element of matrix Q_1	
$Q_{\min}$, $Q_{\max}$	bounded values of airflow rate	(m^3/s or CFM)

Q_{set}	desired airflow rate	(m^3/s or CFM)
Q_1	state weighting matrix	
Q_2	control weighting factor	
Q2-down	the value of Q_2 in step-down process for OTA-VP	
RLS	recursive least squares	
ROCA	robust optimal control algorithm	
RTS001	zone temperature of room 1	(^oC or ^oF)
RTS002	zone temperature of room 2	(^oC or ^oF)
SFP	specific fan power	
SISO	single-input-single-output	
SOAC	simplified optimal adaptive control	
SPVOP	the smallest positive non-zero value of the processor	
T_a	discharge air temperature as system output	(^oC or ^oF)
T_{a0}	entering air temperature	(^oC or ^oF)
T_c	time constant for FOPDT model	
T_s	sampling time	
T_{set}	desired discharge air temperature	(^oC or ^oF)
T_{ws}	supply chilled water temperature	(^oC or ^oF)
T_z	zone temperature	(^oC or ^oF)
T_{zset}	desired zone temperature	(^oC or ^oF)
T_{z0}	zone temperature with no cooling	(^oC or ^oF)
T_2	discharge warm air temperature of heating coil	(^oC or ^oF)

T_{2s}	desired discharge warm air temperature of heating coil	(^{o}C or ^{o}F)
u	controller output	
uq	control output of controller $C_q(z)$	
u_{max}, u_{min}	bounded values of controller output u	
ut	control output of controller $C_t(z)$	
u_v	control output of controller	
	for the heating coil system	(0 to 100%)
	for the adaptive neural network control	(0 to 10V)
u_{vn}	neural network control value of the adaptive neural network controller's output	
u_{vp}	PID control value of the adaptive neural network controller's output	
UD	a unitary upper triangular matrix (U) and diagonal matrix (D)	
UpValue	the upper bound of P_{ss}	
$U(z)$	the z transform of u	
V	water flow control valve	
ValKi	integral gain of PI of DAS	
ValKp	proportional gain of PI of DAS	
ValSP	desired discharge air temperature of DAS	

VALVE	controller output to the chilled water flow rate control valve	(V)
VAV	variable air volume	
VAV-VT	variable air volume variable temperature	
w_{ii}	element of W_i	
w_{0i}	element of W_0	
$w(k)$	weighting function	
W	weighting function matrix	
W_i	weight matrix for a hidden unit	
W_0	weight matrix for the output unit	
x	a column matrix of state variables	
x_1 , x_2	state variables	
x_1 , x_2 , x_3 , x_4 , x_5	input units of neural network	
X	input vector	
y	the difference between T_{a0} and T_a	
$\hat{y}$	estimated output of plant	
y_{max}	the maximum value of y	
YTAEC3GLCBS	proportional gain of PI for the heating coil control	
$Y(N)$	a $(N-l)\times 1$ matrix	
$Y(z)$	the z transform of y	
ZTAEC3GLCBS	integral gain of PI for the heating coil control	

ZTS001	zone temperature setpoint of room 1	(^{o}C or ^{o}F)
ZTS002	zone temperature setpoint of room 2 for experiment	(^{o}C or ^{o}F)
ZT1 , ZT2	zone temperature sensors	
Z-N	Ziegler-Nichols	

α	a parameter of weighting function for system parameter identifications
α_e, α_u	weighting factors for computing $IndexP_i$ weighting factors for computing E_T
α_w	a boolean variable to avoid over training
α_v	an adaptive weight factor to avoid slow response
α_4	a weight parameter for filtering input data x_4
α_5	a weight parameter for filtering input data x_5
β	a constant number used as initial value for diagonal elements of P
β_1	a coefficient for computing α_v
γ	adjustable parameter of weighting function for system parameter identifications
δ	a selectable small positive value to avoid dividing by zero
ε	a $(N-l)\times 1$ matrix

η, η_1	learning rates	
η_h	time-varying learning rate for Δw_{0i}	
η_x	time-varying learning rate for Δw_{ij}	
η_0	a selected constant learning rate	
θ	predictive parameter value of plant	
$\hat{\theta}$	estimated parameter value of plant	
θ^0	true parameter value of plant	
λ	a Lagrange multiplier vector	
μ	a scalar parameter for computing L_1 and L_2	
σ	a scalar parameter for computing $\hat{a}$ and $\hat{b}$	
ς	a scalar parameter to avoid dividing by zero	
τ	dead-time of FOPDT system	(s)
ψ	a 2×1 measurand matrix	
Σ	a scalar parameter for analysis of P_{ss}	
Ψ	a $2\times(N-l)$ matrix	

1. Introduction

Efficient control strategies in heating, ventilating, and air-conditioning (HVAC) systems have become more important recently in the world because of the increasing energy requirements and diminishing energy sources. Incorporating several optimizing functions in energy-management control (EMC) systems and performing real-time adjustments to HVAC processes can improve the energy efficiency of HVAC systems (Zheng, 1997). Global optimization of an entire HVAC system is a powerful strategy for the improvement of energy efficiency of HVAC systems, but it must be executed by efficient local controls for every loop in the controlled HVAC system. Variable air volume (VAV) is the most popular operating mode in HAVC systems, because it has the potential to save energy.

This thesis deals with the development of online adaptive control strategies for local loops in VAV-HVAC systems. Emphasis is placed on the application of modern control theories combined with classical PID control to develop implementable and improved controllers for VAV systems.

1.1 HVAC Systems

HVAC systems play a significant role in reducing the environmental impact on occupied spaces. The primary function of an HVAC system is to provide and maintain a healthy and comfortable indoor environment. The goal of HVAC control system design is to provide effective control strategies to maintain comfort with adequate air quality for the occupants of an occupied space under variable load conditions with minimal use of

energy. Reducing energy consumption and relevant practical techniques are therefore the most important aspects in HVAC control system design in view of the fact, that "Among building services, the growth in HVAC systems energy use is particularly significant (50% of building consumption and 20% of total consumption in the USA)." (Pérez-Lombard, Ortiz, & Pout, 2008, p. 394).

Typical all-air HVAC systems provide energy transfer via heating/cooling coils, airflow regulation to maintain air pressure or temperature via fan speed regulation or/and damper position changes, and central water supply servicing heating/cooling coils or multiple units. All-air HVAC systems are generally operated in two modes: constant volume (CV) and variable air volume (VAV). In CV mode of operation, air-supply temperature is varied in response to zone loads while maintaining the airflow rate constant. This concept is usually used for single duct constant volume systems. One drawback of the CV systems is that the fan energy consumption remains the same irrespective of zone loads. Another drawback is that the single duct CV system cannot supply conditioned air at different temperatures to meet the needs of individual zones. To overcome this problem, reheat systems are needed. For a cooling case, the supply air temperature is cooled to satisfy the zone with maximum load and then reheated to meet the needs of zones experiencing lower loads. The reheat system used in CV systems contributes to energy waste. In contrast, VAV systems enjoy a significant advantage over CV systems in terms of the economy of operation (Zaheer-uddin & Zheng, 2001), and result in the lower energy consumption (Arguello-Serrano & Velez-Reyes, 1999).

1.2 VAV and VAV-VT Systems

In the VAV mode, air-supply temperature is held at some constant setpoint while airflow rate is varied to satisfy zone load, in contrast to the CV mode of operation, where air-supply temperature is varied in response to zone loads while holding the airflow rate constant. During low load periods, reduced airflow rates can be achieved in a VAV system, and this can lead to significant reduction in fan energy consumption because of the fact that "fan energy consumption is proportional to cubic power of airflow rate" (McQuistion, Parker, & Spitler, 2000). Zaheer-uddin et al. (2001) have further shown that the variable air volume mode of operation in which both airflow rate and air-supply temperature are continuously modulated is a more energy efficient strategy. This mode is identified as the variable air volume variable temperature (VAV-VT) mode.

1.3 Zone Temperature Controls

In all-air HVAC systems, zone temperature is controlled by airflow regulation of supply air. Typical airflow regulation in zone temperature controls of HVAC systems includes pressure independent control and pressure dependent temperature control. In pressure independent control, it will be easier to get a stable response but zone temperature set-point may not be satisfied because of plant uncertainty. In contrast, in pressure dependent temperature control zone temperature set-point can be reached but the control action responding to pressure disturbance effect of airflow rate may not be faster. In addition, for a multi-zone system operating in VAV or VAV-VT mode, damper position change or fan speed change for a new airflow requirement of a zone will affect other zones' airflow because of the coupled nature of airflow system. These limitations of

typical airflow regulation in zone temperature controls will be further illustrated in chapter 6.

1.4 Supervisory Control in HVAC Systems

In most buildings the VAV systems provide air at constant temperature year round. This practice is not necessarily the most economical, because of this practice that numerous problems occur during part load operation of VAV systems, such as, poor air distribution, inadequate ventilation, and high humidity within the controlled space because of too low airflow rate. Therefore, it is recognized that the basic principle of a VAV system should be to control both the airflow rate and the temperature of supply air into the controlled space for heating, ventilation, and air-conditioning. In addition, building HVAC controls should be operated to minimize energy consumption and/or operating cost.

To achieve this objective, a supervisory control system should have the capabilities to provide the desired time-of-day optimal setpoint profiles under dynamic outside conditions and indoor loads for local controllers. The local controllers track the optimal setpoint profiles so that the HVAC system runs optimally from the current state to the new state at the provided setpoints. The control strategy with the supervisory control will improve the performance of a VAV system in terms of providing good temperature and humidity control as well as in reducing the energy costs significantly. The typical local controls in VAV systems are zone temperature control, discharge air temperature control, airflow rate control, variable speed fan control, reheat control, outdoor ventilation flow control, chilled water temperature control (or heat exchanger

water temperature control), water flow rate control, etc. These local controls will affect the performance of supervisory control.

1.5 Motivation

Providing energy efficient, healthy and comfortable indoor environment in buildings is the main goal of the modern HVAC controls. However, to achieve this goal many practical problems must be considered such as different operating conditions, varying environmental conditions, and real-time implementation considerations. These will affect the performance of control strategies. To guarantee optimal operation of VAV systems, several adaptive, intelligent, optimal control strategies for local controls will be explored in this thesis.

1.6 Scope and Objectives

In the context of background and motivation cited above this thesis presents several practical adaptive, intelligent, optimal online control strategies for VAV and VAV-VT local loop controls for HVAC systems. The specific objectives include:

1. To augment the existing RLS online identification algorithm for FOPDT systems to improve its online reliability.
2. To develop an optimal control strategy with improved ability in rejecting the effects of disturbances acting on FOPDT systems.
3. To design an online intelligent control strategy with learning property that can be implemented in existing HVAC control systems.

4. To develop an online adaptive control strategy to reduce the effects of airflow interaction and system uncertainty in zone temperature control in VAV systems.

5. To test the developed control strategies in a VAV laboratory HVAC system using an existing energy management control system platform.

1.7 Thesis Outline

This thesis is divided into seven chapters. In Chapter 1, an introduction to the VAV control systems and the objectives of this thesis are given. The motivation for studying online adaptive and intelligent control strategies for multi-zone VAV systems is also discussed.

Chapter 2 consists of literature survey related to modeling and different controls in HVAC systems. The review further supports the objectives of this thesis.

In Chapter 3, a robust online identification technique is developed by adopting a matrix-reset technique. It is an improved RLS identification algorithm for FOPDT model from an earlier study (Qu, 2002).

Chapter 4 presents an on-line optimal proportional-integral plus feedforward (PI-FF) controller with H_∞ tuning rules for FOPDT model systems with improved A new index is introduced to evaluate the control performance. Simulation studies in an adaptive control configuration showed the added improvement of the proposed control algorithm. In addition, a simplified optimal control algorithm is developed. Its applications to a heating coil control loop in the Concordia University's HVAC system

and the DAS in the HVAC Test Facility are studied and improvement in robustness is illustrated through experimental results.

In Chapter 5, an implementable neural network control is developed. It is derived by integrating adaptive control, neural network control and PID control. Simulation and experimental studies for a local control of HVAC systems are also presented.

In Chapter 6, an online adaptive control strategy to reduce the effects of airflow interaction and system uncertainty on zone temperature control in VAV systems is proposed. This control strategy is derived by adopting a two loop control structure. The limitations of classical typical airflow regulation in zone temperature controls (pressure independent control and pressure dependent temperature control) are also discussed in this chapter. Comparisons between the proposed control strategy and the classical airflow regulation controls are presented. The improvements in performance of the proposed control are illustrated.

Finally, conclusions, main contributions of this thesis and recommendations for future research are given in Chapter 7.

2. Literature Review

Extensive research on various aspects of HVAC controls and building systems have been motivated by the growing concerns about indoor environments and energy efficiency. The related aspects of HVAC controls will be surveyed in this Chapter.

2.1 Introduction

Many aspects related to HVAC controls, such as modeling, design of controllers, PID controls, intelligent (fuzzy, neural networks, adaptive) controls, experimental controls and energy management control system (EMCS), have been studied by several researchers in recent years. In the following sections, the relevant papers will be reviewed and summarized.

2.2 Modeling and Simulation of HVAC Systems

In recent years, there has been a growing interest in the mathematical modeling of HVAC systems and its components (Tashtoush, Molhim, & Al-Rousan, 2005). Many researchers have studied HVAC dynamic models using either theoretical or experimental approach. The studies related to modeling done by several researchers will be summarized below.

Tashtoush et al. (2005) described a procedure for deriving a dynamic model of an HVAC system that consists of a zone, heating, cooling and dehumidifying coil, humidifier, ductwork, fan, and mixing box. They investigated the tuning technique using the Ziegler-Nichols rule from a practical viewpoint, and gave simulation results showing

the open loop and the closed loop responses of indoor temperature and humidity ratio. The results show that the system is capable of controlling the disturbances efficiently within a small period of time and with less error. They concluded that the dynamic model can be especially useful for control strategies that require knowledge of the dynamic characteristics of HVAC systems.

Zheng and Zaheer-uddin (1996) developed dynamic models of HVAC system components for optimizing the thermal processes in a variable air volume (VAV) heating, ventilating and air conditioning (HVAC) system. The constrained optimal control problem was formulated and solved. Typical daily optimal operating trajectories for the system were presented. Results showed that to achieve thermal comfort, both zone temperature and humidity ratio should be controlled, and the optimization of outdoor air economy cycle results in significant energy savings.

Mei and Levermore (2002) presented the results of modeling and simulating a laboratory variable air volume (VAV) test rig. They developed models for each component, such as fan, duct and VAV terminal box, with control systems, in the test rig. They also performed the simulations via the logical connection of the component models by means of an HVACSIM+ platform (Clark, 1985). They used a polynomial curve fitting method and a ten neuron sigmoid artificial neural network (ANN) model to model the non-linear characteristic of the fan. The ANN based model is shown to give better results. A non-linear characteristic terminal box model based on the experimental modeling was developed. The ANN fan model and the terminal box model were included

in HVACSIM+ program as new component subroutines. The simulation results for the VAV test rig via HVACSIM+ were validated by real system operation performance.

Huang, Zaheeruddin and Cho (2006) used detailed system dynamic models to evaluate energy management control (EMC) functions such as outside air (OA) economizer cycle, programmed start and stop lead time, load reset and occupied time adaptive control strategy. They also presented a real time system embedded with the above EMC functions. The simulation results manifest that energy savings of 17% can be achieved when the system is operated with the EMC functions and optimal set points compared with the system without such functions. These results do point out that the optimal set point strategy is very useful in achieving energy efficient operation of HVAC systems.

Wang, Lee, Fung, Bi, and Zhang (1999) developed dynamic models to simulate the thermal, hydraulic, environmental and mechanical characteristics and energy performance of a building and VAV air-conditioning system under the control of Energy Management and Control Systems (EMCS). Wang et al. (1999) also developed three on-line supervisory strategies and programs based on integrated EMCS stations to optimize the VAV static pressure set-point, AHU outlet air temperature set-point and outdoor ventilation air flow set-point. The strategies and programs were commissioned and evaluated under the simulated 'real-life' environment.

Wang and Jin (2000) proposed a system approach for optimizing multi-zone building systems, based on predicting the responses of overall system environment and energy performance to the changes in control settings of VAV air-conditioning systems.

Incremental dynamic models with `self-tuning' of the VAV system were developed and used. A genetic algorithm was used to solve the on-line optimization problem of multiple parameters. The strategy was tested and evaluated in a simulated `living' environment under various weather conditions.

Maxwell, Shapiro and Westra (1989) developed an empirical model of chilled water coil and used it to predict the system response to inputs with P, PI and PID control algorithms. The empirical model is not suitable for online control as the model needs to be updated.

Kasahara et al. (2000) described a procedure for deriving a dynamic model of an air-conditioned space by applying physical laws, such as energy and mass balance principles. These models are useful in energy efficiency simulation studies.

Kasahara et al. (2001) have presented a stability limit analysis and a new tuning method for PID controllers in bilinear systems with time-delayed feedback. The bilinear systems they considered are variable air volume (VAV) systems, which are defined as air-handling units that use variable airflow rate to satisfy the heating, ventilating, and air-conditioning (HVAC) operation requirements – such as indoor temperature (thermal comfort.) In this reference, they have developed a normalized bilinear model of VAV systems by identifying the energy flow to and from the environmental space and presented a generalized parameter analysis of the stability limits by simulation. The results of the analysis reveal that controller parameters can be determined by assuming that the plant is linear. The proposed tuning method of PID controller requires a gain reduction factor for practical applications. The main limitation of the online application

of the tuning method is that it requires extensive computations to find the gain reduction factor. The methodology in this study relies on bilinear models which are not suitable for systems with time delay.

Wang et al. (2004) presented a technique for developing a simple and accurate cooling coil unit (CCU) model. The modeling technique is based on energy balance and heat transfer principles. They used commissioning information to estimate, at most, three model parameters by either a linear or nonlinear least squares method. They have done experiments to show that the method is robust and gives a better match to real performance over the entire operating range compared to other methods.

Kulkarni and Hong (2004) explored the problem of using a single-zone, two-position control system and presented a proportional control system for the residential building by setting up the dynamic simulation for the building and the control system. They used state-space method to model the building system and implemented the simulation code on MATLAB. They also implemented optimization of the controller using this model. The thermal comfort and energy efficiency were compared under different schemes. They found that proportional control is advantageous to the two-position control for thermal comfort while there is not much difference in energy consumption between two control schemes. However, in their work the furnace was operated without any minimum run time with continuous data sampling.

From the above modeling and simulation studies it is noted that the major focus of the model development has been for energy simulation and thermal comfort evaluation. These models are either static or dynamic from less rigorous to detailed. Because of

higher computational and memory requirements, these models are not suitable for implementation on existing building control systems.

2.3 Design of Controllers for HVAC Systems

An HVAC system includes many local control loops. They are required for regulation of temperature, airflow rate etc in many processes in HVAC systems. Many researchers have worked on design of local controllers for HVAC systems. The popular techniques are PID control, optimal control, intelligent (fuzzy, neural networks, adaptive) control, H_∞ control, pattern recognition control, predictive control and nonlinear control. Since many studies have been done on PID control, optimal control, and intelligent control, the literature review for them will be shown in later sections. Here, the summary includes literature related to H_∞ control (Al-Assadi, Patel, Zaheer-ruddin, Verma, & Breitinger, 2004; Qu et al., 2004), preview control (Zaheer-uddin, Al-Assadi, & Patel, 1994; Kasahara et al., 1998), pattern recognition control (Seem, 1997), predictive control (Dexter & Haves, 1989), decoupled control (Rentel-Gómez & Vélez-Reyes, 2001; Semsar, Yazdanpanah, & Lucas, 2003), and nonlinear control (Argüello-Serrano et al., 1999).

Al-Assadi et al. (2004) presented the results of a study on the use of H_∞ constraints in an optimization technique for the design of robust decentralized output feedback control of a heating, ventilation and air conditioning (HVAC) system. They used robust stability and performance specifications to achieve temperature control in multi-zone HVAC system in the presence of disturbances and model uncertainties and under constraints on control input energy. The resulting fixed-gain decentralized output

feedback controller, which is based on a linear model, was implemented via simulation on a full bilinear model of the HVAC system. Superior performance of the H_∞ -based design was shown via comparison of these results with those based on ''constrained'' linear-quadratic optimal regulator design. The design methodology is too complex for online implementation.

First-order-plus-dead-time (FOPDT) models are easier to implement in a real system. Tan, Liu and Tam (1998) developed PID tuning rules based on loop-shaping H_∞ control for the FOPDT processes. The application of H_∞ based adaptive PI controller in HVAC systems is demonstrated by Qu et al. (2004). The approach of tuning single-loop controllers in HVAC systems using the H_∞ loop-shaping tuning rules was applied to a discharge air temperature (DAT) control system. The recursive least squares method was used for identification of the HVAC process as a FOPDT model. The output responses of the adaptive PI controller were compared with a LQR optimal adaptive controller. Simulation results showed that the adaptively tuned PI controller is able to track setpoint changes very well in the presence of changes in plant parameters, disturbances and external noise acting on the system.

A decentralized preview controller was designed for temperature control of multi-zone indoor environmental spaces by Zaheer-uddin et al. (1994). A two-zone space heating system considered consisted of a boiler, heat pumps, distribution network and two environmental zones. The decentralized preview controller was designed by using a parameter optimization method under the assumption that the outdoor temperature variations are "previewable". They compared the output responses of the resulting

decentralized closed-loop bilinear system acted upon by single and multiple disturbances with and without preview action, and gave results showing the robustness property of the controller, and the 24-hour building operation with unoccupied and occupied setpoint tracking using preview control. However, experimental validation is necessary to evaluate the effectiveness of the preview control.

Kasahara et al. (1998) presented a multivariable autoregressive (AR) model which is a three input/two output model obtained by using observed data for an HVAC system. They used a combination of the model and the preview control that is a linear quadratic Gaussian (LQG) optimal control with feedforward compensation to control process variables such as indoor temperature and indoor humidity. The comparison of measured data and simulation results shows that the plant model is adequately formulated. Also, experimental results on a commercial-sized test plant with LQG control system and preview control system are presented. They showed that the optimal control system based on statistical modeling with the multivariable AR model is quite useful for the control of interactive HVAC systems, and the preview control system produces excellent control under normal operating conditions compared to LQG control system. The limitations of the optimal control system based on statistical modeling with the multivariable AR model are that the modeling and the control design are very difficult to implement online, and the model obtained off-line may not match the model dynamics undergoing variable operating conditions.

Seem (1997) presented a method for implementing a new pattern recognition adaptive controller (PRAC) developed through optimization, for automatically adjusting

the parameters of PI controllers while under closed loop control. Depending on patterns of the closed loop response, PRAC will determine the parameters of the digital PI controller used in an HVAC system. Simulation results subject to random noise and load disturbance modeled by either one or zero are presented. Some field test results are also given. The results showed that PRAC is robust, easy to use and has low computational and memory requirements. From the results presented, it can be noted that PRAC responses are either sluggish or oscillatory. It takes a long time to reach stable state. The limitation of this study is that PRAC was developed for systems that can be characterized by a first-order plus dead-time model with the ratio of dead time to time constant between 0.25 and 1, and the ratio of sampling time to time constant is between 0.1 and 1 for "good control."

Dexter et al. (1989) developed a robust self-tuning predictive controller based on the Generalized Predictive Control algorithm (Clarke, Mohtadi, & Tuffs, 1987) for HVAC applications. The controller uses default values for most of its parameters and requires selection of only one commissioning parameter: the control-sampling interval. In the controller, a parameter estimator for the HVAC plant, which is based on the UD filter form of the recursive least-squares algorithm, using a simple form of variable exponential forgetting (Dexter, 1983), is used. To implement a set of expert rules, which supervise the operation of the on-line parameter estimator and the calculation of control action, Dexter et al. (1989) developed special jacketing software. Also, they have used a component-based computer simulation package (HVACSIM+) to examine the behavior of the controller in both the zone and supply air temperature control loops. The robust behavior of the self-tuning controller is demonstrated and its superior performance to that of a

manually tuned PI controller is suggested by the results. Application of the self-tuning controller in a cascaded control configuration is also discussed and they concluded that the use of two self-tuning controllers within a cascaded control scheme worked well when care was taken to deal with the interactions that occurred between the inner and outer loops during the tuning period. The controller is too complex for implementation on existing building control hardware. Also the accuracy of the estimator over extended period of operation is not proven in the simulation.

Rentel-Gómez et al. (2001) developed a nonlinear noninteracting control system for temperature and relative humidity in a thermal-space conditioned by a variable-air-volume (VAV) heating, ventilating, and air conditioning (HVAC) system. They showed the importance of decoupling techniques in controlling temperature and relative humidity independently and accurately for some industrial processes. They demonstrated how decoupled control of temperature and relative humidity is possible using a multivariable cascade control with two loops. The inner-loop used the non-interacting control law for decoupling, and the outer-loop is a PD controller used for stabilization and control. This is a simulation based study and requires experimental validation.

Semsar et al. (2003) introduced a Back-Stepping controller for a nonlinear, MIMO HVAC System. They used feedback linearization method with introduction of a feedback of states and disturbances for the purposes of disturbance decoupling and nonlinear model linearization. They also applied the Back-Stepping controller to the linearized model of the system. It has been shown that using this method, heat and moisture loads can be compensated, considering them as measurable disturbances.

Finally they provided the simulation results to show the ability of the method with high disturbance decoupling and good tracking properties. The methodology is suitable for simulation study and is too complex for implementation in real systems.

Argüello-Serrano et al. (1999) presented a non-linear disturbance rejection state feedback controller for an HVAC system. The controller was designed by using Lyapunov stability theory and consists of a regulator and a disturbance rejection component. To reduce the effect of thermal loads other than design loads on the system, they also proposed a thermal load estimator that allows the controller to obtain on-line estimates of the thermal loads affecting the thermal space. In addition, they have shown simulation results for a variable air volume (VAV) HVAC system. The results demonstrated the potential for the controller to keep comfort levels and save energy in a variable air volume HVAC system operating in the cooling mode. The main limitation of the design for the controller is its complexity for online implementation.

2.4 PID Controls in HVAC Systems

In this section a survey of the published literature on the applications of PID techniques for HVAC systems will be given. Studies by Seem (1997), Qu et al. (2004), and Kasahara et al. (2001) summarized in the previous sections have also used PID control technique.

Kasahara et al. (1999) have developed a design and tuning method in which the gains of a robust PID controller for HVAC systems are obtained by solving a two-disk type of mixed sensitivity problem. The PID gains obtained by the conventional Ziegler-Nichols rule were modified by applying this technique. To illustrate the method, the

temperature control of a single-zone environmental space and the HVAC plant which was approximated by a first-order lag plus dead-time system was considered. The numerical simulation and the experiments on a commercial-size test plant for air conditioning were presented. The study showed that the robust PID gains could be expressed as simple linear functions of the ratio of the dead-time to the time constant. However, for every plant, the use of this method requires the determination of six parameters off-line to compute the three gain reduction factors.

Krakow (1998) has proposed the relationship between the sampling interval and digital PI control system performance by using experimental and simulated response characteristics for a PI-controlled mixing valve air heating system. The PI tuning rules were specified based on the analytical and experimental study by Krakow, Lin and Zeng (1995a and 1995b), Krakow and Lin (1995), and Hussein (1996), for the first-order system (without storage) and second-order system (with storage.) The study showed that, long sampling intervals may yield more satisfactory response characteristics, than short sampling intervals if the system is tuned appropriately. Appropriate tuning implies using PI coefficients based on (non-conventional) theory developed specifically for long sampling intervals. A long sampling interval implies a complete response of the controlled variable to the change in the control signal. The limitation of the paper is that the results obtained are specific to a system and cannot be generalized.

Nesler (1986a) has reported the implementation of three automated controller-tuning methods, which include a computer-assisted controller tuning program, an automatic tuning controller, and a self-tuning controller for HVAC processes. A

computer-assisted controller-tuning program allows novice users to tune DDC controllers reliably and quickly. An automatic tuning controller fully automates the open-loop step-test tuning procedure and has self-monitoring capability that leads the automatic tuning routine, once initiated, can operate without supervision. Nesler (1986a) concluded that automated controller tuning addresses two fundamental problems in HVAC control applications: the time-consuming initial tuning of the controller and the requirement for periodic controller retuning as system loads change. A self-tuning control system adjusts PI control parameters in real-time using closed loop control data. Experimental results from applying the self-tuning controller to a discharge air temperature control loop are given. It is noted that unmodeled load disturbances, drifting parameters and actuator nonlinearity are limitations of self-tuning controllers.

Nesler (1986b) has presented the implementation of a self-tuning controller to control typical HVAC processes (the model can be considered as a first-order plus dead-time). The self-tuning controller consists of five independent software blocks. The five blocks include an automatic tuning routine used to establish initial parameter estimates, a recursive least-squares estimator for making parameter estimates on-line, a controller design block, which computes the gains of PI controller depending on the new parameter estimates, a PI controller, and a performance monitor, which supervises the self-tuning controller operation. The open-loop step test method is used for the automatic tuning routine. The PI gains are computed by minimizing the integrated absolute error (IAE). In addition, the performance monitor is introduced to determine when retuning is required. The use of the performance monitor can also increase system flexibility and robustness. The main limitation of RLS (Recursive Least Squares) estimation is that self-tuners can

occasionally fail to produce useful estimates under certain conditions such as self-tuning control loops subjected to large and unmodeled load disturbances which occur in HVAC processes.

Huang and Lam (1997) presented an adaptive learning strategy based on genetic algorithms (GA) for automatic tuning of PID controllers in HVAC systems to achieve optimal performance. They used genetic algorithms, since they have been proved to be robust and efficient in finding near-optimal solutions in complex problem spaces. They also modified the modular dynamic simulation software package HVACSIM+ and incorporated the genetic algorithm-based optimization program to provide a complete simulation environment for detailed study of controller performance. In addition they considered three performance indicators (overshoot, settling time, and mean squared error) in the objective function of the optimization procedure for evaluation of controller performance. The simulation results showed that the genetic algorithm-based optimization procedures as implemented in the research study are useful for automatic tuning of PID controllers for HVAC systems, yielding minimum overshoot and minimum settling time. This is a simulation study and not implemented on real systems.

Wang, Shi and Cai (2001) developed a simple and efficient PID autotuner and presented its application to HVAC systems. A second order plus dead time model is identified by the autotuner based on two continuous relay feedback experiments. The PID controller was designed on the basis of gain- and phase-margin specifications. The methodology requires more computation and memory as such is not suitable for online application.

Zaheer-uddin and Tudoroiu (2004) explored the problem of improving the performance of a discharge air temperature (DAT) system using a PID controller and augmenting it with neural network based tuning and tracking functions. They modeled the DAT system as a SISO (single input single output) system, and presented the architecture of the real time neuro-PID controller and simulation results obtained under realistic operating conditions. The simulation results show that the network assisted PID controller is able to track both constant and variable set point trajectories efficiently in the presence of disturbances acting on the DAT system.

Kotaki, Yamakawa, Yamazaki, Kamimura and Kurosu (2005) described tuning PID controllers using optimization, subject to constraints on derivatives of control input, and considering model uncertainty caused by changes in system dynamics. To obtain optimal PID parameters, they presented graphs as functions of a normalized dead-time and a perturbation of system parameters. In addition, the control performance in disturbance suppression and reference tracking properties was presented and the comparisons with the partial model matching method and the H_∞ compensator designed for the same system were shown. Moreover, to avoid making the control system sensitive to measurement noise, a PI controller with a relaxation filter was developed. It was shown that there is very little difference in control performance between the PI controller and the H_∞ compensator. Like most previous studies, this is also a simulation based study and has not been experimentally validated.

2.5 Optimal Controls in HVAC Systems

A survey of the published literature about optimal controls in HVAC systems is presented in this section. The studies of Al-Assadi et al. (2004), Wang et al. (2000), Zaheer-uddin et al. (1994), Kasahara et al. 1998, Huang et al. (1997), Kulkarni et al. (2004), and Kotaki et al. (2005) discussed in the previous section also deal with optimal control issues in HVAC systems.

Zaheer-uddin et al. (2001) explored the application of a multistage optimization technique to determine optimal operating strategies for HVAC systems. Simulation results are shown for a single-zone space heating system consisting of a heat pump, a storage tank, a heating coil, a fan, and ductwork. The optimization problem was solved using a typical building operation schedule, consisting of off-normal, start-up, and normal occupied periods, assuming time-of-day rates. Results are presented, for the two most widely used operating strategies, namely, constant-volume (CV) and variable-air-volume (VAV) system. It is shown that the variable-air-volume mode of operation in which both air-supply temperature and flow rate are continuously modulated is the most energy efficient strategy. The limitations of the study are that the optimal result depends on exact dynamic models, and in real systems, to track the setpoints exactly may be extremely difficult.

Singh, Zaheer-uddin and Patel (2000) studied the application of adaptive control for a class of multivariable processes in heating, ventilating and air conditioning (HVAC) systems. They simulated the thermal dynamics of a two zone fan-coil heating (FCH) system and environmental zones by a nonlinear model, and designed a multivariable

adaptive controller based on Linear Quadratic Regulator (LQR) theory. Simulation results showing the closed loop response of the system to changes in operating points, external disturbances, changes in system parameters and unmodeled dynamics were presented. They showed that the adaptive controller is able to adapt to a wide range of operating conditions and is able to maintain the zone temperatures and the boiler temperature close to their respective setpoints. Like most optimal control solutions, this one is computationally extensive and therefore suitable in off-line studies.

Lu, Cai, Soh, Xie and Li (2004) presented a model-based optimization strategy for the condenser water loop of centralized heating, ventilation and air conditioning (HVAC) systems. They analyzed each component characteristics and interactions within and between cooling towers and chillers, and formulated the optimization problem as that of minimizing the total operating cost of all energy consuming devices with mechanical limitations, component interactions, outdoor environment and indoor cooling load demands as constraints. They also proposed a modified genetic algorithm for this particular problem to obtain the optimal set points of the process. Simulations and experimental results on a centralized HVAC pilot plant were shown and it was concluded that the operating cost of the condenser water loop can be substantially reduced compared with conventional operation strategies.

Sun and Reddy (2005) presented a general and systematic methodology, termed complete simulation-based sequential quadratic programming (CSB-SQP), for determining the optimal control of building HVAC&R systems. This approach allows the coupling of a detailed simulation program with an efficient optimization method, namely

the sequential quadratic programming (SQP) algorithm. This approach allows the use of accurate component models of the system as against empirical models as currently used, while providing efficient optimal solutions to be determined. Sun et al. (2005) developed the mathematical basis of the methodology and applied it to a simple cooling plant system to illustrate the accuracy, efficiency and robustness of this method. Experiments were not conducted but they discussed the issue of implementing such an optimization under real-time control.

Zaheer-uddin (1993) explored the application of modern control theory to design control systems for buildings. Example problems dealing with HVAC systems and indoor environment control are considered. He used pole-placement technique, optimal regulator theory and adaptive control to design controllers. The responses of the systems subject to disturbances were investigated. The simulation results illustrated the advantage of one method over the other and emphasized the importance of the use of improved methods to design control systems for intelligent buildings.

2.6 Intelligent Controls in HVAC Systems

The most popular intelligent controls applied in HVAC systems are fuzzy logic control, neural networks control and adaptive control. In this section, a review of literature in these areas will be given.

2.6.1 Adaptive Controls in HVAC Systems

From the literature (Zaheer-uddin 1993), it is known that adaptive control has advantage over the pole-placement technique and optimal regulator theory in design of

control systems for intelligent buildings. In addition to the work on adaptive controls by Singh et al. (2000), Seem (1997), Nesler (1986b), Zaheer-uddin (1993), and Qu et al. (2004), the following additional survey on adaptive controls in HVAC systems is presented.

Bai and Zhang (2007) have presented an adaptive PI controller for use in HVAC systems. They used recursive least squares (RLS) with exponential forgetting combined with model matching of a zero frequency method to estimate the model's parameters while the system remained in closed loop. Bai et al. (2007) developed a tuning formula for a PI controller with robustness based on the estimated parameters to adjust the controller's parameters automatically while under closed loop. The simulation results show that the new adaptive PI controller has improved performance. However, the controller was not experimentally validated.

Åström, Hägglund and Wallenborg (1993) have presented a tuning method based on the relay feedback for a general digital controller. The method was developed for tuning digital control laws and the control design method used is based on pole placement. There is an interesting feature in the tuning method that the sampling period and the desired closed loop poles are determined from an experiment with relay feedback. The conclusion from extensive simulations stated that the method works very well for low-order systems with time delay. Two test results applied to HVAC plants are presented. A limitation noted by Åström et al. (1993) is that the direct approach does not work well for systems with large pole in continuous time models.

Chen, Lee and Wepfer (May 1990) have presented an adaptive robust control scheme applied to a single-zone HVAC system. A single-zone HVAC system with modeling uncertainty (which includes thermal storage effect, heat and moisture generation, and outside temperature and humidity variation) is established for a single zone HVAC system in a generic room. It is a nonlinear system, and the uncertainty is assumed bounded but the bound is unknown. Then, a class of adaptive robust controls which was originally designed by Corless and Leitmann (1984) is used to achieve the control objective to drive the room's state (which is related to its temperature and humidity) into a comfort region. A comparison between the use of on-off control and the use of the adaptive robust control from simulation results is given. Chen et al. (May 1990) conclude that simulation results depict a satisfactory transient performance in the sense of maintaining small overshoot under a significant deviation of the initial state from the comfort region. A drawback noted by Chen et al. (May 1990) is that the steady state performance has certain oscillations.

Calvino, Gennusa, Rizzo and Scaccianoce (2004) presented the problems of predicted mean vote (PMV) index in monitoring and controlling HVAC equipment and described a fuzzy control for HVAC system to overcoming these problems. They represented a simple approach, focused on the application of an adaptive fuzzy controller that avoids the modeling of indoor and outdoor environments. They also presented some simulation results which are not validated experimentally.

Salsbury (2002) has proposed a new switching control law (pulse modulation adaptive controller, PMAC) that implements pulse-width-pulse-frequency modulation.

Pulse durations are determined to maintain the amplitude of variation in the controlled variable at or below a user-defined level. In addition to providing quantifiable control performance, PMAC can reduce component wear by issuing fewer switches than conventional control schemes. The control law is developed around a first-order system characterization but incorporates an adaptive loop, which allows application to a wide range of non-first-order and also time-variant systems. The author presented test results from applying PMAC to both simulated and real HVAC systems. Application of such methods on available HVAC control platforms requires significant resources.

2.6.2 Fuzzy Logic Controls in HVAC Systems

Fuzzy logic control is one of the popular intelligent controls in HVAC systems. A survey of the published literature about fuzzy logic controls in HVAC systems is presented in this section.

Alcalá, Casillas, Cordón, González and Herrera (2005) proposed the use of weighted linguistic fuzzy rules in combination with a rule selection process to develop fuzzy logic controllers (FLCs) dedicated to the intelligent control of HVAC systems concerning energy performance and indoor comfort requirements. They developed a genetic optimization process considering an efficient approach to perform rule weight derivation and rule selection for FLCs and tested the proposed technique considering a physical modelization of a real test site. The conclusion was that the proposed technique yielded much better results than the classical on-off controller showing good performance on these kinds of complex problems. The application of fuzzy logic for online applications is not studied.

Chu, Jong and Huang (2005) proposed a least enthalpy estimator (LEE) that combines the definition of thermal comfort level and the theory of enthalpy into a load predicting way to provide timely suitable settings for a fan coil unit (FCU) fuzzy controller used in HVAC. The fuzzy controller can make decisions and adjust the output of the FCU system depending on the settings, including temperature and relative humidity. Some actual experiments were done to show the application of the LEE-based FCU fuzzy controller in evaluating thermal comfort, energy efficiency and reliability. The methodology needs to be tested in real building systems to evaluate their performance.

He, Cai and Li (2005) presented a multiple model predictive control (MMPC) strategy based on Takagi–Sugeno (T–S) fuzzy models for temperature control of air-handling unit (AHU) in HVAC systems. They constructed the control system in two levels that the higher level is a fuzzy partition based on AHU operating range to schedule the fuzzy weights of local models in lower level, and the lower level is composed of a set of T–S models based on the relation of manipulated inputs and system outputs. In addition, they divided the complex nonlinear AHU system into a set of T–S models through a fuzzy satisfactory clustering (FSC) methodology and selected a fuzzy integrated linear varying parameter (LVP) model for the global system. Then, they developed the hierarchical MMPC strategy using parallel distribution compensation (PDC) method, in which different predictive controllers are designed for different T–S fuzzy rules and the global controller output is integrated by the local controller outputs through their fuzzy weights. Finally, they presented simulation and real process testing

results to show that the proposed MMPC approach is effective in HVAC system control applications.

2.6.3 Neural Networks in HVAC Systems

Because of the difficulty in modeling HVAC systems for controls, the neural networks controls have become more popular in recent years. Several researchers (Wang, Jing, & An, 2006; Mei et al., 2002 (reviewed in Section 2.2); Zaheer-uddin et al., 2004 (reviewed in Section 2.4); Abbassi & Bahar, 2005; Massie, Kreider, & Curtiss, 2004a, & 2004b; Ben-Nakhi & Mahmoud, 2004; Yang, Yeo, & Kim, 2003; Ahmed, Mitchell, & Klein, 1998a, 1998b, & 1998c; Jeannette, Assawamartbunlue, Curtiss, & Kreiser, 1998; Atthajariyakul & Leephakpreeda, 2005) have applied neural network (NN) methods to HVAC systems.

Wang et al. (2006) have studied a neuron adaptive PID control which is applied in a single-zone HVAC system for adaptively adjusting the PID parameters. The simulation results they presented illustrate that neuron PID controller has the capability of self-adapting.

Abbassi et al. (2005) used artificial neural network (ANN) to do the thermodynamic modeling of an evaporative condenser under steady state and transient conditions for establishing control of thermal capacity. The authors used predictive neural network, capable of understanding dynamic behavior and predicting the preset output to train the system under dynamic condition. The principle operation of such neural networks is based on the reduction of gradients of errors existing between the predicted output and the actual output of the system. They used neural controller based on training

to control the system thermal capacity. The conclusion made is that artificial neural network controller is suitable substitute for PID controllers for thermal systems. ANN controllers are complex and require carful training to be effective in real building HVAC systems.

Massie et al. (2004a) described the construction and measured performance of a neural network-based optimal controller for an ice thermal storage system. The controller was constructed with four neural networks, three of which map equipment behavior and one that acts as a global controller. The controller self-learns equipment responses to the environment and then determines the control settings that should be used. The optimization was conducted by addressing cost function under a selected planning window to determine the sequence of control actions. Massie et al. (2004b) reported the verification of the results using computer simulation and with the operation in a full-scale HVAC laboratory.

Massie et al. (2004b) described the validation and performance of an optimal neural network-based controller for an ice thermal storage system. The controller learns equipment responses and determines the control settings. As such, there is minimal need to calibrate the controller to installed equipment. Massie et al. (2004b) verified the results by conducting tests in a full-scale HVAC laboratory.

Ben-Nakhi et al. (2004) designed and trained general regression neural networks (GRNN) to investigate the feasibility of using this technology to optimize HVAC thermal energy storage in public buildings as well as office buildings. They used state of the art building simulation software, ESP-r (Clarke, 2001), to generate a database covering the

years 1997–2001 and to calculate hourly cooling loads for three office buildings using climate records in Kuwait. They used the cooling load data for 1997–2000 for training and testing the neural networks (NN), while robustness of the trained NN was tested by applying them to a "production" data set (2001 data) that the networks have never "seen" before. In addition, they determined optimum GRNN design parameters that best predict cooling load profiles for each building by performing parametric studies. They assumed external hourly temperature readings for a 24 h period as network inputs, and the hourly cooling load for the next day as the output. They also evaluated the performance of the NN using a statistical indicator (the coefficient of multiple determination) and by statistical analysis of the error patterns, including confidence intervals of regression lines, as well as by examination of the error patterns. Finally, they concluded that a properly designed NN is a powerful instrument for optimizing thermal energy storage in buildings based only on external temperature records. The application is shown for load predication and does not address HVAC control.

Yang et al. (2003) presented an application of the ANN in a building control system. The objective of this study is to develop an optimized ANN model to determine the optimal start time for a heating system in a building. For this, programs for predicting the room air temperature and the learning of the ANN model based on back propagation learning were developed, and learning data for various building conditions were collected through program simulation for predicting the room air temperature using systems of experimental design. Then, the optimized ANN model was used to determine the optimal start time.

Ahmed et al. (1998a) proposed a combined feedforward and feedback control approach for a laboratory HVAC system. A general regression neural network (GRNN) is utilized in the feedforward component for HVAC system identification and control, while the feedback component provides a control signal to offset any steady-state error. A typical variable-air-volume laboratory HVAC control system is considered by the authors. They studied pressure control in this paper. They also show the simulation results obtained by using a laboratory simulator. The simulation results indicate that the combined approach performs better than the feedback approach over widely varying operating conditions and different damper characteristics. The main limitation of this paper is that the simulation results were obtained for six cases of damper characteristics separately, that is, the results do not include the dynamic situation of the damper characteristics that exist in real systems.

Ahmed et al. (1998b) presented the second application of the combined feedforward and feedback control approach. In the application, the internal heat generation in the laboratory space is considered as a disturbance. The implementation for temperature control is studied by using two closed loops: a supply air flow rate control loop and an exhaust air flow rate control loop so that the laboratory pressure constraint is met. In the control sequence the supply flow rate is increased by first opening the general exhaust damper to increase the total laboratory exhaust flow rate. They show that the FFPI control loop works well under a wide range of operating conditions. But in the cooling temperature control system, the controlled variable is not the room temperature, so that some offset of the room temperature may appear in steady state if the model is not exactly correct.

Ahmed et al. (1998c) presented the third application of the combined feedforward and feedback control approach. In this application, two separate disturbance sequences are considered for heating, and then the implementation for temperature control has been studied by using two closed loops, a temperature control loop and a supply airflow rate control loop. In addition, they also provided a summary and recommendations for the three systems, pressure control system, temperature control system for cooling and temperature control system for heating. They concluded that the FF part requires only a single smoothing parameter to be estimated, which can be held constant for most of the HVAC processes. The proposed FFPI controller may not need to be retuned. The main limitation in the three application papers (Ahmed et al., 1998a, 1998b, & 1998c) is that the identification results of GRNN were kept constant in the simulations.

Jeannette et al. (1998) have presented experimental results of a predictive neural network (PNN) controller applied to an unstable hot water system in an air-handling unit. The PNN controller works with a PID controller. The neural network learns the system while it is operating under the PID controller, and depending on the predictions, the NN used is "good" or not, the NN will or will not take control from the PID algorithm to control the processes. The term "good" means that the average of the past ten COVs, where COV is the coefficient of variation defined by Kreider and Haberl (1994) goes below 0.45. When the NN is active and the average COV rises above 0.55, then the NN model needs to be updated with new data and the controller reverts to PID control. Actual laboratory testing of the PNN and PID controllers shows favourable results for the PNN controller. The main limitation of the method is that the NN needs the PID controller's support for training and works only under specified range of operating conditions.

Atthajariyakul et al. (2005) presented a practical approach to determine human thermal comfort quantitatively via neural computing. The neural network model, as an explicit function of the relation of the predicted mean vote (PMV) index to accessible variables, i.e. the air temperature, wet bulb temperature, globe temperature, air velocity, clothing insulation and human activity, allows real time determination of the thermal comfort index. The authors used experimental results for an air conditioned office room to demonstrate the effectiveness of the proposed methodology and show good agreement between the thermal comfort index calculated from the neural network model in real time and those calculated from the conventional PMV model.

2.7 EMCS in HVAC&R Systems

To reduce energy consumption of HVAC systems, EMCS (energy management control systems) play a key part in building control. How to implement EMCS is still a challenging research area. The survey of few studies on EMCS will be shown in this section. In addition to the papers by Wang et al. (1999), Zheng et al. (1996), Wang et al. (2000), Huang et al. (2006) reviewed in the previous sections, in the following several papers related to EMCS will be reviewed.

Fong, Hanby and Chow (2006) proposed a simulation-optimization approach for the effective energy management of HVAC system, and developed a metaheuristic simulation–EP (evolutionary programming) coupling approach using evolutionary programming, which can effectively handle the discrete, non-linear and highly constrained optimization problems, such as those related to HVAC systems. They also demonstrated the effectiveness of this simulation–EP coupling suite through the

establishment of a monthly optimum reset scheme for both the chilled water and supply air temperatures of the HVAC system in a local subway station. This reset scheme is shown to have a saving potential of about 7% as compared to the existing operational settings, without any extra cost.

Engdahl and Johansson (2004) presented the theory for an optimal supply air temperature in a variable air volume (VAV) system to minimize the system energy use. The optimal supply air temperature can be set dependent on the load, specific fan power (SFP), chiller coefficient of performance, outdoor temperature and the outdoor relative humidity. They also calculated the heating, ventilation and air-conditioning (HVAC) energy use depending on supply air temperature control strategy, average U-value of the building envelope. After analysis of energy use, they concluded that controlling the supply air temperature optimally results in a significantly lower HVAC energy use than with a constant supply air temperature.

Jin, Ren and Xiao (2005) developed an optimal strategy for outdoor air control using a system approach based on prediction to minimize energy consumption. They used ARMA (autoregressive moving average) model to predict the energy performance expressed by an energy-increment equation. The energy-increment equation was formed to involve the real-time variations of AHU (air handling unit) load and energy use of reheaters of VAV terminals. By minimizing the energy-increment equation using genetic algorithm, the optimal settings of outdoor air ratio of AHU and reheating were obtained. The strategy was tested and evaluated in a simulated environment under various outdoor and indoor conditions.

Lu, Cai, Soh and Xie (2005a) presented the global optimization technique for overall heating, ventilating and air conditioning (HVAC) systems. They formulated the objective function of global optimization and constraints based on mathematical models of the major components. All these models are associated with power consumption components and heat exchangers for transferring cooling load. They introduced the characteristics of all the major components, then transformed and simplified the complicated original optimization problem for overall HVAC systems into a compact form ready for optimization according to the characteristics of the operating components.

Lu, Cai, Soh and Xie (2005b) presented the solution for the global optimization problem for overall heating, ventilating and air conditioning (HVAC) systems using a modified genetic algorithm. They showed the implementation procedure of the proposed optimal method. They concluded that the proposed method indeed improves the system performance significantly compared with traditional control strategies through simulation studies for a pilot scale centralized HVAC plant controlled by the optimal method (Lu et al., 2005a).

Lu, Cai, Soh, Li and Xie (2005) presented a practical method to optimize in-building section of centralized HVAC systems which consist of indoor air loops and chilled water loops. First, they established mathematical models associated with energy consuming devices. Then, they adopted adaptive neuro-fuzzy inference system (ANFIS) to model duct and pipe networks and obtain optimal differential pressure (DP) set points based on limited sensor information to adapt variation of cooling load of each end user. In addition, they formulated a mixed-integer nonlinear constraint optimization problem of

system energy and used a modified genetic algorithm to solve it. The optimization obtained by using a systematic approach in optimizing the overall system energy consumption. They made comparisons between the proposed optimization method and traditional ones for a typical centralized HVAC system. They provided the results and showed that the proposed method improves the system performance.

2.8 Experimental Research in HVAC Controls

Experimental work on control methods in HVAC systems has been investigated by several researchers. Kasahara et al. (1999) presented experimental results for PID tuning methods in HVAC systems (reviewed in Section 2.4). Krakow (1998) (reviewed in Section 2.4) used experimental responses for a PI-controlled mixing valve air heating system to show the relationship between sampling interval and digital PI control system performance. Application of adaptive PID control methods to HVAC systems were studied by Seem (1997) (reviewed in Section 2.3) and Nesler (1986a and 1986b) (reviewed in Section 2.5). A tuning method based on relay feedback, to a HVAC system was presented by Åström et al. (1993) (reviewed in Section 2.6.1).

Wang, Lee, Fung, Bi and Zhang (1999) proposed a PID controller design method that achieves high performance for a wide range of linear self-regulating processes. The PID tuning rules were developed using a second-order plus dead-time modeling technique and a closed loop pole allocation strategy. The technique was applied to processes with various dynamics, including those with low- and high-order, small and large dead-time, and monotonic and oscillatory responses. Simulation examples and comparisons with Ho's gain and phase margin method (GPM) (Ho, Hang, & Cao, 1995)

were presented and the results showed that improved performance can be obtained. Also, real-time experiments were carried out both in the laboratory and in the industry. The test in the laboratory was conducted on a Dual Process Simulator KI 100 manufactured by KentRidge Instruments, and the results from using both the proposed tuning method and Ho's method for one oscillatory process were presented. The industrial test was performed on an HVAC digital control system called Enflex, for a supply air pressure loop and a zone air temperature loop, in the Supersymmetry Services PTC LTD, Singapore. The process responses for both the proposed tuning method and Åström's modified Ziegler and Nichols method (Åström & Hägglund, 1984) were presented. The experimental results showed that improved performance is achieved by using the PID tuning method they developed. The main limitation of the tuning method is that robustness to uncertainties in the models is not considered and uncertainties in the models certainly exist and have an effect on performance since an exact cancellation method is used in their analysis.

Wallonborg (1991) proposed a control algorithm for a self-tuning controller. The control algorithm depends on discrete-time process transfer function parameters, and the parameters based on the wave form of a periodic oscillation obtained with a relay feedback tuning experiment. The self-tuning controller is a general linear discrete-time controller and was designed by using pole placement based on input-output models. In addition, the self-tuning controller also has a feature that the sampling period and the desired closed loop poles is determined automatically with respect to the process dynamics and the desired closed loop performance can be easily modified by the The experimental results for applying the control algorithm to a supply air temperature

control and an air duct pressure control are shown. Wallonborg concluded that the algorithm has worked well in many different HVAC applications, and a substantial reduction in commissioning can be achieved compared with manual tuning of conventional controllers. The main drawback of the algorithm is that in some cases it may be difficult to obtain the necessary steady-state conditions for a tuning experiment.

J. Wang, Y. Wang, and Shao (2005) noted that variable air volume (VAV) air conditioning control system has the feature of multi-control loops, so while all the control loops are working together, they interfere and influence each other. Therefore, they designed the decoupling unit in VAV air conditioning system using the method of diagonal matrix decoupling, and adopted Lonworks technology into VAV air conditioning decoupling control system so that data could be exchanged among multi-loops. Experimental results demonstrate that the combination of the diagonal matrix decoupling and Lonworks technology (decoupling compensation coefficients among multi-loops are handled as network variables of Lonworks technology) can improve the performance of the VAV air conditioning control system.

2.9 Summary and Discussion

In this chapter, the literature related to HVAC systems was reviewed. The literature reviewed includes modeling, design of controllers, intelligent controls, experimental controls and energy management control system (EMCS).

The modeling of HVAC systems is one of the most important aspects in system design. The modeling effort has been focused at two levels. One is for simulation and the other is for control design. The models for simulation of HVAC performance have been

developed by many researchers such as Tashtoush et al. (2005), Mei et al. (2002), Huang et al. (2006), and Wang et al. (1999). The models for control design, especially for auto tuning and adaptive controls, have received little attention. A frequently used model for local loop control is based FOPDT modeling approach. This is considered adequate if it is used as a part of robust identification for parameter update.

From the literature review presented in this chapter, it is noted that while there have been several studies on the design of controllers for HVAC systems most can be grouped into simulation based energy efficiency analysis studies and control studies which use either computer control or industrial controls. Such developed algorithms can hardly be implemented on building control platforms currently available. Therefore, the focus of this research has been to develop PI control tuning methods which can be implemented on existing building control systems. Both online adaptation, robustness issues have been addressed and the feasibility of NN control for HAVC systems has been demonstrated.

PID controller is still the most popular controller in HVAC field today. However, there is a need to augment the PID controller with energy optimal and robustness properties. Although some studies on the combination of intelligent control and PID control have been done by some researchers such as Seem (1997), Nesler (1986b), and Qu et al. (2004), the developed control strategies have to be implemented in existing building control hardware platform. This aspect is lacking in many of the studies done in the literature.

The interaction in HVAC systems makes control difficult. To solve this kind of problem some researchers such as Wang et al. (2005), Rentel-Gómez et al. (2001), and Semsar et al. (2003) have used decoupling control. For zone temperature controls in multi-zone systems the interaction of airflow into zones could be solved by adopting innovative two loop control structure. Such a control strategy will be studied in this research.

EMCS in HVAC systems plays key part in implementing supervisory control strategies to achieve energy savings. To achieve the energy saving goal, the local controls in HVAC systems must be efficient and robust. The emphasis of this thesis is to develop suitable and simple control strategies for local controls of HVAC systems that can be implemented in real systems with EMCS. The detailed proposed control strategies will be presented in the following chapters.

3. Modified RLS Identification Algorithm for FOPDT Systems

In order to develop improved adaptive control strategies a robust online identification technique needs to be developed. Therefore, the objective here is the development of a modified RLS algorithm that is suitable for online implementation.

An RLS identification algorithm for FOPDT model that uses a 2×2 matrix P was developed in an earlier study (Qu, 2002). To improve the robustness property of the RLS algorithm developed earlier, a matrix-reset technique is designed. Simulation results show that with this technique a more robust online identification of plant parameters was achieved.

3.1 RLS Algorithm for Online Identification of FOPDT Systems

The recursive least squares (RLS) method is an effective approach in online identification because a new estimate can be obtained easily. In order to implement the RLS algorithm for online identification of a system, consider the following diagram (Franklin, Powell, & Workman, 1997).

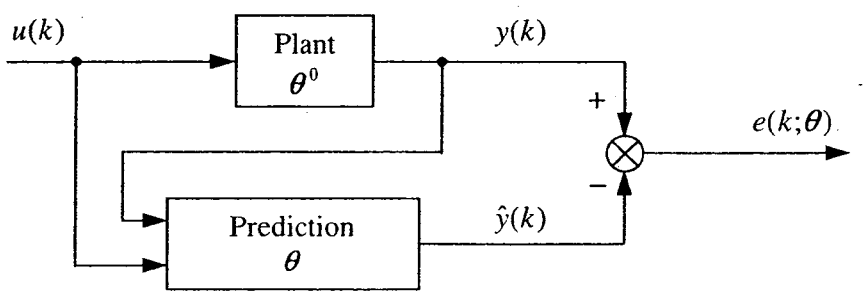

Figure 3.1 Block diagram showing the generation of output prediction error

Considering the system as a FOPDT model (3.1), it is noted that, if l is fixed, the system identification reduces to the estimation of parameters a and b of the system.

$$G(z)=\frac{Y(z)}{U(z)}=\frac{bz^{-l-1}}{1-az^{-1}} \tag{3.1}$$

Using measured or computed values of $y(k)$ and $u(k)$ for some k, we have

$$y(k)-ay(k-1)-bu(k-l-1)=e(k;\theta) \tag{3.2}$$

Let

$$\theta=[a \quad b]^T \tag{3.3}$$

and

$$\psi(k)=[y(k-1) \quad u(k-l-1)]^T \tag{3.4}$$

then, through analysis, we can write the error equation as

$$Y(N)=\Psi(N)\theta+\varepsilon(N;\theta) \tag{3.5}$$

where

$$\Psi(N)=[\psi(l+1) \quad \psi(l+2) \quad \cdots \quad \psi(N)]^T$$

$$\varepsilon(N;\theta)=[e(l+1;\theta) \quad \cdots \quad e(N;\theta)]^T$$

$$Y(N)=[y(l+1) \quad \cdots \quad y(N)]^T$$

Assume that we observe a set of inputs and outputs

$$\{u(0),u(1),\cdots,u(N),y(0),y(1),\cdots,y(N)\},$$

and that we need to estimate the parameter θ^0 of the system and the prediction is θ. The least-squares method can be expressed as

$$\min_{\theta} J(\theta) \tag{3.6}$$

where $J(\theta)=\sum_{k=l+1}^{N} w(k)e^2(k;\theta)=\varepsilon^T W\varepsilon$ and the weighting function $w(k)$ is positive.

For $w(k)=\alpha\gamma^{N-k}$, $\hat{\theta}=\begin{bmatrix}\hat{a}\\ \hat{b}\end{bmatrix}$ is the minimum of $J(\theta)$, the vector $L(k)=\begin{bmatrix}L_1(k)\\ L_2(k)\end{bmatrix}$ and the 2×2 matrix $P(k)=\begin{bmatrix}P_{11}(k) & P_{12}(k)\\ P_{21}(k) & P_{22}(k)\end{bmatrix}$, the scalar form of RLS algorithm for FOPDT model described in the previous study (Qu, 2002) can be summarized as follows:

Step 1: Select $N\,(>2\times l)$

Step 2: Select α, γ

Comment: $\alpha=\gamma=1$ is ordinary least squares; $\alpha=1-\gamma$ and $0<\gamma<1$ is exponentially weighted least squares

Step 3: Select initial values for $P(N)$ and $\hat{\theta}(N)$. One possibility is that set $\hat{\theta}(N)=\begin{bmatrix}0\\ 0\end{bmatrix}$, $P(N)=\begin{bmatrix}\beta & 0\\ 0 & \beta\end{bmatrix}$, where β is a large scalar. This requires less memory and matrix inversion is not needed, and the computations can be reduced to calculate $P(N)$ and $\hat{\theta}(N)$

Step 4: Collect $y(N)$ and $u(N-l)$ and form $\psi^T(N+1)=\begin{bmatrix}y(N) & u(N-l)\end{bmatrix}$

Step 5: Let $k\leftarrow N$

Step 6: $L(k+1)\leftarrow\dfrac{P(k)}{\gamma}\psi(k+1)\left(\dfrac{1}{\alpha}+\psi^T(k+1)\dfrac{P(k)}{\gamma}\psi(k+1)\right)^{-1}$ can be done by

step 6-1:

$$\mu(k+1)\leftarrow\frac{1}{\dfrac{1}{\alpha}+\left(P_{11}(k)y^2(k)+(P_{12}(k)+P_{21}(k))y(k)u(k-l)+P_{22}(k)u^2(k-l)\right)/\gamma} \tag{3.7}$$

step 6-2: $L_1(k+1)\leftarrow\dfrac{\mu(k+1)}{\gamma}\left(P_{11}(k)y(k)+P_{12}(k)u(k-l)\right)$ (3.8)

and step 6-3: $L_2(k+1) \leftarrow \frac{\mu(k+1)}{\gamma}\left(P_{21}(k)y(k)+P_{22}(k)u(k-l)\right)$ (3.9)

Step 7: Collect $y(k+1)$ and $u(k-l+1)$

Step 8: $\hat{\theta}(k+1) \leftarrow \hat{\theta}(k)+L(k+1)\left(y(k+1)-\psi^T(k+1)\hat{\theta}(k)\right)$ can be done by

step 8-1: $\sigma(k+1) \leftarrow y(k+1)-\left(\hat{a}(k)y(k)+\hat{b}(k)u(k-l)\right)$ (3.10)

step 8-2: $\hat{a}(k+1) \leftarrow \hat{a}(k)+L_1(k+1)\sigma(k+1)$ (3.11)

and step 8-3: $\hat{b}(k+1) \leftarrow \hat{b}(k)+L_2(k+1)\sigma(k+1)$ (3.12)

Step 9: $P(k+1) \leftarrow \frac{1}{\gamma}\left[I-L(k+1)\psi^T(k+1)\right]P(k)$ can be done by

step 9-1: $PLY_1(k+1) \leftarrow P_{11}(k)L_2(k+1)y(k)$ (3.13)

step 9-2: $PLY_2(k+1) \leftarrow P_{12}(k)L_2(k+1)y(k)$ (3.14)

step 9-3: $P_{11}(k+1) \leftarrow \frac{1}{\gamma}\left[P_{11}(k)\left(1-L_1(k+1)y(k)\right)-P_{21}(k)L_1(k+1)u(k-l)\right]$ (3.15)

step 9-4: $P_{12}(k+1) \leftarrow \frac{1}{\gamma}\left[P_{12}(k)\left(1-L_1(k+1)y(k)\right)-P_{22}(k)L_1(k+1)u(k-l)\right]$ (3.16)

step 9-5: $P_{21}(k+1) \leftarrow \frac{1}{\gamma}\left[-PLY_1(k+1)+P_{21}(k)\left(1-L_2(k+1)u(k-l)\right)\right]$ (3.17)

and step 9-6: $P_{22}(k+1)=\frac{1}{\gamma}\left[-PLY_2(k+1)+P_{22}(k)\left(1-L_2(k+1)u(k-l)\right)\right]$ (3.18)

Step 10: $k \leftarrow k+1$

Step 11: Form $\psi(k+1)$

Step 12: Go to step 6.

Note that all equations of the algorithm are expressed in scalar form (no matrix inversion is required), so they can be directly implemented on the existing EMCS. This

algorithm uses less memory than the original RLS (Franklin et al., 1997) for higher value of l ($l \geq 2$ normally) and no matrix inversion is required.

3.2 Issues in Using the RLS Algorithm for Online Identification

Numerical instability in the RLS algorithm may cause absolutely wrong identification results. To avoid this situation, a robust RLS algorithm is developed. The basis of the development strategy is described in the following.

First of all, in the RLS algorithm, we need to compute the elements of $P(k+1)$ as in step 9 of the algorithm, which uses the following equations.

$$P(k+1) = \frac{1}{\gamma}\left[I - L(k+1)\psi^T(k+1)\right]P(k) \tag{3.19}$$

where $L(k+1) = \frac{P(k)}{\gamma}\psi(k+1)\left(\frac{1}{\alpha} + \psi^T(k+1)\frac{P(k)}{\gamma}\psi(k+1)\right)^{-1}$ and

$\psi(k) = [y(k-1) \quad u(k-l-1)]^T$.

The above equations do not guarantee that all elements in $P(k+1)$ with their absolute values do not go to infinity. For example, in the case of $P_{11}(k) < 0$, $|P_{11}(k)| > M$ (M is a large positive value which is close to the maximum operating value of the system and $2M$ will be greater than the maximum operating value of the system) at a time k, and $|L_2(k+1)| > 2$ at the time $k+1$, from equation (3.13) we can see that $|PLY_1(k+1)|$ will be greater than the maximum operating value for $y(k) \geq 1$. From the step 6 and step 9 of the program, we can see that if $P_{11}(k) < 0$ and $P_{22}(k) < 0$ at a time k then the result $|P_{11}(k)| > M$, $|P_{22}(k)| > M$ or one of $|P_{11}(k)|$ and $|P_{22}(k)|$ may tend to infinity for a

symmetrical initial matrix P, $0<\gamma<1$ and $\mu(k+1)>0$ because the following equations exist under the symmetrical initial matrix condition.

$$P_{12}(k+1)=P_{21}(k+1)$$

$$P_{11}(k+1)=\frac{P_{11}(k)}{\gamma}-\frac{\mu(k+1)}{\gamma^2}\left(P_{11}(k)y(k)+P_{12}(k)u(k-l)\right)^2 \quad \text{and}$$

$$P_{22}(k+1)=\frac{P_{22}(k)}{\gamma}-\frac{\mu(k+1)}{\gamma^2}\left(P_{12}(k)y(k)+P_{22}(k)u(k-l)\right)^2$$

In addition, $\hat{\theta}(k+1)=\hat{\theta}(k)+L(k+1)\left(y(k+1)-\psi^T(k+1)\hat{\theta}(k)\right)$ shows that we need to avoid $L(k+1)=0$ over a long interval which causes incorrect identification result because in this case, even if $y(k+1)\neq\psi^T(k+1)\hat{\theta}(k)$, there still exists $\hat{\theta}(k+1)=\hat{\theta}(k)$. This observation can be drawn from $P(k)=0$ through some analysis for the FOPDT system.

As a result, we can say that $P(k)=0$ causes incorrect identification and also significantly higher absolute values of $P(k)$ cause incorrect identification (the infinity problem). Resetting the matrix $P(k)$ in such cases is one way to solve this problem.

In the equation (3.7) in step 6-1, a division operation is required. However, by computing $\varsigma(k)$ first as in Equation (3.20), we can verify whether $\varsigma(k)$ goes to zero or not. Therefore, we should guarantee that $\varsigma(k)\neq 0$ for validly computing $\mu(k+1)$ by modifying the online identification algorithm.

$$\varsigma(k)=\frac{1}{\alpha}+\left(P_{11}(k)y^2(k)+\left(P_{12}(k)+P_{21}(k)\right)y(k)u(k-l)+P_{22}(k)u^2(k-l)\right)/\gamma \qquad (3.20)$$

3.3 Matrix-Reset Technique

To avoid incorrect identification results or infinity problem, a matrix-reset technique is developed. The basis for this is that we can set an upper bound on the sum of the square values of elements in matrix P to solve the infinity problem and set a lower bound on the sum of the square values of elements in matrix P to solve the incorrect identification problem. That is, we should keep

$$LowValue < P_{ss} < UpValue \quad (\text{where } P_{ss} = P_{11}^2 + P_{12}^2 + P_{21}^2 + P_{22}^2) \tag{3.21}$$

and resetting to initial values for matrix P whenever the value of P_{ss} is out of the bounds.

To choose the lower bound (*LowValue*), we must avoid all elements of P which are less than the smallest positive non-zero value of the processor (SPVOP) and at the same time avoid $L(k+1) = 0$ for $k \rightarrow \infty$. Also, to keep the algorithm running in a normal way which guarantees that the identification is converging, frequent resetting should be avoided. Therefore, based on the above

$$1 > LowValue > SPVOP \tag{3.22}$$

is an acceptable choice for the lower bound (*LowValue*).

Here we discuss how to choose the *UpValue* --- the upper bound. First the computed values in the algorithm must not lead to infinity. That can be ensured by satisfying the following inequality

$$UpValue < \frac{\sqrt{\delta\gamma^2 LPVOP + 1} - 1}{y_{\max} + u_{\max}} \tag{3.23}$$

Where, *LPVOP* is the largest positive non-zero value of the processor. y_{max} is the maximum value of y and u_{max} is the maximum value of u.

Second, we need to also ensure that the following inequality is satisfied. $P(k)=\begin{bmatrix}\beta & 0\\ 0 & \beta\end{bmatrix}$, then $P_{ss}(k+1)<UpValue$.

Therefore, for $P(k)=\begin{bmatrix}\beta & 0\\ 0 & \beta\end{bmatrix}$, we have

$$P_{11}(k+1)=\frac{\beta}{\gamma}\left(1-\frac{\beta y^2(k)}{\gamma\left(\frac{1}{\alpha}+\beta y^2(k)+\beta u^2(k-l)\right)}\right) \tag{3.24}$$

$$P_{12}(k+1)=P_{21}(k+1)=-\frac{\beta}{\gamma}\frac{\beta y(k)u(k-l)}{\gamma\left(\frac{1}{\alpha}+\beta y^2(k)+\beta u^2(k-l)\right)} \tag{3.25}$$

$$P_{22}(k+1)=\frac{\beta}{\gamma}\left(1-\frac{\beta u^2(k-l)}{\gamma\left(\frac{1}{\alpha}+\beta y^2(k)+\beta u^2(k-l)\right)}\right) \tag{3.26}$$

Let $\Sigma=\frac{1}{\alpha}+\beta y^2(k)+\beta u^2(k-l)$, then $0\le\frac{\beta\left(y^2(k)+u^2(k-l)\right)}{\Sigma}<1$. Therefore,

$$P_{ss}(k+1)=\left(\frac{\beta}{\gamma}\right)^2\left[\left(1-\frac{\beta y^2(k)}{\gamma\Sigma}\right)^2+\frac{2\beta^2y^2(k)u^2(k-l)}{\gamma^2\Sigma^2}+\left(1-\frac{\beta u^2(k-l)}{\gamma\Sigma}\right)^2\right]$$

$$=\left(\frac{\beta}{\gamma}\right)^2\left[2-\frac{2\beta y^2(k)}{\gamma\Sigma}+\frac{\beta y^2(k)}{\gamma^2\Sigma}\left(\frac{\beta\left(y^2(k)+u^2(k-l)\right)}{\Sigma}\right)\right.$$

$$\left.-\frac{2\beta u^2(k-l)}{\gamma\Sigma}+\frac{\beta u^2(k-l)}{\gamma^2\Sigma}\left(\frac{\beta\left(y^2(k)+u^2(k-l)\right)}{\Sigma}\right)\right]$$

$$< \left(\frac{\beta}{\gamma}\right)^2 \left[2 - \frac{2\gamma - 1}{\gamma^2 \Sigma} \beta \left(y^2(k) + u^2(k-l)\right)\right]$$

$$< \begin{cases} 2\left(\frac{\beta}{\gamma}\right)^2, & \gamma \geq 0.5 \\ 2\left(\frac{\beta}{\gamma}\right)^2 \left(1 + \left(\frac{1-\gamma}{\gamma}\right)^2\right), & 0 < \gamma < 0.5 \end{cases} \tag{3.27}$$

Therefore, we can choose

$$\frac{\sqrt{\delta\gamma^2 LPVOP + 1} - 1}{y_{\max} + u_{\max}} > UpValue \geq 2\left(\frac{\beta}{\gamma}\right)^2 \text{ for } \gamma \geq 0.5, \tag{3.28}$$

$$\frac{\sqrt{\delta\gamma^2 LPVOP + 1} - 1}{y_{\max} + u_{\max}} > UpValue \geq 2\left(\frac{\beta}{\gamma}\right)^2 \left(1 + \left(\frac{1-\gamma}{\gamma}\right)^2\right) \text{ for } 0 < \gamma < 0.5. \tag{3.29}$$

In the above algorithm, the value of α is between $0 < \alpha \leq 1$. From the RLS algorithm, we know that α and γ are related to weighting factors. For a fixed value of γ, choosing larger α means more weight is placed on the current measurement. If we let $\gamma = 1$ and α be infinity, the parameter α will have no effect on the algorithm. In the next section, simulation result will show that this modification makes the estimation process fast. However, this modification must be combined with a reset technique to have better robustness in real time applications.

To avoid the infinity problem, we must avoid division by zero in computing $\mu(k+1) = 1/\varsigma(k)$ (step 6-1). This can be ensured by considering the online identification program to do reset to initial values for matrix P, when $\varsigma(k) \leq \delta$. Where, δ is a small value (we can choose $\delta \geq \frac{\gamma}{\beta} > 0$ and $\delta > SPVOP$).

In addition, to avoid $L(k+1)=0$ for $k \rightarrow \infty$, $LowValue < P_{ss}$ and inequality (3.27) should be checked and reset the matrix P to the initial status if any inequality is not satisfied. Where, *LowValue* is a selected small positive value. If we let the initial values of $P_{12}=P_{21}$ be zero and $P_{11}=P_{22}$ be positive, then we have $P_{12}(k)=P_{21}(k)$. In a real application, to avoid wrong measurement effect the identified parameters must be bounded. To this end, the modified RLS identification algorithm can be stated as follows.

Initialization: Initialize the model parameters a, b and l obtained by applying any off-line system identification method using a set of open-loop experimental data, select or compute $a_{\max}$, $a_{\min}$, $b_{\max}$, and $b_{\min}$ by considering such as 75% changes in T_c and K_c shown in Figure 4.3

Step 1: Select $N\,(>2\times l)$, *LowValue* and *UpValue*

Step 2: Select α, γ

Comment: $\alpha=\gamma=1$ is ordinary least squares; $\alpha=1-\gamma$ and $0<\gamma<1$ is exponentially weighted least squares; $\gamma=1$ and $\alpha=\infty$ is recommended.

Step 3: Set $P_{11}(N)=P_{22}(N)=\beta$, $P_{12}(N)=0$, $\hat{a}(N)=a$, and $\hat{b}(N)=b$, where β is a positive large scalar that satisfies the inequality (3.28) for $\gamma\geq 0.5$, and satisfies the inequality (3.29) for $0<\gamma<0.5$.

Step 4: Collect $y(N)$ and $u(N-l)$

Step 5: Let $k \leftarrow N$

Step 6: $\varsigma(k+1) \leftarrow 1/\alpha+(P_{11}(k)y^2(k)+2P_{12}(k)y(k)u(k-l)+P_{22}(k)u^2(k-l))/\gamma$ (3.30)

Step 7: If $|\varsigma(k+1)| \leq \delta$ then go to step 20 else go to step 8 (avoid dividing by zero)

Step 8: $L_1(k+1) \leftarrow \left(P_{11}(k)y(k) + P_{12}(k)u(k-l)\right)/\varsigma(k+1)/\gamma$ (3.31)

Step 9: $L_2(k+1) \leftarrow \left(P_{12}(k)y(k) + P_{22}(k)u(k-l)\right)/\varsigma(k+1)/\gamma$ (3.32)

Step 10: Collect $y(k+1)$ and $u(k-l+1)$

Step 11: $\sigma(k+1) \leftarrow y(k+1) - \left(\hat{a}(k)y(k) + \hat{b}(k)u(k-l)\right)$ (3.33)

Step 12: $\hat{a}_c(k+1) \leftarrow \hat{a}(k) + L_1(k+1)\sigma(k+1)$ (3.34)

Step 13: $\hat{b}_c(k+1) \leftarrow \hat{b}(k) + L_2(k+1)\sigma(k+1)$ (3.35)

Step 14: $PLY_2(k+1) \leftarrow P_{12}(k)L_2(k+1)y(k)$ (3.14)

Step 15: $P_{11}(k+1) \leftarrow \frac{1}{\gamma}\left[P_{11}(k)\left(1 - L_1(k+1)y(k)\right) - P_{12}(k)L_1(k+1)u(k-l)\right]$ (3.36)

Step 16: $P_{12}(k+1) \leftarrow \frac{1}{\gamma}\left[P_{12}(k)\left(1 - L_1(k+1)y(k)\right) - P_{22}(k)L_1(k+1)u(k-l)\right]$ (3.16)

Step 17: $P_{22}(k+1) = \frac{1}{\gamma}\left[-PLY_2(k+1) + P_{22}(k)\left(1 - L_2(k+1)u(k-l)\right)\right]$ (3.18)

Step 18: $P_{ss}(k+1) \leftarrow P_{11}^2(k+1) + 2P_{12}^2(k+1) + P_{22}^2(k+1)$ (3.37)

Step 19: If $LowValue < P_{ss} < UpValue$ then go to step 21 else go to step 20

Step 20: Set $P_{11}(k+1) = P_{22}(k+1) = \beta$ and $P_{12}(k+1) = 0$ (do reset)

Step 21: If $a_{\min} \le \hat{a}_c(k+1) \le a_{\max}$ and $b_{\min} \le \hat{b}_c(k+1) \le b_{\max}$ then go to step 22 else go to step 23 (only computed value in the considered range will be updated)

Step 22: $\hat{a}(k+1) \leftarrow \hat{a}_c(k+1)$ and $\hat{b}(k+1) \leftarrow \hat{b}_c(k+1)$ then go to step 24

Step 23: $\hat{a}(k+1) \leftarrow \hat{a}(k)$ and $\hat{b}(k+1) \leftarrow \hat{b}(k)$

Step 24: $k \leftarrow k+1$

Step 25: Go to step 6.

3.4 Simulation Studies for the Modified RLS Algorithm

Real systems always have some delay and dynamics. The proposed modified RLS identification algorithm will reduce the maximum delay and response time under realistic operating conditions. Simulation results show that the proposed modified RLS identification algorithm has smoother (smaller offset) response than the previous RLS algorithm (Franklin, 1997; Qu, 2002). The simulation implementation in Simulink is depicted in Figure 3.2.

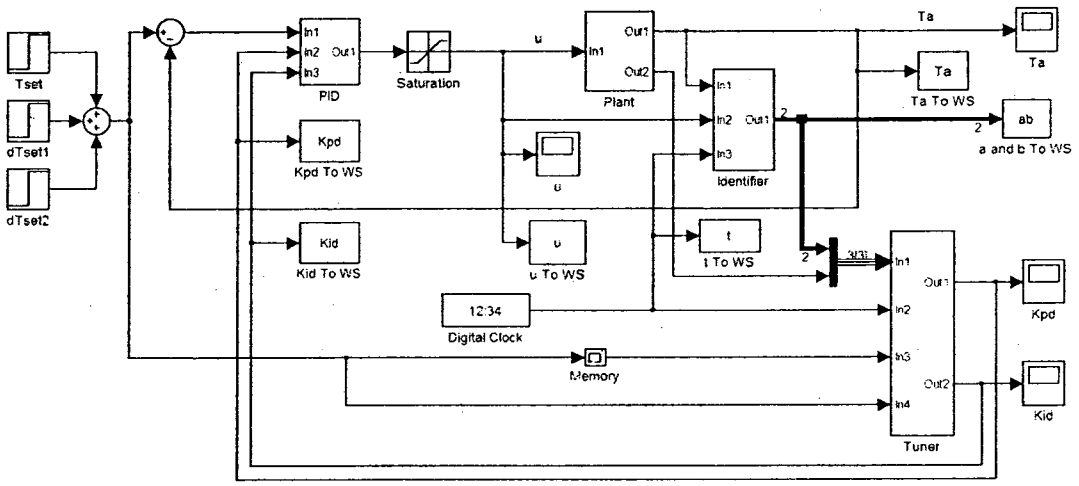

Figure 3.2 Simulation scheme for on-line adaptive control

In Figure 3.2, the plant model is given by Equation (3.1) and the delay l is known. The identifier is implemented by using RLS algorithm with or without the matrix-reset technique. The H_∞ PI tuning algorithm is applied for the tuner in this section. Eight cases are considered in the simulation study. The matrix-reset technique is not used in Case 3.1 ($\alpha=\gamma=1$), Case 3.3 ($\alpha=0.5$ and $\gamma=0.5$), Case 3.5 ($\alpha=\infty$ and $\gamma=1$) and Case 3.7 ($\alpha=0.05$ and $\gamma=0.95$). In Case 3.2 ($\alpha=\gamma=1$), Case 3.4 ($\alpha=0.5$ and $\gamma=0.5$), Case

3.6 ($\alpha=\infty$ and $\gamma=1$) and Case 3.8 ($\alpha=0.05$ and $\gamma=0.95$), the matrix-reset technique is applied with $\delta=\gamma/\beta$, $LowValue$=0.85 and $UpValue$=$8\times10^{12}>2(\beta/\gamma)^2$.

The parameters of the simulated plant processes are as follows.

$$a=\begin{cases}0.98 & t<5000\\ 0.9866 & t\geq5000\end{cases},\quad b=\begin{cases}0.1278 & t<5000\\ 0.0427 & t\geq5000\end{cases},\quad l=9 \text{ (plant process 3.1),}$$

$$a=\begin{cases}0.98 & t<5000\\ 0.9735 & t\geq5000\end{cases},\quad b=\begin{cases}0.1278 & t<5000\\ 0.2112 & t\geq5000\end{cases},\quad l=9 \text{ (plant process 3.2) and}$$

$$a=\begin{cases}0.98 & t<5000\\ 0.9604 & t\geq5000\end{cases},\quad b=\begin{cases}0.1278 & t<5000\\ 0.3796 & t\geq5000\end{cases},\quad l=9 \text{ (plant process 3.3).}$$

The parameter limits were set as $a_{\max}=0.9885$, $a_{\min}=0.9224$, $b_{\max}=0.8681$ and $b_{\min}=0.0183$. The simulation was made with $T_{a0}=78.0°F$, $N=25$, $P(0)=\begin{bmatrix}\beta & 0\\ 0 & \beta\end{bmatrix}$, $\beta=8\times10^5$ and the sampling time T_s = 4s. The simulation results for different plant processes and the cases are shown in Figures 3.3 to 3.8. Figures (c) and (d) are partially enlarged views of Figures (a) and (b).

Figures 3.3 to 3.5 show that the identification of the plant Processes 3.1, 3.2 and 3.3 under Case 3.1 (α = γ = 1 without matrix reset technique) is incorrect. The dynamic time of the identification (convergence to the real plant parameter values) for Processes 3.1, 3.2 and 3.3 under Case 3.2 (α = γ = 1 with the matrix reset technique) are 32s, 220s and 68s. The dynamic time of the identification (convergence to the real plant parameter values) for plant Processes 3.1, 3.2 and 3.3 under Case 3.6 (α = ∞ and γ = 1 with the

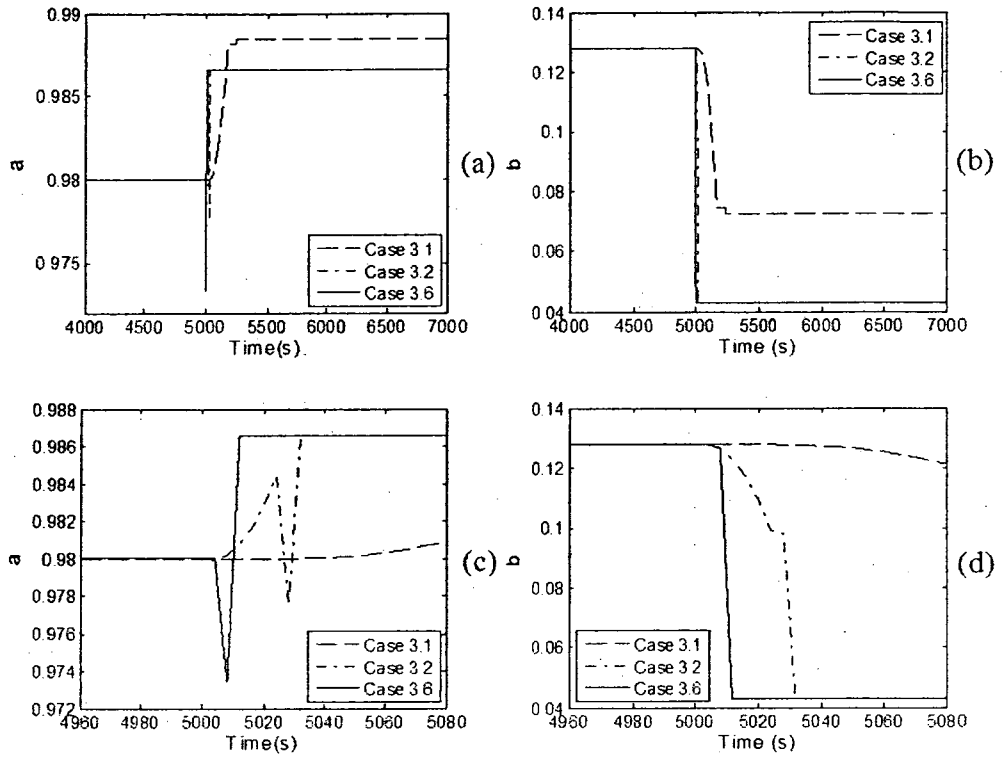

Figure 3.3 Identification simulation results for process 3.1 under Cases 3.1, 3.2, 3.6

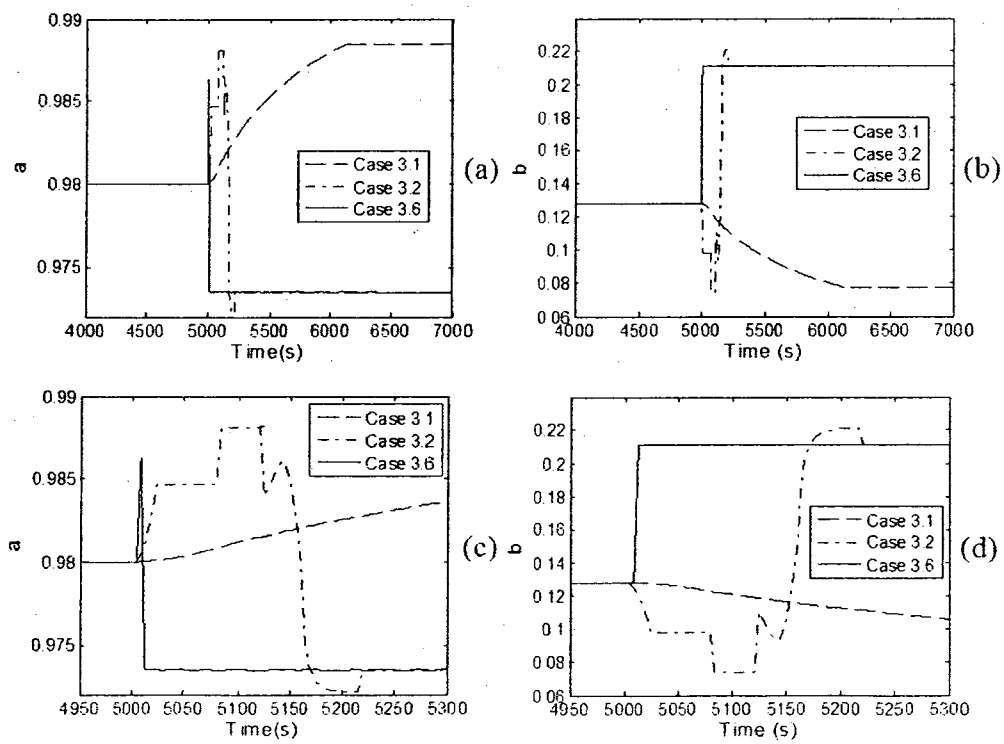

Figure 3.4 Identification simulation results for process 3.2 under Cases 3.1, 3.2, 3.6

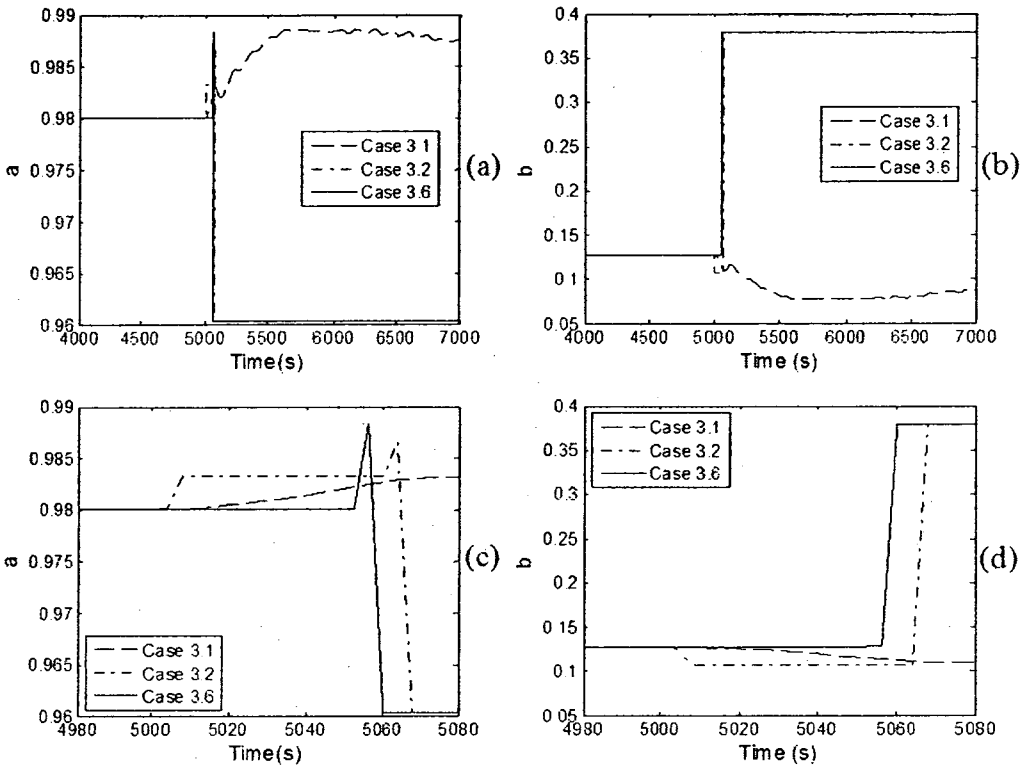

Figure 3.5 Identification simulation results for process 3.3 under Cases 3.1, 3.2, 3.6

matrix reset technique) are 12s, 12s and 60s. The results indicate that to have correct identification it is necessary to use the matrix reset technique. In addition, the results show that choosing $\alpha = \infty$ and $\gamma = 1$ with the matrix reset technique (Case 3.6) resulted improved identification of the system parameters.

The identification results for Case 3.3 ($\alpha = 0.5$ and $\gamma = 0.5$ without the matrix reset technique) could not be shown in Figures 3.6 to 3.8, because simulation run was interrupted due to infinity problem ($|PLY_2| = Inf$). The simulation runs for Processes 3.1 to 3.3 were tried for Case 3.5 ($\alpha = \infty$ and $\gamma = 1$ without the matrix reset technique), however, they were interrupted too due to infinity problem ($|PLY_2| = Inf$). Therefore, no figures for Case 3.5 could be recorded.

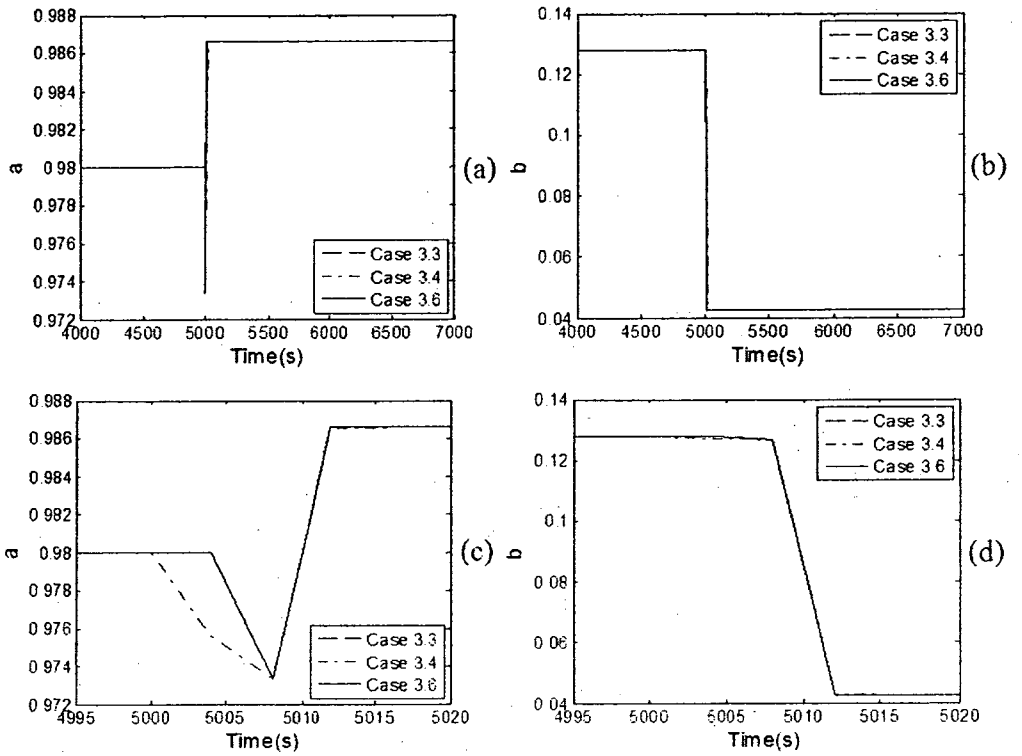

Figure 3.6 Identification simulation results for process 3.1 under Cases 3.3, 3.4, 3.6

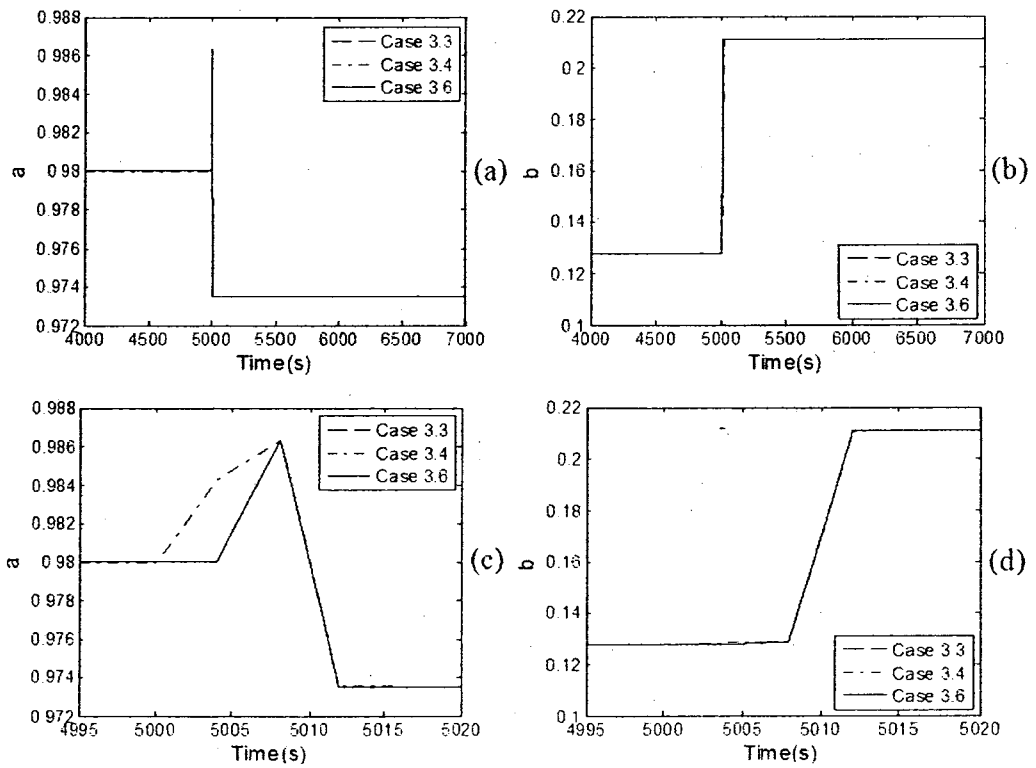

Figure 3.7 Identification simulation results for process 3.2 under Cases 3.3, 3.4, 3.6

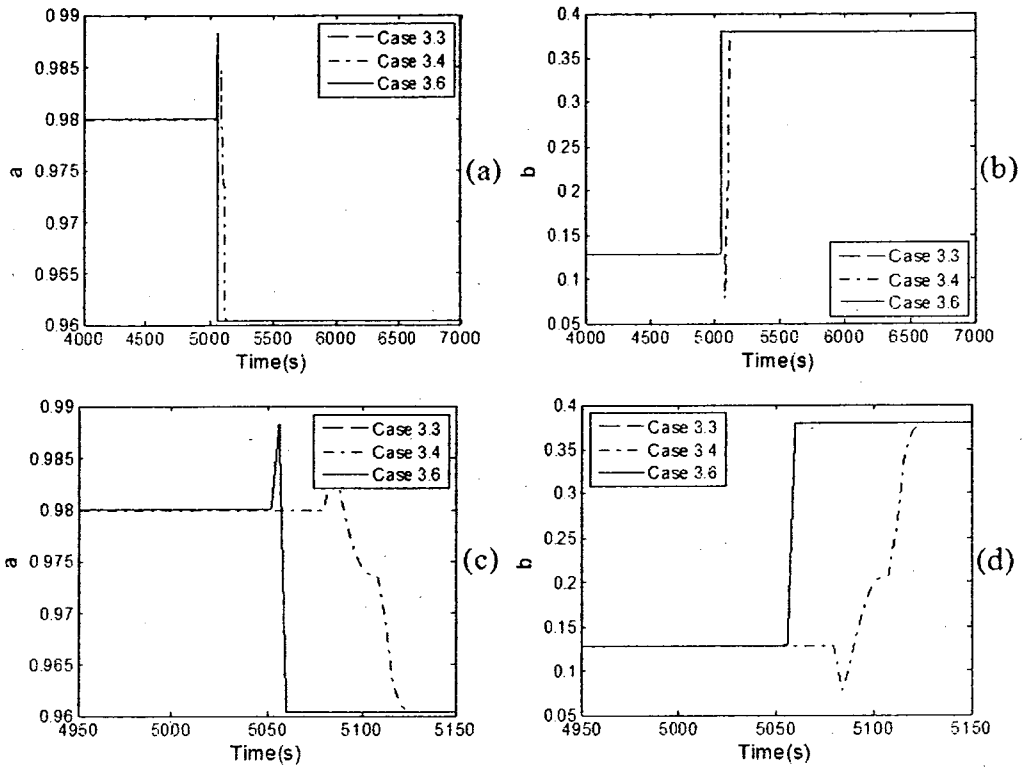

Figure 3.8 Identification simulation results for process 3.3 under Cases 3.3, 3.4, 3.6

As shown in Figures 3.6 and 3.7, the response times of the identification for plant Processes 3.1 and 3.2 for Case 3.4 ($\alpha = 0.5$ and $\gamma = 0.5$ with the matrix reset technique) and Case 3.6 ($\alpha = \infty$ and $\gamma = 1$ with the matrix reset technique) are the same (12s). But, the inflection point for Case 3.6 is closer to the real value compared with the inflection point for Case 3.4. From Figure 3.8, it is noted that the response time of the identification for plant Process 3.3 for Case 3.6 (60s) is much smaller than the response time of the identification for plant Process 3.3 for Case 3.4 (124s).

It is clear that by using the matrix reset technique we can avoid the infinity problem and better identification results can be obtained in most of the cases. But, in some cases with the exponentially weighted least squares one can obtain better results without the matrix reset technique. This is illustrated in Figure 3.9. The limit set in Figure

3.9 refers to the plant parameter limits. The limit set 1 is same as chosen before, that is, $a_{max}=0.9885$, $a_{min}=0.9224$, $b_{max}=0.8681$ and $b_{min}=0.0183$. The limit set 2 parameter limits are $a_{max}=0.9999$, $a_{min}=0.9224$, $b_{max}=0.8681$ and $b_{min}=0.0001$. The identification of plant Process 3.1 for Case 3.7 (without the matrix reset technique) with Limit set 1 (16s) is faster than for Case 3.8 (with the matrix reset technique) with Limit set 1 (more than 1000s to reach real plant parameter values). The main reason for the long response time for plant Process 3.1 for Case 3.8 (with the matrix reset technique) is plant parameter limit selection. Figure 3.9 shows that the identification for plant Process 3.1 for Case 3.8 with Limit set 2 (108s to reach real plant parameter values) has better performance. Figure 3.9 also shows that Case 3.6 (12s to reach real plant parameter values) still is the fastest choice for the identification.

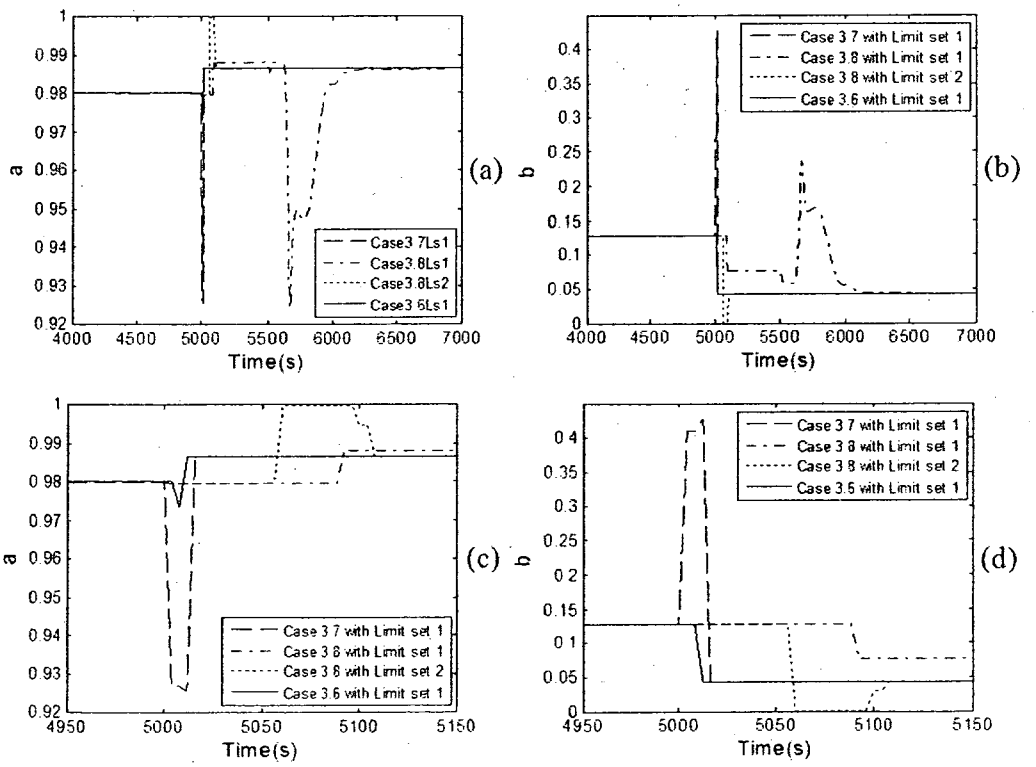

Figure 3.9 Identification result comparison for Cases 3.7, 3.8, 3.6

In summary, the identification method with $\alpha=\infty$ and $\gamma=1$ (with the matrix reset technique) gives fast and smooth identification responses. In addition, there is no trial required to select α and γ values in this method. Therefore, it is recommended to use $\alpha=\infty$ and $\gamma=1$ with the matrix reset technique for the online identification of the FOPDT plants.

3.5 Experimental Tests with the Modified RLS Algorithm

To test the modified RLS algorithm, we have applied the algorithm for online identification and control of discharge air temperature in an HVAC test facility. The results are plotted in Figures 3.10 – 3.12. The system was controlled by the simplified optimal adaptive control (with modified RLS algorithm). Figure 3.10 shows the identification of plant parameters. a_v is the estimated value of the parameter a and b_v is the estimated value of the parameter b in the identification process.

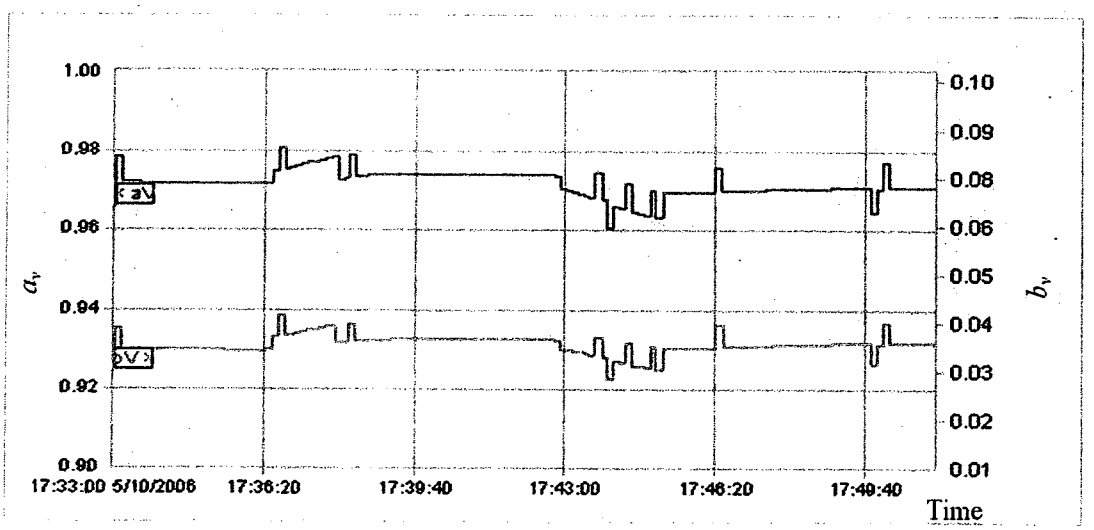

Figure 3.10 Identification results of the experimental tests

Figure 3.11 shows evolution of controller gains and Figure 3.12 shows the discharge air temperature responses. The experimental results show that the simplified optimal adaptive controller with modified RLS algorithm gives good setpoint tracking responses.

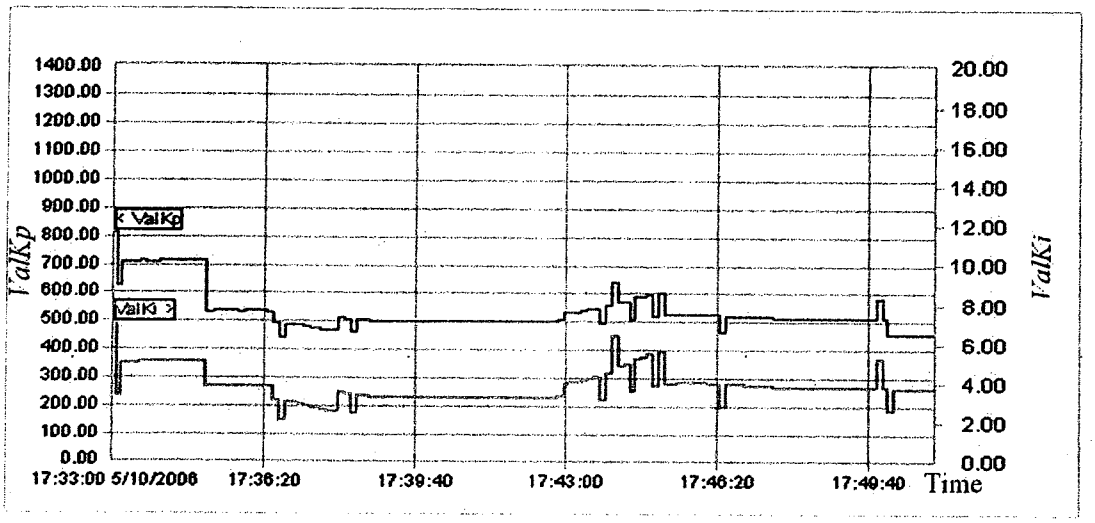

Figure 3.11 System PI parameters of the experimental tests

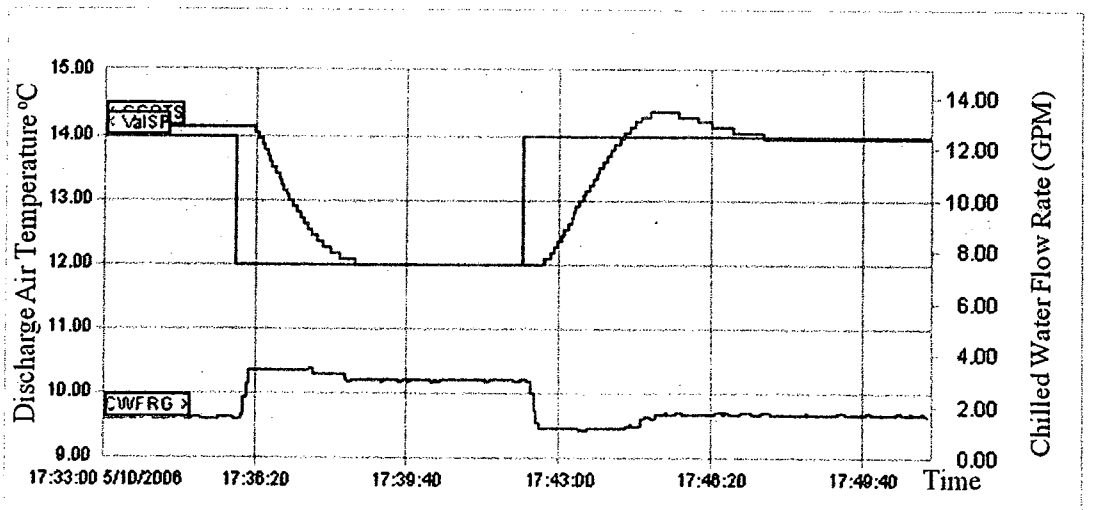

Figure 3.12 Step responses of the experimental tests

3.6 Summary

In this chapter, a modified RLS identification algorithm with the matrix-reset technique for online identification was developed. The modified RLS algorithm was tested by using computer simulations and experiment. The results show that the modified RLS identification algorithm is able to track changes in the system parameters rapidly. The matrix-reset technique makes the identification algorithm more reliable and stable.

4. An Adaptive Control Strategy with a Robust Optimal Control Algorithm for FOPDT Systems

In this chapter an on-line optimal proportional-integral plus feedforward (PI-FF) controller tuning algorithm for single-input-single-output (SISO) thermal processes in HVAC systems is presented. A discharge air system (DAS) is considered. The DAS is modeled as a FOPDT system in discrete time domain. An optimization problem is formulated and solved to derive the optimal PI-FF tuning algorithm combined with H_∞ based PI tuning rules. The proposed tuning algorithm has a weighting factor Q_2 that can be a new freedom parameter to improve the ability in rejecting the effect of system parameter changes. Simulation runs in an adaptive control structure are made under various operating conditions. The results show that the on-line tuned optimal PI-FF controller in the adaptive control system is able to track setpoint changes rapidly and smoothly, and has improved ability in rejecting the effect of system parameter changes under suitably selected values of Q_2 compared with other methods. Guidelines for choosing Q_2 in balancing different requirements are proposed. Finally, a specific case of the optimal controller is proposed and experimentally tested and validated.

4.1 Introduction

Heating, ventilating and air conditioning (HVAC) systems in commercial buildings account for more than half of commercial building's energy consumption. Therefore, reducing energy consumption of HVAC systems remains a challenging area of research with significant potential for economic benefits. To this end, optimal control strategies offer a practical method for energy efficient operation of HVAC systems. In

addition, improving robustness to system parameter changes is an important part of the ongoing research.

A Discharge Air System (DAS), which is one of the basic components of a heating, ventilating and air-conditioning system, is considered. Several different discharge air system configurations exist depending on heating or cooling applications. Figure 4.1 shows the DAS for sensible cooling of air. The discharge air temperature is maintained close to a chosen setpoint by modulating the mass flow rate of chilled water via valve control (u). The control of DAS represents an important control problem of practical interest in HVAC. Because of the importance several studies have been done. See for example, the work done on discharge air temperature system by McCullagh, Green and Chandraseker (1969), Gartner (1972), Hamilton, Leonard and Pearson (1974 and 1977), Stoecker, Rosario, Heidenreich and Phelan (1978), Shavit and Brandt (1982), Nesler and Stoecker (1984). A discharge air temperature system model was developed by Hamilton et al. (1977). Stoecker et al. (1978) have studied the stability of the air temperature control-loop. The dynamic performance of a discharge air temperature system with a PI controller is examined by Nesler et al. (1984). Note that in the above studies only the classical proportional-integral (PI) control problem is addressed. Here we explore online optimal control of DAS which is robust.

In real HVAC systems, loads and system conditions change without schedule. This implies that system parameters in a fixed model for an HVAC system will change without schedule. Some researchers have used H_∞ technique to improve robustness to parameter changes for HVAC systems (Qu et al., 2004; Al-Assadi et al. 2004). However,

it is also important to design optimal controllers for DAS because good regulation of discharge air temperature with strong robustness improves overall energy-use efficiency of HVAC systems. Motivated by these considerations, we propose a methodology for on-line optimal control of DAS applied in an adaptive control system and show results under various operating conditions specially in improving the ability in rejecting the effect of system parameter changes.

4.2 The DAS Model

In this section, we are going to derive state equations for closed loop DAS system with a PI controller.

4.2.1 Physical Model

Figure 4.1 shows a schematic diagram of a DAS system. Mixed air enters the cooling coil at temperature T_{a0}. It is cooled and dehumidified in the cooling coil by using chilled water. The temperature of the air leaving the cooling coil T_a is controlled by modulating the chilled water flow rate in the coil as shown by the feedback control loop.

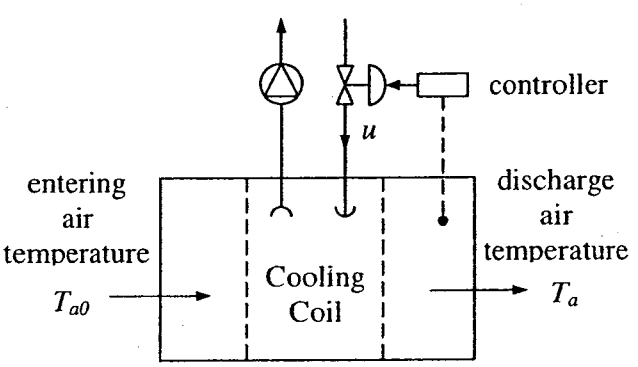

Figure 4.1 Schematic diagram of DAT system

4.2.2 Temperature Control

In a typical HVAC system, several thermal processes are controlled simultaneously to monitor and maintain temperature, pressure and flow rates at optimum levels. This is achieved by using feedback control systems. The number of feedback control loops, often referred to local control loops, varies depending on the complexity of an HVAC system. The discharge air temperature control, zone temperature control, airflow control etc are the most important local control loops in HVAC systems. The objective of this study is to develop an optimal control method that can be applied to local control loops in HVAC systems. The methodology is described by considering a discharge air temperature system.

From a practical standpoint, the DAS controller should be: (1) simple for implementation using available hardware, (2) adaptive to load changes and (3) stable, and (4) giving near optimal temperature control. The major focus of this development will be that the models should be suitable for on-line implementation and control.

In the following sections, a robust on-line optimal control combined with H_∞ tuning rules for thermal processes in HVAC systems is developed. First, state equations for the closed loop DAS system with a PI controller are derived (Sections 4.2.3 and Secondly, the optimal control problem is formulated as a standard constrained-minima problem and solved using the method of Lagrange multipliers in Section 4.3. It is shown that the optimal solution consists of PI control signal and feedforward control signal. Then, an algorithm for tuning of PI-FF controller parameters is proposed in Section 4.4. Simulation results in an adaptive control system showing the operation of the optimal PI-

FF controller under several operating conditions are presented in Section 4.5. A simplified optimal control algorithm is proposed in Section 4.6 and its applications and experimental validations are presented in Sections 4.7 and 4.8.

4.2.3 The First-order-plus-dead-time (FOPDT) Model

Assuming sensible cooling of air, the input-output model can be represented by Figure 4.2 where u, the chilled water flow rate, is the input and T_a, the discharge air temperature (DAT), is the output. The entering air temperature T_{a0} is considered as disturbance on the system.

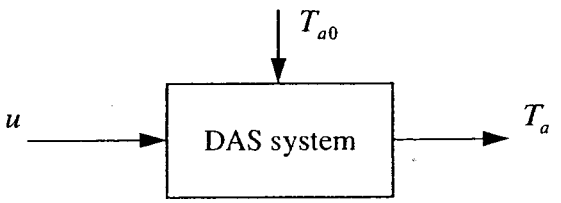

Figure 4.2 Block diagram of DAS system

From the point of view of implementation, it is necessary to reduce the computational effort required in the identification and control of the DAS system. To this end, we model the DAS system as a first-order plus dead-time (FOPDT) system. The model can be represented as Figure 4.3a. Where, T_{a0} is the output of the system when $u = 0$; T_a is the output of the system and u is the input of the system. Assume that T_s is the sampling time and

$$l = \frac{\tau}{T_s} \tag{4.1}$$

is an integer. Then, the discrete model can be expressed as Figure 4.3*b*.

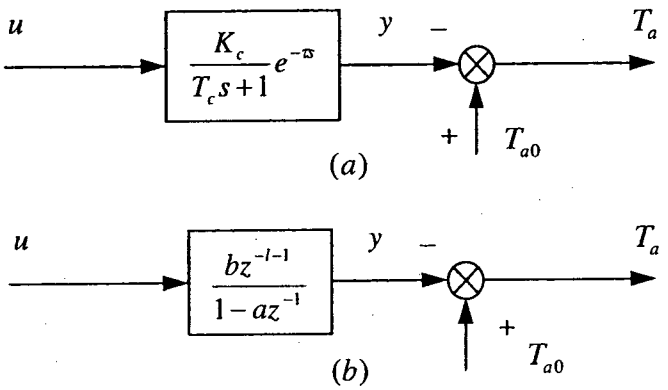

Figure 4.3 First-order plus dead-time model

Where, the parameters a and b have the relationship with the parameters T_c and K_c as in Equations 4.2 and 4.3.

$$a = e^{-\frac{T_s}{T_c}} \tag{4.2}$$

$$b = K_c(1-a) \tag{4.3}$$

From the discrete time FOPDT model of DAS shown in Figure 4.3b, the outputs of the model can be described by Equations 4.4 and 4.5.

$$y(k+1) = \begin{cases} 0 & k < l \\ ay(k) + bu(k-l) & k \geq l \end{cases} \tag{4.4}$$

$$T_a(k) = T_{a0} - y(k) \tag{4.5}$$

In the above FOPDT model, the dead-time l can be obtained by applying least squares identification techniques to the output data obtained from open-loop experiments. The parameters a and b will be computed on-line by applying the modified RLS identification algorithm with the matrix-reset technique. The details of the algorithm are given in Chapter 3.

4.2.4 The Closed-Loop DAS Model

The closed-loop control diagram of the DAS with a PI controller is shown in Figure 4.4. A digital PI controller with feedback gains K_{pd} and K_{id} as in Equation 4.6

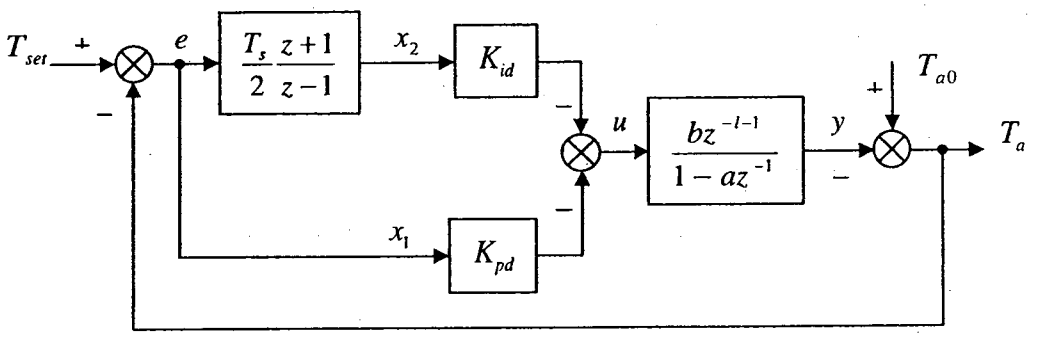

Figure 4.4 Closed-loop diagrams of DAS with a PI controller $K_d(z)$

was used where T_s is the sampling time. The DAS model is described by Equations 4.4 and 4.5.

$$K_d(z) = -\frac{\left(K_{pd} + \frac{K_{id}T_s}{2}\right)z + \left(\frac{K_{id}T_s}{2} - K_{pd}\right)}{z-1} \tag{4.6}$$

Let $K_{PI} = [K_{pd} \quad K_{id}]$, then we have

$$u(k) = -K_{PI}x(k) \tag{4.7}$$

where

$$x(k) = \begin{bmatrix} x_1(k) \\ x_2(k) \end{bmatrix} \tag{4.8}$$

$$x_1(k) = e(k) \tag{4.9}$$

$$x_2(k) = x_2(k-1) + \frac{T_s}{2}\left(e(k) + e(k-1)\right) \tag{4.10}$$

By considering

$$e(k) = T_{set} - T_{a0} + y(k) \tag{4.11}$$

we have

$$x_1(k) = \begin{cases} T_{set} - T_{a0} & 0 \le k \le l \\ y(k) + T_{set} - T_{a0} & k > l \end{cases} \tag{4.12}$$

$$x_2(k) = \begin{cases} kT_s(T_{set} - T_{a0}) & 0 \le k \le l \\ kT_s(T_{set} - T_{a0}) + \dfrac{y(k)}{2}T_s + T_s\sum_{i=l+1}^{k-1} y(i) & k > l \end{cases} \tag{4.13}$$

For $k > l$ where l is the delay time, the model equations (Equations 4.12 and 4.13) of the closed-loop DAS can be expressed in terms of states and control input and the system parameters as shown in Equation 4.14.

$$x(k+1) = \begin{cases} \begin{bmatrix} T_{set} - T_{a0} \\ (k+1)T_s(T_{set} - T_{a0}) \end{bmatrix} & -1 \le k < l \\ \begin{bmatrix} a & 0 \\ \dfrac{1+a}{2}T_s & 1 \end{bmatrix} x(k) + \begin{bmatrix} b \\ \dfrac{bT_s}{2} \end{bmatrix} u(k-l) + \begin{bmatrix} b \\ \dfrac{bT_s}{2} \end{bmatrix} \dfrac{1-a}{b}(T_{set} - T_{a0}) & k \ge l \end{cases} \tag{4.14}$$

4.3 Optimization

It is worth noting that the energy consumption of HVAC systems during the start-up dynamics over a period of time equal to the length of transportation delay l is much less than the energy consumption over the time span to reach the target operating setpoint. By noting this fact, we have formulated and solved the optimization problem for the case when $k \ge l$. For the system given by

$$\begin{aligned} x(k+1) &= \begin{bmatrix} a & 0 \\ \dfrac{1+a}{2}T_s & 1 \end{bmatrix} x(k) + \begin{bmatrix} b \\ \dfrac{bT_s}{2} \end{bmatrix} u(k-l) + \begin{bmatrix} 1-a \\ \dfrac{(1-a)T_s}{2} \end{bmatrix} (T_{set} - T_{a0}) \\ &= Ax(k) + Bu(k-l) + C(T_{set} - T_{a0}), \qquad k \ge l \end{aligned} \tag{4.15}$$

where $x(k)=\begin{bmatrix} y(k)+T_{set}-T_{a0} \\ k(T_{set}-T_{a0})T_s+\dfrac{y(k)}{2}T_s+T_s\sum_{i=l+1}^{k-1}y(i) \end{bmatrix}$

$$A=\begin{bmatrix} a & 0 \\ \dfrac{1+a}{2}T_s & 1 \end{bmatrix}$$

$$B=\begin{bmatrix} b \\ \dfrac{bT_s}{2} \end{bmatrix}$$

$$C=\begin{bmatrix} 1-a \\ \dfrac{(1-a)T_s}{2} \end{bmatrix}$$

we wish to select $u(k-l)$ so that a cost function

$$J=\frac{1}{2}\sum_{k=l}^{N}\left[x^T(k)Q_1x(k)+u^T(k-l)Q_2u(k-l)\right] \tag{4.16}$$

is minimized. In Equation 4.16 Q_1 is the symmetric weighting matrix and Q_2 ($Q_2 \neq 0$) is weighting on control energy. They are nonnegative definite. The above problem can be considered as a standard constrained-minima problem that we wish to minimize J subject to the constraint

$$-x(k+1)+Ax(k)+Bu(k-l)+C(T_{set}-T_{a0})=0, \quad k=l,l+1,\cdots,N \tag{4.17}$$

By using the method of Lagrange multipliers (Franklin et al. 1997), the cost function is written as

$$J'=\frac{1}{2}\sum_{k=l}^{N}\left[x^T(k)Q_1x(k)+u^T(k-l)Q_2u(k-l) + \lambda^T(k+1)(-x(k+1)+Ax(k)+Bu(k-l)+C(T_{set}-T_{a0}))\right] \tag{4.18}$$

where $\lambda(k+1)$ is a Lagrange multiplier vector.

By minimizing J' with respect to $x(k)$, $u(k-l)$, and $\lambda(k)$ an optimal control solution for $Q_1 = \begin{bmatrix} q_{11} & 0 \\ 0 & 0 \end{bmatrix}$ was found. The optimal control has the following structure

$$u(k) = -K_{PI}x(k) - K_{FF}(T_{set} - T_{a0}) \tag{4.19}$$

where

$$K_{PI}(k) = \begin{cases} K\begin{bmatrix} 1 & 0 \\ 0 & 0 \end{bmatrix} & k = 0 \\ K(A-BK)^k \begin{bmatrix} 1 & 0 \\ 0 & l/k \end{bmatrix} & 1 \le k \le l \\ K(A-BK)^l & k > l \end{cases} \tag{4.20}$$

$$K_{FF}(k) = \begin{cases} K\begin{bmatrix} 0 \\ lT_s \end{bmatrix} & k = 0 \\ K\left(\sum_{i=0}^{k-1}(A-BK)^i\right)C & 1 \le k \le l \\ K\left(\sum_{i=0}^{l-1}(A-BK)^i\right)C & k > l \end{cases} \tag{4.21}$$

with $K = \begin{bmatrix} K_p & K_i \end{bmatrix}$ (4.22)

$$K_p = \frac{bq_{11}}{(1+a)Q_2} \tag{4.23}$$

$$K_i = \frac{2bc_2}{(1+a)Q_2} \tag{4.24}$$

From the above optimal results, we note that the control as in Equation 4.19 can be implemented as a PI controller with a feedforward action as depicted in Figure 4.5.

From Equations 4.23 and 4.24, it is noted that the magnitudes of controller gains K_p and K_i are functions of the parameters (q_{11} and c_2) and the weighting factor (Q_2). The parameters q_{11} and c_2 can be chosen such that control response is fast and smooth.

To this end, we have used the H_∞ tuning rules (Qu et al., 2004) developed by a loop-shaping and robust stabilization technique (Tan et al., 1998). By assuming $Q_2 = 1$ it is noted that the controller gain Equations 4.23 and 4.24 are the same as those obtained by the H_∞ tuning rules. After some algebraic manipulations, we have

$$q_{11} = \frac{(0.265\gamma + 0.307)(1-a^2)}{b^2}\left(-\frac{1}{l\ln a} + 0.5\right)\frac{5.314\gamma + 0.951}{2 - l\ln a} \tag{4.25}$$

$$c_2 = \frac{(0.265\gamma + 0.307)(1-a^2)}{b^2}\left(-\frac{1}{l\ln a} + 0.5\right)\frac{\ln a}{(l\ln a - 2)T_s} \tag{4.26}$$

with $\gamma = 0.1974$ for all l or $\gamma = \dfrac{-l\ln a - 0.951}{5.314}$ for $-\dfrac{2}{\ln a} \le l \le -\dfrac{8.922}{\ln a}$.

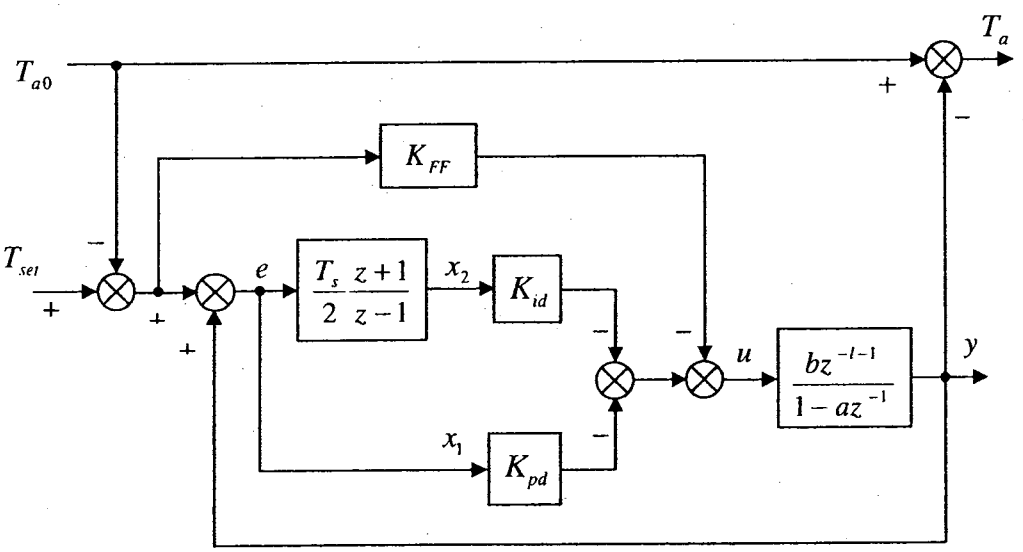

Figure 4.5 Closed-loop diagram of the optimal PI controller with feedforward action

According to the above selection, q_{11} and c_2 dependent on the model parameters, and the weighting factor Q_2 gives an additional degree of freedom to optimize the performance of PI controller.

4.4 Tuning Algorithm

In this section, we will present the developed optimal tuning algorithm, and introduce a new index to evaluate the performance of the optimal PI-FF controller.

4.4.1 Optimal Tuning Algorithm

Here we give a set of tuning equations for the optimal PI controller derived in the previous section. From the definitions of A, B, K, and by assuming

$$A-BK=\begin{bmatrix} g_{11} & g_{12} \\ g_{21} & g_{22} \end{bmatrix}=g,$$

$$(A-BK)^i=\begin{bmatrix} h_{11}(i) & h_{12}(i) \\ h_{21}(i) & h_{22}(i) \end{bmatrix}=h(i), \text{ and}$$

$$\sum_{i=0}^{j}(A-BK)^i=\begin{bmatrix} m_{11}(j) & m_{12}(j) \\ m_{21}(j) & m_{22}(j) \end{bmatrix}=m(j),$$

the following discrete time tuning equations for the controller parameters K_{pd}, K_{id} and K_{FF} were derived. These are:

$$K_{pd}(k)=\begin{cases} K_p & k=0 \\ K_p h_{11}(k)+K_i h_{21}(k) & 1\le k\le l \\ K_p h_{11}(l)+K_i h_{21}(l) & k>l \end{cases} \tag{4.27}$$

$$K_{id}(k)=\begin{cases} 0 & k=0 \\ \dfrac{l}{k}\left(K_p h_{12}(k)+K_i h_{22}(k)\right) & 1\le k\le l \\ K_p h_{12}(l)+K_i h_{22}(l) & k>l \end{cases} \tag{4.28}$$

$$K_{FF}(k)=\begin{cases} K_i l T & k=0 \\ (1-a)\left(K_p m_{11}(k-1)+K_i m_{21}(k-1)+\dfrac{T}{2}\left(K_p m_{12}(k-1)+K_i m_{22}(k-1)\right)\right) & 1\le k\le l \\ (1-a)\left(K_p m_{11}(l-1)+K_i m_{21}(l-1)+\dfrac{T}{2}\left(K_p m_{12}(l-1)+K_i m_{22}(l-1)\right)\right) & k>l \end{cases} \tag{4.29}$$

Equations (4.22 – 4.29) describe the optimal tuning equations for FOPDT processes in discrete time domain. We refer to this algorithm as Optimal Tuning Algorithm (OTA). The algorithm can be implemented by following the steps given below. However, it requires more memory and computation than the H_∞ PI tuning rules.

Initialization: Initialize the model parameters a, b and l obtained by applying any off-line system identification method using a set of open-loop experimental data

Step 1: Update the model parameters a and b using a selected RLS identification method at time $k\ (>2\times l+1)$ or keep the model parameters a and b as initialized at time $k\ (\leq 2\times l+1)$

Step 2: Update parameter c_2 and weighting parameter q_{11} (related to smooth response)

Step 3: Choose weighting parameter Q_2 (related to energy and robustness to system parameter changes)

Step 4: Calculate K_p and K_i

Step 5: Update g, $h(i)$, and $m(i-1)$ with $h_{11}(0)=h_{22}(0)=1$, $h_{12}(0)=h_{21}(0)=0$ and $m_{11}(-1)=m_{22}(-1)=m_{12}(-1)=m_{21}(-1)=0$ until $i=k$ for $1\leq k\leq l$ or $i=l$ for $k>l$

Step 6: Calculate K_{pd}, K_{id} and K_{FF} from Equations 4.27, 4.28 and 4.29

Step 7: $k \leftarrow k+1$ and go to Step 1.

4.4.2 Guideline for Choosing the Control Input Weighting Parameter Q_2

In the discharge air temperature cooling control system, an increase in the discharge air temperature setpoint (step-up) would require less mass flow rate of chilled water which in turn decreases energy consumption. On the other hand, a decrease in setpoint temperature (step-down) will have the opposite effect. Therefore, it can be reasoned that when the setpoint temperature is increased it would require less energy and as such a smaller value of Q_2 would be appropriate so that the control response is not over damped. Likewise, a higher value of Q_2 would be needed when the setpoint is decreased. To this end, we introduce two parameters Q2-down and a reduction factor. The value of Q2-down indicates the value of Q_2 that the system adopts in step-down process and the reduction factor is the multiplier used to compute the value of Q_2 that the system adopts in step-up process. The reduction factor is always positive and less than one. That is, Q_2 = Q2-down × reduction factor is the value of Q_2 in the step-up process. We refer to this technique as Optimal Tuning Algorithm with Variable Parameter (OTA-VP).

To develop guidelines in the selection of Q2-down and reduction factor, the following index is defined. Where, n is the number of the total considered processes and $IndexP_i$ is index of the i th process.

$$IndexT = \frac{1}{n}\sum_{i=1}^{n} IndexP_i \tag{4.30}$$

By defining α_u as the weighting factor for energy and α_e the weighting factor for dynamic response, and noting that weighting factors should satisfy $\alpha_u + \alpha_e = 1$, the

$IndexP_i$ is formulated as follows:

$$IndexP_i = \alpha_u \left(\sum_{k=k_0}^{k_{end}} \frac{1}{2}(u(k)+u(k-1))T_s \right) \Big/ SumRU + \alpha_e \left(\sum_{k=k_0}^{k_{end}} \frac{1}{2}(|e(k)|+|e(k-1)|)T_s \right) \Big/ SumRE \tag{4.31}$$

$$SumRU = \left(\sum_{k=k_0}^{k_{end}} \frac{1}{2}(u(k)+u(k-1))T_s \right)_{reference} \tag{4.32}$$

$$SumRE = \left(\sum_{k=k_0}^{k_{end}} \frac{1}{2}(|e(k)|+|e(k-1)|)T_s \right)_{reference} \tag{4.33}$$

Note that the $IndexP_i$ is normalized with a reference value which in this case is based on H_∞ PI tuning rules. When the value of $IndexT$ is less than one for selected α_u and α_e, it means that the system has better performance than the reference system during the time interval $[k_0 \quad k_{end}]$. In addition to using the index for the purpose of comparison, we can minimize $IndexT$ with respect to Q2-down and reduction factor to select the optimal values.

In the next section the impact of Q_2 on temperature regulation, energy consumption of DAS, and robustness changes in system parameters will be investigated, and further guidelines for choosing the control input weighting parameter Q_2 in balancing different requirements will be given.

4.5 Simulation Studies in an Adaptive Control System

The tuning algorithm should reduce control energy and be robust to changes in system parameters. To test the developed algorithms, the DAS model parameters *a* and *b*

were varied. To this end, seven different sets of models as shown on Table 4.1 were used. We assumed 4s to be the sampling time (T_s), and refer to these models as processes 4.1, 4.2, 4.3, and combined processes 4.1, 4.2, 4.3, 4.4.

Parameters \ Process		Process 4.1	Process 4.2	Process 4.3	Combined Process 4.1	Combined Process 4.2	Combined Process 4.3	Combined Process 4.4
a	t<3000s	0.9538	0.969	0.9097	0.9538	0.9538	0.9538	0.9538
	3000s≤t<5000s	0.9538	0.969	0.9097	0.9538	0.969	0.9538	0.9097
	t≥5000s	0.9538	0.969	0.9097	0.969	0.969	0.9097	0.9097
b	t<3000s	0.1329	0.0446	0.3896	0.1329	0.1329	0.1329	0.1329
	3000s≤t<5000s	0.1329	0.0446	0.3896	0.1329	0.0446	0.1329	0.3896
	t≥5000s	0.1329	0.0446	0.3896	0.0446	0.0446	0.3896	0.3896
l		9	9	9	9	9	9	9

Table 4.1 Plant parameter changes for considered processes

The simulation implementation in Matlab Simulink is depicted in Figure 4.6. $T_{a0} = 66.0F$ is assumed. The identification process is omitted in the simulation study for simplicity. The current plant parameter values of a and b are directly sent to the tuner. According to a new set of the input parameters, the tuner generates a new set of the PID controller parameter values and sends to the PID controller. By setting Q2-down equal to Q_2 and reduction factor equal to one as the input values of the tuner in Figure 4.6 a constant Q_2 PI-FF control system can be simulated. This strategy with constant Q_2 is referred to here as Optimal Tuning Algorithm (OTA).

A time-scheduled operation of DAS involving change in setpoint temperature of air leaving the coil was simulated. Three cases were considered. These are referred to as Cases 4.1, 4.2 and 4.3 respectively and shown below.

$$T_{set} = \begin{cases} 60F & t < 3000 \\ 61F & 3000 \le t < 5000 \\ 60F & t \ge 5000 \end{cases}, \quad T_{set} = \begin{cases} 60F & t < 3000 \\ 61F & t \ge 3000 \end{cases}, \text{ or } T_{set} = \begin{cases} 61F & t > 3000 \\ 60F & t \le 3000 \end{cases}$$

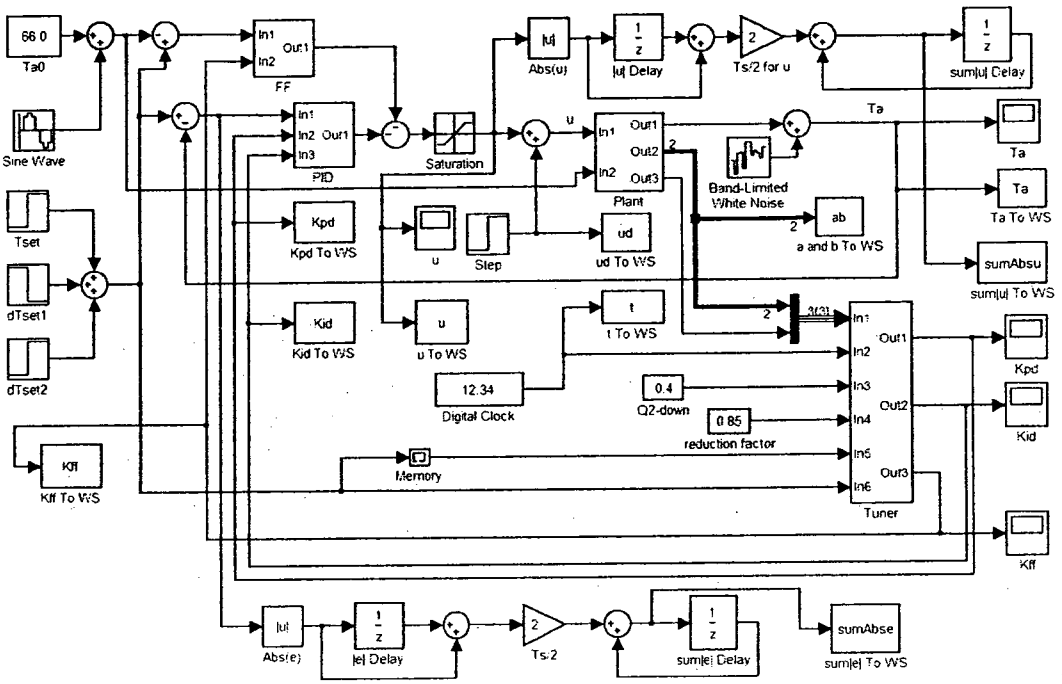

Figure 4.6 Simulation structure for OTA and OTA-VP

4.5.1 Control Input Energy

Table 4.2 shows the simulation results for Processes 4.1, 4.2 and 4.3 with Case 4.1 using the optimal tuning algorithm (OTA) with six different sets of constant Q_2 values. The integral of the mass flow rate was computed in each case as a measure of control input energy. This will enable comparison of different Q_2 values. A lower value of the integral of u would signify lower energy consumption. Therefore, from the results depicted in Table 4.2, it can be reasoned that in order to save energy one must choose a higher Q_2 value when the setpoint is changed from higher to a lower value and a smaller value of Q_2 when the setpoint is changed from lower to a higher value. Figure 4.7 illustrates the response, using the optimal tuning algorithm (OTA).

Magnitude of Q_2	$\sum_{k=751}^{1250} \frac{T_s}{2}(u(k)+u(k-1))$ for step-up			$\sum_{k=1251}^{1750} \frac{T_s}{2}(u(k)+u(k-1))$ for step-down		
	Process 4.1	Process 4.2	Process 4.3	Process 4.1	Process 4.2	Process 4.3
0.25	3445.4	6860.4	2306.6	4203.5	8433.6	2793.0
0.5	3453.7	6877.2	2312.1	4195.0	8416.7	2787.4
0.75	3462.1	6893.6	2317.7	4186.5	8399.8	2781.7
1.0	3470.5	6910.4	2323.4	4178.0	8382.7	2775.9
1.25	3479.0	6927.3	2329.1	4169.4	8365.6	2770.2
1.5	3487.6	6944.3	2334.9	4160.7	8348.4	2764.4

Table 4.2 Effect of Q_2 on energy efficiency

The above results offer an important insight that it is important to choose the magnitude of Q_2 based on the direction of setpoint change. We refer to this technique as Optimal Tuning Algorithm with Variable parameter (OTA-VP). The implementation scheme of OTA-VP is depicted in Figure 4.6.

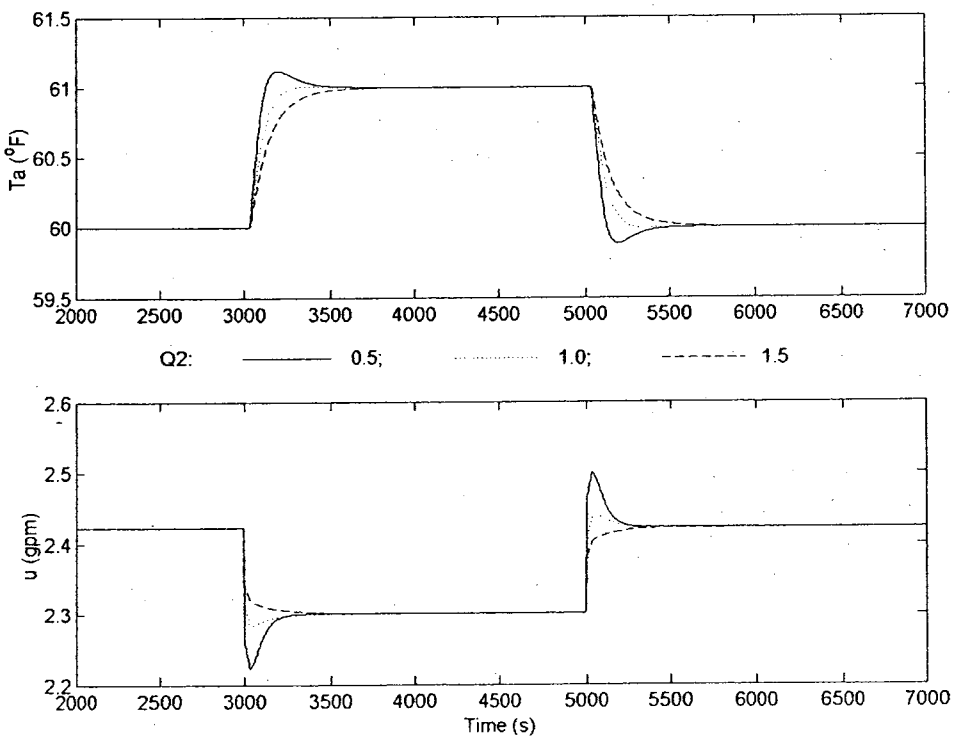

Figure 4.7 Responses with the optimal tuning algorithm (Process 4.1; Case 4.1)

4.5.2 Index Comparison with Other Methods

Simulation studies were made to compare the performance of OTA and OTA-VP algorithms with the H_∞ and the Ziegler-Nichols (Z-N) tuning rules. The results using the three processes namely Processes 4.1, 4.2 and 4.3 with Case 4.1, were evaluated with $\alpha_u = 0.8$ and $\alpha_e = 0.2$ over the time interval $k_0 = 751$ to $k_{end} = 1750$. Figure 4.8 shows how the index value changes as a function of Q2-down weighting for different reduction factors. IndexHT in the figure refers to the index based on the comparison with the H_∞ tuning rules and IndexZNT refers to the index with reference as the Ziegler-Nichols tuning method. The results show that a minimum exists with respect to Q2-down and reduction factor. The simulation results also show that the OTA (reduction factor = 1) and the OTA-VP algorithms with good selection of Q_2 could give better performance compared to the H_∞ and the Ziegler-Nichols tuning rules. It is also noted that the OTA-VP with a good choice of Q_2 could yield better performance than the OTA because a minimum *IndexT* for OTA-VP exists. It was found that a reduction factor = 0.85 and Q2-down = 0.4 is close to the optimal result in minimizing the index. Likewise, Q2-down = 0.6 gives near optimal result for the OTA. Figure 4.9 shows the dynamic responses to setpoint changes for the H_∞ and the Ziegler-Nichols tuning rules and for the OTA and OTA-VP with near optimal Q_2 values. The responses for H_∞ tuning rules, OTA and OTA-VP algorithms are good. The dynamic responses of Z-N method are different for different processes and show some oscillations.

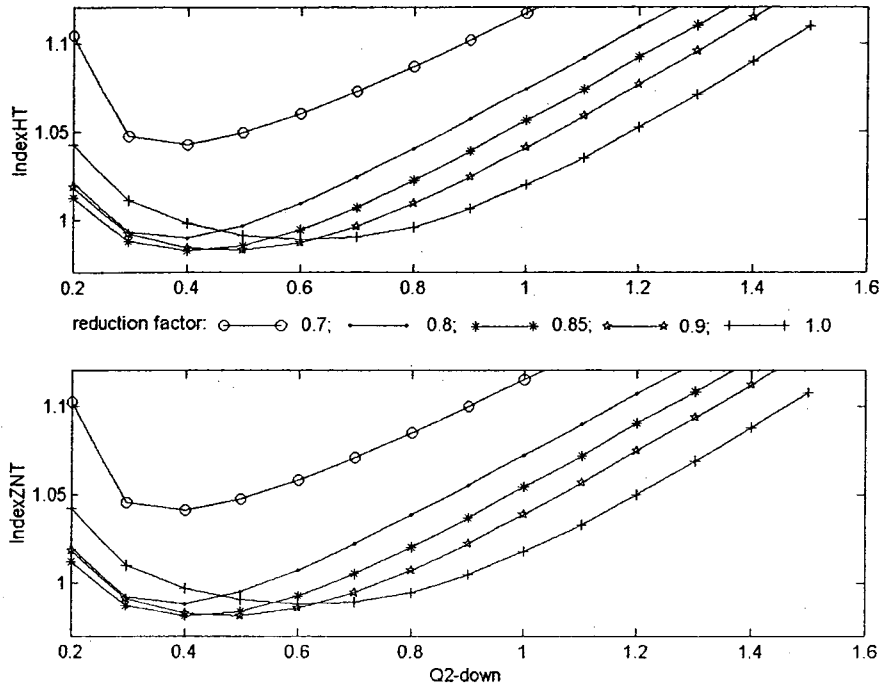

Figure 4.8 Index with respect to reduction factor and Q2-down

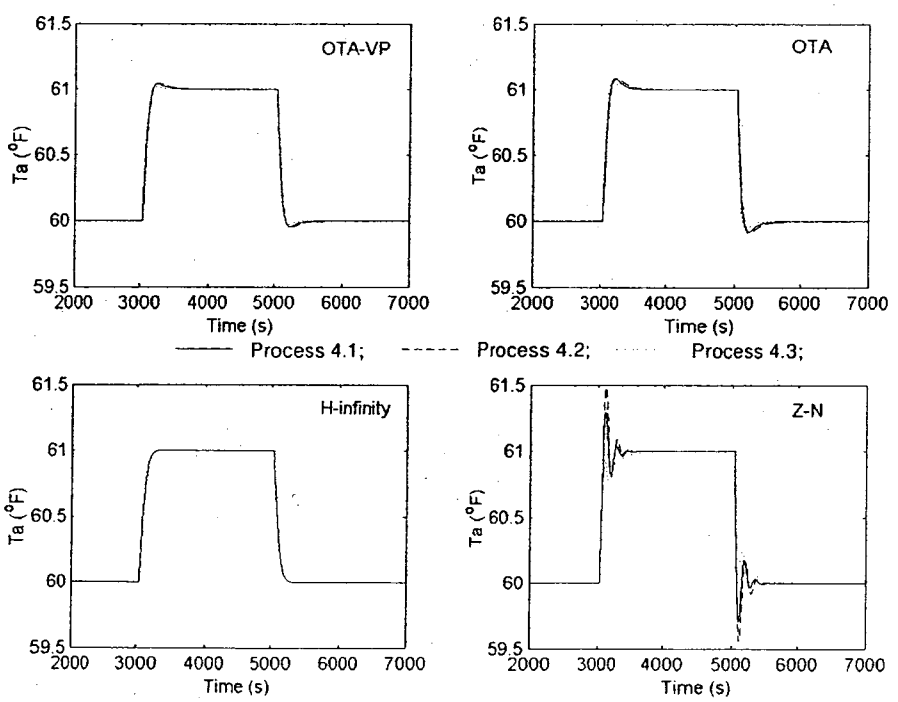

Figure 4.9 Response comparisons between OTA-VP, OTA, H_∞ tuning rules and Z-N method

4.5.3 Robustness Studies

In order to test the robustness property of the optimal tuning algorithm, four different DAS models referred to before namely, Combined Processes 4.1, 4.2, 4.3, and 4.4 were used. These combined processes simulate load changes that typically occur in an HVAC system. This could impact the system parameters of the FOPDT model and may require discharge air temperature to be regulated in a VAV system. The performance of optimal tuning algorithm (OTA) in compensating for parameter changes assumed as combined processes 4.1 to 4.4 and regulating the discharge air temperature was studied. he results depicted in Figures 4.10 and 4.11 show that the OTA and the OTA-VP with the near optimal parameters have improved ability to reject the effect of changes in

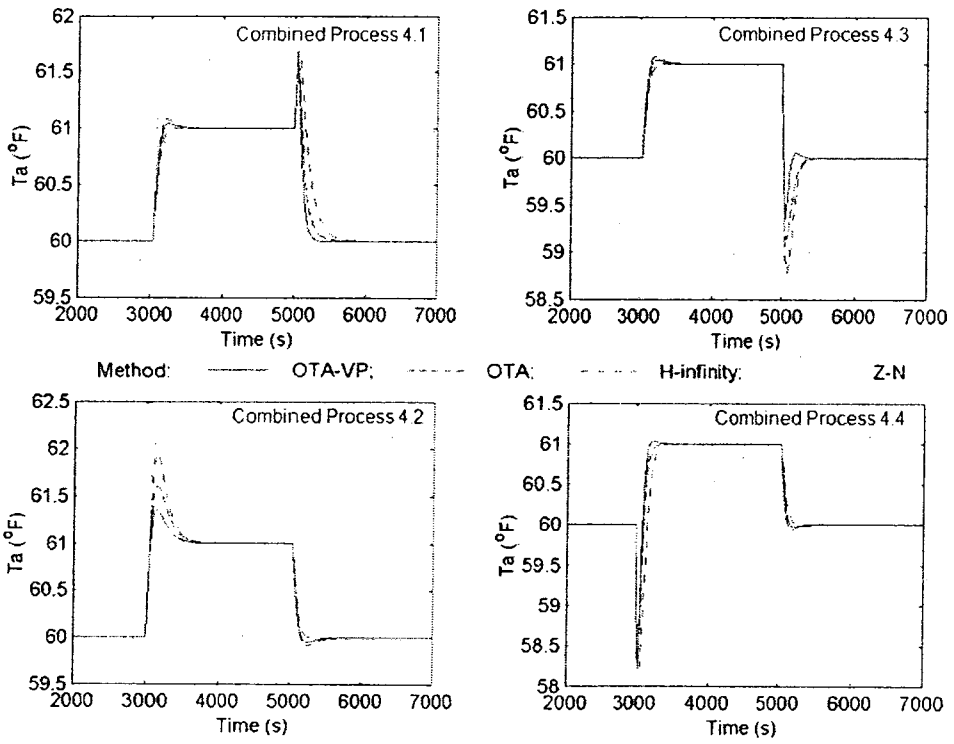

Figure 4.10 Robustness comparisons in the CPs 4.1 to 4.4 with Case 4.1

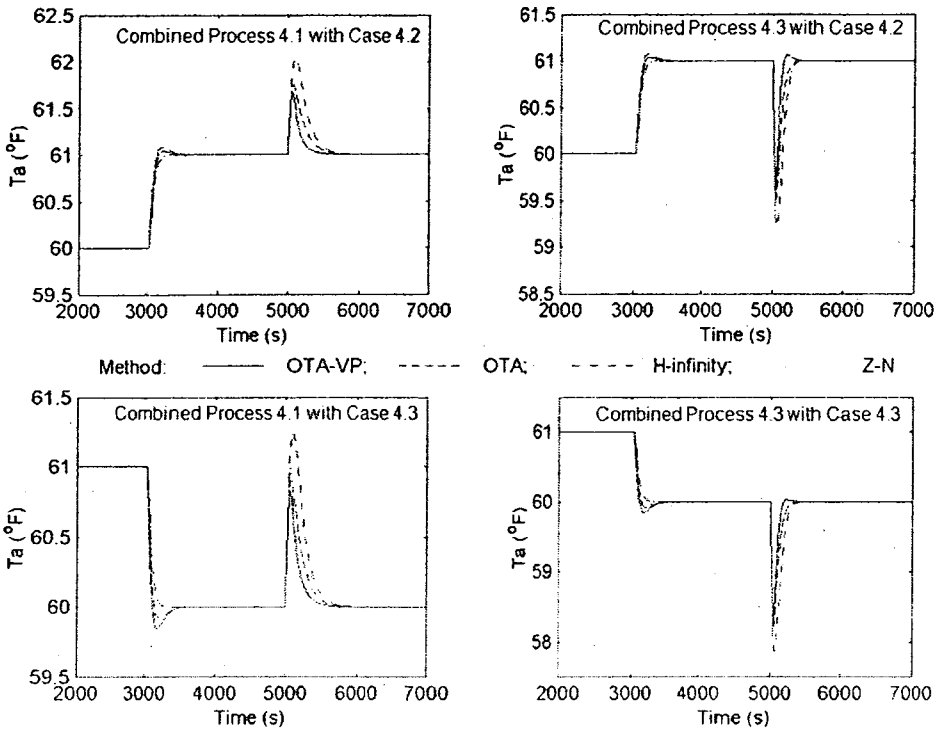

Figure 4.11 Robustness comparisons in CPs 4.1 and 4.3 with Cases 4.2 and 4.3

the system parameters (lower maximum shooting and fast convergence) compared with H_∞ tuning rules and Zeigler-Nichols method.

Method	$IndexP_i$ ($\alpha_u = 0.8$ and $\alpha_e = 0.2$)				*IndexT*
	CP 4.1	CP 4.2	CP 4.3	CP 4.4	
H_∞ tuning rules	1.0000	1.0000	1.0000	1.0000	1.0000
OTA-VP with Q2-down = 0.4 & reduction factor = 0.85	0.9256	0.9036	0.9233	0.9154	0.9170
OTA with $Q_2 = 0.6$	0.9480	0.9551	0.9663	0.9309	0.9501
Ziegler-Nichols	0.9159	1.0082	0.9405	1.0235	0.9720

Table 4.3 Index comparisons between methods for CPs with Case 4.1

The results depicted in Tables 4.3, 4.4 and 4.5 indicate that the OTA and the OTA-VP with the near optimal parameters have lower index values (*IndexT*) compared to

H_∞ tuning rules or Zeigler-Nichols method. The improvement achieved with the OTA-VP is significant.

Method	$IndexP_i$ ($\alpha_u = 0.8$ and $\alpha_e = 0.2$)		$IndexT$
	CP 4.1	CP 4.3	
H_∞ tuning rules	1.0000	1.0000	1.0000
OTA-VP with Q2-down = 0.4 & reduction factor = 0.85	0.9152	0.9104	0.9128
OTA with $Q_2 = 0.6$	0.9505	0.9421	0.9463
Ziegler-Nichols	0.9107	1.0099	0.9603

Table 4.4 Index comparisons between methods for CPs 4.1 and 4.3 with Case 4.2

Method	$IndexP_i$ ($\alpha_u = 0.8$ and $\alpha_e = 0.2$)		$IndexT$
	CP 4.1	CP 4.3	
H_∞ tuning rules	1.0000	1.0000	1.0000
OTA-VP with Q2-down = 0.4 & reduction factor = 0.85	0.9254	0.9182	0.9218
OTA with $Q_2 = 0.6$	0.9499	0.9429	0.9464
Ziegler-Nichols	0.9091	1.0152	0.9622

Table 4.5 Index comparisons between methods for CPs 4.1 and 4.3 with Case 4.3

4.5.4 Disturbance Rejection

From the above simulation results, it is clear that the OTA and the OTA-VP with near optimal parameters have stronger robustness to changes in system parameters. In a discharge air system, the disturbance effect such as those due to T_{a0} always exists and the measurements from the sensors have some white noise. To this end, the temperature changes in T_{a0}, were assumed to follow a Sine function with frequency of $2\pi/86400 = 7.27\times10^{-5}$ *rad / s*. To simulate these scenarios, we assumed the changes in T_{a0} given by $3\sin(0.0000727t)$ and with a noise power of 0.1 added to the discharge air

temperature sensor readings. Table 4.6 shows the simulation results for the four control methods and Figure 4.12 illustrates robustness to disturbance using OTA-VP control. The results also indicate that the OTA and the OTA-VP with near optimal parameters have a slightly improved performance compared with the H_∞ tuning rules and the Ziegler-Nichols method.

Method	$IndexP_i$ ($\alpha_u = 0.8$ and $\alpha_e = 0.2$)			$IndexT$
	Process 1	Process 2	Process 3	
H_∞ tuning rules	1.0000	1.0000	1.0000	1.0000
OTA-VP with Q2-down = 0.4 & reduction factor = 0.85	0.9968	0.9981	0.9945	0.9965
OTA with $Q_2 = 0.6$	0.9949	0.9974	0.9905	0.9943
Ziegler-Nichols	0.9976	1.0073	0.9958	1.0002

Table 4.6 Index comparisons under disturbances and Case 4.1 between methods

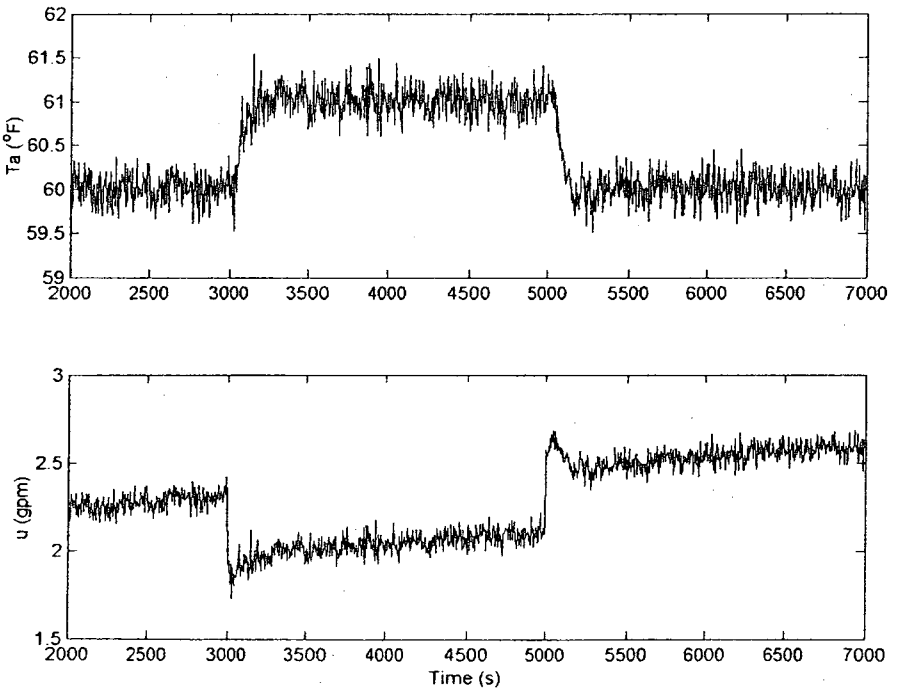

Figure 4.12 Response with disturbance effect for OTA-VP control

4.6 Simplified Optimal Control Algorithm

Reliability of a control system in real applications sometimes relies on its control's simplicity because simple control algorithm will reduce human error and is easy to implement. From the robust optimal tuning rules given in Equations (4.27), (4.28) and (4.29), if we assume $h_{11}(l) \approx 1$, $h_{21}(l) \approx 0$, $h_{12}(l) \approx 0$, $h_{22}(l) \approx 1$, and $a \approx 1$ we will have $K_{pd} \approx \frac{bq_{11}}{(1+a)Q_2}$, $K_{id} \approx \frac{2bc_2}{(1+a)Q_2}$ and $K_{FF} \approx 0$ for $k > l$. This simplified form is very easy to implement in an HVAC system similar to the H_∞ PI tuning rules (Qu et al. 2004). Also, it is close to OTA control in robustness and has improved robustness compared to the H_∞ PI tuning rules as shown in Figure 4.13. Note that $Q_2 = 0.6$ was used in the simulation study for the simplified control and OTA control. For $Q_2 = 1$, K_{pd} and K_{id} shown above are identical to the H_∞ PI tuning rules.

The simplified optimal control algorithm is summarized as follows.

$$K_{pd} = \frac{bq_{11}}{(1+a)Q_2} \tag{4.34}$$

$$K_{id} = \frac{2bc_2}{(1+a)Q_2} \tag{4.35}$$

The coefficients of q_{11} and c_2 are defined by equations of 4.25 and 4.26 respectively. In the next two sections, the experimental results for two applications of the simplified optimal control algorithm will be presented. In the first application the heating coil control identified as node 77 in the Concordia University's HVAC system will be considered. In the second application the discharge air temperature control in the VAV

laboratory test facility will be studied. The weight parameter Q_2 in the simplified optimal control algorithm gives freedom to adjust the system performance to improve robustness and step response. Experimental results show improvement in robustness and step response performance.

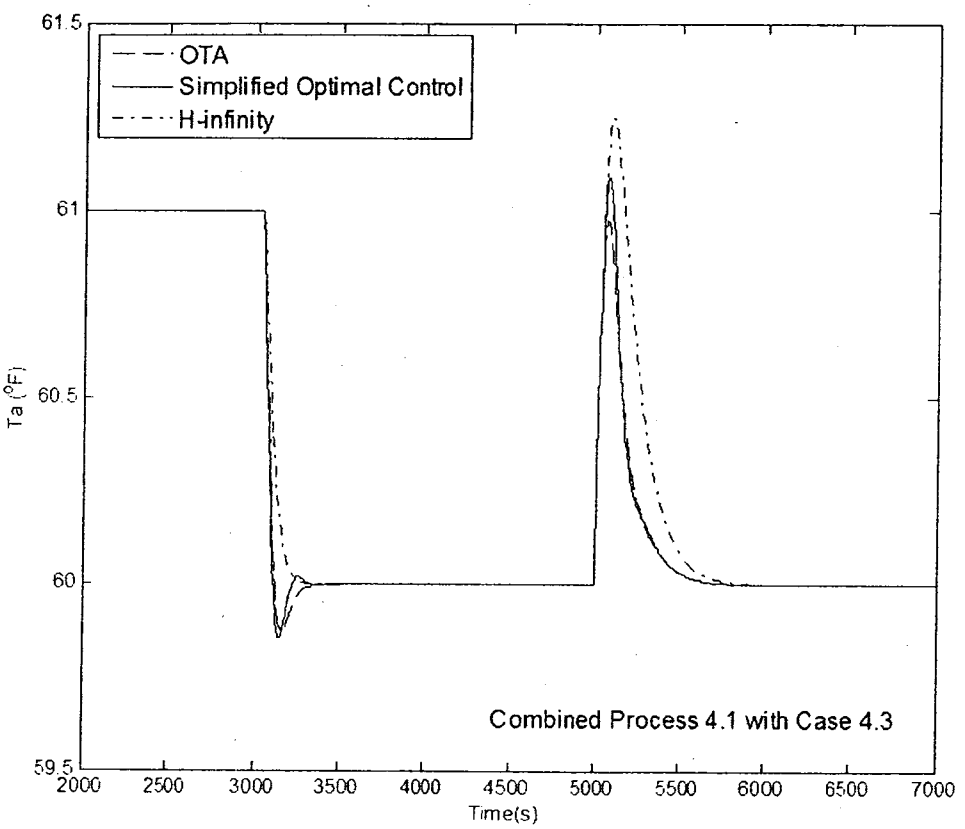

Figure 4.13 Robustness comparisons for different controls

4.7 Application to a Heating Coil System

In this section, we first present the problem of the original PI control system. Then, the application of the modified H_∞ PI tuning rules to the heating coil control system in an adaptive control structure is described. Finally, experimental results showing comparisons between the two will be presented.

4.7.1 The Problem in the Original Heating Coil Control System

The original control system was a PI control system. It is shown in Figure 4.14. The problem in the original temperature control system was oscillations in warm air temperature response by about 3 ^{o}C, when the outside weather was cold. The test results of the original PI control heating coil system are shown in Figure 4.15. The red line (*MTAEC3GLCB*) is the output air temperature from the heating coil system and the blue line (*ATAEC3GLCB*) is the setpoint. The result shows the problem in the original heating coil temperature control system that the response of the control system was oscillatory and the maximum offset was great than 1.6 ^{o}C.

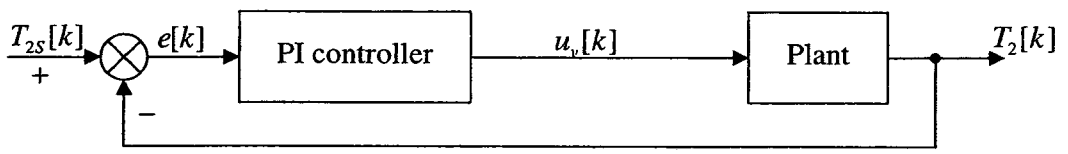

Figure 4.14 Original heating coil PI control system

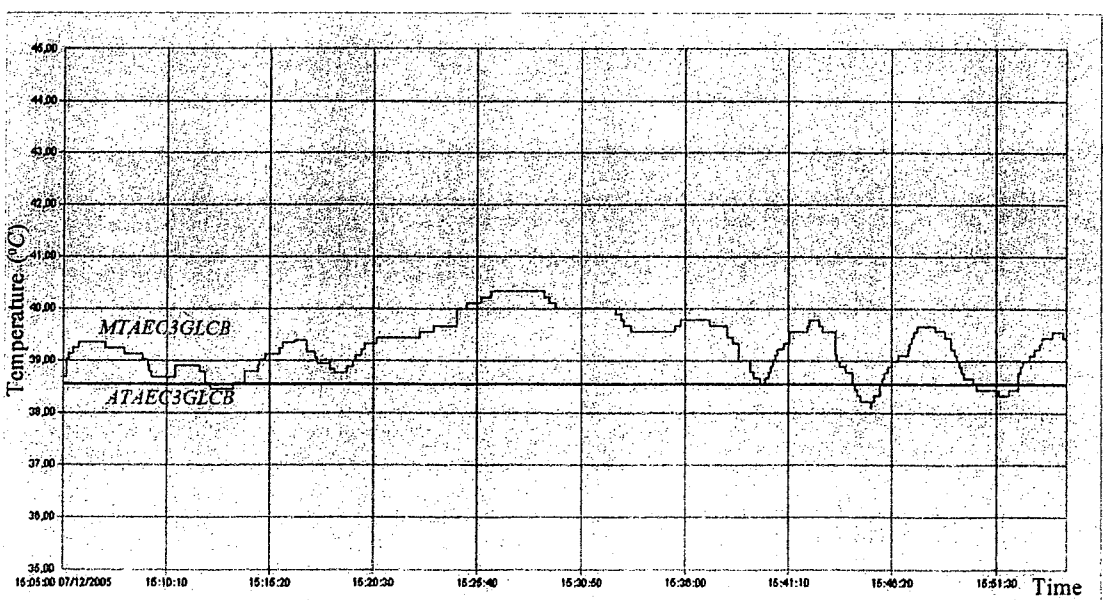

Figure 4.15 Bad performance of the original heating coil PI control system

4.7.2 Online Adaptive PI Control Strategy for the Heating Coil Control System

To solve the problem mentioned in Section 4.7.1, we consider adopting the online adaptive PI control strategy with the simplified optimal control algorithm. The simplified optimal control algorithm has improved robustness compared to the H_∞ adaptive PI tuning rules. The adaptive PI control structure is shown in Figure 4.16. To have the adaptive ability, we add two new functional blocs to the original PI control system. These are an identifier and a PI tuner. The identifier does the estimation of the system parameters and the PI tuner does the PI parameters updating following the identified system parameters online.

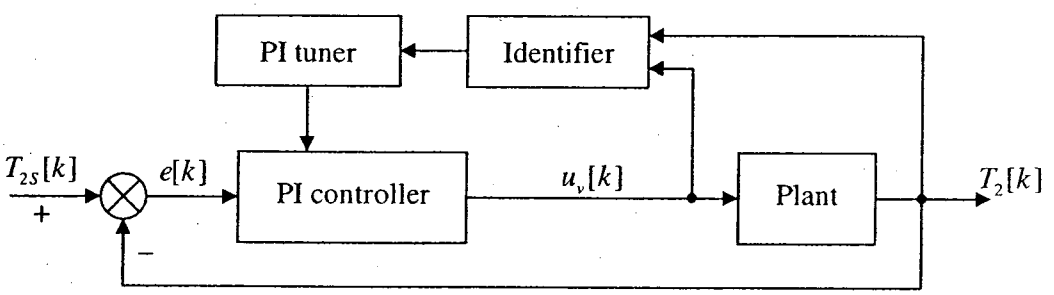

Figure 4.16 Adaptive PI control system for the heating coil system

4.7.3 Variables in the Heating Coil Control System

The heating coil air temperature is the controlled variable T_2 that is named as *MTAEC3GLCBS* in PPCL program. The setpoint is T_{2s} that is named as *ATAEC3GLCBS*. The setpoint value is in the range of 26 to 43 °C. The control variable u_v is the input of the hot water valve flow rate in percentage and named as *CBCGLC470BS* (0 to 100%).

The PI parameters of the heating coil control system are K_{pd} and K_{id} named as *YTAEC3GLCBS* and *ZTAEC3GLCBS* in PPCL program. The inlet air temperature of the heating coil system is T_{20}.

4.7.4 Identification of the Plant

The plant (the heating coil) is modeled as a first order plus dead-time (FOPDT) system. That is,

$$\frac{T_2(z)-T_{20}}{u_v(z)}=\frac{bz^{-(l+1)}}{1-az^{-1}} \tag{4.36}$$

and $$y(k)=T_2(k)-T_{20}. \tag{4.37}$$

The transportation time delay l is considered as a constant that can be determined by an open-loop test. The identifier program estimates the parameters of a and b online.

The open-loop test was made on December 14, 2005. The experimental result is shown in Figure 4.17. The green line is the percentage of the valve opening and the red line is the output air temperature of the heating coil. The percentage of the valve opening was set as follows.

$$u_v=\begin{cases}39\% & before \quad 14:15:03 \\ 49\% & after \quad 14:15:03 \quad before \quad 14:24:02 \\ 39\% & after \quad 14:24:02\end{cases}$$

From the open-loop response, the delay time in the step-up mode of operation was 42s and the delay time in the step-down case was 55s. If we choose $T_s=8\,\mathrm{s}$ as the sampling time, the model delay l should be chosen as 7 because $7\times 8=56\,\mathrm{s}$. The online identification algorithm proposed in Charter 3 was used for the identification of the heating coil plant.

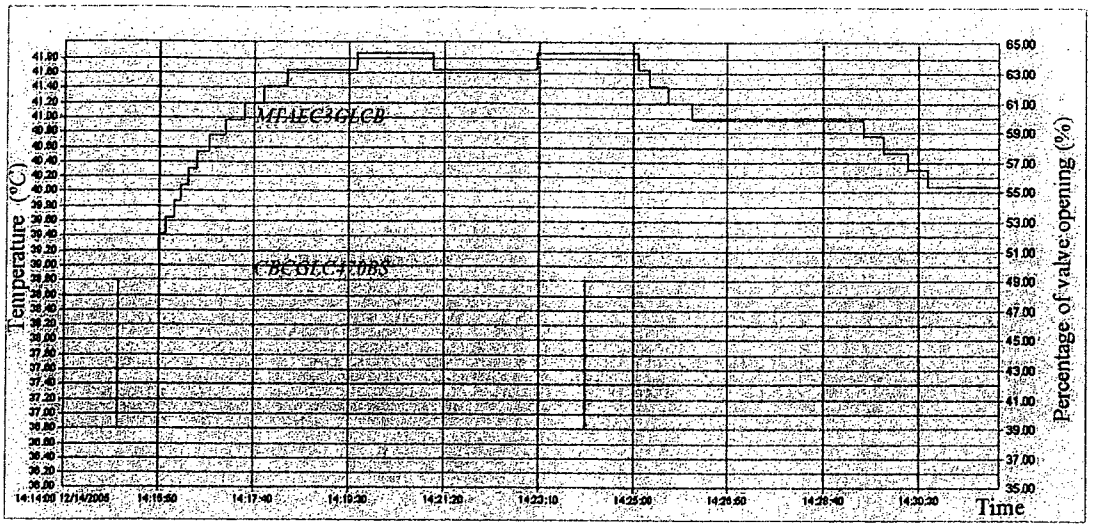

Figure 4.17 Open-loop tests for determination of the heating coil system delay

4.7.5 Algorithm for the Heating Coil Control System

We keep the original PI control for the heating coil control system unchanged. In order to have the adaptive PI control active, we add new functions that include both the identifier and the PI tuner. The new algorithm does the identification of the system, and then updates the PI parameters according to the simplified optimal control algorithm based on the new identification result. The adaptive PI control with the simplified optimal control algorithm is called simplified optimal adaptive control (SOAC). The new algorithm is expressed in the following diagram. SECND5 is one of the system timers. We use it to control the sampling time.

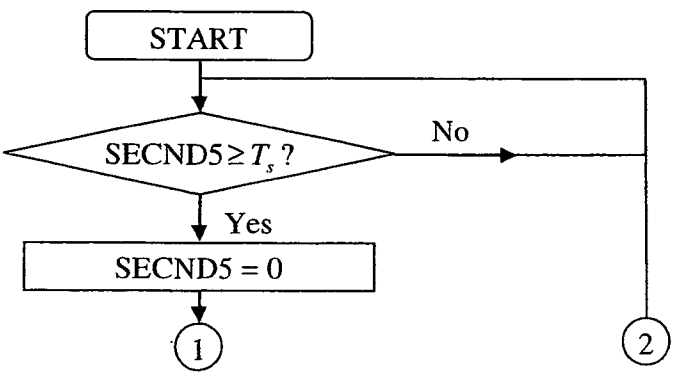

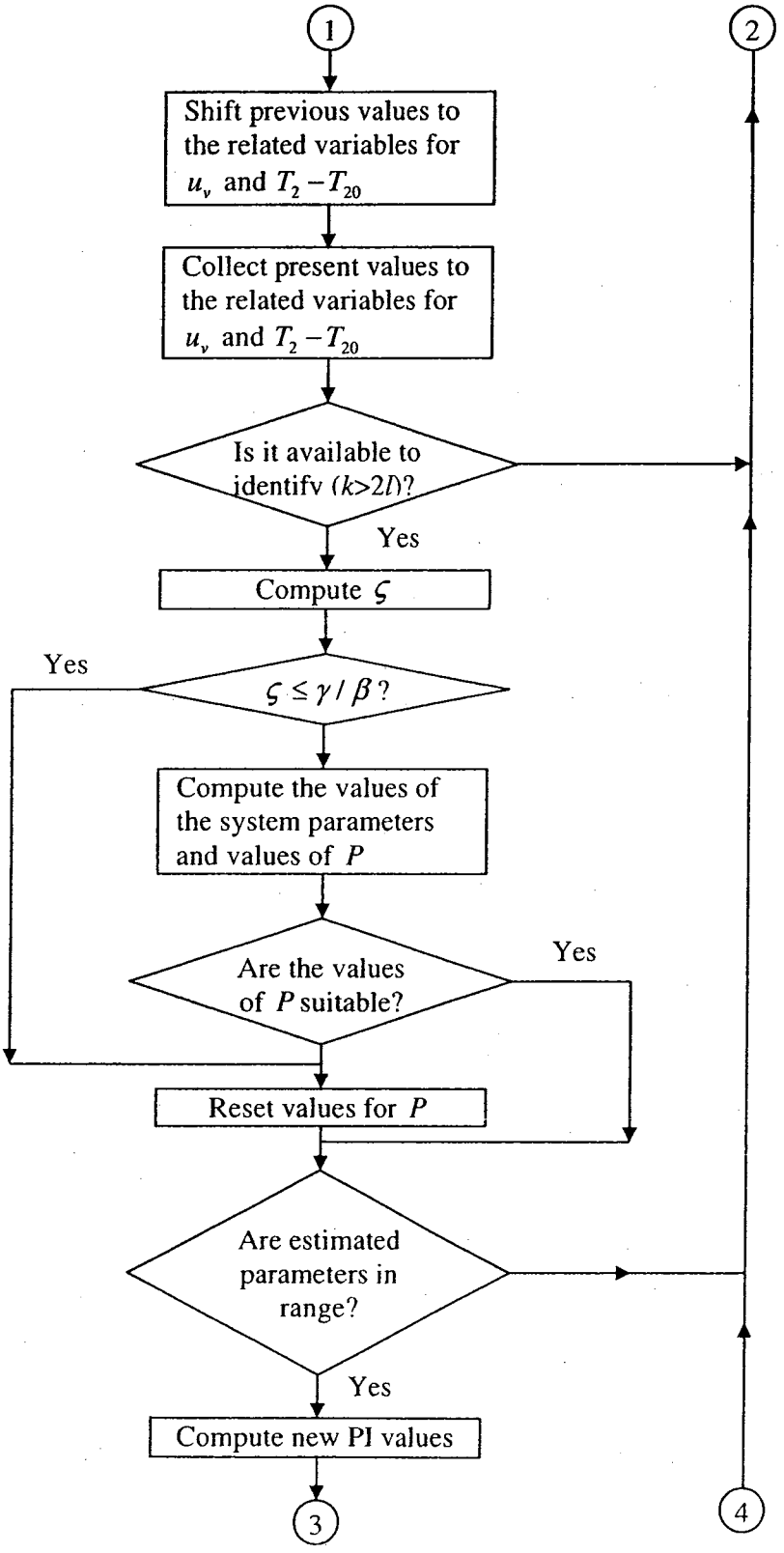
1
2
Shift previous values to the related variables for u_v and $T_2 - T_{20}$
Collect present values to the related variables for u_v and $T_2 - T_{20}$
Is it available to identifv (k>2l)?
Yes
Compute ς
Yes
$\varsigma \leq \gamma / \beta$?
Compute the values of the system parameters and values of P
Are the values of P suitable?
Yes
Reset values for P
Are estimated parameters in range?
Yes
Compute new PI values
3
4

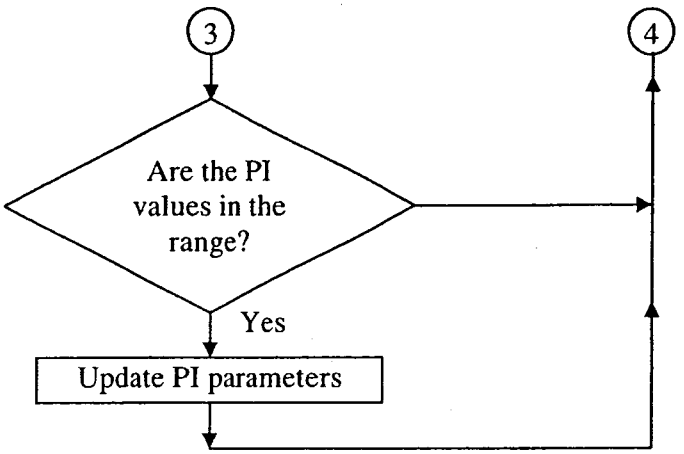

Figure 4.18 Flowchart of the SOAC for the heating coil control

4.7.6 Experimental Results of SOAC for the Heating Coil Control System

The experimental results shown in Figure 4.19 were compared. The blue line is the setpoint, and the red and green lines are the output warm air temperature and the percentage of the valve opening respectively.

The original PI control was active before 11:32:33. After that, the control was changed to SOAC with $Q_2 = 1$. Because the internet communication was taking time and the changes needed to be done one by one, this resulted in a big offset as shown in Figure 4.19. However, after few minutes the adaptive PI control (SOAC) made the system converge and stay at the setpoint closely.

To show the advantage of the adaptive PI control, somewhat longer experimental data was recorded. It is shown in Figure 4.20. The response is much closer to the setpoint compared to Figure 4.15, but the offset is still greater than $0.8^{\circ}C$ and the response is

below the setpoint over a long time. This may imply that SOAC (becomes H_∞ adaptive PI control for $Q_2 = 1$) can be further improved to reduce the effect of load changes.

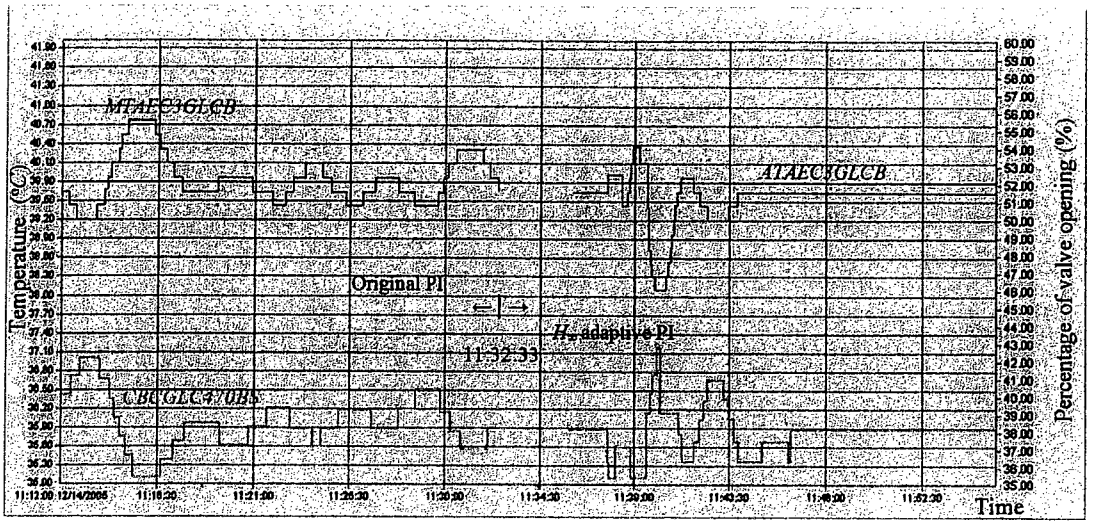

Figure 4.19 Comparison between the original PI and the adaptive PI controls

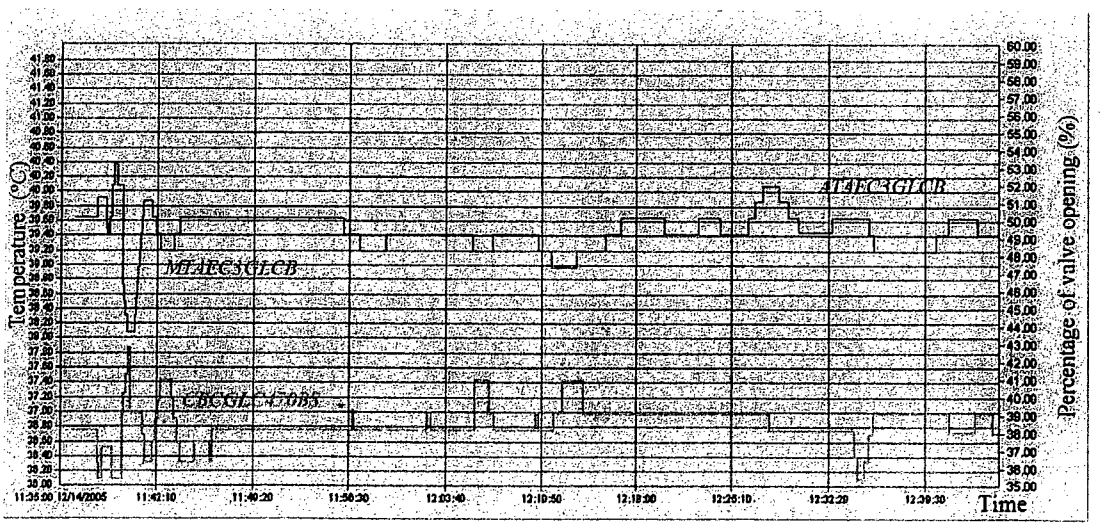

Figure 4.20 Experimental result of SOAC with $Q_2 = 1$

To improve the performance of SOAC, the weight factor Q2 < 1 is appropriate. Figure 4.21 shows the response for SOAC with $Q_2 = 0.5$. The response in Figure 4.21 seems to be closer to the setpoint compared to the response with $Q_2 = 1$ shown in Figure

4.20 and has balanced offset on both sides. The maximum offset in Figure 4.21 is less than $0.6^{\circ}C$. It is clear that the response has been improved. The small oscillation in Figure 4.21 shows the possibility that a further increase in Q_2 would be appropriate. The experimental results in Figure 4.22 show the response of SOAC with $Q_2 = 0.6993$.

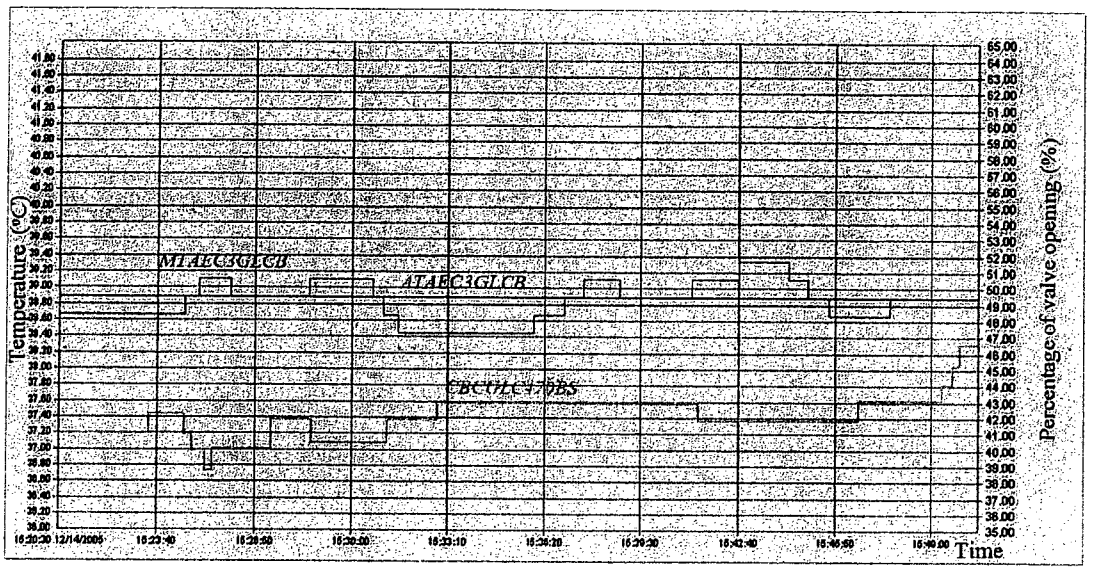

Figure 4.21 Experimental result of SOAC with $Q_2 = 0.5$

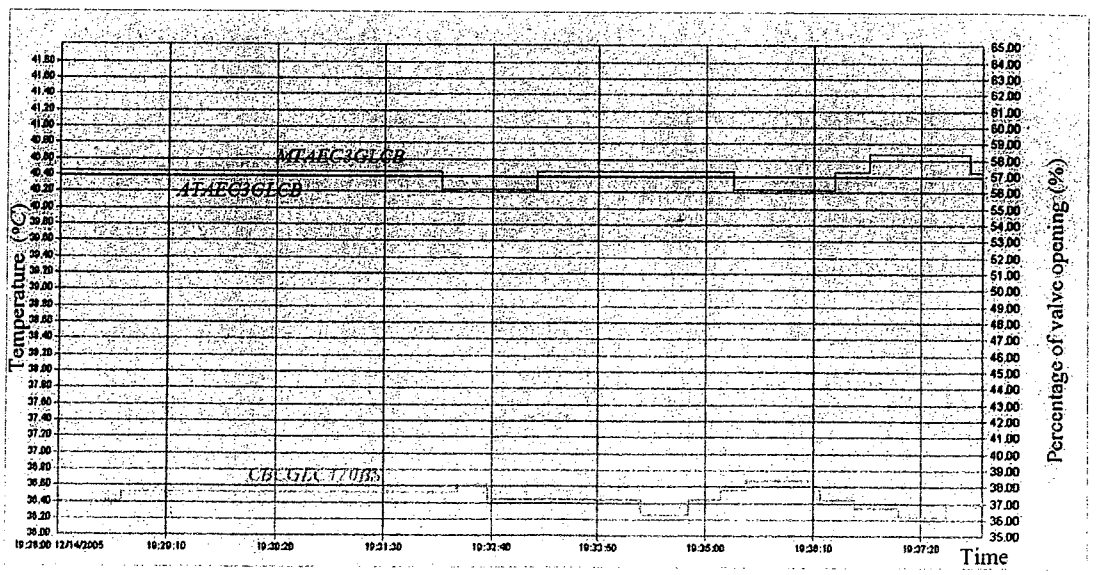

Figure 4.22 Experimental result of SOAC with $Q_2 = 0.6993$

It can be seen that the response in Figure 4.22 has been further improved, because the maximum offset is less than $0.4^{\circ}C$ and the offsets on both sides are balanced. It is apparent from these results that by properly selecting the value of Q_2, the system response can be improved.

We have also made the tests of step responses with Q_2 = 1 and the original PI control. The step response test result for the original PI control is shown in Figure 4.23. The original PI control started at 16:20:00 and ended at 17:24:00 on December 14, 2005. The step changes are *ATAEC3GLCBS* = 38.79°*C* from 39.79°*C* at 16:49:00 and

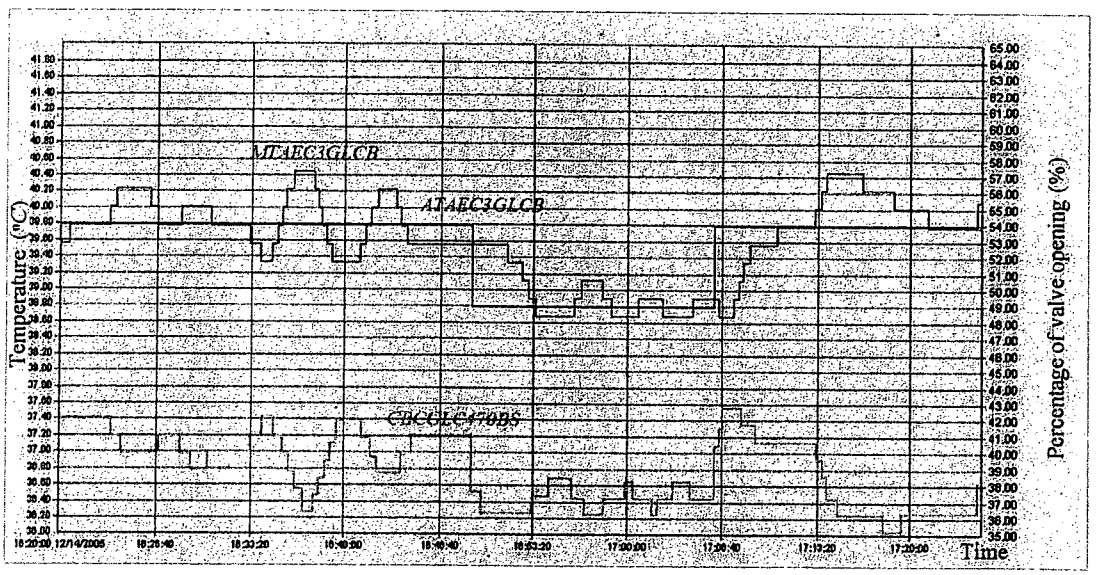

Figure 4.23 Step response of the original PI control

ATAEC3GLCBS = 39.79°*C* from 38.79°*C* at 17:06:00. The overshoots are 66% for the step-up setpoint change and 12% for the step-down setpoint change. The settling time for the step-up setpoint change to within 0.22°*C* is 774s and the settling time for the step-down setpoint change to within 0.22°*C* is 571s.

Figure 4.24 presents the step response test result for SOAC with Q_2 = 1 and the identification results and the system PI parameters (which are 1000 times of the tuned PI parameters, that is, *YTAEC3GLCBS* = K_{pd} and *ZTAEC3GLCBS* = K_{id}) are shown in Figures 4.25 and 4.26 respectively. The step changes in Figure 4.24 are *ATAEC3GLCBS* =40.49°*C* from 39.79°*C* at 12:50:35 and *ATAEC3GLCBS* = 39.49°*C* from 40.49°*C* at 13:10:19. The overshoot for the step-up setpoint change is 69% and there is no overshoot

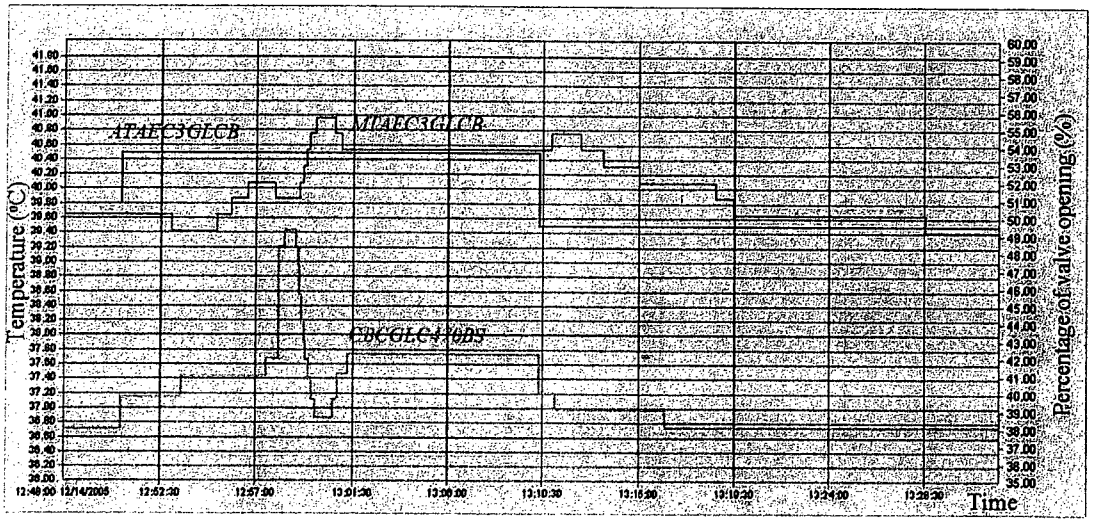

Figure 4.24 Step response for SOAC with Q_2 = 1

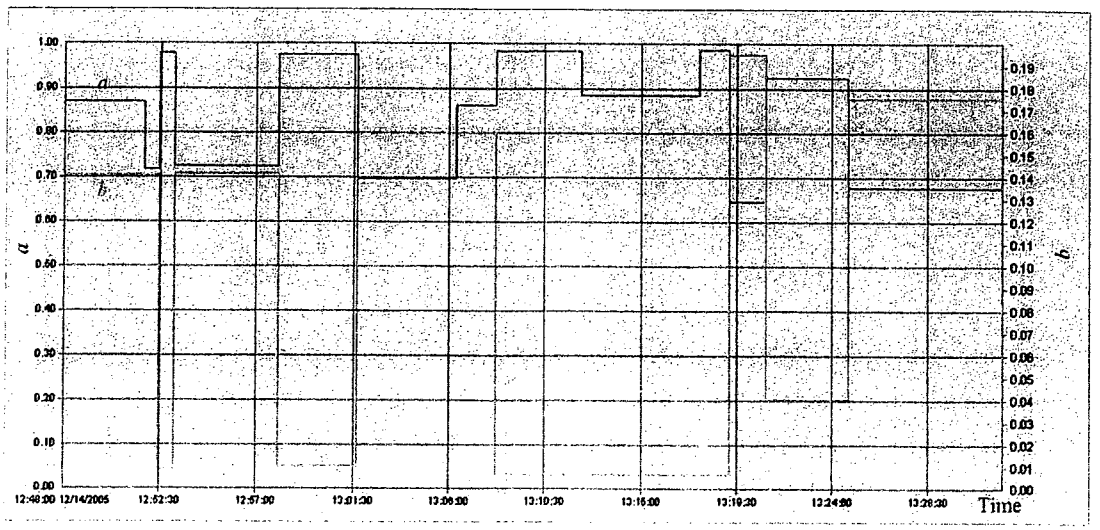

Figure 4.25 Identification result in SOAC with Q_2 = 1

for the step-down setpoint change. The settling time for the step-up setpoint change to within $0.22^{\circ}C$ is 610s and the settling time for the step-down setpoint change to within $0.22^{\circ}C$ is 549s.

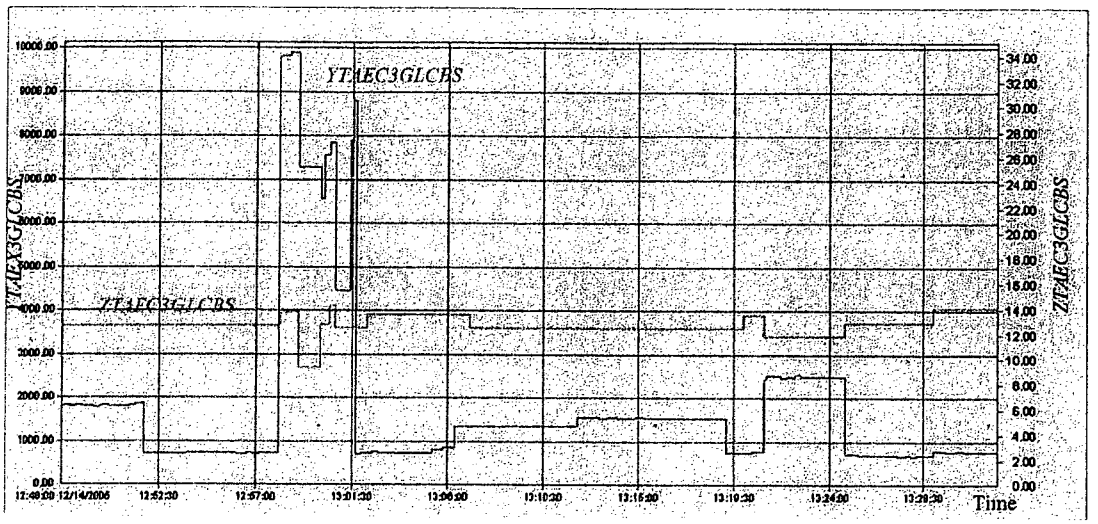

Figure 4.26 PI parameter evolution of SOAC with $Q_2 = 1$

The above results indicate that SOAC with $Q_2 = 1$ is faster than the original PI control system. It is also worth noting that if we increase the accuracy of the controlled variable the identification will be more smooth which will lead to much better step response for SOAC.

4.8 Application to the DAS

We have also done the experimental tests with the simplified optimal adaptive PI control (SOAC) applied to the DAS in the laboratory HVAC test facility. The DAS model remains the same as in Section 4.2.3. Figure 4.27 shows the step responses controlled by SOAC with two different weighting factors $Q_2 = 1.3889$ and $Q_2 = 1.6667$ respectively. Figure 4.28 presents the system PI parameters tuned by the simplified

optimal control algorithm and Figure 4.29 shows the identification results of the DAS model parameters.

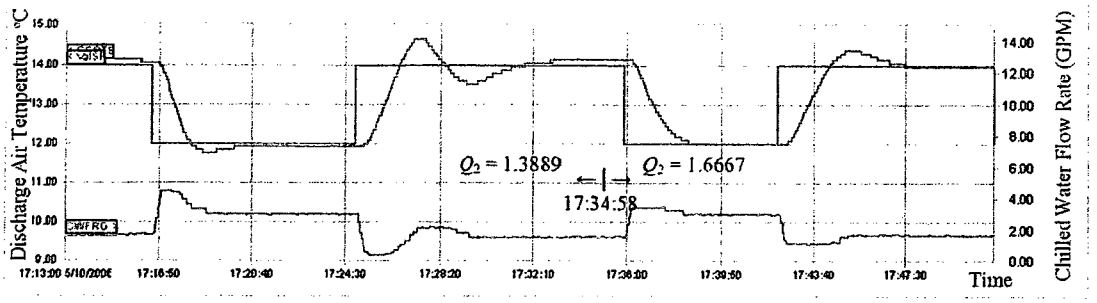

Figure 4.27 Step responses of SOAC with Q_2 = 1.3889 and 1.6667

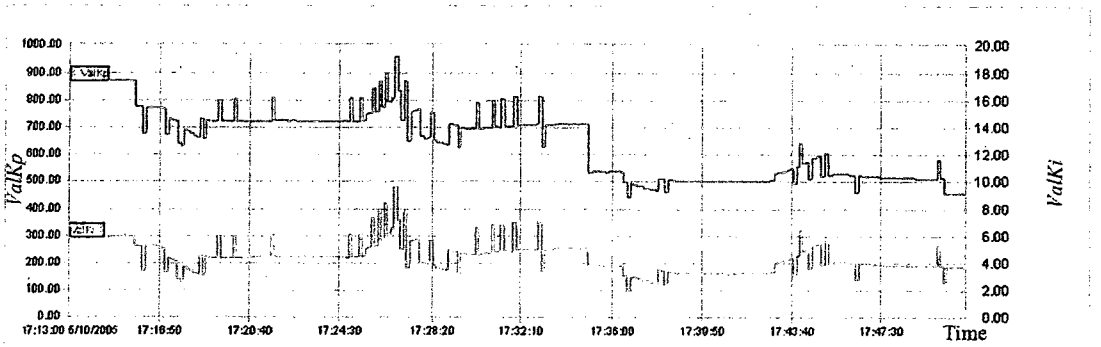

Figure 4.28 PI gains of SOAC with Q_2 = 1.3889 and 1.6667

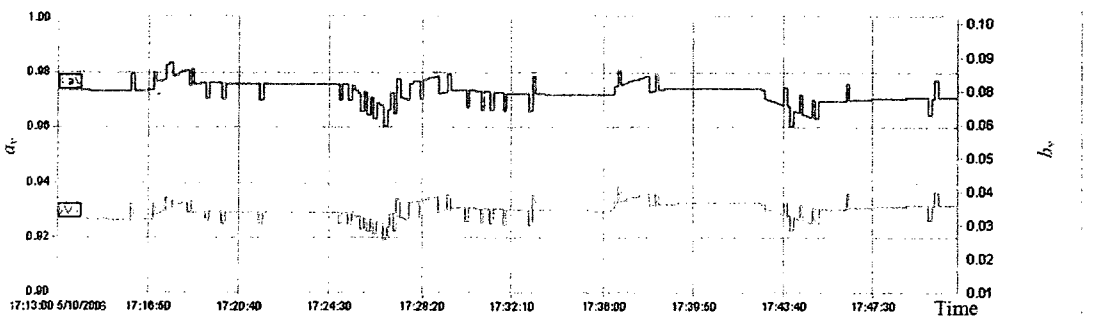

Figure 4.29 Identification in SOAC with Q_2 = 1.3889 and 1.6667

ValSP in Figure 4.27 is the setpoint of the discharge air temperature (*CCOTS*) and *CWFRG* is the chilled water flow rate in GPM. The PI parameters (*ValKp* and *ValKi*) in

Figure 4.28 are 1000 times the tuned PI parameters to account for the scaling factor. In Figure 4.29, a_v is the estimated value of the parameter a and b_v is the estimated value of the parameter b responses obtained from the identification process.

The step responses in Figure 4.27 confirm that SOAC is able to give good step response performance by changing the weighting factor Q_2. The step response results also show that increasing the weighting factor reduces overshoot and gives smooth step response.

4.9 Summary

By describing the dynamics of a discharge air system (DAS) using a FOPDT model, an online optimal control algorithm combined with the H_∞ tuning rules was developed. The developed tuning rules were tested using computer simulations in an adaptive control system. The results show that the proposed optimal tuning algorithm is able to track changes in discharge air temperature setpoints efficiently and reduces the effect of changes in system parameters significantly. Results also showed that the control input weighting factor of the controller in response to a demand for an increase in setpoint should be lower than the corresponding weighting parameter in the case of a decrease in setpoint.

In this Chapter, we have also designed an adaptive PI control with the simplified optimal control algorithm (SOAC). Applications to the heating coil control system in a real building control system of Concordia University and the DAS in the laboratory HVAC test facility are illustrated. The experimental results indicate that SOAC with a suitable weighting factor has improved robustness and better step response.

5. Adaptive Neural Network Strategy for DAS

In this chapter, an adaptive neural network controller is developed. The proposed controller is constructed by augmenting the PID control structure with a neural network control algorithm. Simulation study shows that the proposed controller has strong robustness, improved regulation and tracking functions for FOPDT type plants compared to classical PID controllers. Experiments were also conducted to compare the developed strategies with some of the existing control strategies used in HVAC systems.

5.1 Introduction

In Chapter 4, we have developed a robust optimal tuning algorithm which has strong robustness property. However, it relies on plant model and needs plant parameter identification in the adaptive control application. Neural network control is a kind of model-less control strategy. Therefore, it is of interest to explore realizable neural network control algorithms for HVAC controls.

The Discharge Air System (DAS) is one of the basic components of a heating, ventilating and air-conditioning system. It was chosen again as a controlled plant for the proposed adaptive neural network controller, also due to the fact that the DAS model has dead zone nonlinearity. In the experimental studies section we will show the dead zone nonlinearity observed from open-loop responses. Figure 4.1 shows the DAS for sensible cooling of air. The discharge air temperature is maintained close to a chosen setpoint by modulating the mass flow rate of chilled water via valve control (u). In previous studies, as mentioned in Chapter 4, only the classical proportional-integral (PI) control problem

for the control of DAS is addressed. Here we explore on-line adaptive neural network control (ANNC) of DAS which is useful for real-time implementation.

The methodology for on-line adaptive neural network control of DAS is presented in sections 5.2 and 5.3. In section 5.2, the on-line adaptive NN control system configuration is explained and the NN learning algorithm is described in section 5.3. Simulation studies are conducted in section 5.4 and experimental studies are presented in section 5.5.

5.2 Adaptive Neural Network Control System

The adaptive neural network control of DAS is shown in Figure 5.1. The entering air temperature T_{a0} and the supply chilled water temperature T_{ws} are measurable; so we use them as additional inputs of the neural network controller to improve its adaptive ability.

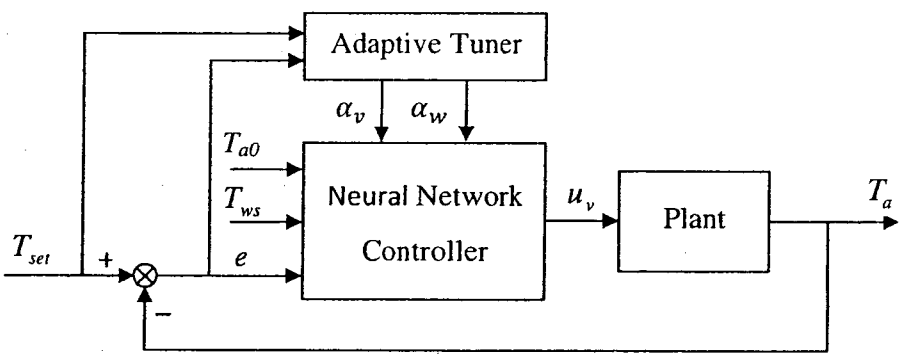

Figure 5.1 Adaptive NN control system

In addition, the neural network controller has learning ability to changes in the dynamics of the system. The adaptive tuner performs update function for adaptive parameters. The adaptive tuner is designed to avoid over training and slow response.

The adaptive neural network controller configuration is shown in Figure 5.2. In this controller, we use PID structure to have three inputs x_1 to x_3 for the normal neural network controller based on only one input e. α_v is an adaptive weight factor to avoid slow response. α_w is a boolean variable to avoid over training.

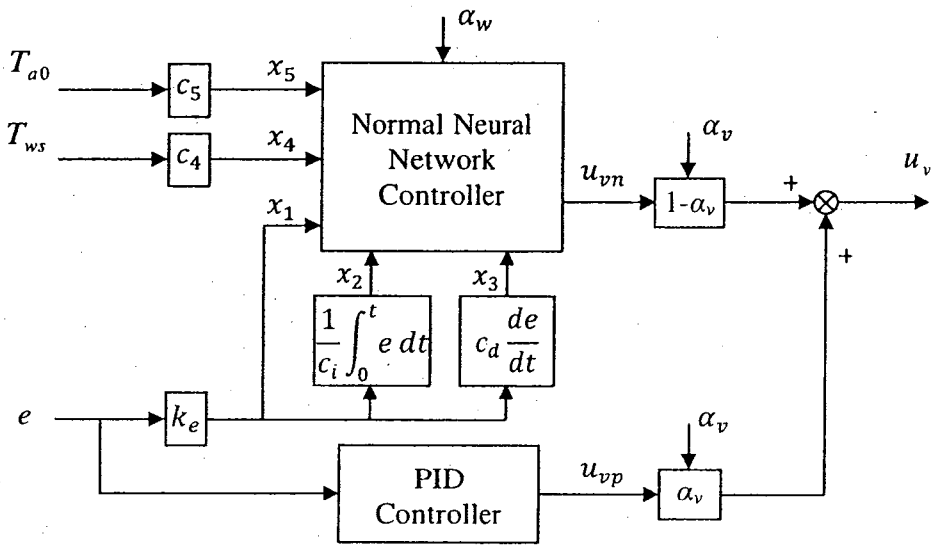

Figure 5.2 The adaptive neural network controller

For the normal neural network controller, we select a 5-5-1 two layer network structure with hyperbolic tangent activation function as shown in Figure 5.3. The controller output u_{vn} is proportional to the output o_1 with a proportionality constant c_1.

The hyperbolic tangent ($tanh(1.5x)$) is chosen as the activation function for both hidden and output layers because it has several advantages of equalizing training over layers (Kalman & Kwasny, 1992).

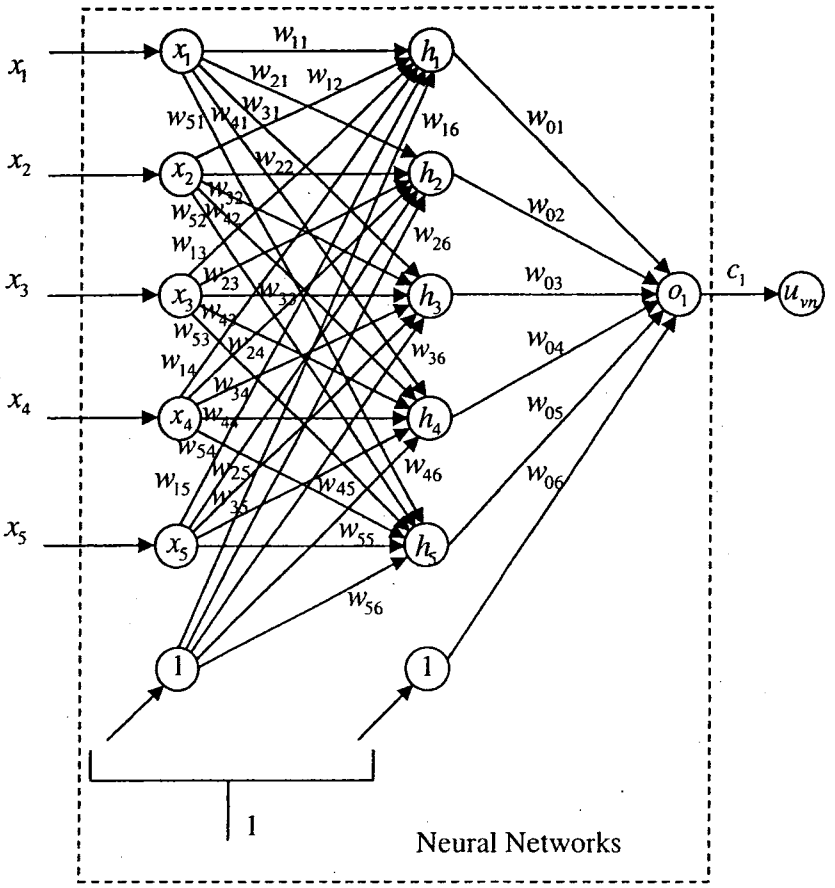

Figure 5.3 Selected normal neural network controller

5.3 Neural Network Learning Algorithm

The adaptive controller design objective was defined as the minimization of performance index

$$E_T = \alpha_e \frac{1}{2}\sum_{k=1}^{n}\left(T_{set}(k) - T_a(k)\right)^2 + \alpha_u \frac{1}{2}\sum_{k=1}^{n}\left(u_v(k)\right)^2 \tag{5.1}$$

Such that both set-point tracking error and energy consumption are minimized. We have

$$\min_{w} E(k) = \min_{w}\left[\alpha_e \frac{1}{2}(T_{set}(k)-T_a(k))^2 + \alpha_u \frac{1}{2}(u_v(k))^2\right] \tag{5.2}$$

The network weights were updated along-vector gradient of error E (Gradient Descent Method) such as

$$\Delta w^{(l)} = -\eta \frac{\partial E(k)}{\partial w^{(l)}} \tag{5.3}$$

Where η is learning rate parameter (>0); $\Delta w^{(l)}$ is weight vector from $l-1^{st}$ to l^{th} layer.

Following the chain rule, the above equation can be rewritten as:

$$\Delta w^{(l)} = -\eta \frac{\partial E(k)}{\partial w^{(l)}} = -\eta\left(\frac{\partial E(k)}{\partial T_a(k)}\frac{\partial T_a(k)}{\partial u_v(k)} + \frac{\partial E(k)}{\partial u_v(k)}\right)\frac{\partial u_v(k)}{\partial o_1(k)}\frac{\partial o_1(k)}{\partial w^{(l)}} \tag{5.4}$$

$$\Delta w^{(l)} = \eta\left(\alpha_e(T_{set}(k)-T_a(k))\frac{\partial T_a(k)}{\partial u_v(k)} - \alpha_u(u_v(k))\right)c_1\frac{\partial o_1(k)}{\partial w^{(l)}} \tag{5.5}$$

α_u was approximated as follows,

$$\alpha_u = -(T_{set}(k)-T_a(k-1))^2\frac{\partial T_a(k-1)}{\partial u_v(k-1)} \approx -(T_{set}(k)-T_a(k))^2\frac{\partial T_a(k)}{\partial u_v(k)} \tag{5.6}$$

thus, we have

$$\Delta w^{(l)} = \eta\left(\alpha_e(T_{set}(k)-T_a(k))\frac{\partial T_a(k)}{\partial u_v(k)} + (T_{set}(k)-T_a(k))^2\frac{\partial T_a(k)}{\partial u_v(k)}u_v(k)\right)c_1\frac{\partial o_1(k)}{\partial w^{(l)}}$$

$$= \eta(T_{set}(k)-T_a(k))\frac{\partial T_a(k)}{\partial u_v(k)}(\alpha_e + (T_{set}(k)-T_a(k))u_v(k))c_1\frac{\partial o_1(k)}{\partial w^{(l)}} \tag{5.7}$$

The calculation of the partial derivative of the network output with respect to the weight vector is calculated based on the network architecture, the only term cannot be

analytically calculated is the partial derivative of the discharge air temperature (T_a) with respect to the controller output (u_v) at each time step.

The actual value of $\partial T_a / \partial u_v$ is not important due to scaling of the term based on the coefficient η (equation (5.3)), but the sign of the above mentioned term needs to be determined. By performing a step change on the controller output (Δu_v), a negative proportional reaction of the discharge air temperature is obtained (ΔT_a). Thus, the system can be characterized as negative and monotone relevant to the command (u_v), since the partial derivative of the system output (T_a) relevant to the controller output (u_v) is always negative. The above assumption is correct only if the partial derivative exists for every time step, which leads to continuous changes in the controller output. Equation (5.7) can be written as

$$\Delta w^{(l)} = -\eta_l c_1 (T_{set}(k) - T_a(k))(\alpha_e + (T_{set}(k) - T_a(k))u_v(k)) \frac{\partial o_l(k)}{\partial w^{(l)}} \tag{5.8}$$

Considering the choice of the hyperbolic tangent ($tanh(1.5x)$) as the activation function for both hidden and output layers and assuming

$$H = [h_1 \quad h_2 \quad \cdots \quad h_{m_i} \quad 1]^T \tag{5.9}$$

$$X = [x_1 \quad x_2 \quad \cdots \quad x_{m_j} \quad 1]^T \tag{5.10}$$

$$W_0 = [w_{01} \quad w_{02} \quad \cdots \quad w_{0m_i} \quad w_{0(m_i+1)}] \tag{5.11}$$

$$W_i = [w_{i1} \quad w_{i2} \quad \cdots \quad w_{im_j} \quad w_{i(m_j+1)}] \tag{5.12}$$

$$o_{1in} = W_0 H \tag{5.13}$$

$$h_{iin} = W_i X \tag{5.14}$$

$$g_w(k) = k_1 c_1 (T_{set}(k) - T_a(k))(\alpha_e + (T_{set}(k) - T_a(k))u_v(k)) \tag{5.15}$$

where m_i is the number of the hidden nodes and m_j is the number of inputs, we have

$$o_1(k)=\frac{1-e^{-3o_{1in}(k)}}{1+e^{-3o_{1in}(k)}} \tag{5.16}$$

$$h_i(k)=\frac{1-e^{-3h_{iin}(k)}}{1+e^{-3h_{iin}(k)}} \tag{5.17}$$

Considering the fact that

$$\left(\frac{1-e^{-3x}}{1+e^{-3x}}\right)^{\cdot}=\frac{3e^{-3x}\left(1+e^{3x}\right)+3e^{-3x}\left(1-e^{-3x}\right)}{\left(1+e^{-3x}\right)^2}=\frac{6e^{-3x}}{\left(1+e^{-3x}\right)^2}=f'(1.5x) \tag{5.18}$$

we have

$$\Delta w_{0i}=-\frac{\eta_1}{k_1}g_w(k)f'(1.5(W_0H))h_i$$

$$=-\frac{\eta_1}{k_1}g_w(k)\frac{6e^{-3o_{1in}}}{\left(1+e^{-3o_{1in}}\right)^2}h_i \quad (i=1,\ 2,\ \cdots,\ m_i+1) \tag{5.19}$$

$$\Delta w_{ij}=-\frac{\eta_1}{k_1}g_w(k)f'(1.5(W_0H))w_{0i}f'(1.5(W_iX))x_j$$

$$=-\frac{\eta_1}{k_1}g_w(k)\frac{6e^{-3o_{1in}}}{\left(1+e^{-3o_{1in}}\right)^2}w_{0i}\frac{6e^{-3h_{iin}}}{\left(1+e^{-3h_{iin}}\right)^2}x_j \tag{5.20}$$

$$(i=1,\ 2,\ \cdots,\ m_i+1,\ j=1,\ 2,\ \cdots,\ m_j+1)$$

To achieve global convergence, we introduce two time-varying learning rates instead of η_1/k_1. For Δw_{0i}, we use

$$\eta_h=\frac{\eta_0}{1+h_1^2+h_2^2+\cdots+h_{m_i}^2} \tag{5.21}$$

and for Δw_{ij}, we use

$$\eta_x = \frac{\eta_0}{1 + x_1^2 + x_2^2 + \cdots + x_{m_j}^2} \tag{5.22}$$

where, η_0 is a selected constant learning rate.

The inputs and the output of the normal neuron network controller can be expressed as follows.

$$x_1(k) = k_e e(k) = k_e(T_{set}(k) - T_a(k)) \tag{5.23}$$

$$x_2(k) = x_2(k-1) + \frac{k_e T_s}{2c_i}(e(k) + e(k-1)) \tag{5.24}$$

$$x_3(k) = c_d k_e \frac{e(k) - e(k-1)}{T_s} \tag{5.25}$$

$$x_4(k) = \alpha_4 c_4 (T_{ws}(k) - c_{40}) + (1 - \alpha_4) x_4(k-1) \tag{5.26}$$

$$x_5(k) = \alpha_5 c_5 (T_{a0}(k) - c_{50}) + (1 - \alpha_5) x_5(k-1) \tag{5.27}$$

$$o_{1in}(k) = \sum_{i=1}^{m_i} w_{0i}(k) h_i(k) \tag{5.28}$$

$$\eta_h(k) = \frac{\eta_0}{1 + h_1^2(k) + h_2^2(k) + \cdots + h_{m_i}^2(k)} \tag{5.29}$$

$$\eta_x(k) = \frac{\eta_0}{1 + x_1^2(k) + x_2^2(k) + \cdots + x_{m_j}^2(k)} \tag{5.30}$$

$$h_{iin}(k) = \sum_{j=1}^{m_j} w_{ij}(k) x_j(k) \tag{5.31}$$

To save computing time, we assume $h_{ii}(k) = e^{3h_{iin}(k)}$, then (5.32)

$$h_i(k) = \frac{h_{ii}(k) - 1}{h_{ii}(k) + 1} \tag{5.33}$$

and assuming $o_{11}(k) = e^{3o_{1in}(k)}$, (5.34)

we have

$$o_1(k)=\frac{o_{11}(k)-1}{o_{11}(k)+1} \tag{5.35}$$

Let

$$o_{1d}(k)=\frac{6o_{11}(k)}{(o_{11}(k)+1)^2} \tag{5.36}$$

we can update the weights and the output of the controller as follows.

$$w_{0i}(k+1)=w_{0i}(k)-\eta_h(k)g_w(k)o_{1d}(k)h_i(k) \tag{5.37}$$

$$w_{ij}(k+1)=w_{ij}(k)-\eta_x(k)g_w(k)o_{1d}(k)w_{0i}(k)\frac{6h_{ii}(k)}{(h_{ii}(k)+1)^2}x_j(k) \tag{5.38}$$

$$u_v(k)=c_1o_1(k)+c_{10} \tag{5.39}$$

From the equations (5.23) to (5.39), we note that to implement the controller we need to determine the values of c_1, c_{10}, c_4, c_{40}, c_5, c_{50}, c_i, c_d, T_s, α_4, α_5, α_e, k_e, k_1 and η_0. The coefficients c_1 and c_{10} depend on the performance of the actuator for the chilled water control valve. c_{10} is the maximum input value of the actuator for zero water flow, and c_1 can be computed by using equation (5.39) at $o_1(k)=1$ when $u_v(k)$ is equal to the maximum input of the actuator for maximum water flow rate. c_4 and c_{40} are selected to obtain a suitable range for x_4. The value of c_{40} should be less than the minimum value of T_{ws} in order to keep the controller monotone relevant to T_{ws}. The selection of c_4 is related to the balance between x_1 and x_4. α_4 is a filter parameter for x_4 since T_{ws} is measured and contains noise. Similarly, c_5 and c_{50} are selected to have a suitable range for x_5. Again the value of c_{50} should be less than the minimum value of

T_{a0} to keep the controller monotone relevant to T_{a0}. α_s is a filter parameter. T_s is the sampling time. c_i and c_d are control parameters. We can use Cohen Coon Method, or Ziegler-Nichols Method or other tuning methods to determine c_i and c_d from a reference plant. k_e is a parameter that reduces the sudden impact of inputs on system responses. k_1 is a scale factor to adjust the learning rate η_0.

To achieve smooth response, we need to stop training process of neural network control at certain point. To this end, an absolute index is considered as defined in equation (5.40). A small positive A0 will yield small overshoot when Index0 is close to IndexSet (equation (5.41)).

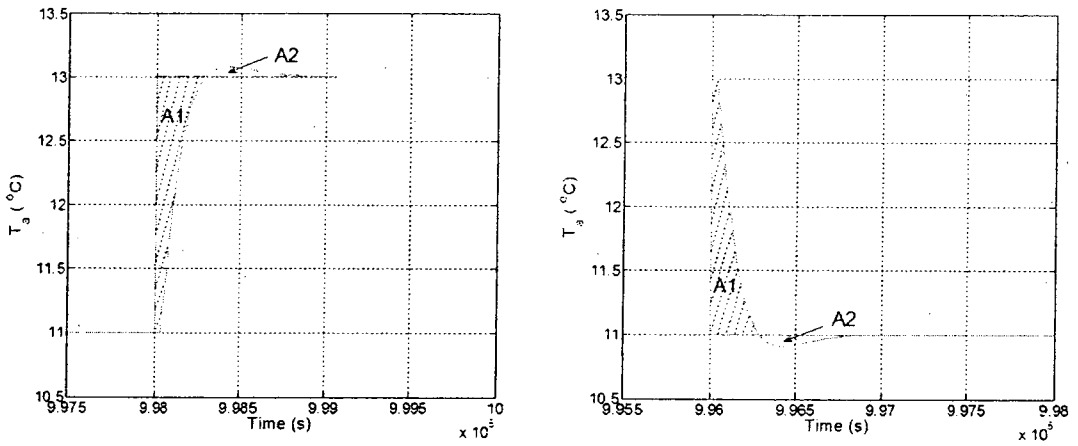

Figure 5.4 Index and IndexSet consideration

In Figure 5.4, two kinds of responses with areas A1 and A2 are shown. From this figure, we can define Index0 and IndexSet as shown below.

$$Index0 = IndexAbs - A0 = \frac{A1 + A2}{CT_s} - A0 \tag{5.40}$$

$$IndexSet = \frac{A1 - A2}{CT_s} \tag{5.41}$$

Where $C = abs(T_{set}(k) - T_{set}(k-1))$ (5.42)

To avoid slow response, we need to tune the adaptive parameter α_v online. Figure 5.5 shows the flow chart of the algorithm.

The flow chart shown in Figure 5.6 summarizes the adaptive neural network algorithm. First we need to compute and select several specific parameters (as shown in the chart) by the rules explained above and to initialize the weights. Then, following the data collection and analysis the weights are updated. The data collection, computing and decision are repeated automatically as shown in the flow chart.

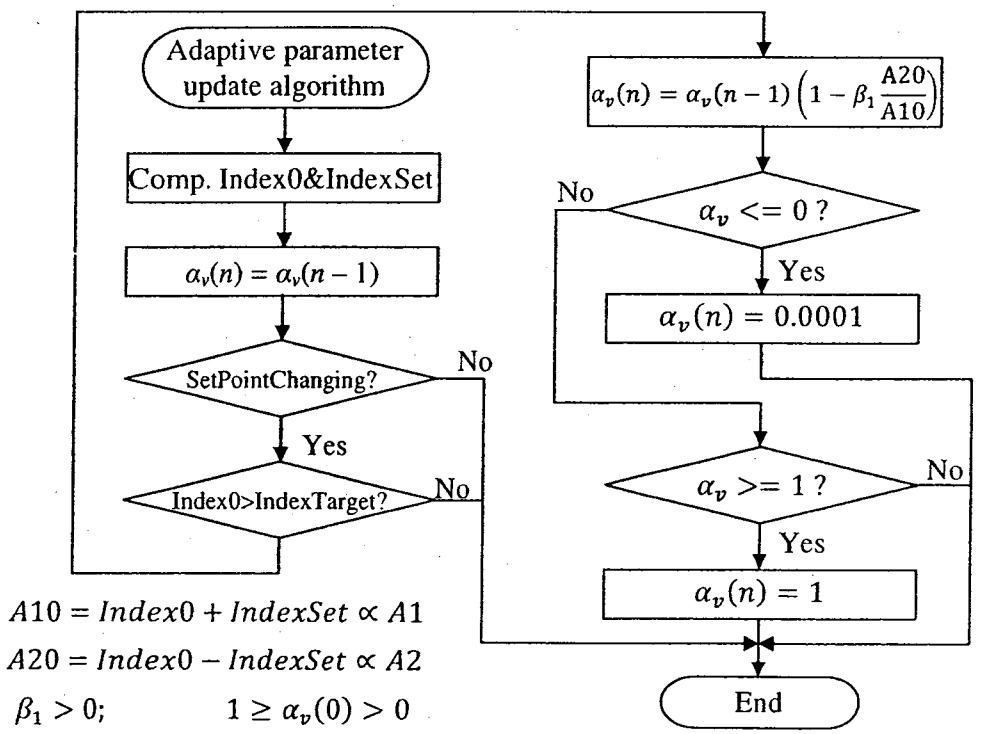

Figure 5.5 Flow chart of the adaptive tuning algorithm

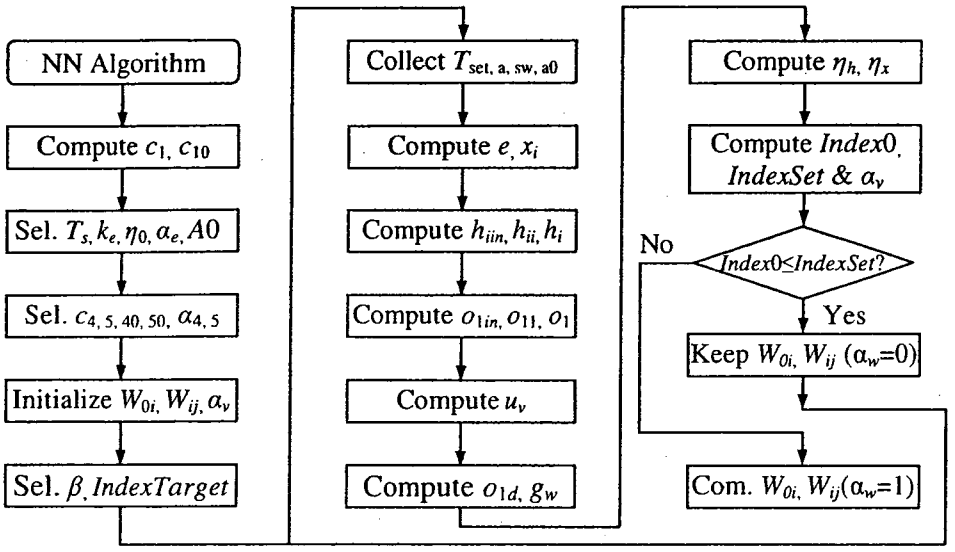

Figure 5.6 Flow chart of the adaptive neural network algorithm

The following initial weights $w_{11} = w_{22} = w_{33} = -0.5$, $w_{01} = w_{02} = w_{03} = 0.6$ and others weights close to 0 resulted in faster training process.

5.4 Simulation Results

The adaptive neural network algorithm should be robust to changes in system parameters. To test the developed algorithms, the DAS system was considered as FOPDT model. Parameters in the model were varied. To this end, twenty-seven different sets of parameters were used. Comparison with the classical PID control was made. The result demonstrated that the proposed adaptive neural network control has stronger robustness and good learning speed.

The FOPDT model is described in equations (5.43) and (5.44). It is assumed that the original plant has $a = 0.98$, $b = 0.1278$, and $l = 9$ with the sampling time of T_s = 4s. We consider 50% changes in the parameters in continuous time domain. Twenty-seven

sets of parameter changes in a, b and l were used for simulation study and these are shown in Tables 5.1 to 5.3.

$$T_a(k)=T_{a0}-y(k) \tag{5.43}$$

$$y(k)=\begin{cases} 0 & k\le l \\ ay(k-1)+bu(k-l-1) & k>l \end{cases} \tag{5.44}$$

Par.\Set	01	02	03	04	05	06	07	08	09
a	0.9604	0.9604	0.9604	0.9604	0.9604	0.9604	0.9604	0.9604	0.9604
b	0.1265	0.1265	0.1265	0.253	0.253	0.253	0.3796	0.3796	0.3796
l	4	9	14	4	9	14	4	9	14

Table 5.1 Sets 1 to 9 of the plant parameter changes

Par.\Set	11	12	13	14	15	16	17	18	19
a	0.98	0.98	0.98	0.98	0.98	0.98	0.98	0.98	0.98
b	0.0639	0.0639	0.0639	0.1278	0.1278	0.1278	0.1917	0.1917	0.1917
l	4	9	14	4	9	14	4	9	14

Table 5.2 Sets 11 to 19 of the plant parameter changes

Par.\Set	21	22	23	24	25	26	27	28	29
a	0.9866	0.9866	0.9866	0.9866	0.9866	0.9866	0.9866	0.9866	0.9866
b	0.0427	0.0427	0.0427	0.0855	0.0855	0.0855	0.1282	0.1282	0.1282
l	4	9	14	4	9	14	4	9	14

Table 5.3 Sets 21 to 29 of the plant parameter changes

The simulation runs were made using Simulink. Two main implementation blocks in Simulink are shown in Figures 5.7 and 5.8. Because T_{a0} and T_{ws} change very slowly we chose T_{a0} to simplify the implementation in the simulation study. This resulted in a network with 4 inputs and 4 hidden nodes. T_{set} was set to $11^{\circ}C$ or $13^{\circ}C$ in the following simulations.

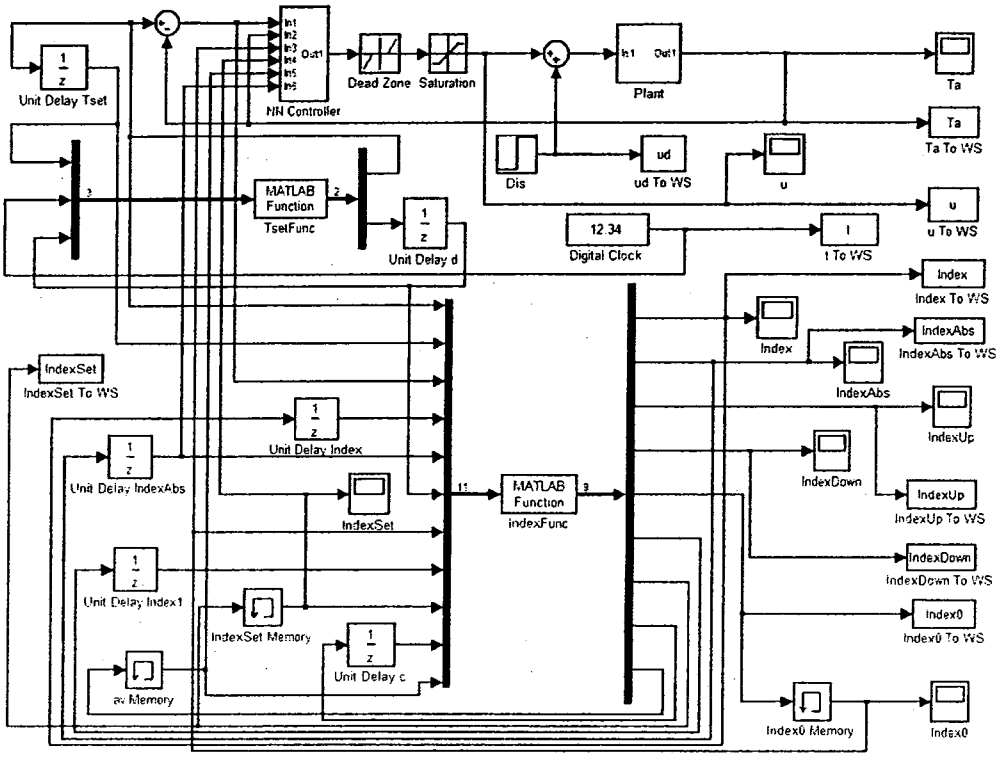

Figure 5.7 Adaptive neural network control system implementation in Simulink

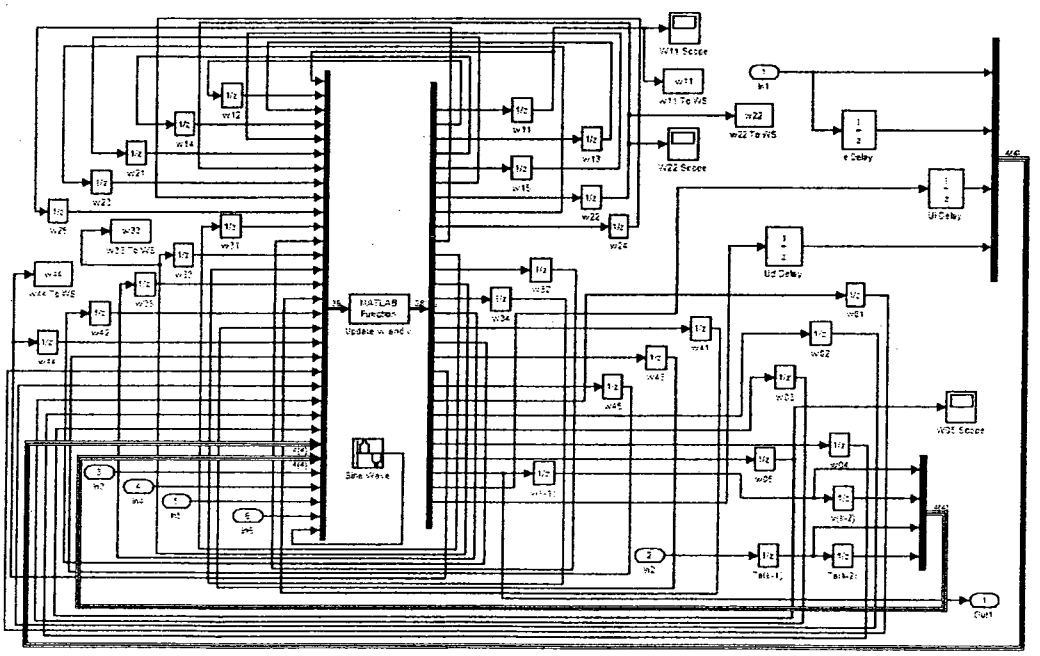

Figure 5.8 Adaptive neural network controller implementation in Simulink

Figure 5.9 shows a sample comparison of the step responses and the performance index values for the proposed adaptive neural network controller without ($\alpha_v = 0$) and with ($\alpha_v \neq 0$) adaptive tuning property. The step responses shown in Figure 5.9 (c) and the

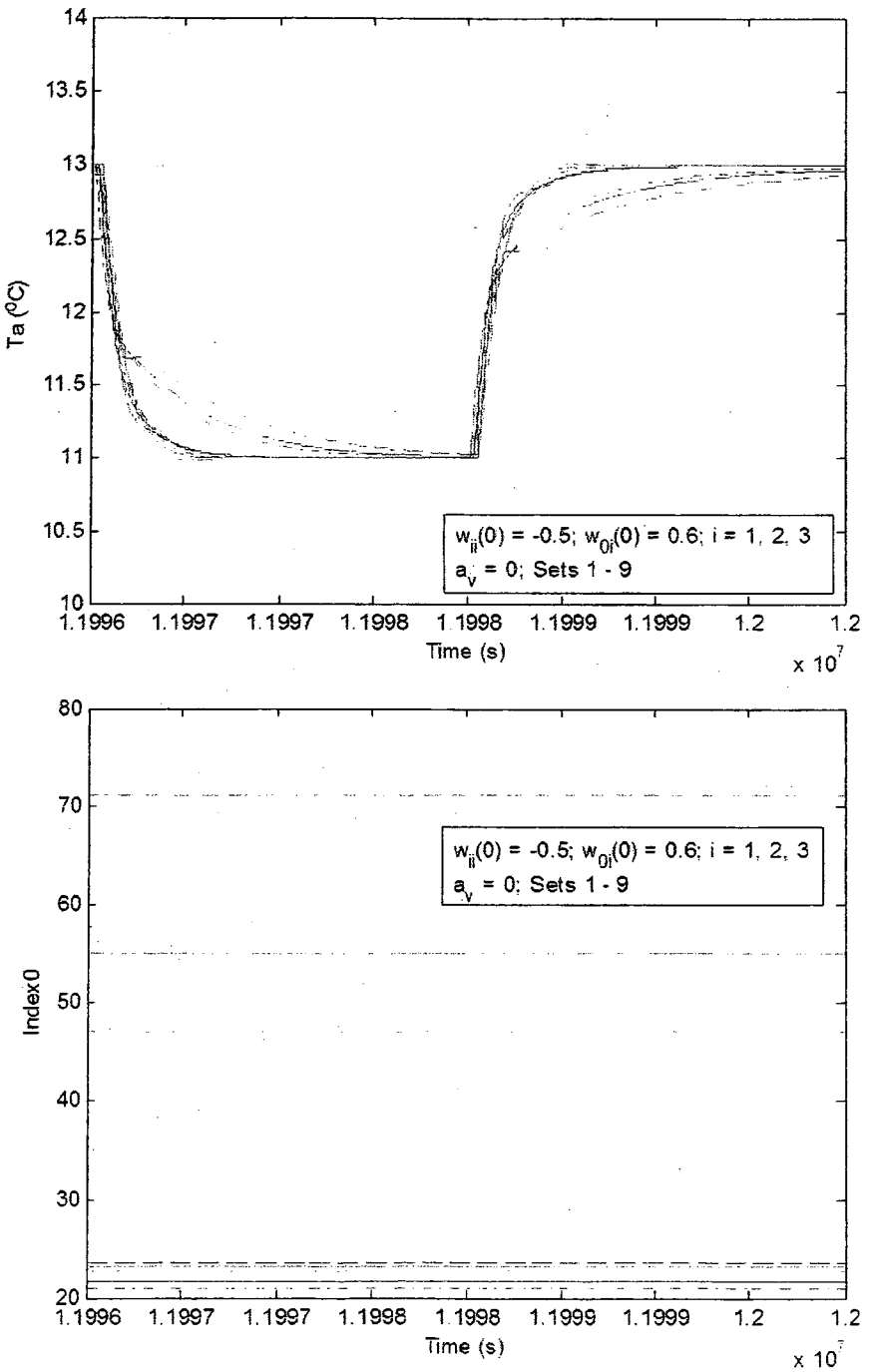

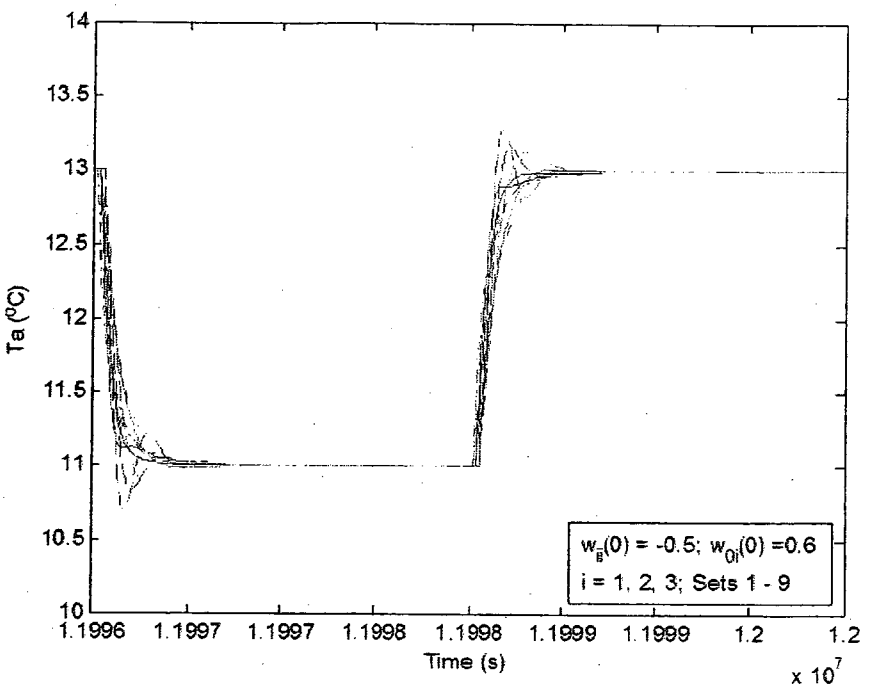

(c)

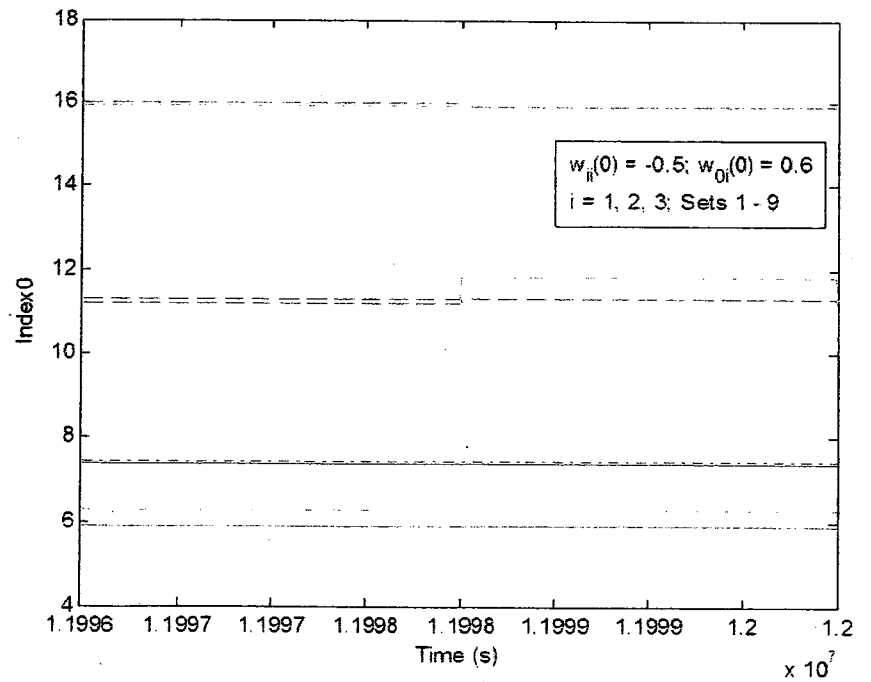

(d)

Figure 5.9 Comparison for the adaptive neural network control with $\alpha_v = 0$ and $\alpha_v \neq 0$

performance indexes depicted in Figure 5.9 (d) with adaptive tuning are superior to those without adaptive training shown in Figures 5.9 (a) and 5.9 (b). The controller without

adaptive tuning property could not achieve fast response for all plants. However, the controller with the adaptive tuning property did improve step responses even in the presence of 50% change in plant parameters (Figure 5.9 (c)) with lower index values as shown in Figure 5.9 (d).

In the above simulations the following parametric values were used: $\beta_1 = \alpha_v(0) = 0.03$, $\alpha_e = 12.0$, $c_1 = 5.0$, $k_1 = 0.018$, $c_{10} = 5.0$, $\alpha_4 = 1.0$, $c_4 = 0.1$, $c_{40} = 5.0$, $\eta_0 = 0.000747$, $k_e = 0.05$, $k_p = -1.2$, $k_i = -0.0143$, $k_d = -15.4497$, $c_i = k_p/k_i = 83.9161$, $c_d = k_d/k_p = 12.8748$, $A0 = IndexTarget = 16.0$ and $T_{a0} = 27^{\circ}C$. k_p, k_i and k_d were obtained by using Cohen-Coon tuning rules for the original plant. The results for all simulated plants indicate that the adaptive neural network controller has the ability to minimize performance index for all plants close to or even less than the target index. Figure 5.9 (c) and Figure 5.9 (d) partially illustrate the results. The legends used in Figure 5.9 are defined in Table 5.4.

Plant Set	j1	j2	j3	j4	j5	j6	j7	j8	j9
Color	Green			Blue			Red		
Line	-.	-	--	-.	-	--	-.	-	--

Table 5.4 Legends for different plant sets (j = 0, 1, 2)

The responses from the classical CCM-PID control and the proposed adaptive neural network control were compared for Plant Sets 1-9, 11-19 and 21-29. It was observed that almost half of the step responses of CCM-PID control were oscillatory (Figure 5.10(a)). On the other hand, all step responses converged in the proposed adaptive NN control (Figure 5.10(b)). As an example, the step responses for Plant Sets 21-29 are shown in Figure 5.10. The corresponding index values are shown in Figure 5.11.

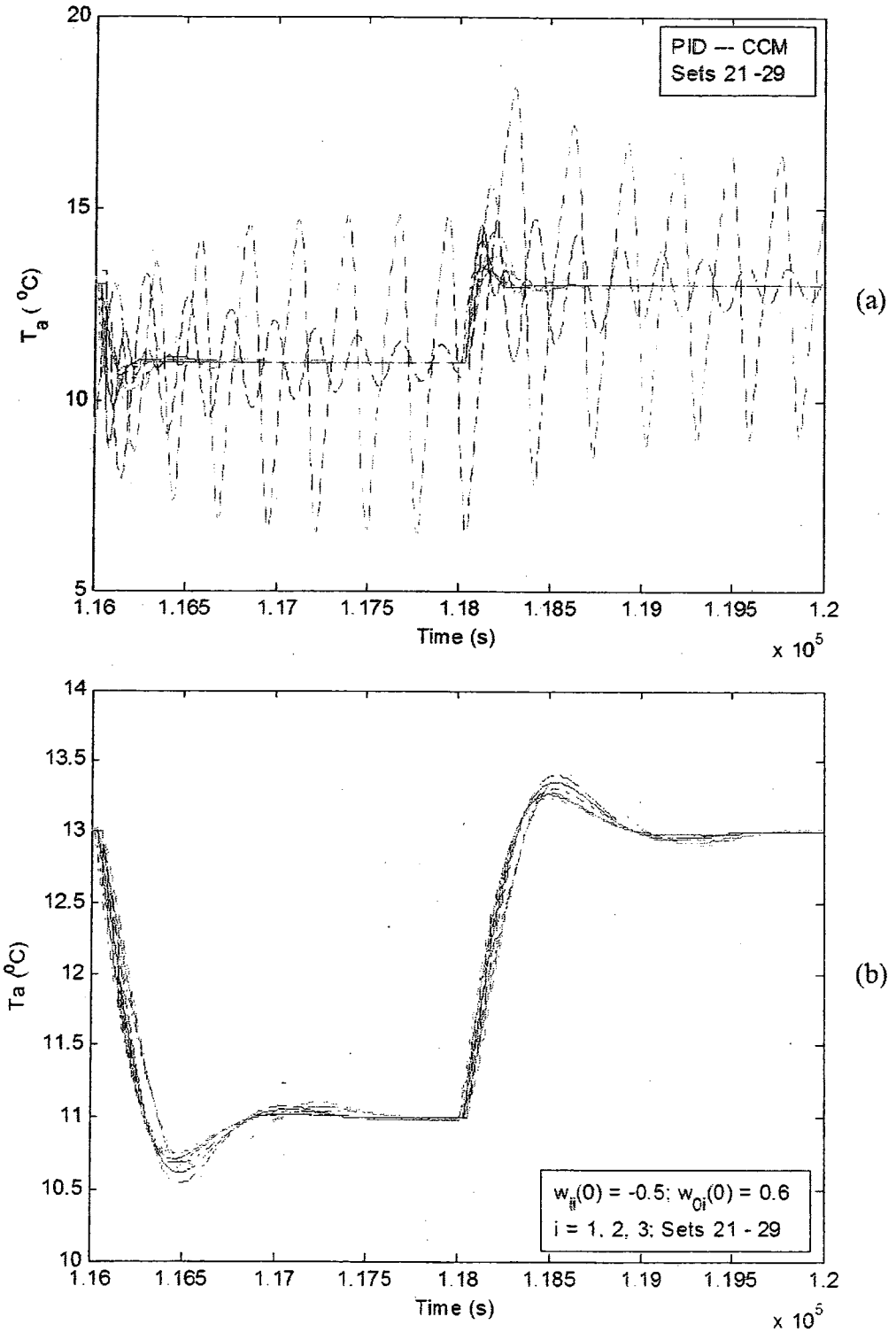

Figure 5.10 Comparison of step responses of CCM-PID and Adaptive NN control for plant sets 21 to 29

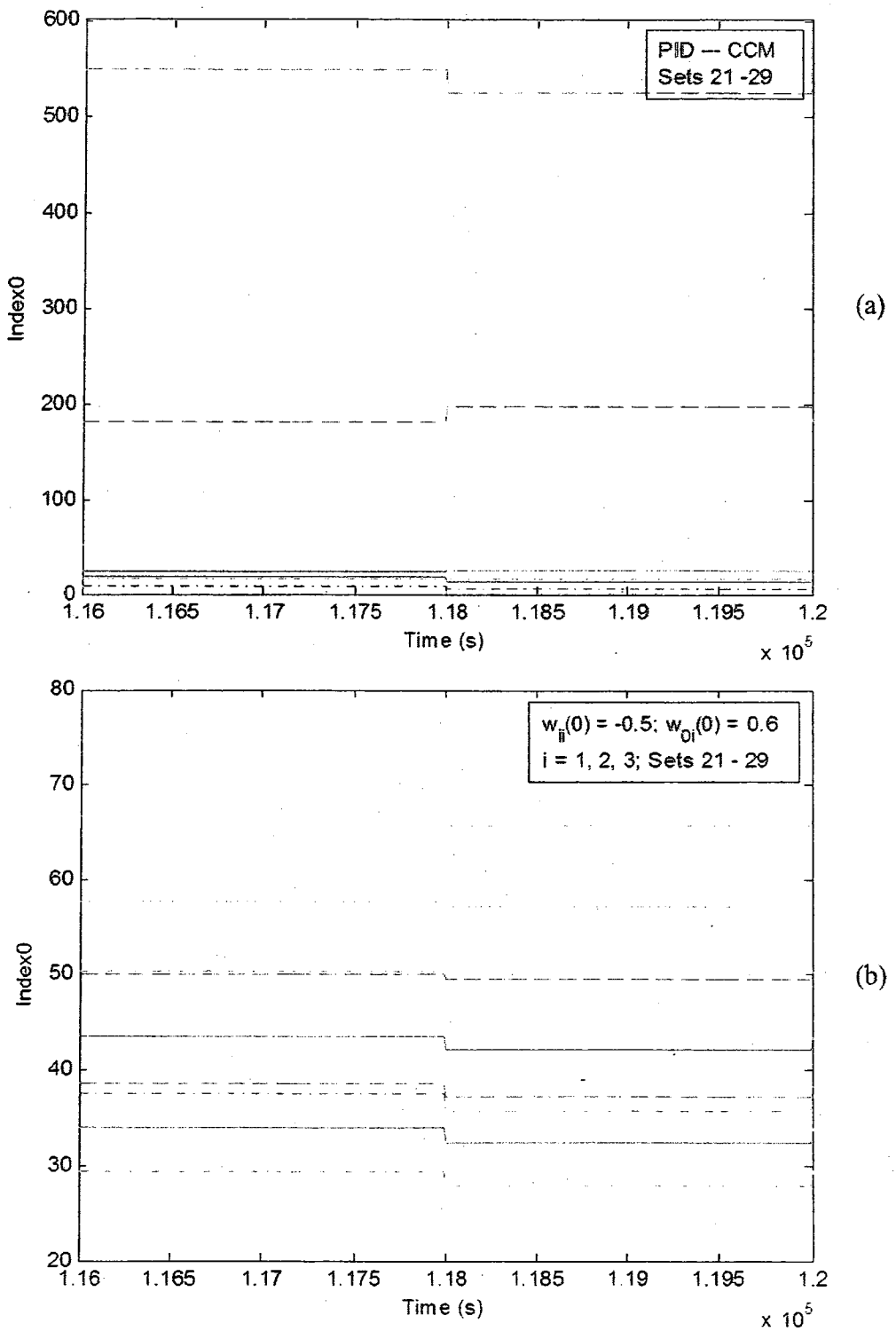

Figure 5.11 Comparison of CCM-PID and Adaptive NN control Index for plant sets 21 to 29

In the following the impact of the initial values of w_{ii}, w_{0i}, and $A0$ on training and convergence is illustrated. Consider plant set 26. With the previous values chosen in Figure 5.10 the step response was not fast enough. To achieve faster step response and shorter training process, it was observed that a smaller initial value of w_{ii} is needed. From Figure 5.12 (a), we can see that the step response for $w_{ii}(0)$ = -2.0 is faster than the step response for $w_{ii}(0)$ = -0.5, and has less overshoot than the step response for $w_{ii}(0)$ = -3.5. From Figure 5.12 (b), we note that the maximum index value for $w_{ii}(0)$ = -2.0 is the smallest of the three. In addition, a lower value of $A0$ combined with $w_{ii}(0)$ = -2.0 resulted in improved step response and lower absolute index value. Figure 5.12 (c) and (d) show the improved responses.

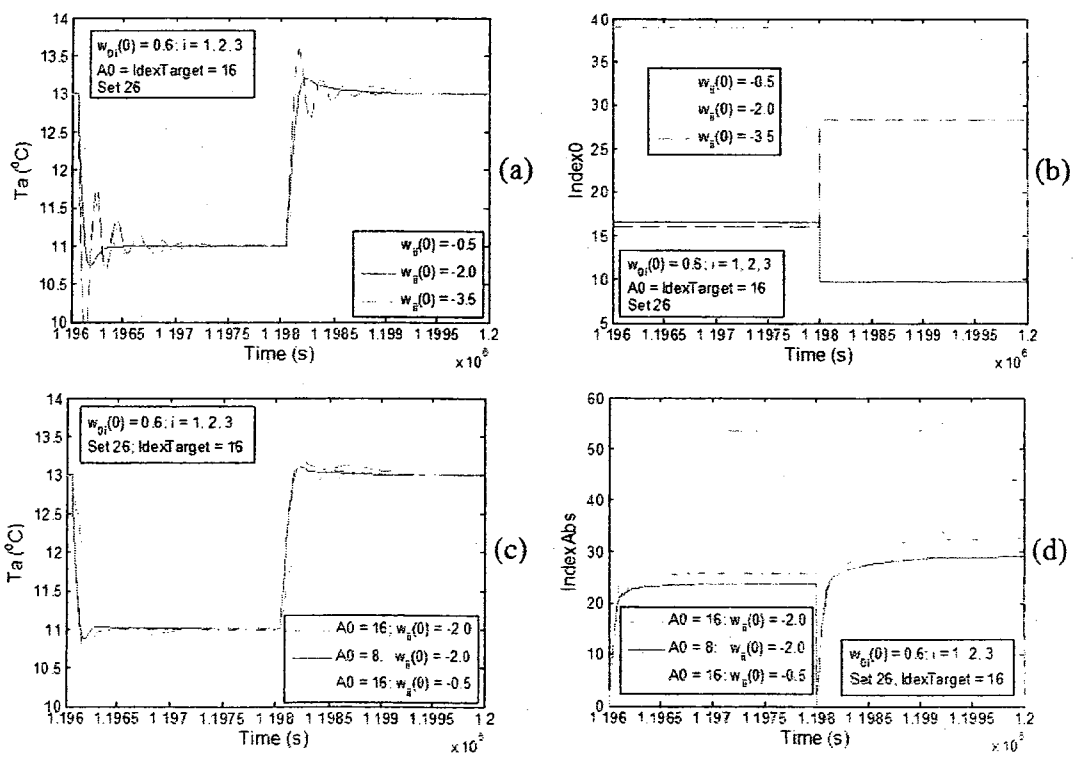

Figure 5.12 Effect of w_{ii} and $A0$ for Plant Set 26

Figure 5.13 illustrates the impact of training parameter $w_{05}(0)$ and index target on step responses. As shown in Figure 5.13 (c) and (d) $w_{05}(0) = 0.5$ gives better performance than $w_{05}(0) = 0.25$, 0.75 and 1.0. Figure 5.13 (a) and (b) show that $w_{05}(0) = 0.5$ with *IndexTarget* = 20 has very good performance and can reach the index target in the chosen simulation time. Also $w_{05}(0) = 0.5$ with *IndexTarget* = 16 has good performance too, but the index target is too high and hard to reach.

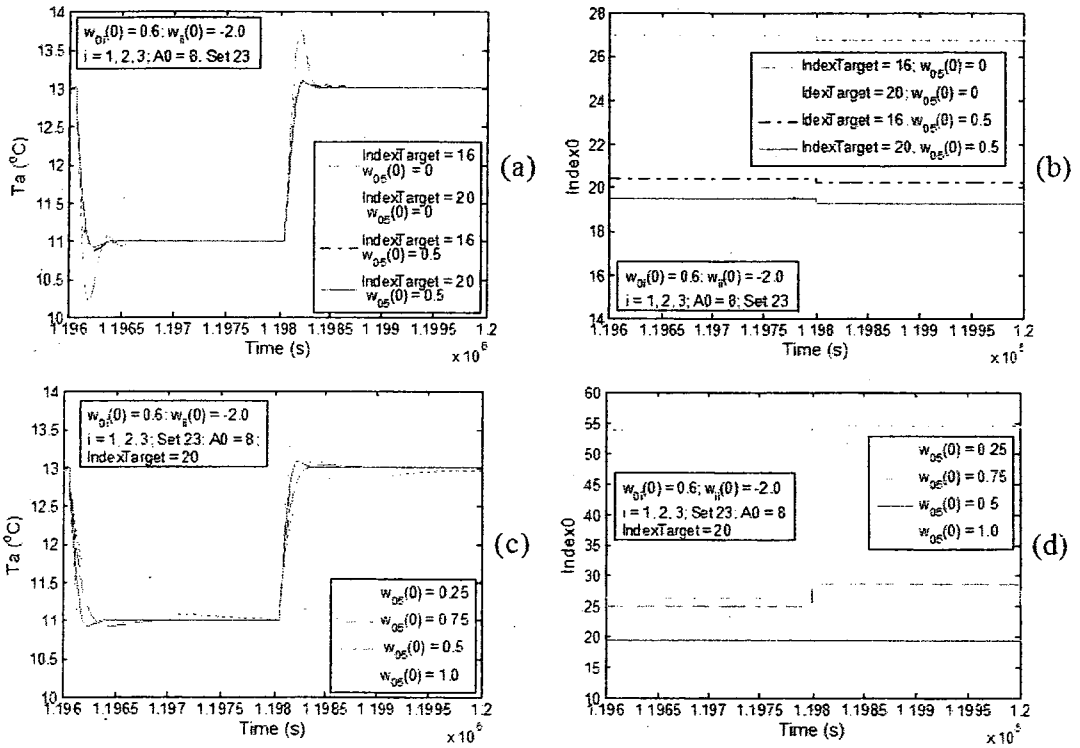

Figure 5.13 Effect of w_{05} and IndexTarget for Set 23

In the following the impact of learning rate is explored. The learning rate cannot be too high or too low. A too high learning rate will never reach the target solution and a too low learning rate will take too long time to get to the target solution. Figure 5.14 (a) and Figure 5.14 (b) show that the learning parameter $\eta_0 = 0.0022$ is too large for Plant

Set 23. The learning rate η_0 = 0.0022 resulted in oscillatory step response and higher Index0 than the target value. Figure 5.14 (b) shows that η_0 = 0.0003735 is too small because the target index hasn't been reached. However, the learning rates between η_0 = 0.000747 to 0.0015 are suitable for Plant Set 23 for training because the value of Index0 is equal to or less than the index target over the evaluation time. From Figure 5.14 (c) and Figure 5.14 (d), we can see that η_0 = 0.0011 is the best choice of the three because in a short time Index0 has already reached the target index and has faster response.

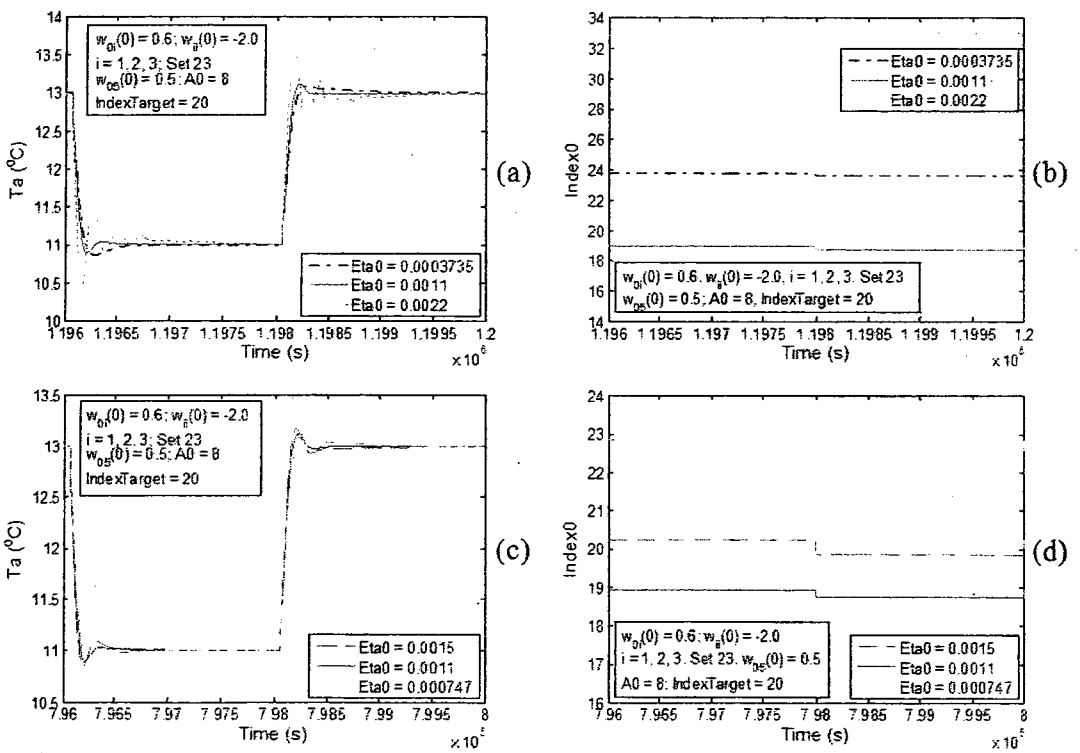

Figure 5.14 Step responses and Index0 on effect of η_0 for Set 23

Figure 5.15 shows the effect of unsuitable initial set of $w_{05}(0)$ and η_0 on responses and training time of the adaptive NN controller. Figures 5.15(a) - (b) show responses with

an unsuitable initial set. However, as the training time is increased the responses improved progressively as shown in Figures 5.15 (c) – (d). Good initial values can be obtained from a few trial and error simulation runs.

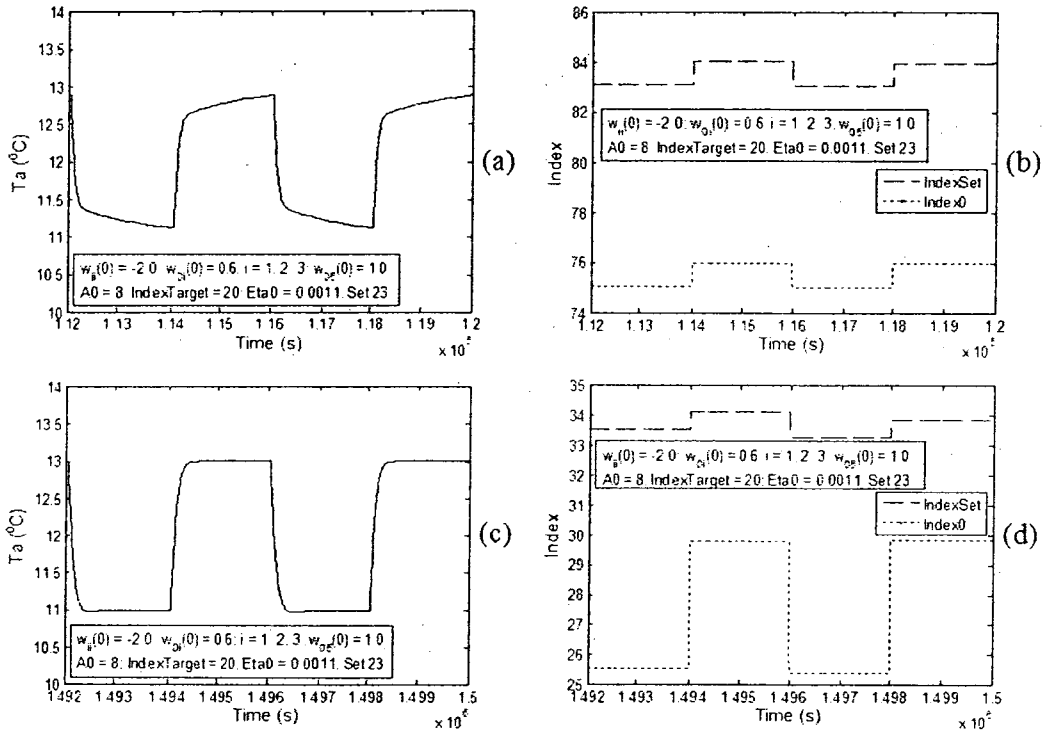

Figure 5.15 Step responses and Indexes with poor parameter selection for Set 23

Set	1	2	3	4	5	6	7	8	9
$w_{ii}(0)$	-1.2	-1.2	-1.2	-0.6	-0.6	-0.6	-0.5	-0.5	-0.5
$w_{05}(0)$	0.38	0.38	0.38	0.0	0.0	0.0	0.0	0.0	0.0
Set	11	12	13	14	15	16	17	18	19
$w_{ii}(0)$	-2.0	-2.0	-2.0	-1.3	-1.3	-1.3	-0.9	-0.9	-0.9
$w_{05}(0)$	0.51	0.51	0.51	0.15	0.15	0.15	0.05	0.05	0.05
Set	21	22	23	24	25	26	27	28	29
$w_{ii}(0)$	-3.0	-3.0	-3.0	-1.9	-1.9	-1.9	-1.6	-1.6	-1.6
$w_{05}(0)$	0.53	0.53	0.53	0.18	0.18	0.18	0.05	0.05	0.05

Table 5.5 Initial value selection of $w_{ii}(0)$ and $w_{05}(0)$ for fast learning for different plants

Table 5.5 shows suitable initial values of w_{ii} and w_{05} for several plant sets. These initial values resulted in fast learning and better responses and these were obtained by observing the trends from the simulation results.

The entering air temperature T_{a0} is an input of the NN model. To study the effect of T_{a0}, simulations were carried out by assuming an entering air temperature profile over a day by a sine function such as $T_{a0}(t)$ = 3.0sin(0.000072722t) + 27.0 ^{o}C. This requires choosing proper weights associated with the input T_{a0}. To this end we chose two sets $w_{44}(0)$ = 0.1; c_4 = 0.5 and $w_{44}(0)$ = 0.38; c_4 = 0.1. In each case c_{40} = 22.0 was kept constant. The responses in Figures 5.16 and 5.17 show that the adaptive neural network controller has the ability to respond to the effect of sinusoidal changes in the entering air

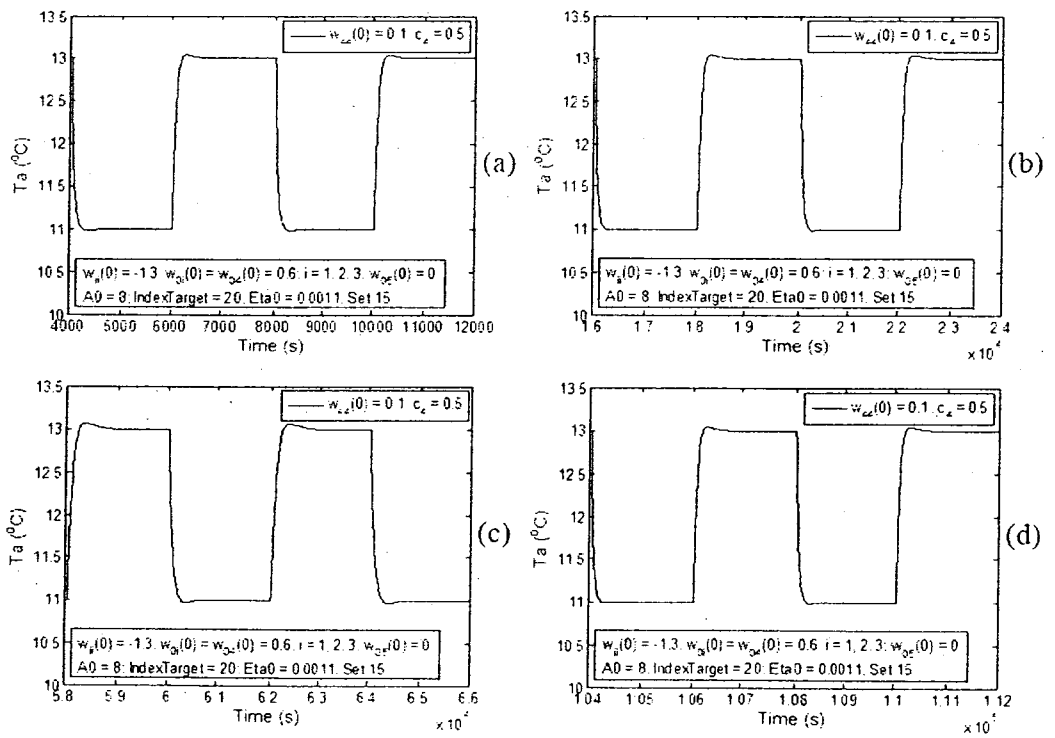

Figure 5.16 Step responses with $w_{44}(0)$ = 0.1 and c_4 = 0.5 for Set 15

temperature. The values of $c_4 = 0.5$ and $w_{44}(0) = 0.1$ were used in Figure 5.16, and $c_4 = 0.1$ and $w_{44}(0) = 0.38$ were used in Figures 5.17. Both the parameter selections resulted in fast learning processes and good responses.

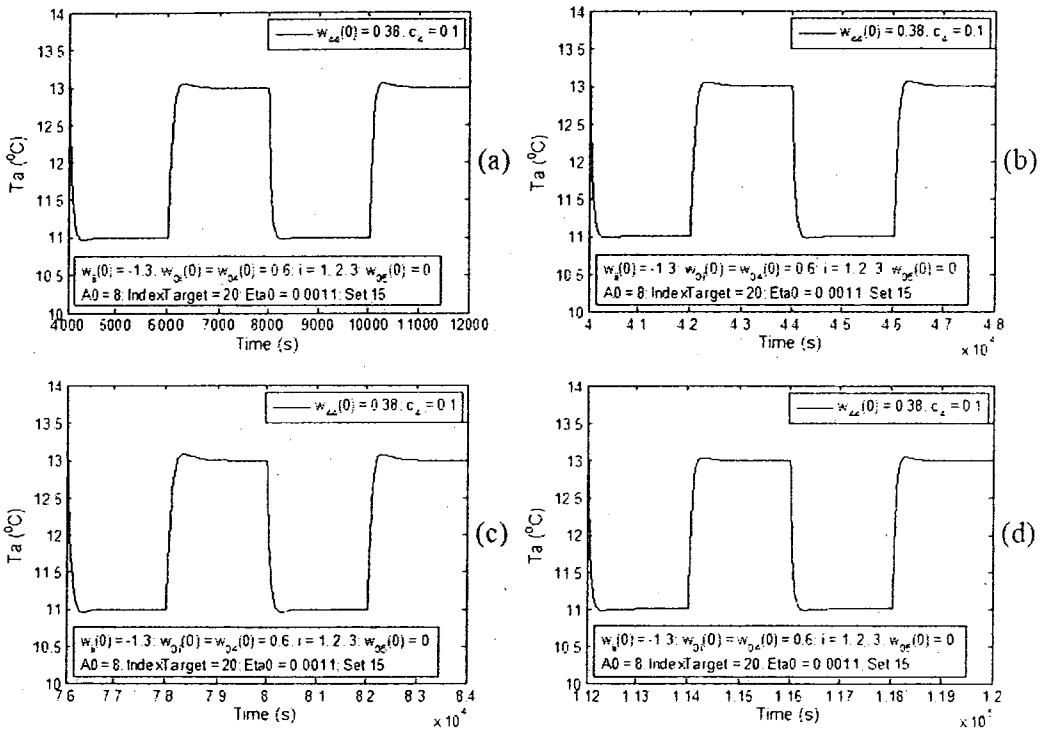

Figure 5.17 Step responses with $w_{44}(0) = 0.38$ and $c_4 = 0.1$ for Set 15

In the above section, we have discussed how to select initial, control (index and learning parameters to achieve stable step responses for the proposed adaptive neural network control to plant parameter changes. Results between the proposed adaptive neural network control and the classical CCM-PID control were made. Also guidelines for selecting proper initial parameters are given. The effect of entering air temperature was studied. The results indicate that the proposed adaptive neural network controller has strong potential to improve robustness and performance of HVAC system. In the next section, experiments will be conducted to verify these findings.

5.5 Experimental Studies

To test the proposed neural network control, experiments were conducted. The experimental control system schematic diagram of the two-zone VAV-HVAC Test Facility is shown in Figure 5.18.

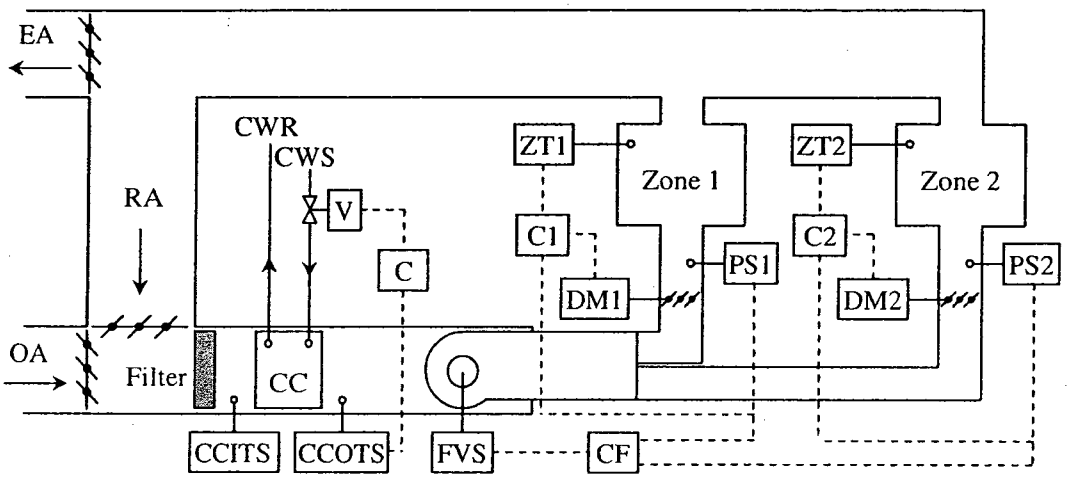

Figure 5.18 Schematic diagram of the VAV-HVAC system and its' controls

The test facility is located in the Thermal Environment Control Lab of Concordia University. In the test facility, DM1 and DM2 are damper motors that adjust the damper position to modulate required airflow rate to zone 1 and zone 2 respectively. The controllers C1 and C2 modulate the dampers. Chilled water is supplied to the cooling coil (CC) from a 2-ton water-cooled chiller and a storage tank unit. The controller C is used to control the discharge air temperature (CCOTS) of the cooling coil through the actuator V to modulate the water flow rate. CF is the controller to adjust total airflow rate in the system by controlling the fan motor speed and FVS is the actuator for the fan motor. The test facility consists of several local control loops including the discharge air control loop. A list of sensors used and their accuracy is given in Appendix. Figure 5.19 shows the discharge air system.

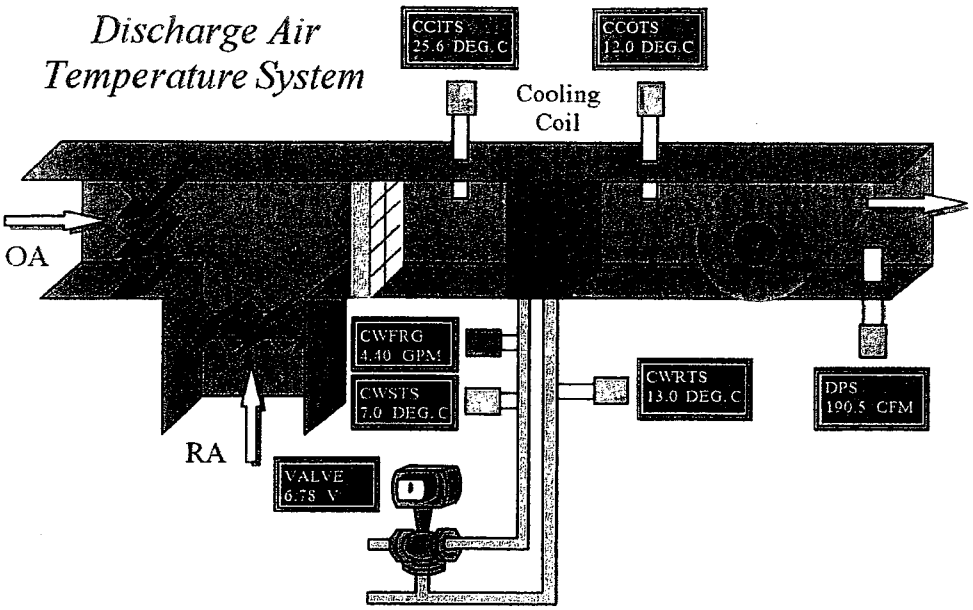

Figure 5.19 Discharge air temperature control system implementation

The proposed neural network controller was tested in the discharge air temperature control loop shown above. In the discharge air temperature control system as shown in Figure 5.19, outdoor air (OA) and room return air (RA) are mixed and filtered before entering the cooling coil. Air entering the cooling coil at temperature (CCITS) is cooled to the discharge air temperature (CCOTS), which should track the desired discharge air temperature (ValSP), by modulating the flow rate of chilled water by a motorized three-way valve controlled by the controller output (VALVE in voltage). The airflow rate in the system is measured by measuring the differential pressure (DPS), which is converted to airflow rate in cubic feet per minute (CFM). The other variable names used in the experimental system are defined as follows. DAMP1 is the control input of the damper in the duct to zone 1. DAMP2 is the control input of the damper in the duct to zone 2. FAN is the control input of the fan. CWSTS is the chilled water supply temperature. CWRTS is the water temperature leaving the cooling coil. The

measured airflow rate to each zone is DPS001 to zone 1 and DPS002 to zone 2 in MA. To simplify the entire system, the dampers and fan were set at constant position (open loop control). The load changes for each zone were simulated by using individual electric baseboard heaters.

An open-loop test for the discharge air temperature control loop was conducted on March 25, 2008. Figure 5.20 shows the test result. From the open-loop test results, we note that the control valve exhibits dead-zone nonlinearity identified in the figure. It is important for the controller to mitigate the effect of dead zone on the output responses of the system. This will be discussed later in this chapter.

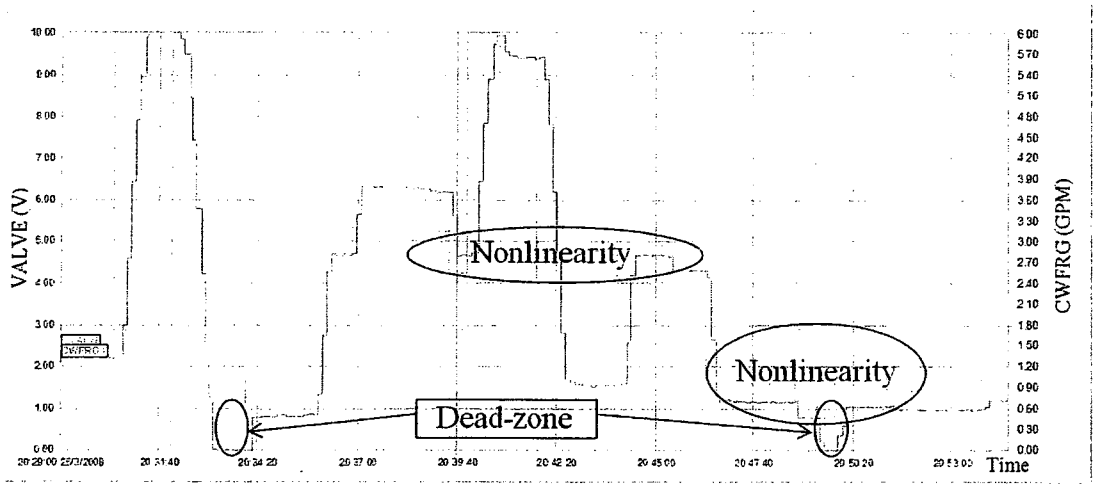

Figure 5.20 Open-loop tests for chilled water flow rate to its controls

Figures 5.21and 5.23 give two example results of step responses controlled by the proposed adaptive neural network controller. Figures 5.22 and 5.24 present the related indexes. The full 5-5-1 neural network structure was implemented in the experimental study using the proposed adaptive neural network controller. That is, the number of inputs of the normal neural network controller is m_j = 5 and the number of the hidden

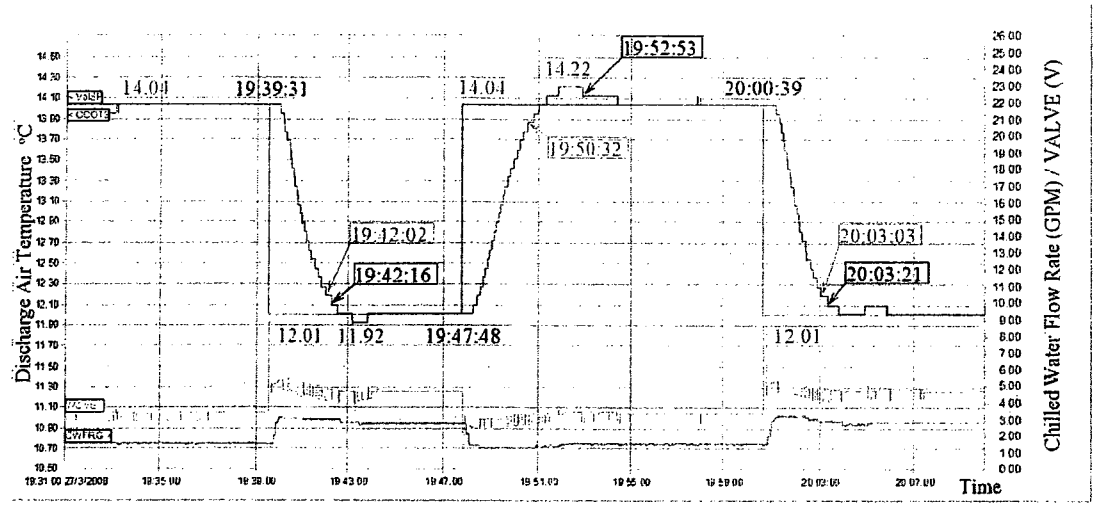

Figure 5.21 Step responses of the proposed controller under normal load conditions

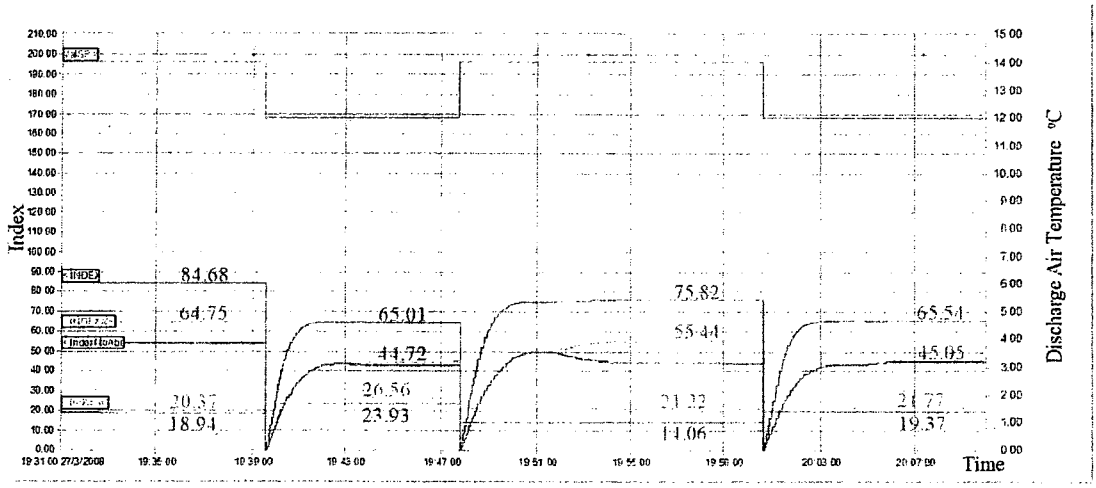

Figure 5.22 Index evolution during step response

nodes of the normal neural network controller is m_i = 5. To evaluate the system performance several indexes were used in this study. The integrated square error (ISE) is labeled as INDEX and the integrated absolute value of the error (IAE) is labeled as INDEXabs. IndexNoAbs is the integrated error and IndexSet depends on it.

The experimental results in Figures 5.21 and 5.22 correspond to the conditions and parameters depicted in Table 5.6.

Conditions		CCITS	CWSTS	DAMP1	DAMP2	FAN	HEAT1	HEAT2
		24.5°C	6.2°C	5.4V	5.8V	5V	500 watts	875 watts
Parameters	Constants	η_0	k_p	k_i	k_d	k_e	k_1	β_1
		0.0005	-1.2	-0.0143	-15.4497	0.068	0.0187	0.03
		c_1	c_{10}	c_4	c_{40}	c_5	c_{50}	α_e
		4.5	5.5	0.068	5.0	0.068	22.0	12.0
		c_i	c_d	α_4	α_5	A0	*IndexTarget*	
		85.71	13.02	0.5	0.5	8.0	25.0	
	Initial values	w_{11}	w_{22}	w_{33}	w_{44}	w_{55}	α_v	
		-0.992	-0.968	-0.96	-0.953	-0.937	0.001	
		w_{01}	w_{02}	w_{03}	w_{04}	w_{05}	w_{06}	
		0.994	0.96	1.002	0.982	0.5	0.795	

Table 5.6 Experimental conditions and parameter set 1

The setpoint (ValSP) was changed as shown in Figures 5.21 and 5.22. The proposed neural network controller is tracking the setpoint changes smoothly and fast as shown in Figure 5.21. The settling times for setpoint step-down are 151s & 144s (to within 0.18°C). The settling time for setpoint-up is 164s. The maximum overshoot is 8.9%. From Figure 5.22, we can see that Index0 < IndexSet and Index0 < IndexTarget. This means that the neural network training process has stopped during this period. The values of INDEX and INDEXabs as shown in Figure 5.22 are 84.68 & 75.82 and 64.75 & 55.44 respectively for step-up, and 65.01 & 65.54 and 44.72 & 45.05 for setpoint-down changes. These results correspond to normal load conditions depicted in Table 5.6.

Another set of experimental results under high load conditions and parameters defined in Table 5.7 are presented in Figures 5.23 and 5.24.

The step responses shown in Figure 5.23 are as fast as those in Figure 5.21 even though the zone load was higher. We note that the main reason for this is due to the fact that lower values of w_{ii} (i = 1, 2 and 3) were used to compensate for the high load.

Conditions		CCITS	CWSTS	DAMP1	DAMP2	FAN	HEAT1	HEAT2
		24.8°C	8.5°C	7.4V	5.8V	3.2V	1500 watts	1000 watts
Parameters	Constants	η_0	k_p	k_i	k_d	k_e	k_1	β_1
		0.0005	-1.2	-0.0143	-15.4497	0.068	0.0187	0.03
		c_1	c_{10}	c_4	c_{40}	c_5	c_{50}	α_e
		4.5	5.5	0.068	5.0	0.068	22.0	12.0
		c_i	c_d	α_4	α_5	A0	*IndexTarget*	
		85.71	13.02	0.5	0.5	8.0	25.0	
	Initial values	w_{11}	w_{22}	w_{33}	w_{44}	w_{55}	α_v	
		-1.282	-1.268	-1.26	1.242	1.234	0.001	
		w_{01}	w_{02}	w_{03}	w_{04}	w_{05}	w_{06}	
		0.994	0.96	1.002	0.978	0.978	0.492	

Table 5.7 Experimental conditions and parameter set 2 for high load

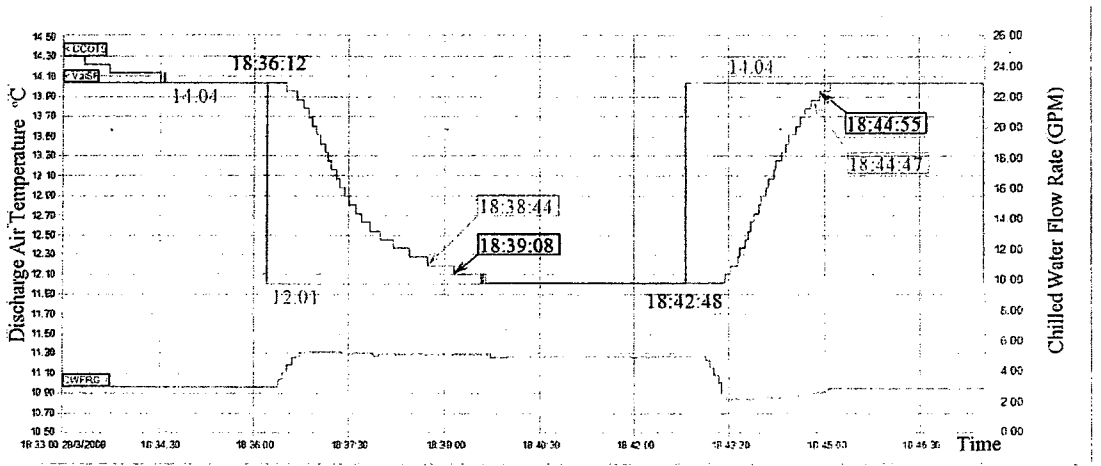

Figure 5.23 Step responses under high load conditions

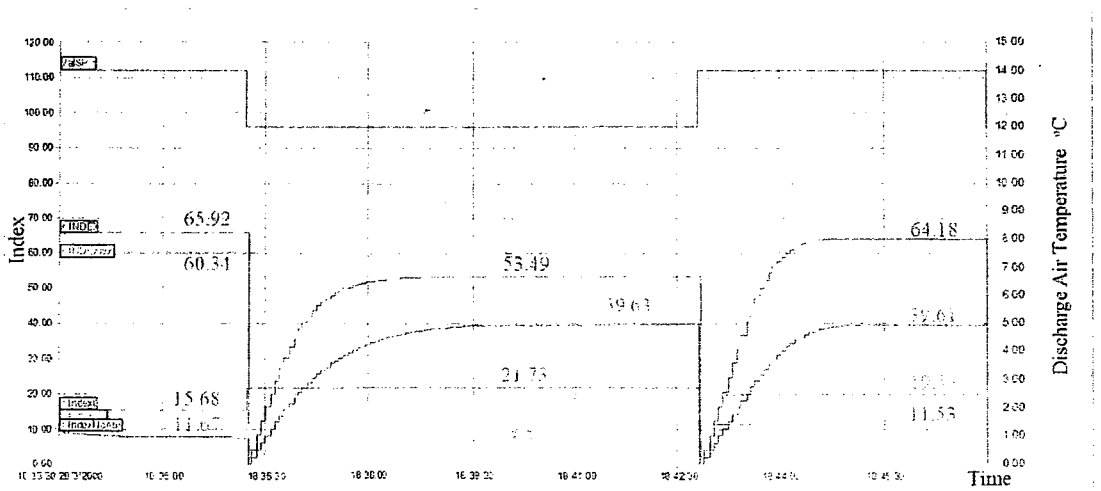

Figure 5.24 Index evolutions under high load conditions

In Figures 5.25, 5.26 and 5.27 the evolution of the training process is presented. We refer to this training as training process 1. The system was started with initial weight parameters at 9:04:12 on March 27, 2008. From Figure 5.27, we can see that the weight parameters are changing from the initial values after 9:04:12. The experimental results show that the settling time is decreasing for the step-up and step-down setpoint changes as the training in progressing (Figure 5.25). The settling times for step-up setpoint

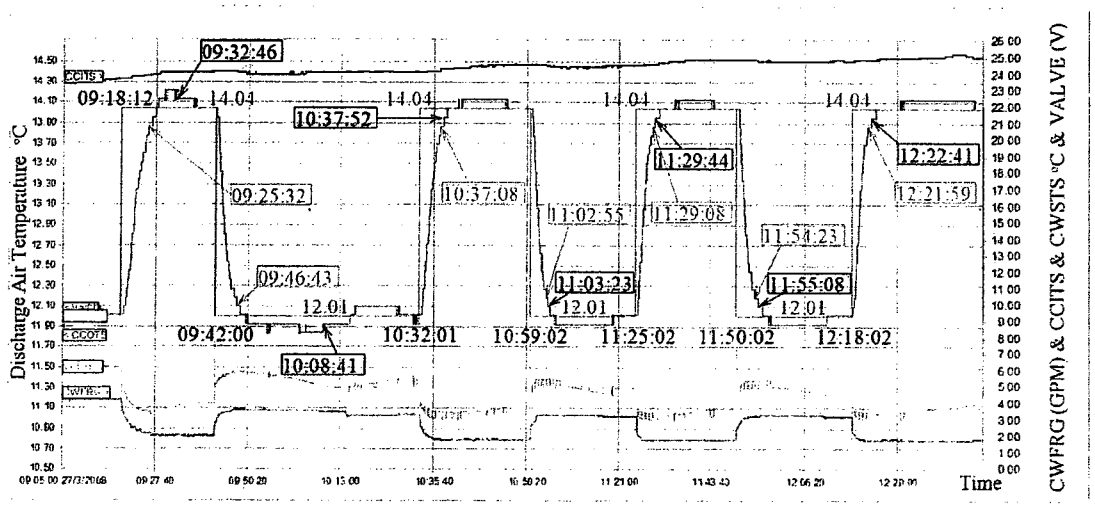

Figure 5.25 Step responses in training process 1

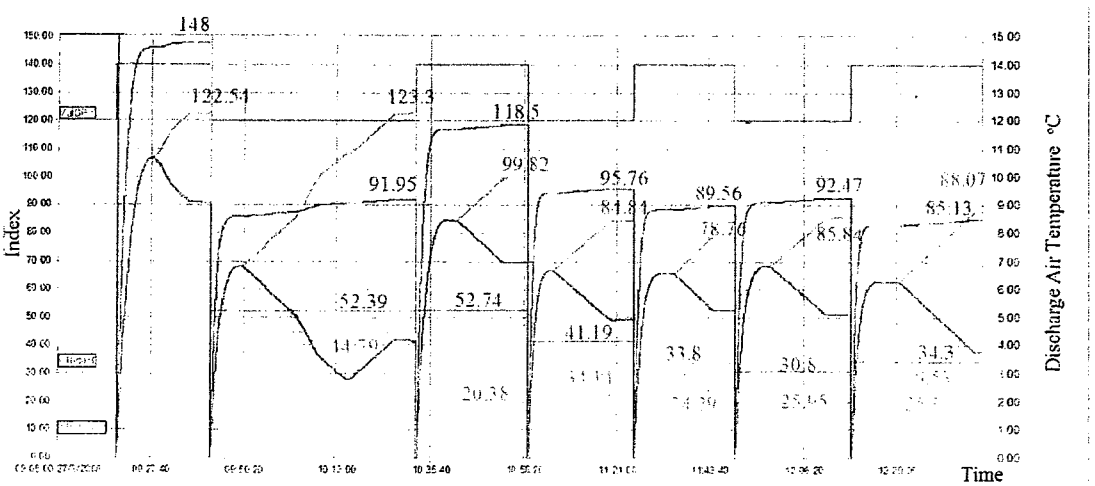

Figure 5.26 Indexes in training process 1

changes to within 0.18°C are 440s, 307s, 246s and 237s. The settling times for step-down setpoint changes to within 0.18°C are 285s, 233s and 261s respectively. From Figure 5.26, we note that INDEXabs has decreased from 122.54 to 84.84 at the fourth setpoint change.

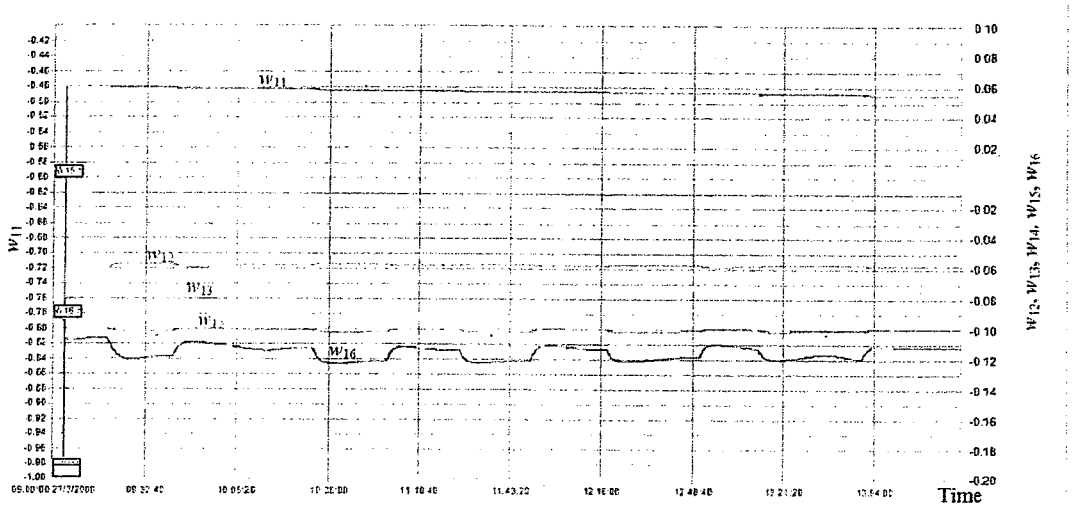

Figure 5.27 Sample weighting parameters in training process 1

From the simulation study in the previous section it was found that by increasing w_{ii} values the rise time can be decreased. The experimental results in Figures 5.28 and 5.29 verify this possibility. The step responses from 14:50:45 to 15:26:40 (settling time to within 0.18°C: 279s for step-up, 164s for step-down) are much faster than the step responses from 14:04:01 to 14:32:00 (settling time to within 0.18°C: 330s for step-up, 351s for step-down cases). The values INDEXabs (Figure 5.29) have been reduced from 83.21 to 69.73 in step-up case and from 92.86 to 50.05 in step-down setpoint case. The performance was improved because w_{ii} was decreased ($w_{ii}^{+} = w_{ii}^{-} - 0.5$) at 14:32:00. Figure 5.30 depicts the evolution of the parameter changes (w_{1j}).

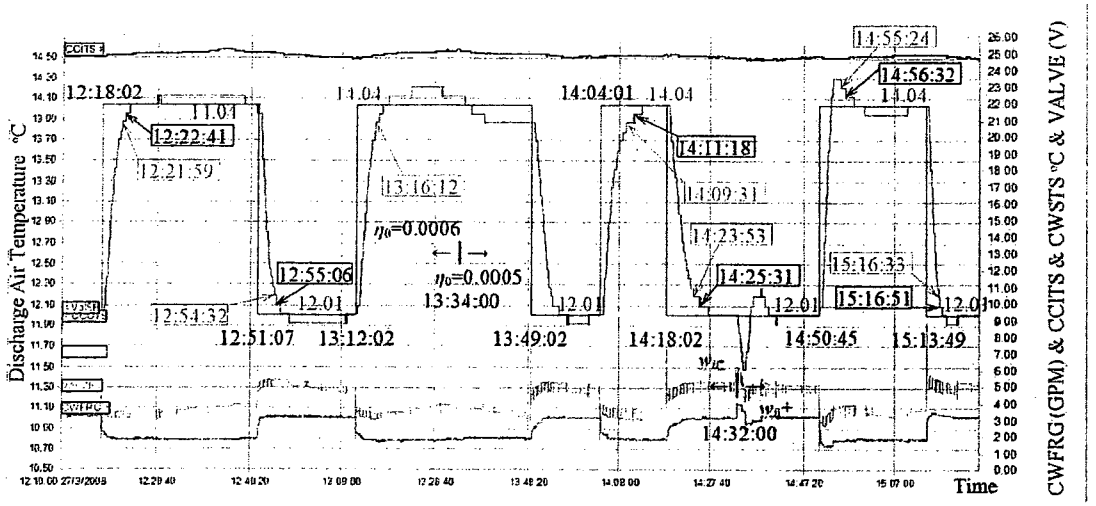

Figure 5.28 Step response comparisons for changing η_0 and w_{ii}

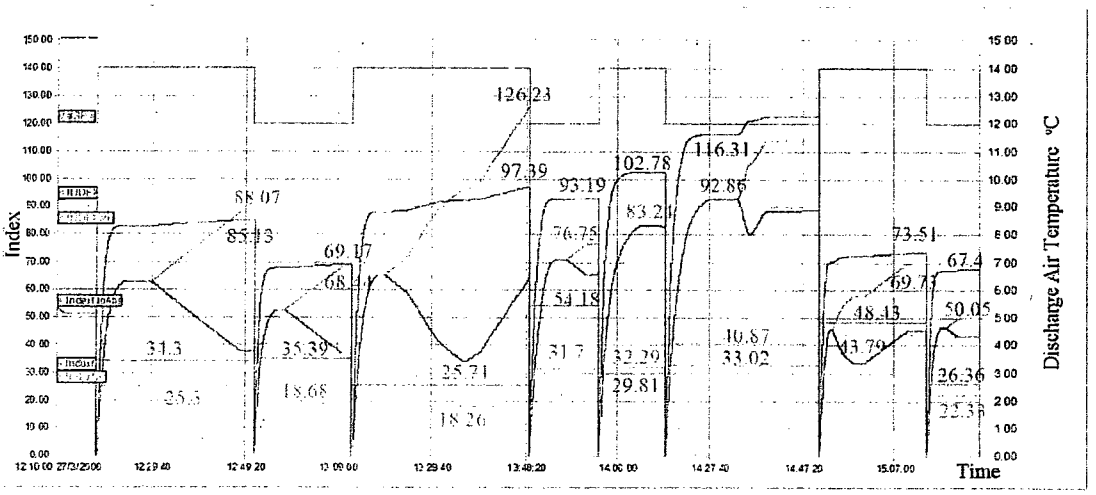

Figure 5.29 Index comparisons for changing η_0 and w_{ii}

Figure 5.28 also shows the impact of leaning rate on the step responses. The learning rate was changed at 13:34:00 from η_0 = 0.0006 to 0.0005 (Figure 5.28). From the step response results, it is noted that lower learning rate gives lower overshoot, and smooth but slow step response. To reduce the settling time with lower learning rate, we need to decrease the values of w_{ii} for i = 1, 2 and 3. Figure 5.28 presents the improvement by decreasing learning rate and w_{ii}.

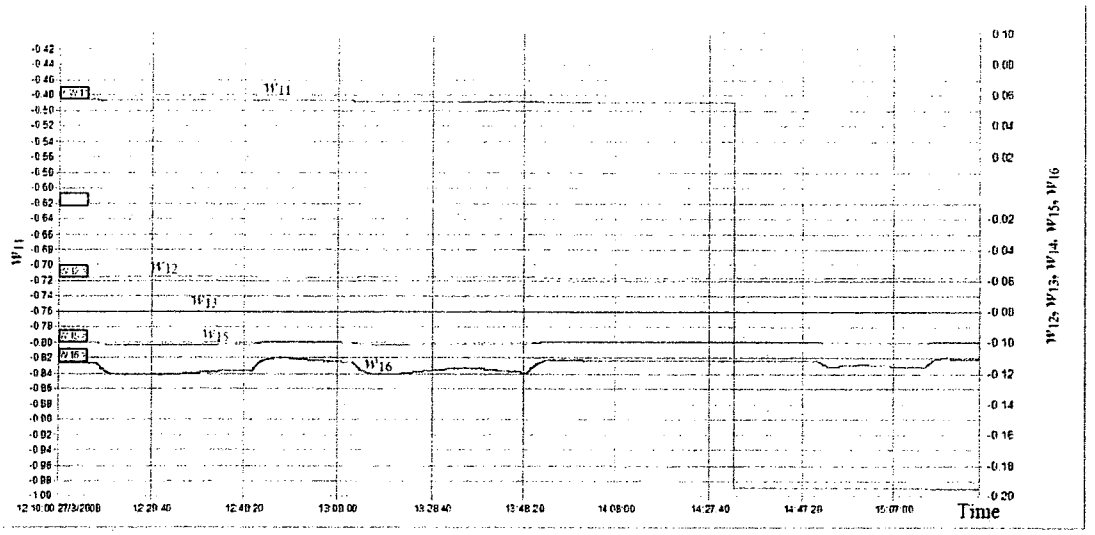

Figure 5.30 w_{1j} **for changing** η_0 **and** w_{ii}

Figures 5.25 and 5.28 also indicate that due to the nonlinearity of the valve, the chilled water flow rate (CWFRG) remains constant even though valve control input is changing. This is attributed to the mechanical dead-zone in the valve actuator system. Even under this type of nonlinearity the neural network controller still can work properly as shown by good responses of the discharge air control system.

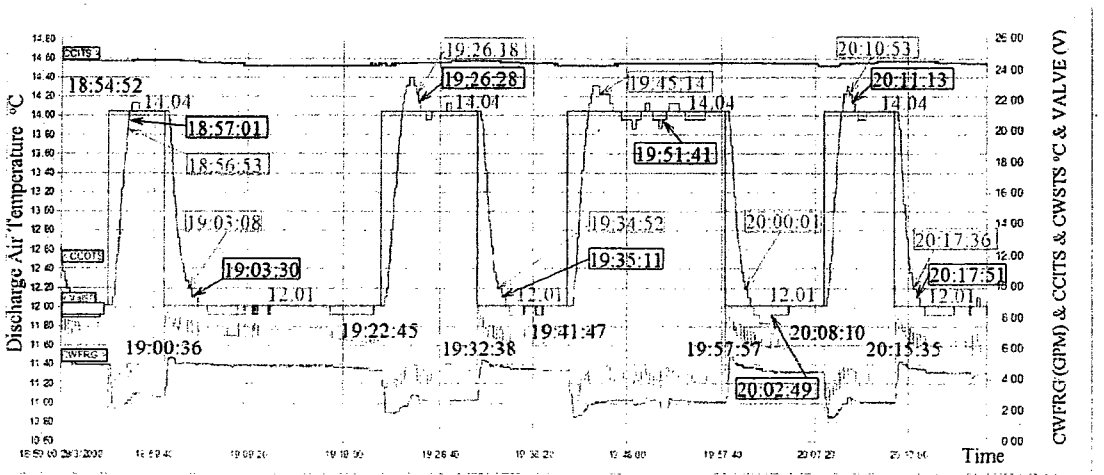

Figure 5.31 Step responses in training process 2 and for different values of FAN

The effects of disturbances on the system responses were studied. Figure 5.33 shows the change in fan speed control input at 19:17:06. This change caused change in airflow rate. As a result, overshoot increased as shown in Figure 5.31. Under those conditions the training processes was continued (Figures 5.31 and 5.32) which results in improved and fast response even though other disturbances such as the chilled water supply temperature and the entering air temperature were also changing on the system.

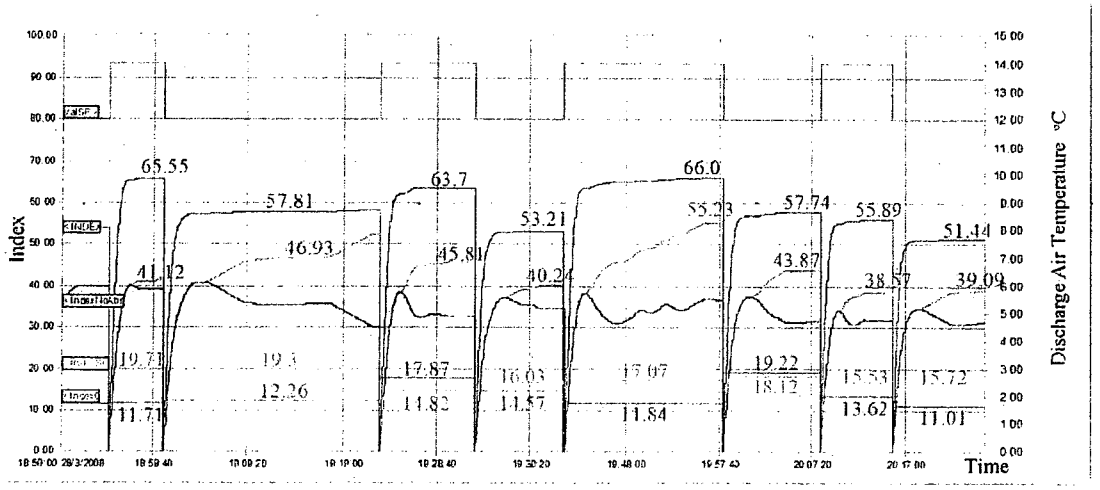

Figure 5.32 Indexes in training process 2 and for different values of FAN

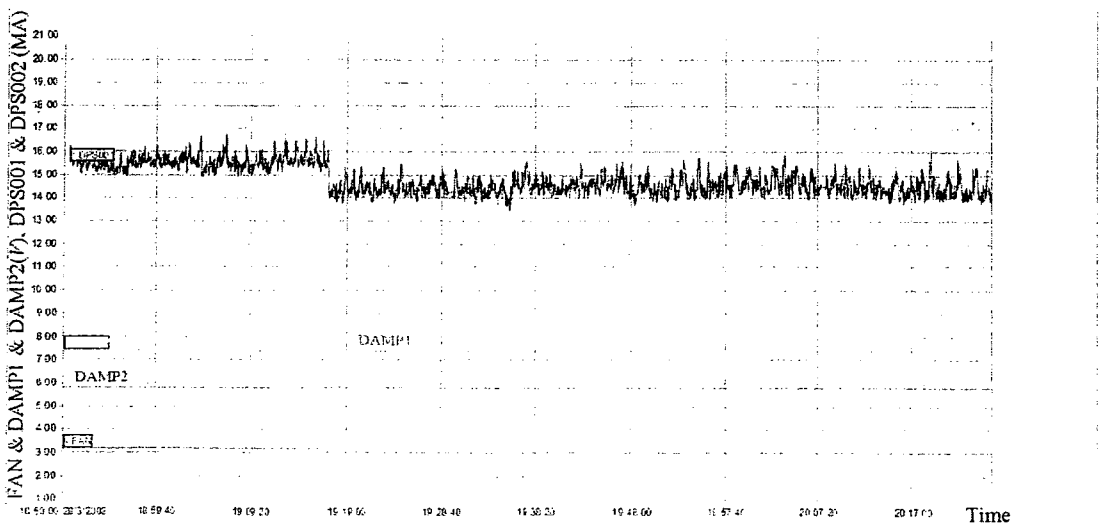

Figure 5.33 Air flow change for training process 2

The effect of load changes were studied by conducting experiments using the proposed adaptive neural network control (ANNC). Figures 5.34 and 5.35 present the results. HEAT2 to zone 2 was increased from 1000 watts to about 2000 watts at 14:35:10 March 29, 2008 and decreased to 0 watts at 15:40:30. The load changes affect the temperature of the entering air and the supply chilled water temperature as shown in Figures 5.34 and 5.35. The increased load mainly increased the entering air temperature (CCITS) and the chilled water supply temperature (CWSTS) in Figure 5.34 and the decreasing the load resulted in decreasing CCITS and CWSTS (Figure 5.35).

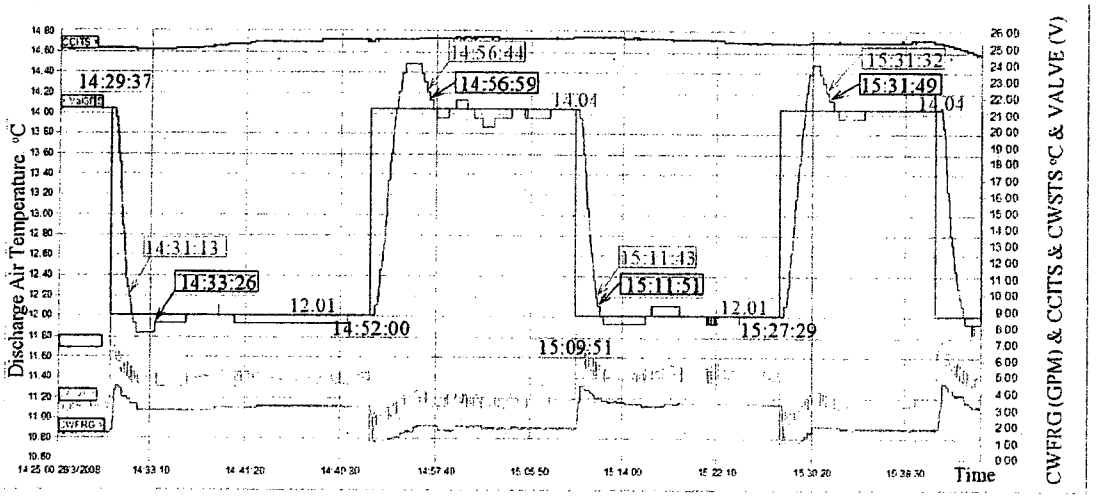

Figure 5.34 Step response of ANNC to increased heat to zone 2

Results / Time	Setpoint-down					Setpoint-up				
	Settling time		Overshoot	INDEX	INDEXabs	Settling time		Overshoot	INDEX	INDEXabs
	0.09°C	0.18°C				0.09°C	0.18°C			
14:29:37	239s	96s	8.87%	45.4	49.27					
14:52:00						299s	284s	21.67%	71.54	66.0
15:09:51	120s	112s	4.43%	51.99	42.57					
15:27:29						260s	243s	21.67%	64.95	52.16

Table 5.8 Performance results of ANNC to increased heat to zone 2

The settling times, overshoot percentages and index values under increasing load are summarized in Table 5.8.

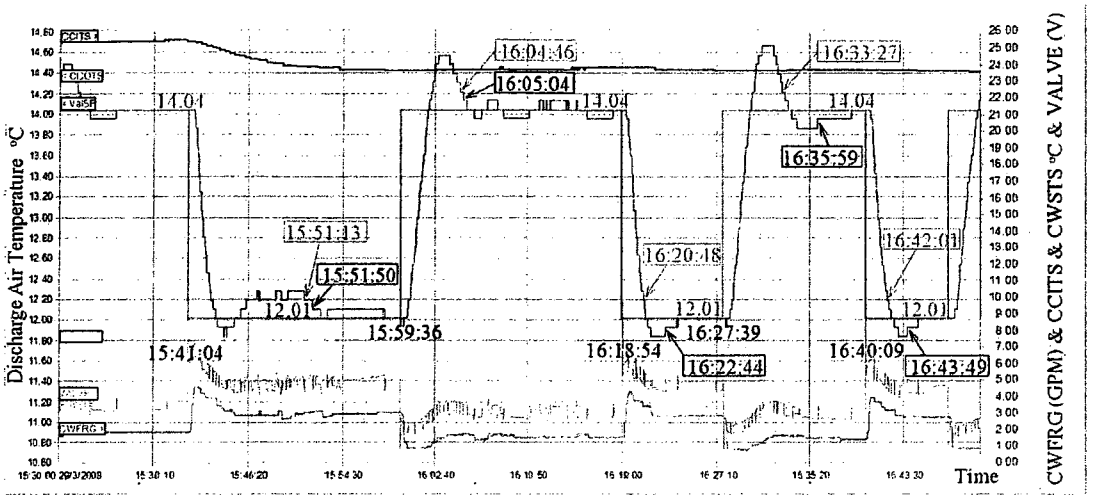

Figure 5.35 Step response of ANNC to decreased heat to zone 2

The settling times, overshoot percentages and index values under decreasing load are summarized in Table 5.9.

Results / Time	Setpoint-down					Setpoint-up				
	Settling time		Overshoot	INDEX	INDEXabs	Settling time		Overshoot	INDEX	INDEXabs
	0.09°C	0.18°C				0.09°C	0.18°C			
15:41:04	646s	609s	8.87%	65.04	66.18					
15:59:36						328s	310s	26.11%	85.12	75.33
16:18:54	230s	114s	8.87%	56.61	40.34					
16:27:39						500s	348s	30.54%	83.78	73.83
16:40:09	220s	112s	8.87%	51.61	37.17					

Table 5.9 Performance results of ANNC to decreased heat to zone 2

From Figures 5.34 and 5.35, we note that the system recognizes change in loads through its training mechanism. This can be observed by noting that increased entering air temperature caused higher chilled water mass flow rate. And a decrease in entering air

temperature due to decreasing load resulted in lower mass flow rate of chilled water (compare Figures 5.34 and 5.35).

The chilled water temperature is decreasing in Figure 5.34 and increasing in Figures 5.35. However, from the two figures we may say that decreased chilled water temperature may increase overshoot for step responses.

The air flow rate effect on the responses was also studied. Figure 5.36 shows the effect with training control parameter set to $\alpha_w = 0$ (before 17:19:21) and $\alpha_w = 1$ (after 17:19:21). The damper control input DAMP2 was changed from 5.8*V* to 7.8*V* at 16:36:00 and 17:32:00 with ValSP = 14.04 (Figure 5.38). As shown in Figure 5.36, the air flow rate change does not affect the response so much and it converges very fast.

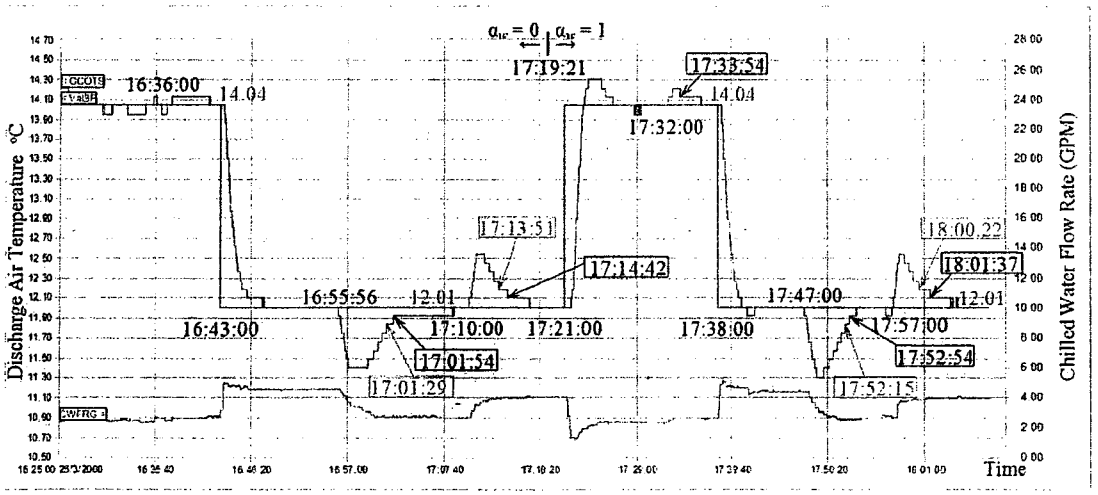

Figure 5.36 Comparison of response to dumper control changes for $\alpha_w = 0$ and $\alpha_w = 1$

With ValSP = 12.01, the changes to the damper control input were made from 7.8*V* to 3.8*V* (at 16:55:56 & 17:47:00) and 3.8*V* to 5.8*V* (at 17:10:00 & 17:57:00) as shown in Figure 5.38. As shown in Figure 5.36, the ANNC is able to maintain the

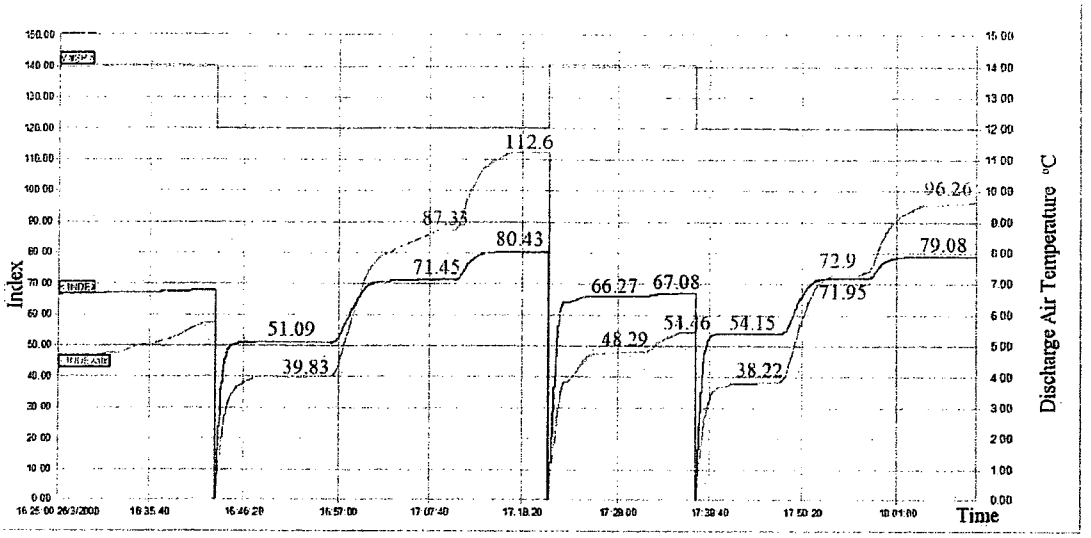

Figure 5.37 Indexes for response comparison under α_w = 0 and 1

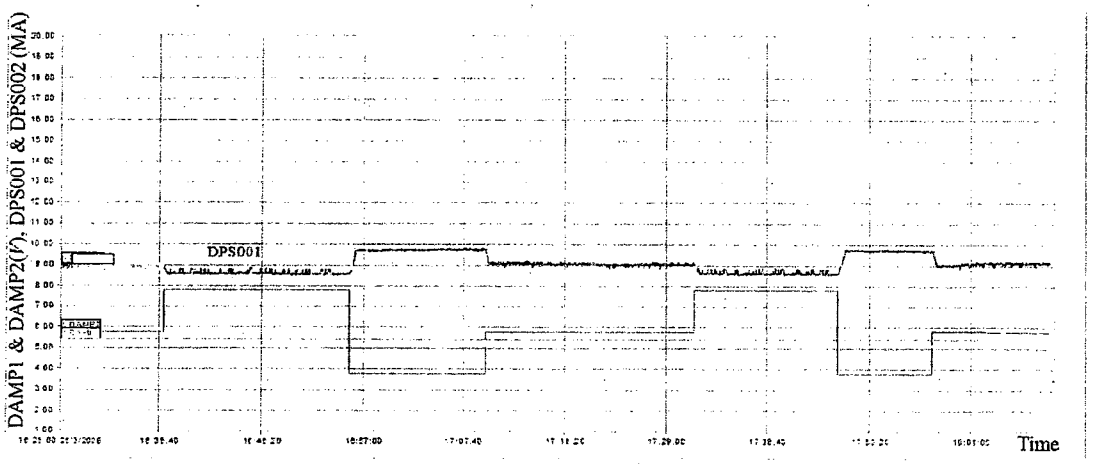

Figure 5.38 Dumper control changes for response comparison under α_w = 0 and 1

discharge air temperature near the setpoint with deviations ranging as high as 0.72°*C*. From the results, we may say that the robustness of the proposed adaptive neural network controller to the air flow changes for both $\alpha_w = 0$ and $\alpha_w = 1$ is similar, however, the robustness to the air flow changes for $\alpha_w = 1$ maybe slightly better.

The responses from the proposed adaptive neural network control (ANNC) and CCM-PID control were compared. Figure 5.39 presents the comparisons. The results

illustrate that the ANNC has better performance in step response but shows weaker performance in disturbance (airflow) rejection.

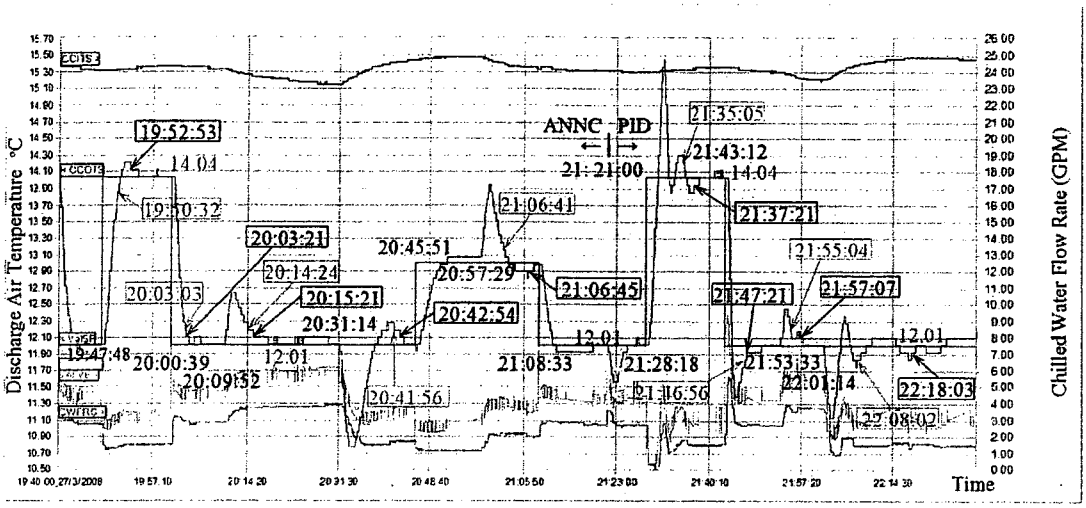

Figure 5.39 Response comparison of ANNC and PID control to dumper control changes

Figure 5.39 shows that the ANNC has lower overshoot to step response (8.87% for step-up setpoint change and 0.00% for step-down setpoint change) compared with the PID control's performance (69.46% for step-up change and 30.05% for step-down change). In addition, the step response controlled by ANNC is much faster than the step response controlled by the PID control.

The settling time and index magnitude comparisons between the two controls are summarized in Table 5.10.

Setpoint direction	Settling time				INDEX		INDEXabs	
	0.09°C		0.18°C					
	ANNC	PID	ANNC	PID	ANNC	PID	ANNC	PID
Step-up	305s	543s	174s	407s	75.82	92.35	55.44	76.35
Step-down	162s	249s	144s	224s	65.54	57.77	45.05	48.27

Table 5.10 Comparisons between ANNC and PID control

The experimental results with airflow changes were compared between the proposed ANNC and CCM-PID control. With ValSP = 12.01, damper settings were changed from 5.4*V* to 7.4*V* (at 20:09:52 & 21:53:33) and 7.4*V* to 3.4*V* (at 20:31:4 & 22:01:14). As shown in Figure 5.39, the ANNC is able to maintain the discharge air temperature near the setpoint with deviations ranging as high as 1.23°*C*. The values of IAE were 40.67 (ANNC) & 12.34 (PID) when damper control changed from 5.4*V* to 7.4*V* and 83.35 (ANNC) & 57.29 (PID) for the change from 7.4*V* to 3.4*V*. The PID control gives a better performance to air flow changes than ANNC in this case, but resulted in higher overshoot. As a result, if we need to improve the disturbance (airflow changes) rejection ability of the ANNC, it may be necessary to add the airflow rate as a new input to the ANNC.

In this section, we have presented the experimental performance results of the proposed neural network controller. The potential abilities of the ANNC were illustrated. The comparisons between the ANNC and PID control were made. It is clear that the ANNC has better step response performance in most cases. The robustness to air flow changes for the ANNC may be not better than PID control in some cases. Some experimental results show that good weight selection will give better performance right away.

5.6 Summary

In this chapter, a new adaptive neural network controller with implementable learning rules is developed. Guidelines for initializing the weights are proposed. Through simulation studies, the robustness of the proposed ANNC to wide range of plant paramter

changes are verified by comparing the results with the classical (CCM) PID controller. The simulation studies also indicate that fast and smooth step response can be achieved by ANNC. In addition, it is shown that if the selected weights are suitable the training process could be shortened; but, if the initial weight values are not good enough the training process could be very long. Experimental studies were conducted. The fastest step responses controlled by the ANNC with no overshoot are shown in Figure 5.23 with the settling time of 152s to reach within $0.18^{o}C$ for step-down setpoint change, and the 119s for step-up setpoint change. The experimental results show that the stable step responses controlled by the ANNC can be achieved in a wide range of operating conditions. Comparisons with PID control were made. The results indicate that the proposed ANNC has smooth, fast and less overshoot step responses compared to the CCM-PID control. The experimental also showed that the proposed ANNC was less responsive than the CMM-PID control in the airflow disturbance rejection. This result indicates that it is necessary to add airflow rate as an input for the ANNC. It was found that with a suitable set of the weight values faster training and better control performance can be achieved.

6. Online Adaptive Two-loop PI Control Strategy

In this chapter, the application of adaptive control strategy for zone temperature control in HVAC systems will be described. An online adaptive two-loop control strategy for VAV systems will be developed.

In modern HVAC systems, VAV control is more popular because of its energy saving potential, however it also induces interaction between zones airflow rates and contributes to uncertainty in plant parameters. Therefore, the airflow regulation in VAV systems causes difficulty in maintaining zone temperature. To adapt and compensate for the interaction and uncertainty in the VAV control system, an on-line adaptive PI&PI controller (a two-loop PI control structure) for zone temperature control is proposed in this chapter. The plant model consists of a two first-order plus dead-time (FOPDT) series models and the interconnecting variable is the airflow rate (or velocity pressure) that is measurable. The proposed controller is implemented by simulation and also on a real VAV system. The system with the proposed controller has both stronger robustness to parameter changes and good disturbance attenuation. At the same time, it makes VAV control much simpler because the velocity pressure set-point or the airflow rate request is automatically updated following the load changes.

6.1 Introduction

Typical airflow regulation in zone temperature controls of HVAC systems includes pressure independent control and pressure dependent temperature control. In the pressure independent control, it is easier to get a stable airflow response but zone

temperature set-point may not be satisfied because of plant uncertainty. In contrast, in the pressure dependent temperature control zone temperature set-point can be reached but pressure disturbance effect remains for long time resulting in a slow response. In in multi-zone systems operating in VAV or VAV-VT mode, a damper position change or a fan speed change for a new airflow requirement of a zone will affect the other zones' airflow as a result of pressure disturbance. These limitations of the typical airflow regulation in zone temperature controls will be addressed in this chapter.

To have both stronger robustness to time-varying thermal loads (reflected in parameter changes of the plant model) and lower sensitivity to airflow rate changes into other zones (disturbance effect), an on-line adaptive PI&PI controller for a VAV-HVAC system will be developed.

6.2 Typical Airflow Regulation

In this section, first the limitations of the typical airflow regulation in zone temperature controls of HVAC systems will be described by examples.

6.2.1 Pressure Independent Zone Temperature Control System

An example of the classical pressure independent zone temperature control system is shown in Figure 6.1. In the system, T_{z0} is the zone temperature with zero airflow rate to the zone and L is a constant that relates the temperature difference between T_{z0} and zone temperature and the airflow rate in the supply duct. The functional block $C_q(z)$ is a PI controller. $G_q(z)$ is the transfer function between damper control cutoff input for minimum airflow rate and difference between supply airflow rate output

and the minimum airflow rate. This relationship can be considered as first-order plus dead-time model. $Q_{\min}$ is the minimum airflow rate to the zone and D is a disturbance to the airflow rate in the supply duct. The function $G_z(z)$ is the transfer function between airflow rate in the duct to the temperature difference between T_{z0} and zone temperature T_z. This process is also considered as a first-order plus dead-time model and its' dead-time will be longer than the dead-time of $G_q(z)$. The combination of $G_q(z)$ and $G_z(z)$ constitutes a two FOPDT series model and the airflow rate is assumed to be measurable.

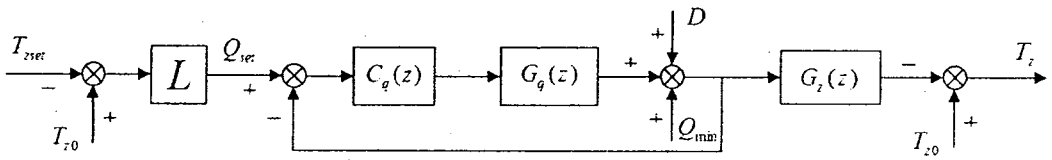

Figure 6.1 A classical pressure independent control for zones

The plant models are

$$G_q(z)=\frac{0.012}{z-0.88}z^{-2},\ G_z(z)=\frac{1}{z-0.99}z^{-9} \tag{6.1}$$

with sampling time of 4s. A maximum airflow rate of 0.0944 m^3/s (200 *cfm*) to the zone is assumed. Considering the minimum airflow rate as 40% of the maximum airflow rate, we have $Q_{\min}=0.0378\ m^3/s$ (80 *cfm*). From the steady state analysis, we have $L\times\lim_{z\to 1}G_z(z)=1$, that is $L=0.01$. Using the adaptive PI control strategy (Qu et al., for the interior control loop and the H_∞ PI tuning rules (Qu et al., 2004) for $C_q(z)$, the system was simulated in Simulink environment as shown in Figure 6.2. A saturator is added to limit the control inputs from exceeding the capacity constraints. In the following simulations, we consider that $T_{z0}=30\ ^\circ C$ and $T_{zset}=23\ ^\circ C$ for $t\geq$5000s from 24 $^\circ C$.

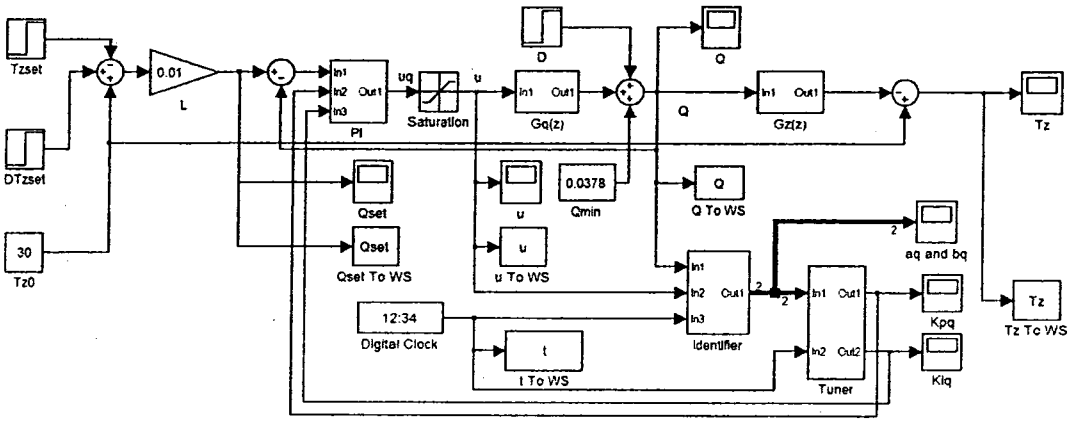

Figure 6.2 Simulation structure for independent pressure control

To show the limitation of the pressure independent control, we choose 0.101% change in the $G_z(z)$ pole value. The simulation results show that for constant L the zone temperature will shift from the original zone temperature response. The results are shown in Figure 6.3. The plot 1 is the original zone temperature response; the plot 2 is the

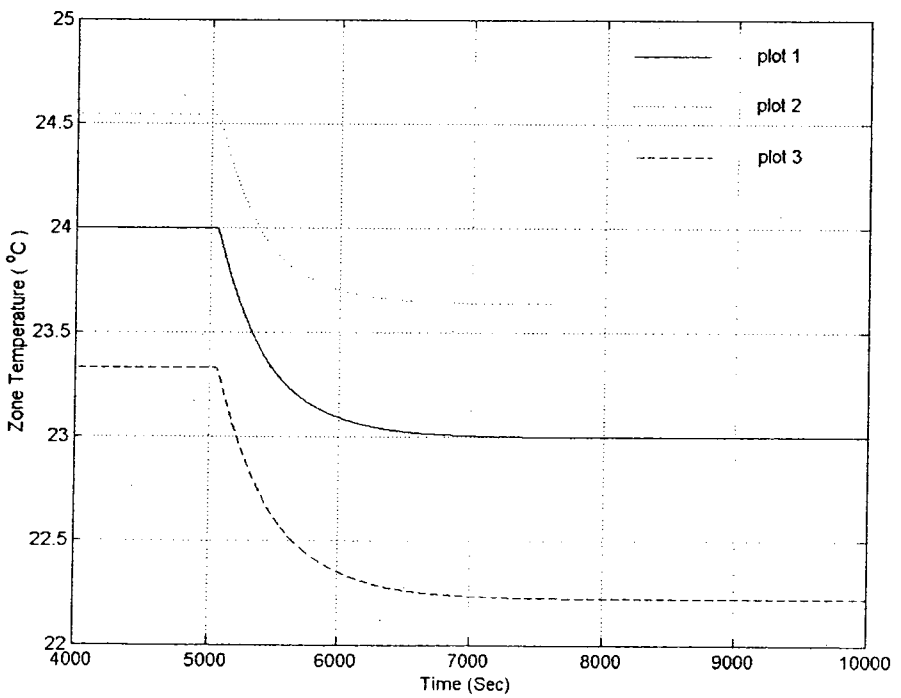

Figure 6.3 Sensibility to parameter changes in the independent pressure control

response with 0.101% decrease in the $G_z(z)$ pole value and the plot 3 is the response with 0.101% increase in the $G_z(z)$ pole value. Even though we can update the value of L by using the information from the plant $G_z(z)$, we still cannot guarantee that the zone temperature will follow the set-point in a real system because 0.101% or more error or uncertainty in parameter estimation usually exists in real systems.

In spite of this, the pressure independent control has good airflow rate (or pressure) response and shows good disturbance reduction. The simulation results in Figure 6.4 show this property of the pressure independent control. The plot 1 is the response without disturbance. The plot 2 is the response with a negative disturbance (25% of maximum

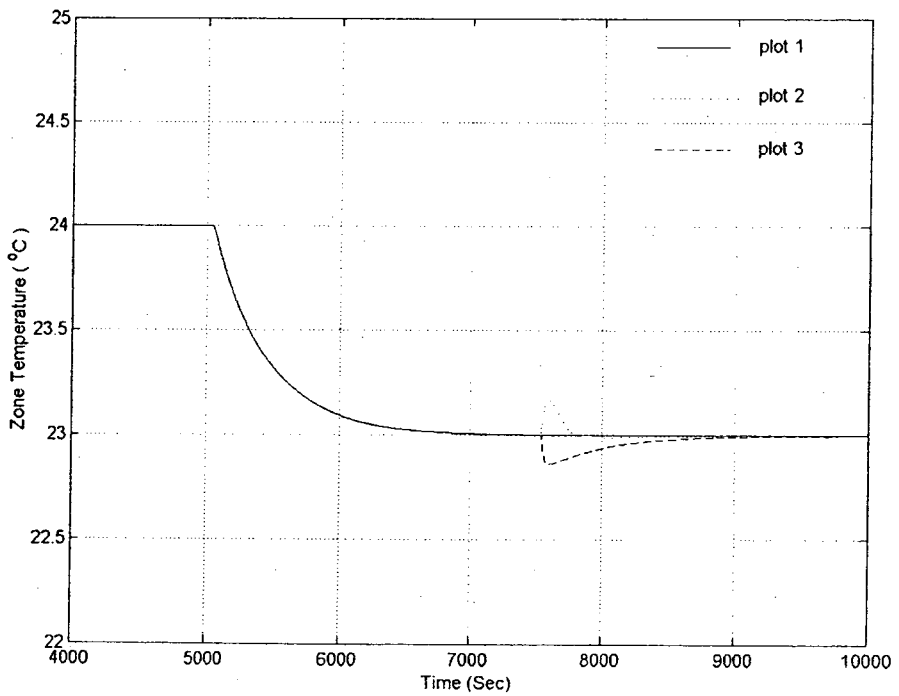

Figure 6.4 Airflow rate disturbance effect reductions in the independent pressure control system

airflow rate) that started at 7500s and the plot 3 is the response with a positive disturbance (25% of maximum airflow rate) that started at 7500s. The good airflow rate (or pressure) disturbance rejection comes from the control loop structure because the controlled variable in the control loop is the airflow rate.

6.2.2 Pressure Dependent Zone Temperature Control System

As it is well known, the pressure dependent zone temperature control system is different from the pressure independent control in terms of the choice of the controlled variable. The controller in the pressure independent control system controls airflow rate (or pressure) signal, in contrast the controller in the pressure dependent control system directly controls the zone temperature. The system diagram for the pressure dependent control is shown in Figure 6.5.

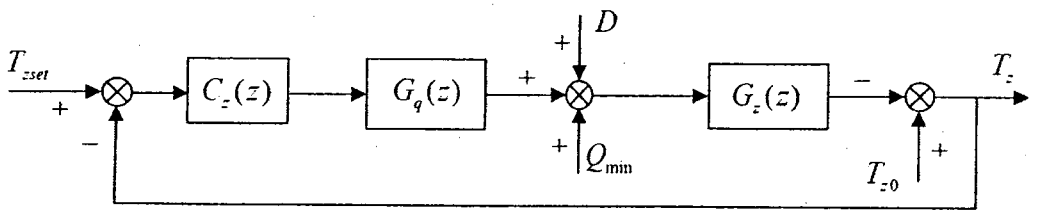

Figure 6.5 A classical pressure dependent control for zones

Considering the same plant as in Equation 6.1, the combination $G_q(z)$ and $G_z(z)$ results in a longer delay that equals to the sum of the both dead-times. Because the pole value of $G_z(z)$ is very close to 1 than the pole value of $G_q(z)$, that is, the pole of $G_z(z)$ is critical in the combination, we consider that the combination model is also FOPDT in order to facilitate the use of the online adaptive PI control strategy. With this consideration, the simulation structure for the pressure dependent control system in Simulink is constructed as shown in Figure 6.6.

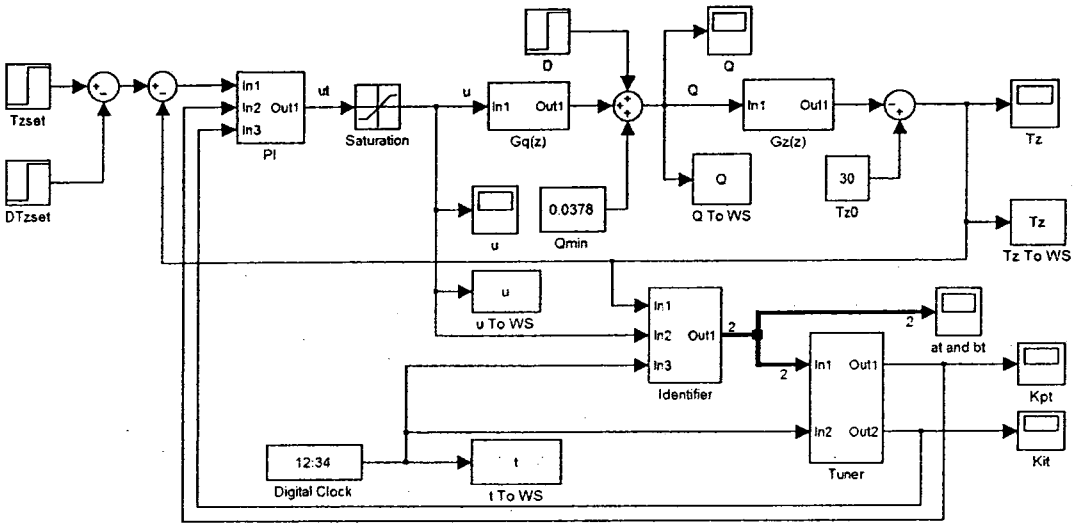

Figure 6.6 Simulation structure in Simulink for the pressure dependent control

As in the previous section, to study the sensitivity to parameter variations, we choose 0.101% changes in the $G_z(z)$ pole value. The simulation results show that the pressure dependent control system is robust to changes in magnitude of $G_z(z)$ pole value than the pressure independent control system. The reason is that $G_z(z)$ is in the inside control loop and the zone temperature is the controlled variable. The results are shown in Figure 6.7. The plot 1 is the original response that is stable and shows fast and good setpoint tracking. The plot 2 is the response with 0.101% decrease in the $G_z(z)$ pole value and the plot 3 is the response with 0.101% increase in the $G_z(z)$ pole value. These are almost the same as the plot 1.

However, the pressure dependent control system is not good in rejecting effect of disturbances in the airflow rate (or pressure) as the pressure independent control system does. In the simulation test, a 25% maximum airflow rate disturbance (increase or decrease in airflow rate) is added to the airflow rate at 7500s, the responses are

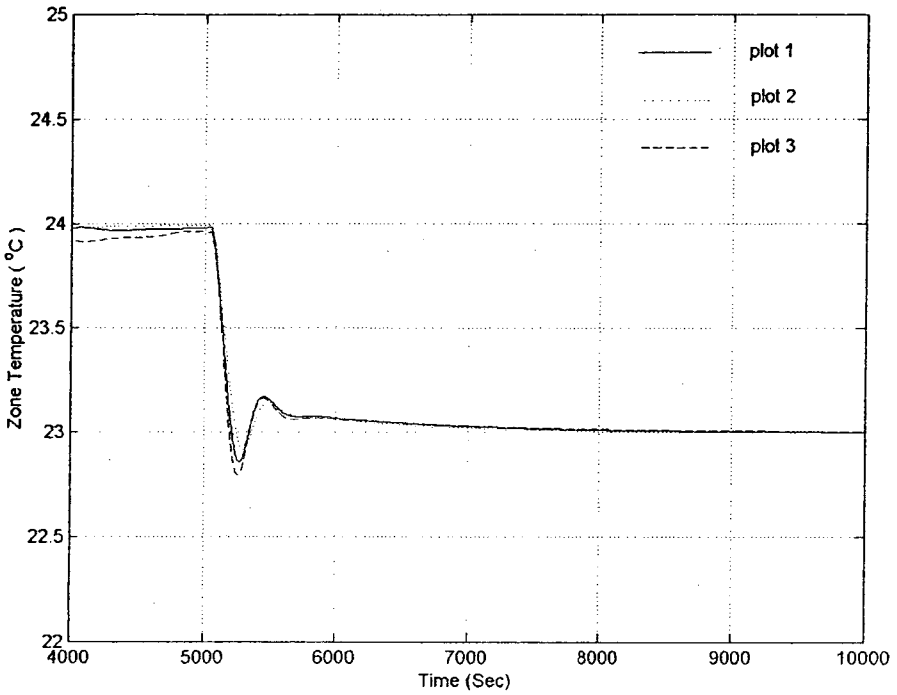

Figure 6.7 Sensibility to parameter changes in the pressure dependent control

converging. But, these are not converging fast enough. These results are shown in Figure 6.8. The plot 2 shows the response has 0.6 °C maximum offset when the airflow rate is decreased, and the plot 3 shows the response has 0.55 °C maximum offset when the airflow rate is increased.

As a result, both of the typical airflow regulation strategies currently used in zone temperature controls in HVAC systems have limitation in terms of robustness to parameter changes or airflow rate disturbance rejection. To improve this limitation a two loop control strategy to improve robustness to parameter changes and the airflow rate disturbance rejection is proposed. This is a new control structure for airflow regulation in zone temperature controls of HVAC systems. The detail will be discussed in the next section.

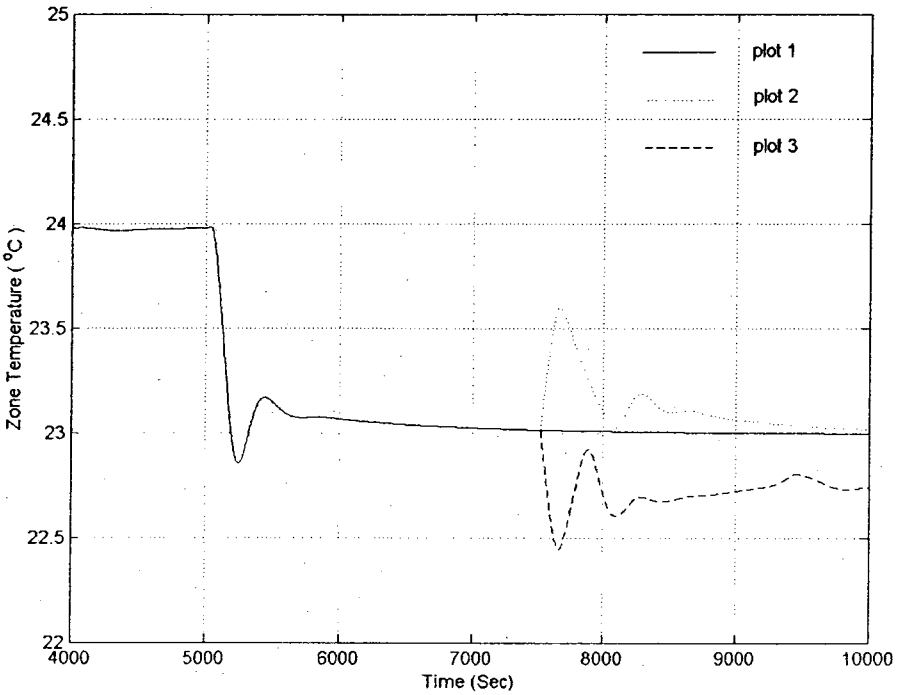

Figure 6.8 **Airflow rate disturbance effect reductions in the pressure dependent control**

6.3 Adaptive Two-Loop PI Control Strategy

To achieve good zone temperature control, robustness to parameter changes and good airflow rate disturbance rejection, an adaptive two-loop PI control structure is proposed as shown in Figure 6.9.

In the proposed adaptive two-loop PI control system, there are two controlled variables (airflow rate and zone temperature) and the sub-plant $G_z(z)$ or $G_q(z)$ is in the inside loop. $C_q(z)$ is a PI controller of the interior loop that maintains airflow rate Q (or pressure) to track the airflow rate setpoint Q_{set}. The airflow rate setpoint is updated by $C_t(z)$ that is also a PI controller in the outer loop to maintain the zone temperature T_z

close to T_{zset}. In addition, the element F is a factor that can be used to adjust the response speed of the outer control loop and give added flexibility to the zone temperature control system in commissioning. In the control structure, Q-Identifier and T-Identifier are the identifiers for the interior and exterior sub-plants respectively. The PI parameters of $C_q(z)$ and $C_t(z)$ are updated by Q-Tuner and T-Tuner respectively.

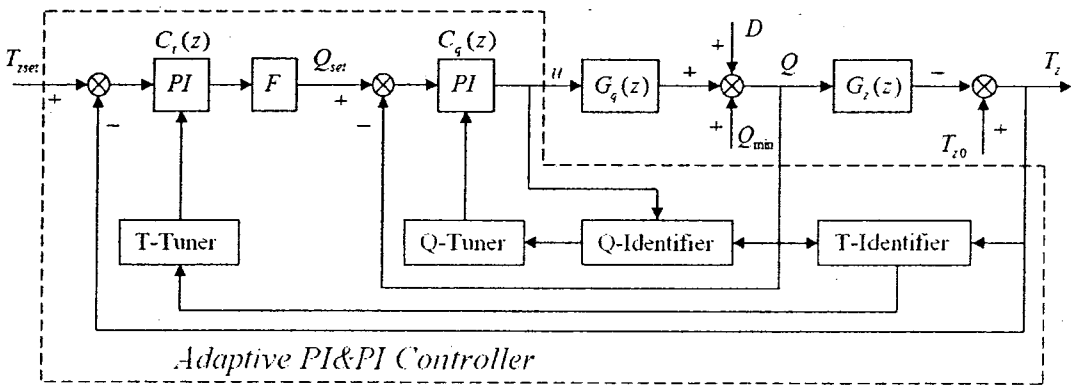

Figure 6.9 Adaptive two-loop control structure for zone temperature controls

6.3.1 Equal Consideration of the Interior Loop for the Exterior Loop

In most zone temperature control systems, the $G_z(z)$ pole value is very close to 1 compared to $G_q(z)$ pole value. In addition, in most control loops the closed loop response will be faster than the open loop response, that is, the bandwidth for the closed loop transfer function will be larger than the bandwidth for the open loop transfer function. Therefore, the bandwidth of the interior closed loop transfer function is very large compared to the bandwidth of the $G_z(z)$ transfer function. This means that the interior closed loop transfer function may be considered as constant within the bandwidth frequency of $G_z(z)$ for the adaptive two-loop control system. As a result, the PI controller

$C_t(z)$ can be designed by considering FOPDT model for the plant as well as for the PI controller $C_q(z)$.

Applying the above concept to the adaptive two-loop control system, and using the H_∞ PI tuning rules (sampling time of $T = 4\,\text{s}$), we obtain the interior PI controller given by $C_q(z) = 13.8041 + 0.4491\dfrac{T}{2}\dfrac{z+1}{z-1}$.

Figure 6.10 shows the bode plots of the interior closed loop transfer function, the transfer function $G_q(z)$ and the transfer function $G_z(z)$. It shows that within the bandwidth of the transfer function $G_z(z)$ the interior loop transfer function becomes

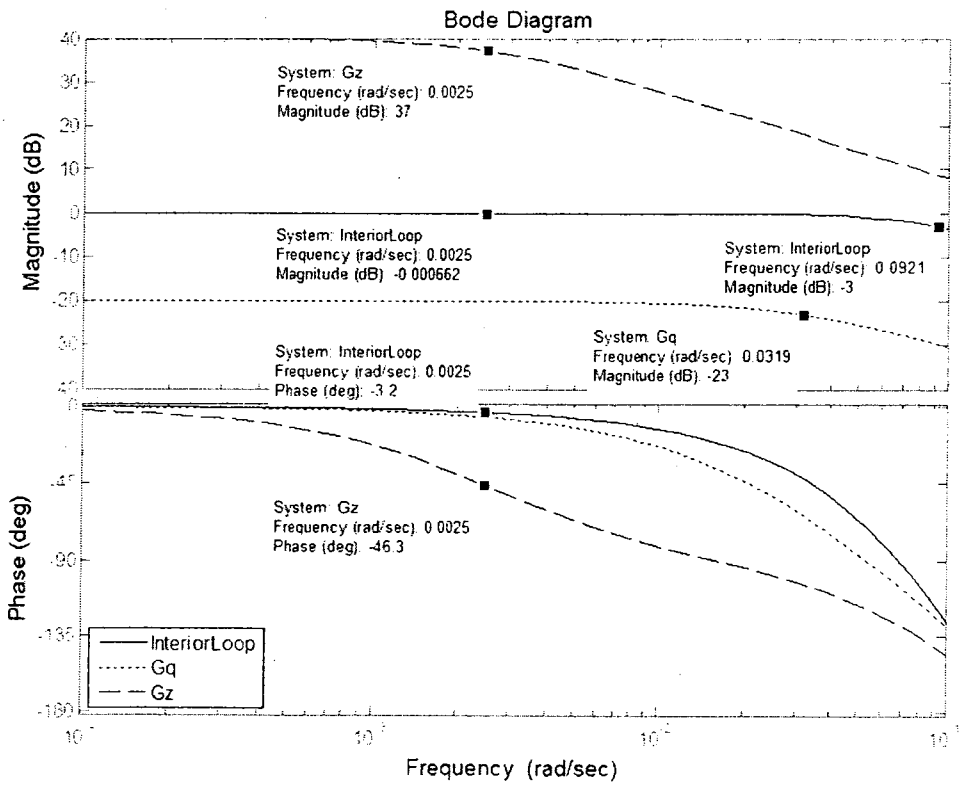

Figure 6.10 Bode plots of $G_z(z)$, $G_q(z)$ and the interior closed loop transfer function

almost a constant one. Therefore, for $F = 1$, we can say that the PI controller $C_t(z)$ can be designed by considering a plant with FOPDT model as well as the PI controller $C_q(z)$. In other words, we can consider $G_z(z)$ as an FOPDT plant to design the PI controller $C_t(z)$ by directly using the H_∞ PI tuning rules, likewise design the PI controller $C_q(z)$ by considering $G_q(z)$ as an FOPDT plant.

6.3.2 Simulation Results for the Adaptive Two-Loop Control System

From the above discussion, the inner closed control loop function with faster sub-plant is constant within the bandwidth of the function for an outer slower sub-plant. This means in the outer closed loop design the inner closed loop function can be considered as a constant. Therefore, the outer closed loop control structure becomes the same as the inner closed loop control structure. From reference (Qu et al., 2004), the H_∞ PI tuning rules and the adaptive PI control strategy can be applied to the FOPDT plant through a closed PI control loop. To this end, the simulation in Simulink for the adaptive two-loop control system for HVAC systems can be implemented as shown in Figure 6.11 and the PI parameters of $C_t(z)$ and $C_q(z)$ can be updated by the H_∞ adaptive PI tuning rules.

In the simulation, two saturators are also considered to maintain system capacity constraints. In order to show the improved performance compared with the typical airflow regulation methods discussed before, simulation runs were made with $F = 0.7$. Through analysis, it can be noted that $FC_t(z)$ updated by the H_∞ adaptive PI tuning rules is the same as the simplified optimal control algorithm with $Q_2 = 1/F$.

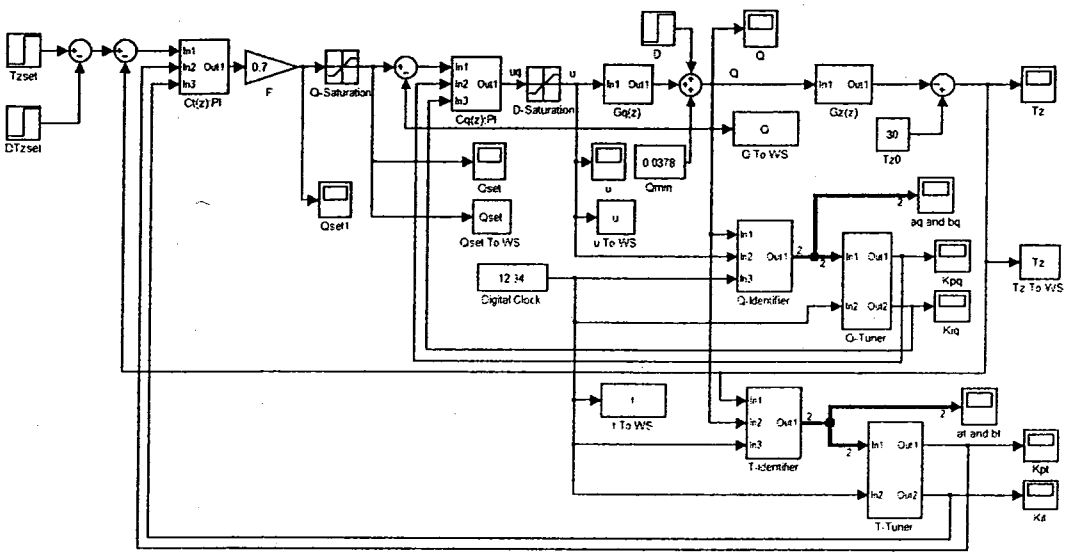

Figure 6.11 Simulation structure for the adaptive two-loop control system

Figure 6.12 shows the simulation results for 0.101% changes in the $G_z(z)$ pole value. The plot 1 is the original response that is stable and is following the setpoint faster.

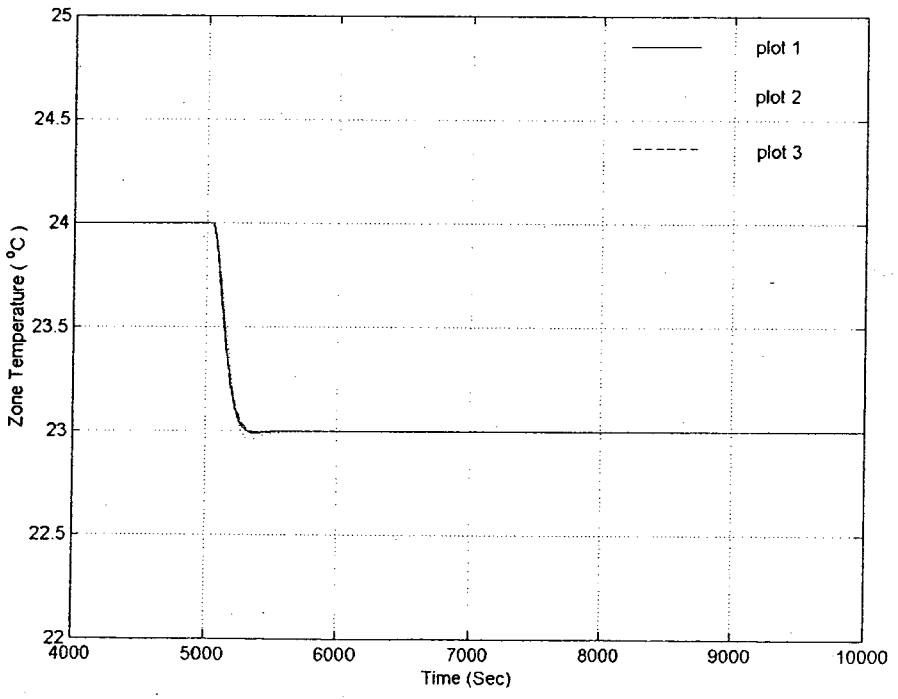

Figure 6.12 Sensibility to parameter changes in the adaptive two-loop control system

The plot 2 is the response with 0.101% decrease in the $G_z(z)$ pole value and the plot 3 is the response with 0.101% increase in the $G_z(z)$ pole value. These are almost the same as the plot 1. Comparing these results with the results in Section 6.2.2, we note that the adaptive two-loop control system has stronger robustness to parameter changes as the pressure dependent control system does and more smooth responses than the pressure dependent control system.

Figure 6.13 shows the airflow rate disturbance rejection for the adaptive two-loop control system. The plot 1 is the response without airflow rate disturbance. The plot 2 is the response with a negative disturbance starting at 7500s and the plot 3 is the response with a positive disturbance. The disturbance is 25% of maximum airflow rate. The

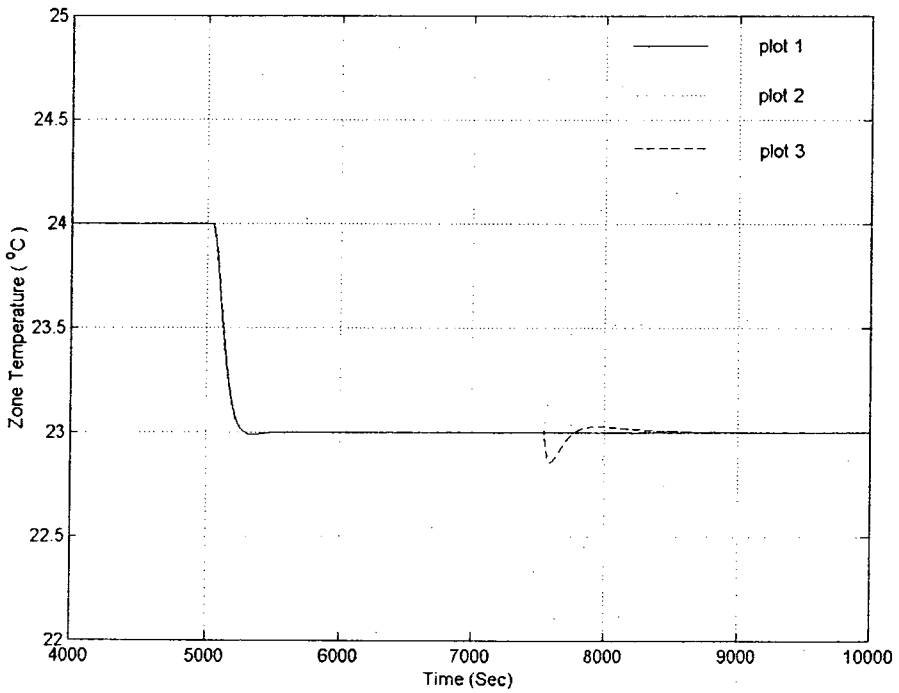

Figure 6.13 Airflow rate disturbance rejections in the adaptive two-loop control system

controller gives good airflow disturbance rejection similar to the pressure independent control system.

The results depicted in Figures 6.12 and 6.13 show robustness to parameter changes of the plant and good airflow disturbance rejection are obtained in the adaptive two-loop control system. Also the zone temperature is maintained close to the setpoint because of the PI controller used in the zone temperature control loop. However, in order to implement the two loop control one must choose F. In the next section, guidelines on the selection of F are given.

6.4 Selection of the Factor F

As mentioned in section 6.3.1, the inner closed loop can be considered as unit (linearity) within the bandwidth frequency of $G_z(z)$. But, the saturator in the inner loop could violate this situation. However, by reducing the maximum input value to the inner loop it may be possible to hold the linearity condition to be true most of the time. The factor F achieves this function in reducing the maximum input value of the inner closed loop by choosing a positive value less than one.

If we assume that the parameters of the controller $C_t(z)$ updated by the H_∞ adaptive PI control rules to the sub-plant $G_z(z)$ are K_{pt1} and K_{it1}, then we can write

$$K_{pt} = FK_{pt1},\ K_{it} = FK_{it1} \tag{6.2}$$

This is a new optimal result for the selected weighting value $Q_2 = 1/F$ which can be shown through analysis. Therefore, a smaller value of F will slow down optimal zone temperature response. The adjustable value of F gives us an additional degree of

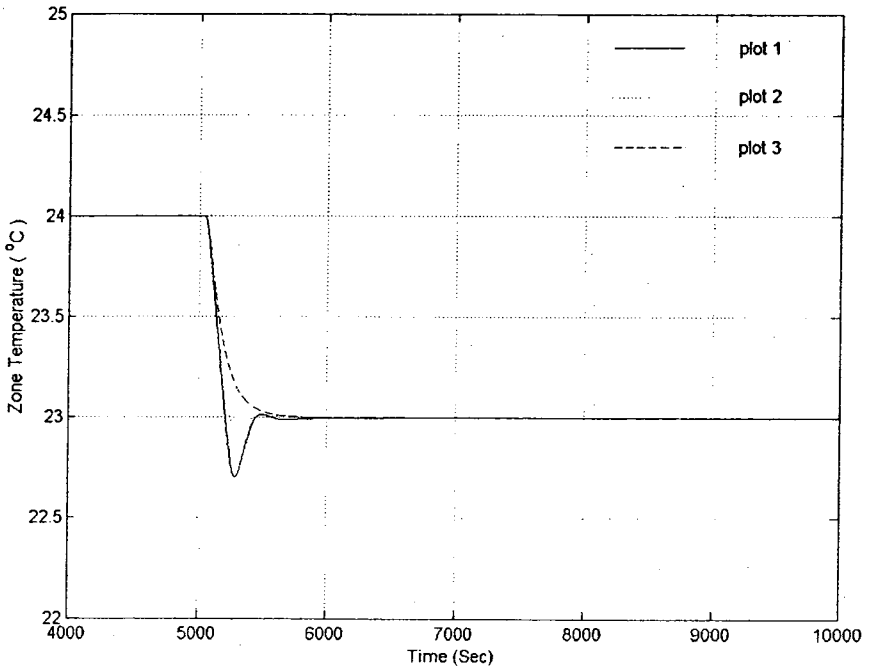

Figure 6.14 Zone temperature response for different F

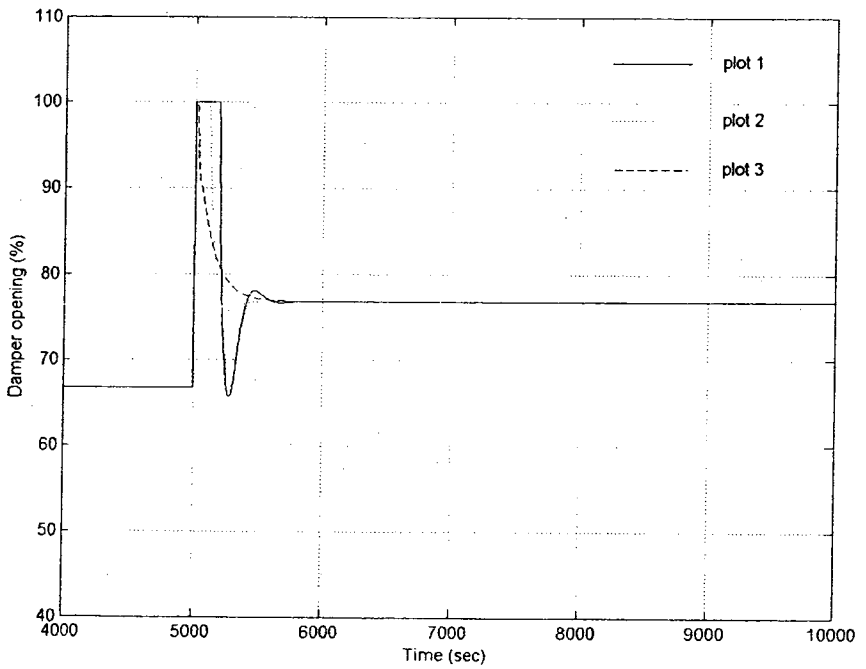

Figure 6.15 Damper opening for different F

freedom to satisfy the linearity condition for the inner closed loop. The simulation results in Figures 6.14 and 6.15 show the effect of the factor F.

In the above two figures, the plot 1 is with $F=1$; the plot 2 is for $F=0.7$ and the plot 3 is with $F=0.5$. As show in the figure, higher value of F displays the longer nonlinearity effect and causes a bigger overshoot. However, a smaller value of F has smaller nonlinearity effect and gives a better response. Therefore, in real systems, with few trials we can get a suitable value of F to achieve good responses using the adaptive two-loop PI control strategy.

6.5 Load Following Property of the Two-Loop Control

Parameter changes in the FOPDT model $G_1(z)$ reflect the load changes that require corresponding changes in airflow rate in VAV system. That is, the load changes require updating Q_{set} in the adaptive two-loop control system.

Online dynamic load changes are extremely difficult to predict. However, in the adaptive two-loop control system the dynamic load changes will lead to Q_{set} changes automatically through the temperature controller $C_1(z)$. Therefore, we only need to consider the maximum airflow rate and the minimum airflow rate for each path in the adaptive two-loop control system design.

The simulation result in Figure 6.16 shows the load following property of the adaptive two-loop control system. The plant model remains the same as given by Equation 6.1 up to 7500s and at this point the $G_2(z)$ pole value is changed to 0.991 as

shown in the first plot in Figure 6.16. The new required airflow rate Q_{set} changes automatically following the parameter change. In the meantime, the zone temperature is maintained to converge to the set-point.

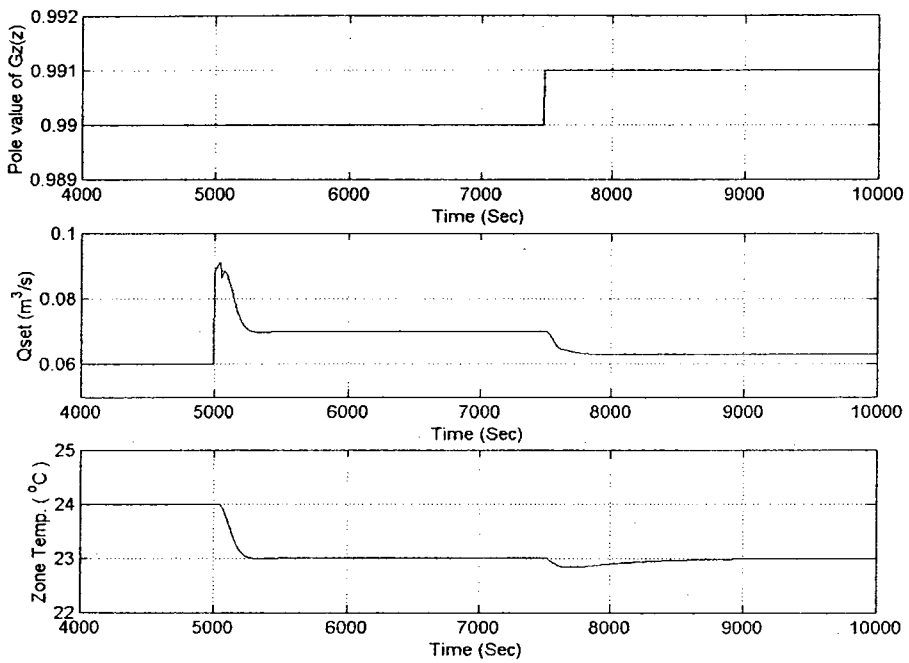

Figure 6.16 Response to the parameter change (load change) in the adaptive two-loop control system

Now, we repeat the simulation with the above mentioned conditions for the pressure independent control system. Figure 6.17 shows that the zone temperature with the change in pole value cannot be maintained close to the setpoint, because Q_{set} does not follow the parameter change as the load changes in the pressure independent control system. Comparing the adaptive two-loop control system and the pressure independent control system, it is clear that the adaptive two-loop control system has the property of

automatically adjusting Q_{set} value according to the load. This property makes the VAV implementation simple and effective.

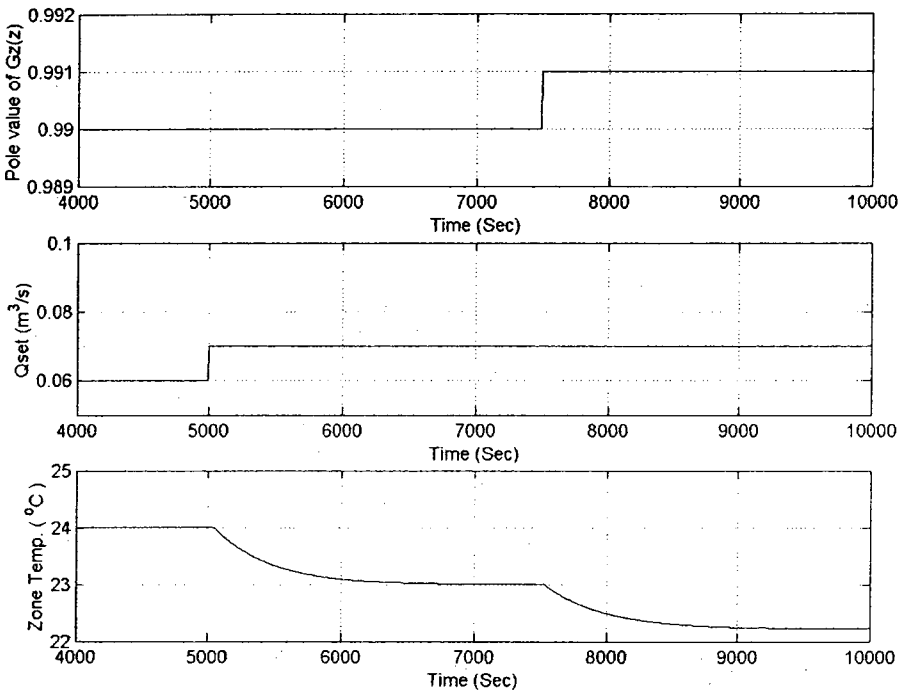

Figure 6.17 Response to parameter change in the pressure independent control system

As discussed before the pressure dependent control system has strong robustness to parameter changes. Therefore, the zone temperature can be maintained to converge to the set-point even though the load changes. However, the airflow rate change in the pressure dependent control system is not smooth as compared to the adaptive two-loop control system. The result is shown in Figure 6.18. The plot 1 is the responses for the two-loop control system and the plot 2 is the responses for the pressure dependent control system.

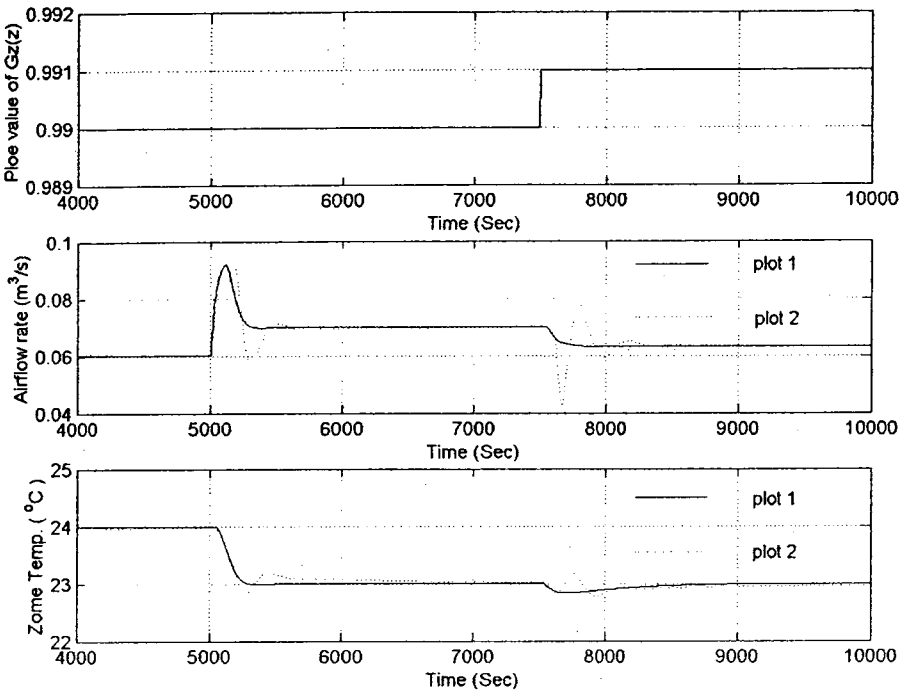

Figure 6.18 Adaptive two-loop control and pressure dependent control responses to the parameter change (load change)

6.6 Implementation in a VAV Test Facility

The adaptive two-loop control strategy was tested in a two-zone VAV-HVAC Test Facility shown in Figure 5.18. The test facility is located in the Thermal Environment Control Lab of Concordia University. In the test facility, DM1 and DM2 are damper motors that adjust the damper position to achieve airflow rate to zone 1 and zone 2 respectively. The controllers C1 and C2 modulate them individually. The output of the controllers is updated by using the two-loop control strategy depending on the zone temperature (ZT1 or ZT2) and the velocity pressure in the supply air duct (PS1 or PS2). Here, the velocity pressure is considered to be the controlled variable directly. Chilled water is supplied to the cooling coil (CC) from a 2-ton water-cooled chiller and a storage

tank unit. The controller C is used to control the discharge air temperature of the cooling coil (CCOT) through the actuator V to modulate the water flow rate. An automatically operated open-loop fan motor speed control is used to adjust total airflow rate in the system. CF is the controller and FVS is the actuator for the fan motor. The output of the controller CF is

$$FAN = k_a \sum Q_{set}(i) + c \tag{6.3}$$

where, i is zone indicator and k is a coefficient that relates to the airflow rate requirement in the VAV system. The coefficient k_a can obtained by Equation (6.3) with $c = 0$ and the required airflow rate values for all zones supplied by FAN. The coefficient k_a was determined by letting the dampers in full open position for each zone (open-loop test). In the two-zone VAV-HVAC Test Facility, $i = 1$ or 2. In addition, we obtained $k_a = 10.5944\ V/(m^3/s)$ and selected $c = 0.4\ V$. The maximum control value of the fan is $FAN = 2.8\ V$. The control strategy improves zone temperature regulation under a wider range of the load changes.

Experiment was done on the two-zone VAV-HVAC Test Facility. The experimental results are shown in Figures 6.19, 6.20, 6.21 and 6.22. The discharge air temperature was maintained at 12 $^{\circ}C$. The zone load was simulated by using two electric heaters.

The plant models require an estimate of the dead times which were obtained by conducting open-loop tests. The obtained dead time was about 3s for the dynamic process from the damper actuator to the velocity pressure (the airflow rate measurement) and the dead time was about 36s for the dynamic process from the velocity pressure to

the zone temperature. Using these dead times, the RLS algorithm with a matrix-reset technique developed in Chapter 3 was used to implement the online identifications of the processes in each zone.

The implementation also requires an estimate of T_{z0} for each zone which is somewhat difficult, but the temperature of the air entering the cooling coil (CCITS) is the closest one can select. Therefore, we use CCITS as substitute for T_{z0} in computing the dynamic output of the process $G_z(z)$ in the parameter estimation. During the experiment, sampling times of 1s for the interior loop and 4s for the exterior loop were used.

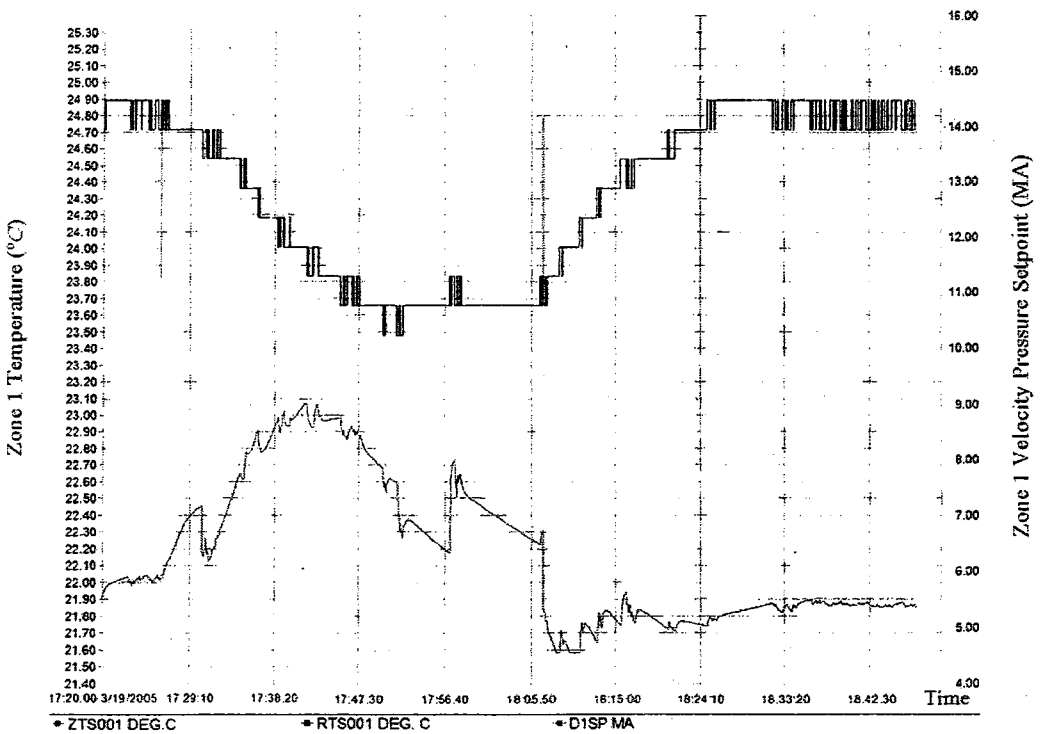

Figure 6.19 Zone temperature response and velocity pressure setpoint for zone 1

In Figure 6.19, ZTS001 is the zone temperature setpoint and RTS001 is the measured value of the temperature for the zone 1. D1SP is the velocity pressure setpoint

(related to zone temperature setpoint and zone load) in the duct connected to the zone 1. The figure shows that the temperature setpoint changes the velocity pressure consequently; the airflow rate changes steer the zone temperature to track the setpoint. Zone 1 temperature shows good response with $F(1)=0.6667$even though the fan control input is changing as shown in Figure 6.20.

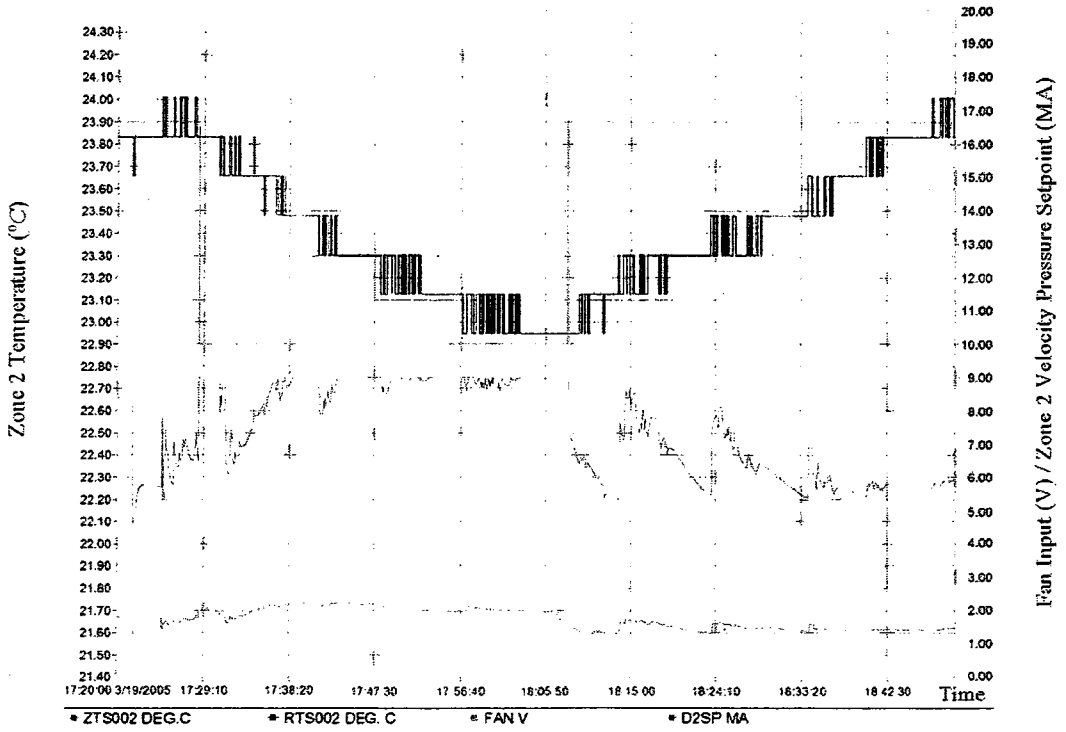

Figure 6.20 Zone temperature response and velocity pressure requirement for zone 2 and fan control

Zone 2 temperature responses are depicted in Figure 6.20. The airflow setpoint Q_{set} was calculated by the following equation.

$$Q_{set}(i)=1.29A\sqrt{0.1\times(DiSP-4)/16}\quad m^3/s \tag{6.4}$$

where, $i = 1$ or 2 and $A = 0.03097m^2$ the duct area.

In the experiments the factor $F(2) = 1$ was used for the zone 2. The experimental results in Figure 6.20 show that because of high cooling load in zone 2, the zone 2 temperature decreases slowly.

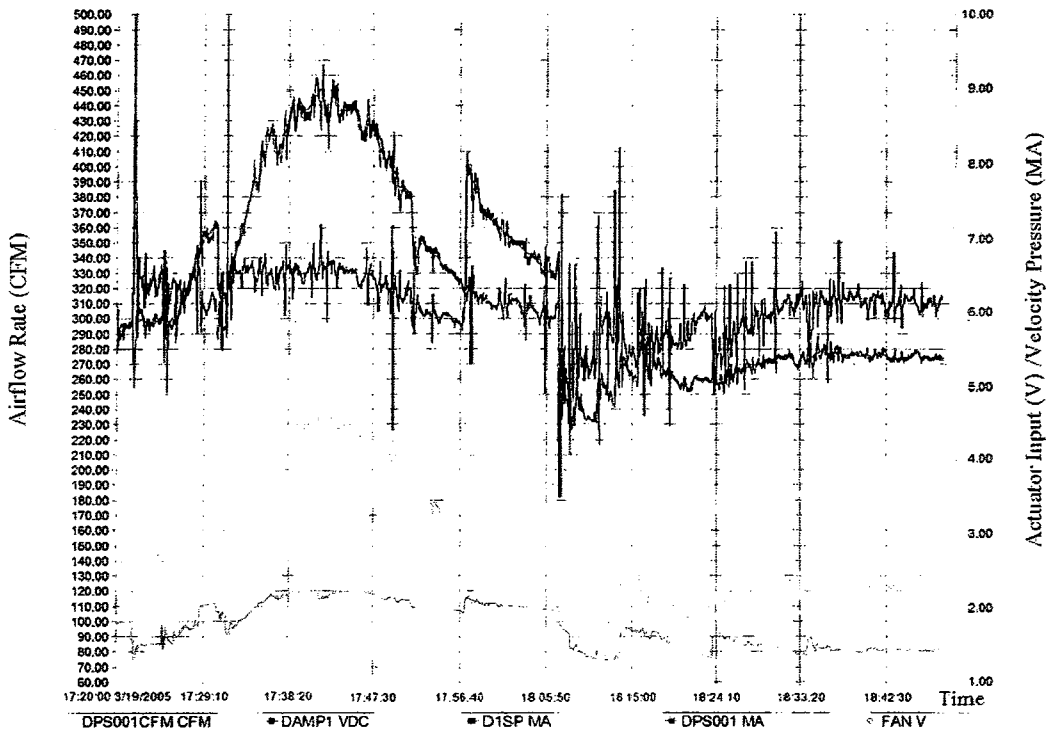

Figure 6.21 Velocity pressure response and airflow rate for zone 1

From the experimental results in Figures 6.21 and 6.22, we note that the selection of F for the both zones did cause saturation of the damper ($10V$ actuator input for dampers) and good tracking was achieved through velocity pressure control (or airflow rate control) for both zones. However, the saturation time of damper opening was very short, so we can say that the selected F values for both zones were acceptable. In Figure 6.21, DPS001CFM, DAMP1, D1SP and DPS001 are the airflow rate, the control input of

the damper, the velocity pressure setpoint, and the velocity pressure sensor measurement respectively in the zone 1 duct. FAN is the fan control input. DPS002CFM, DAMP2, D2SP and DPS002 in Figure 6.22 are the airflow rate, the control input of the damper, the velocity pressure setpoint, and the velocity pressure in the zone 2 duct.

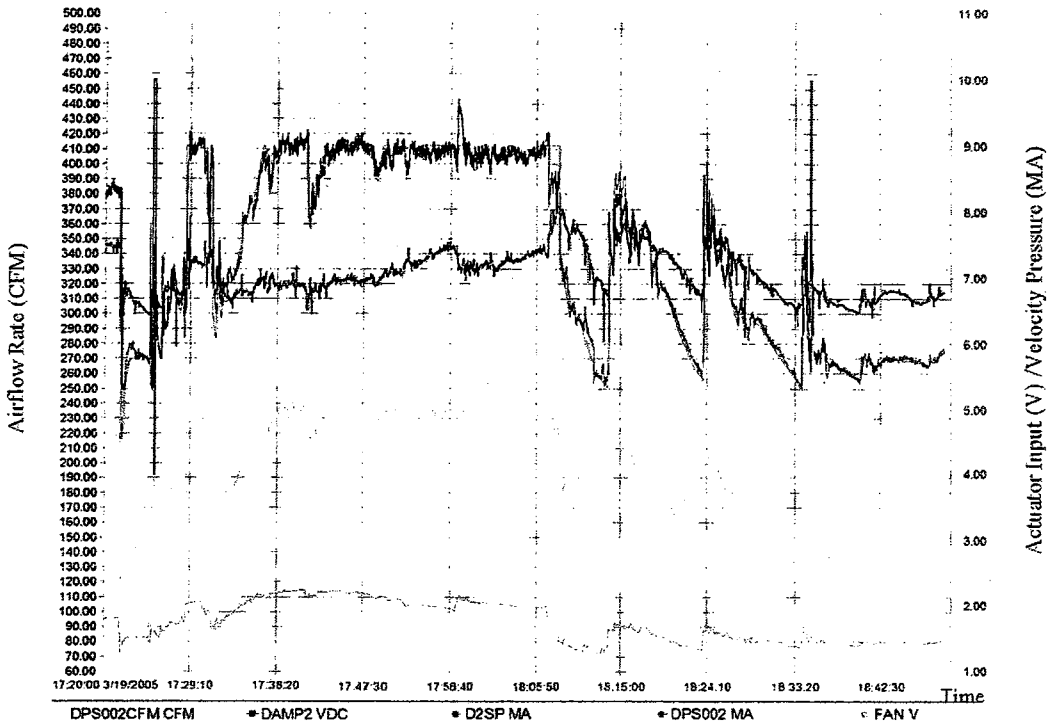

Figure 6.22 Velocity pressure response and airflow rate for zone 2

The experimental results show that the interior loop is very fast compared the exterior loop and the adaptive two-loop PI control strategy is well suited for VAV-HVAC systems.

Keeping the airflow rate between the minimum and the maximum range is essential in the VAV systems to maintain good air quality. By applying upper bound and lower bound limits for the velocity pressure setpoint Q_{set} we can achieve this

The following experimental results (Figures 6.23, 6.24, 6.25, 6.26) show the application of the adaptive two loop control system in maintaining airflow rate within the chosen high and low limits.

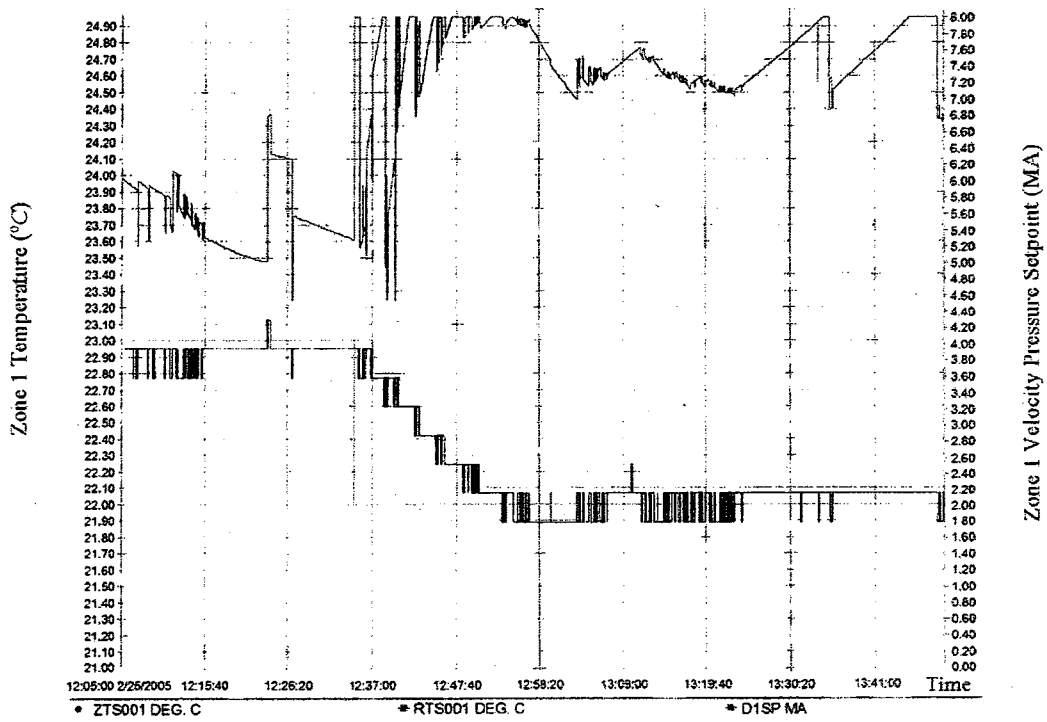

Figure 6.23 Zone temperature response 2 and velocity pressure requirement for zone 1

From Figure 6.24 it is noted that the upper bound (210CFM) was reached for certain times. The zone temperature responses to change in setpoints are shown in Figures 6.23 and 6.25 together with corresponding airflow rates. Similarly, Figure 6.26 shows that the lower bound (80CFM) was reached over short intervals.

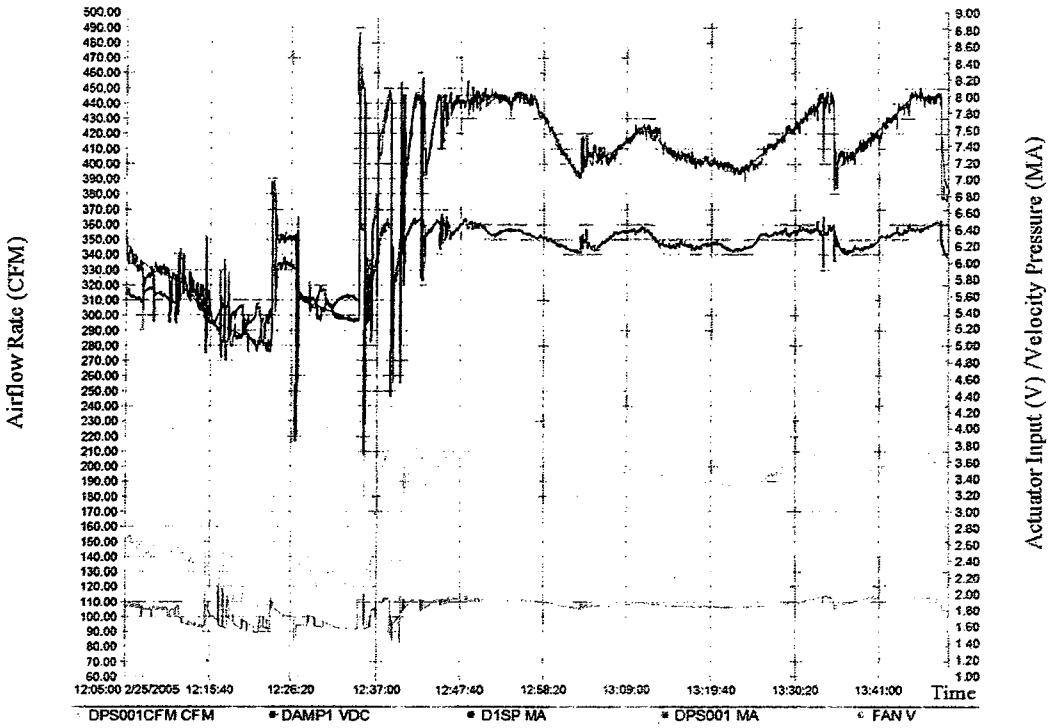

Figure 6.24 Velocity pressure response 2 and airflow rate for zone 1

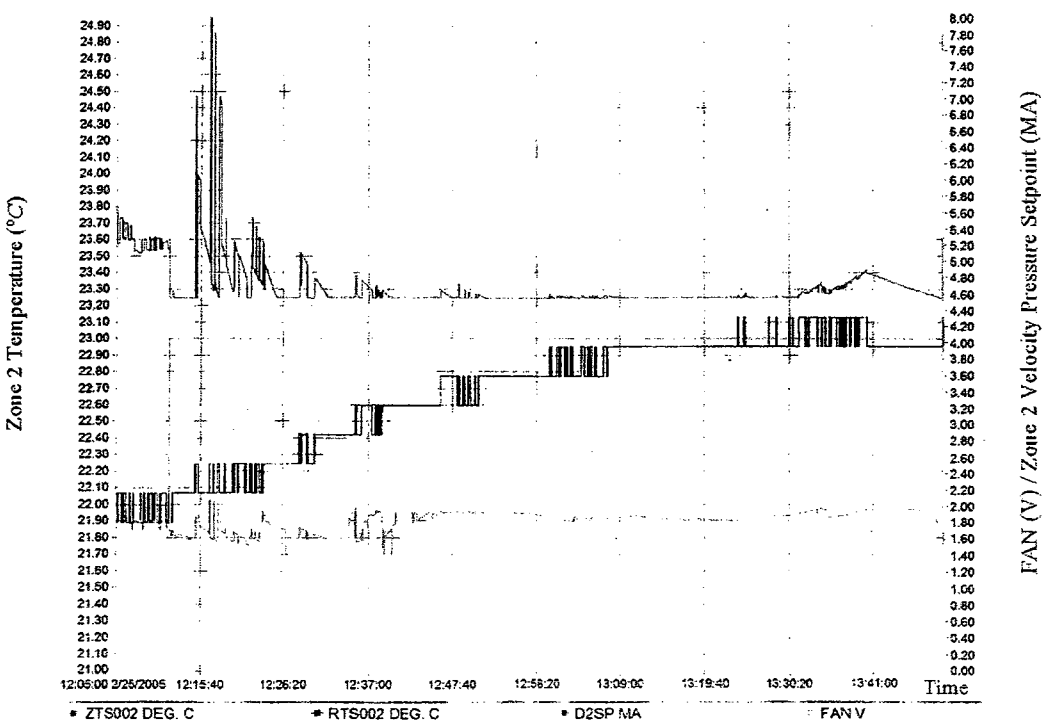

Figure 6.25 Zone temperature response 2 and velocity pressure requirement for zone 2

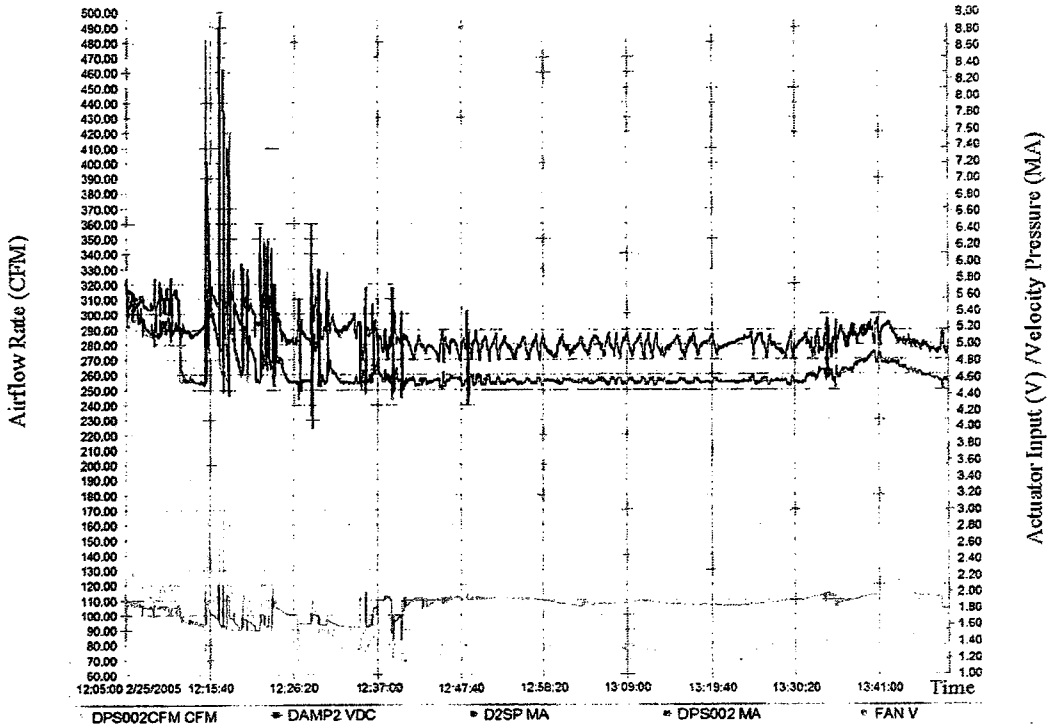

Figure 6.26 Velocity pressure response 2 and airflow rate for zone 2

6.7 Summary

This chapter has presented an online adaptive PI&PI controller for a VAV-HVAC system. The system performance was evaluated through simulations and experiments. The results show that the PI&PI controller gives good zone temperature setpoint tracking, is able to reject pressure disturbances and is robust to load changes compared with classical airflow regulation controls in VAV systems. The controller parameters for both interior and exterior loops can be directly updated by using the H_∞ PI tuning rules.

7. Conclusions and Recommendations

7.1 Conclusions

The conclusions drawn from the four major contributions of this thesis, namely development of, (a) a modified RLS algorithm, (b) on-line optimal control with H_∞ tuning rules, (c) an adaptive neural network strategy and (d) an online adaptive two-loop PI control strategy are summarized below.

A. A modified RLS identification algorithm

A modified RLS identification algorithm with the matrix-reset technique for online identification of the FOPDT system parameters is developed, which is a useful tool for the adaptive controls developed in this thesis. The specific conclusions from this contribution can be summarized as the follows.

1. Numerical instability in the previous RLS algorithm (Franklin, 1997; Qu, 2002) may cause absolutely wrong identification results in some cases. Through analysis it was shown that some equations in the RLS algorithm don't guarantee that all elements in $P(k+1)$ with their absolute values don't go to infinity (infinity problem) and there still exists $\hat{\theta}(k+1)=\hat{\theta}(k)$ if $P(k)=0$ for the FOPDT system (incorrect identification problem) even for $y(k+1)\neq\psi^T(k+1)\hat{\theta}(k)$.
2. To solve this problem it was proposed to keep $LowValue< P_{ss} <UpValue$ (where $P_{ss}=P_{11}^2+P_{12}^2+P_{21}^2+P_{22}^2$) and $|\varsigma(k+1)|>\delta$ to do the identification for a FOPDT system. This strategy was implemented by developing the matrix reset technique.

3. Simulation results show that the identification algorithm (for $\gamma=1$ and $\alpha=\infty$) with the matrix reset technique is able to track changes in the system plant parameters rapidly and gives improved results compared to the ordinary least squares ($\alpha = \gamma = 1$) and some exponentially weighted least squares ($\alpha=1-\gamma$ and $0<\gamma<1$) techniques. The use of existing identification algorithms (without the matrix reset technique) frequently lead to infinity problem ($|PLY_2| = Inf$), consequently require interruption of online simulations. The matrix reset technique avoids such interruptions and gives reliable results.
4. The experimental results show that the modified RLS identification algorithm with the matrix reset technique can be implemented in building EMC systems and is simple (without the need of using $n\times n$ matrix P), reliable and stable for identification in an adaptive control system.

B. An on-line optimal control with H_∞ tuning rules

By describing the dynamics of a discharge air system (DAS) using a FOPDT model, an online optimal control algorithm combined with the H_∞ tuning rules was developed. Some specific conclusions are summarized below.

5. The optimal control problem for DAS was formulated and solved. It was shown that the optimal control consists of PI-FF control structure, that is, $u(k) = -K_{PI}x(k) - K_{FF}(T_{set} - T_{a0})$.
6. In the discharge air temperature cooling control system, it was found that better temperature responses were obtained with smaller weight value of Q_2 weighting

factor during setpoint step-up mode of operation and somewhat higher Q_2 values were found to give better responses during the setpoint step-down mode.

7. For the considered plant, it was found that a reduction factor of 0.85 and Q2-down = 0.4 for the OTA-VP gave results that were close to the optimal results.
8. The developed tuning rules were tested using computer simulations in an adaptive control system. The simulation results show that the proposed OTA and OTA-VP with the near optimal parameters is able to track changes in discharge air temperature setpoints efficiently and to reduce the effect of changes in system parameters significantly.
9. The simulation results show that OTA-VP and OTA have improved performance in disturbance rejection compared with the H_∞ tuning rules and the Ziegler-Nichols method.

Reliability of a control system in real applications sometime relies on its control's simplicity because simple control algorithm will reduce human error. The developed simplified optimal control algorithm is the simplest one. Some specific conclusions for this contribution are summarized below.

10. It was shown that by setting $h_{11}(l) \approx 1$, $h_{21}(l) \approx 0$, $h_{12}(l) \approx 0$, $h_{22}(l) \approx 1$, and $a \approx 1$ the online optimal tuning rules yield $K_{pd} \approx \frac{bq_{11}}{(1+a)Q_2}$, $K_{id} \approx \frac{2bc_2}{(1+a)Q_2}$ and $K_{FF} \approx 0$.

    The simplified optimal control algorithm is simple and easy to implement. It was also shown that for $Q_2 = 1$, the optimal tuning rules converge to H_∞ PI tuning rules.
11. The simplified optimal tuning rules were implemented on Concordia University's heating coil system. The results show that with Q_2 = 0.6993 the adaptive PI

control system had improved response (the maximum offset is less than $0.4^{\circ}C$ and the offsets on both sides of setpoint are balanced) compared with the original PI control response (the maximum offset was great than $1.6^{\circ}C$ and the offsets on both sides were unbalanced).

12. The experimental results on the discharge air temperature control in the HVAC test facility showed that by adjusting the weight parameter Q_2 in the simplified optimal control algorithm improved step responses were obtained.

C. Adaptive neural network control strategy

In contrast to the online optimal control algorithm which requires identification of the model parameters, a new adaptive neural network controller with implementable training rules is proposed, which is a model free method. The specific conclusions from this contribution can be summarized as the follows.

13. An adaptive neural network controller (ANNC) is constructed by augmenting PID control with a neural network control algorithm.
14. Simulation results show that with a suitable set of initial values the training process could be very short for a fixed plant; but, if the initial weight values are not good enough the training process could be very long. Also, decreasing the initial values of $w_{ii}(0)$ decreases the rise time and increasing the initial value of $w_{06}(0)$ can reduce overshoot.
15. The fastest step responses of the ANNC recorded were as follows: the settling time of 152s to within $0.18^{\circ}C$ for a $2^{\circ}C$ step-down setpoint change, and the settling time of 119s to within $0.18^{\circ}C$ for a $2^{\circ}C$ step-up setpoint change.

16. The experimental results demonstrated that stable step responses by the ANNC were achieved over a wide range of operating conditions.
17. The output responses from the PID and ANNC control were compared. The results show that the proposed ANNC has very smooth, fast and less overshoot step responses compared with the CCM-PID control.
18. The experiments showing the disturbance rejection to the airflow rate changes were made. The results show that the proposed ANNC may be not as efficient as the CMM-PID control in the disturbance rejection to the airflow rate changes. This shows that it may be necessary to add airflow rate as input to the ANNC to improve the disturbance rejection property.

D. Online adaptive two-loop PI control strategy

For zone temperature controls in a VAV-HVAC system, an on-line adaptive PI&PI controller is proposed. The system performance of the proposed controller was evaluated through simulations and real applications. Some specific conclusions for this contribution are summarized as follows.

19. The limitations of the typical airflow regulation in zone temperature controls of HVAC systems were illustrated with examples. The simulation results show that the classical pressure independent control results in offset in tracking the zone temperature setpoint, but has stronger robustness to airflow rate (or pressure) disturbance effect. The classical pressure dependent control for zone temperature control system is not good in rejecting the effects of airflow rate (or pressure) disturbance, but has stronger robustness to the parameter changes.

20. The simulation results show that the proposed two loop PI&PI controller has improved the zone temperature setpoint tracking property, better attenuates the pressure disturbance effect and is robust to load changes compared to the classical airflow regulation controls used in VAV systems.
21. The experimental results showed that the proposed on-line adaptive PI&PI controller is tracking airflow rate requirement very quickly and is robust; and the zone temperature setpoints were reached while satisfying the minimum and maximum airflow requirements.

7.2 Contributions of This Study

The main contributions of this thesis are summarized below.

1. A modified RLS identification algorithm with Matrix-Reset Technique for online implementation is proposed. It guarantees that the identification works properly under all possible operating conditions by adopting a matrix-reset technique.

2. A new optimal control for FOPDT system augmented with improved robustness is developed.

   Changes in FOPDT model parameters in HVAC systems require strong robustness property in control design. To achieve this requirement a new optimal control for FOPDT system combined with H_∞ tuning rules (Qu & Zaheeruddin, 2004) is developed. This control improves the ability in rejecting the effect of changes in system parameters.

3. To develop implementable, simple control algorithm with stronger robustness properties, a simplified optimal control algorithm is proposed. The characteristics of this algorithm are verified by two adaptive control applications.

4. An online intelligent control strategy with the integration of adaptive control, neural network control and PID control is developed for local controls of HVAC systems. Simulation and experimental results show that the proposed control strategy has stronger robustness, improved regulation and tracking functions for FOPDT type plants compared to classical PID controls.

5. An online adaptive two-loop PI control strategy (PI&PI) for multi-zone systems is developed. It is combined with classical two-loop structure and H_∞ tuning rules and achieves good zone temperature control, robustness to parameter changes and good airflow rate disturbance effect reduction compared to classical multi-zone controls.

7.3 Recommendations

The results described in this thesis are useful for real implementation of adaptive local loop controllers in HVAC systems. In order to extend these methods to buildings with a large numbers of control loops, the following recommendations are made.

1. Develop implementable supervisory control strategies for the entire HVAC control system in which all control loops can be simultaneously tuned.
2. Conduct more real building experimental tests with the developed control strategies.

Reference

Abbassi, A., & Bahar, L. (2005). Application of neural network for the modeling and control of evaporative condenser cooling load. *Applied Thermal Engineering, 25,* 3176–3186.

Ahmed, O., Mitchell, J., & Klein, S. (1998a). Feedforward-Feedback Controller Using General Regression Neural Network (GRNN) for Laboratory HVAC System: Part I – Pressure Control. *ASHRAE Transactions, 104* (2), 613-625.

Ahmed, O., Mitchell, J., & Klein, S. (1998b). Feedforward-Feedback Controller Using General Regression Neural Network (GRNN) for Laboratory HVAC System: Part II – Temperature Control – Cooling. *ASHRAE Transactions, 104* (2), 626-634.

Ahmed, O., Mitchell, J., & Klein, S. (1998c). Feedforward-Feedback Controller Using General Regression Neural Network (GRNN) for Laboratory HVAC System: Part III – Temperature Control – Heating. *ASHRAE Transactions, 104* (2), 635-643.

Al-Assadi, S. A., Patel, R. V., Zaheer-ruddin, M., Verma, M. S., & Breitinger, J. (2004). decentralized control of HVAC systems using H_∞-performance measures. *Journal of the Franklin Institute, 341,* 543-567.

Alcala, R., Casillas, J., Cordon, O., Gonzalez, A., & Herrera, F. (2005). A genetic rule weighting and selection process for fuzzy control of heating, ventilating and air conditioning systems. *Engineering Applications of Artificial Intelligence, 18,* 279-296.

Arguello-Serrano, B., & Velez-Reyes, M. (1999). Nonlinear control of a Heating, Ventilating, and Air Conditioning system with thermal load estimation. *IEEE Transaction on Control Systems Technology, 7* (1), 56-63.

Åström, K. J., & Hägglund, T. (1984). Automatic tuning of simple regulators with specification on phase and amplitude margins. *Automatica, 20*, 645-651.

Åström, K. J., Hägglund, T., & Wallenborg, A. (1993). Automatic Tuning of Digital Controllers with Applications to HVAC Plants. *Automatica, 29* (5), 1333-1343.

Atthajariyakul, S., & Leephakpreeda, T. (2005). Neural computing thermal comfort index for HVAC systems. *Energy Conversion and Management, 46*, 2553–2565.

Bai, J. B., & Zhang, X. S. (2007). A new adaptive PI controller and its application in HVAC systems. *Energy Conversion and Management, 48*, 1043–1054.

Ben-Nakhi, A. E., & Mahmoud, M. A. (2004). Cooling load prediction for buildings using general regression neural networks. *Energy Conversion and Management, 45*, 2127–2141.

Calvino, F., Gennusa, M. L., Rizzo, G., & Scaccianoce, G. (2004). The control of indoor thermal comfort conditions: introducing a fuzzy adaptive controller. *Energy and Buildings, 36*, 97–102.

Chen, Y. H., Lee, K. M., & Wepfer, W. J. (May 1990). Adaptive Robust Control Scheme Applied to a Single-zone HVAC System. *Proceedings of the 1990 American Control Conference, USA, 2*, 1076-1081.

Chu, C. M., Jong, T. L., & Huang, Y. W. (2005). Thermal comfort control on multi-room fan coil unit system using LEE-based fuzzy logic. *Energy Conversion and Management, 46*, 1579–1593.

Clark, D. R. (1985). *HVACSIM+ building system and equipment simulation program reference manual.* Gaithersburg, Maryland: U.S. Department of Commerce,

National Bureau of Standards, National Engineering Laboratory, Centre for Building Technology.

Clarke, D. W., Mohtadi, C., & Tuffs, P. S. (1987). Generalized Predictive Control – Part The Basic Algorithm; Part II. Extensions and Interpretations. *Automatica, 23* (2), 137-160.

Clarke, J. A. (2001). *Energy simulation in building design.* Oxford: Butterworth–Heinemann.

Corless, M., & Leitmann, G. (1984). Adaptive Control for Uncertain Dynamical Systems. In A. Blaquiere, & G. Leitmann (Eds.), *Dynamical Systems and Microphysics: Control Theory and Mechanics.* Orlando: Academic press.

Dexter, A. L. (1983). Self-tuning control algorithm for single-chip microcomputer implementation. *IEE Proceedings D. Control Theory and Applications, 130* (5), 255-260.

Dexter, A. L., & Haves, P. (1989). A Robust Self-Tuning Predictive Controller for HVAC Applications. *ASHRAE Transactions, 95* (2), 431-438.

Engdahl, F., & Johansson, D. (2004). Optimal supply air temperature with respect to energy use in a variable air volume system. *Energy and Buildings, 36,* 205–218.

Fong, K. F., Hanby, V. I., & Chow, T. T. (2006). HVAC system optimization for energy management by evolutionary programming. *Energy and Buildings, 38,* 220–231.

Franklin, G., Powell, J. D., & Workman, M. (1997). *Digital Control of Dynamic Systems. Reading.* Reading, MA: Addison-Wesley.

Gartner, J. R. (1972). Simplified dynamic response relations for finned-coil heat exchangers. *ASHRAE Transactions, 78* (2), 163-169.

Hamilton, D. C., Leonard, R. G., & Pearson, J. T. (1977). A system model for a discharge air temperature control system. *ASHRAE Transactions, 83* (1), 251-268.

Hamilton, D. C., Leonard, R. G., & Pearson, J. T. (1974). Dynamic response characteristics of discharge air temperature control system at near full and part heating load. *ASHRAE Transactions, 80* (1), 251-268.

He, M., Cai, W. J., & Li, S. Y. (2005). Multiple fuzzy model-based temperature predictive control for HVAC systems. *Information Sciences, 169*, 155–174.

Ho, W. K., Hang, C. C., & Cao, L. S. (1995). Tuning of PID Controllers Based on Gain and Phase Margin Specifications. *Automatica, 31* (3), 497-502.

Huang, W. Z., Zaheeruddin, M., & Cho, S. H. (2006). Dynamic simulation of energy management control functions for HVAC systems in buildings. *Energy Conversion and Management, 47*, 926–943.

Huang, W., & Lam, H. N. (1997). Using genetic algorithms to optimize controller parameters for HVAC systems. *Energy and Buildings, 26*, 277-282.

Hussein, G. M. (1996). *PI control of air temperature and humidity with a chilled water system.* Montreal, Canada: Master's dissertation, Concordia University.

Jeannette, E., Assawamartbunlue, K., Curtiss, P. S., & Kreiser, J. F. (1998). Experimental Results of a Predictive Neural Network HVAC Controller. *ASHRAE 104* (2), 192-197.

Jin, X. Q., Ren, H. G., & Xiao, X. K. (2005). Prediction-based online optimal control of outdoor air of multi-zone VAV air conditioning systems. *Energy and Buildings, 37* (9), 939-944.

Kalman, B. L., & Kwasny, S. C. (1992). Why Tanh: Choosing a Sigmoidal Function. *International Joint Conference on Neural Networks, USA, 4*, 578-581.

Kasahara, M., Kuzuu, Y., Matsuba, T., Hashimoto, Y., Kamimura, K., & Kurosu, S. (2000). Physical model of an air-conditioned space for control analysis. *ASHRAE Transactions, 106* (2), 307-317.

Kasahara, M., Matsuba, T., Hashimoto, Y., Murasawa, I., Kamimura, K., & Kurosu, S. (1998). Optimal Preview Control for HVAC System. *ASHRAE Transactions, 104* (1A), 502-513.

Kasahara, M., Matsuba, T., Kuzuu, Y., Yamazaki, T., Hashimoto, Y., Kamimura, K., et al. (1999). Design and Tuning of Robust PID Controller for HVAC Systems. *ASHRAE Transactions, 105* (2), 154-166.

Kasahara, M., Yamazaki, T., Kuzuu, Y., Hashimoto, Y., Kamimura, K., Matsuba, T., et al. (2001). Stability Analysis and Tuning of PID Controller in VAV Systems. *ASHRAE Transactions, 107* (1), 285-296.

Kotaki, M., Yamakawa, Y., Yamazaki, T., Kamimura, K., & Kurosu, S. (2005). A Tuning Method for PID Controller That Considers Changes in System Characteristics. *ASHRAE Transactions, 111* (2), 13-22.

Krakow, K. I. (1998). Sampling Interval Magnitude Relation to Digital PI Control System Performance. *ASHRAE Transactions, 104* (2), 246-256.

Krakow, K. I., & Lin, S. (1995). PI control of fan speed to maintain constant fan discharge pressure. *ASHRAE Transactions, 101* (2), 398-407.

Krakow, K. I., Lin, S., & Zeng, Z. S. (1995a). Analytical determination of PID coefficients for temperature and humidity control during cooling and

dehumidifying by compressor and evaporator fan speed variation. *ASHRAE Transactions, 101* (1), 343-354.

Krakow, K. I., Lin, S., & Zeng, Z. S. (1995b). Temperature and humidity control during cooling and dehumidifying by compressor and evaporator fan speed variation. *ASHRAE Transactions, 101* (1), 292-304.

Kulkarni, M. R., & Hong, F. (2004). Energy optimal control of a residential space-conditioning system based on sensible heat transfer modeling. *Building and Environment, 39*, 31-38.

Liang, J., & Du, R. (2005). Thermal Comfort Control Based on Neural Network for HVAC Application. *Proceedings of 2005 IEEE Conference on Control Applications, Canada*, 819-824.

Lu, L., Cai, W. J., Soh, Y. C., & Xie, L. H. (2005a). Global optimization for overall HVAC systems—Part I problem formulation and analysis. *Energy Conversion and Management, 46*, 999–1014.

Lu, L., Cai, W. J., Soh, Y. C., & Xie, L. H. (2005b). Global optimization for overall HVAC systems—Part II problem solution and simulations. *Energy Conversion and Management, 46*, 1015–1028.

Lu, L., Cai, W. J., Soh, Y. C., Xie, L. H., & Li, S. J. (2004). HVAC system optimization –condenser water loop. *Energy Conversion and Management, 45*, 613–630.

Lu, L., Cai, W. J., Xie, L. H., LI, S. J., & Soh, Y. C. (2005). HVAC system optimization—in-building section. *Energy and Buildings, 37*, 11–22.

Massie, D. D., Kreider, J. F., & Curtiss, P. S. (2004a). Neural Network Optimal Controller for Commercial Ice Thermal Storage Systems. *ASHRAE Transactions, 110* (2), 361-369.

Massie, D. D., Kreider, J. F., & Curtiss, P. S. (2004b). Verification of a Neural Network-Based Controller for Commercial Ice Storage Systems. *ASHRAE Transactions, 110* (2), 471-478.

Maxwell, G. M., Shapiro, H. N., & Westra, D. G. (1989). Dynamics and control of a chilled water coil. *ASHRAE Transactions, 95* (1), 1243-1255.

McCullagh, K. R., Green, G. H., & Chandraseker, S. (1969). An analysis of chilled water cooling dehumidifying coil using dynamic relationships. *ASHRAE Transactions, 75* (2), 200-209.

McQuistion, F. C., Parker, J. D., & Spitler, J. D. (2000). *Heating, Ventilating and Air Conditioning Analysis and Design* (Fifth ed.). New York: John Wiley & Sons,

Mei, L., & Levermore, G. J. (2002). Simulation and validation of a VAV system with an ANN fan model and a non-linear VAV box model. *Building and Environment, 37,* 277-284.

Nesler, C. G. (1986b). Adaptive Control of Thermal Processes in Buildings. *IEEE Control Systems Magazine, 6* (4), 9-13.

Nesler, C. G. (1986a). Automated Controller Tuning For HVAC Applications. *ASHRAE Transactions, 92* (2B), 189-201.

Nesler, C. G., & Stoecker, W. F. (1984). Selecting the proportional and integral constants in the direct digital control of discharge air temperature. *ASHRAE Transactions, 90* (2B), 834-845.

Perez-Lombard, L., Ortiz, J., & Pout, C. (2008). A review on buildings energy consumption information. *Energy and Buildings, 40*, 394–398.

Qu, G. (2002). *Online strategies for adaptive tuning of PI controllers in HVAC systems.* Montreal, Canada: Master's Dissertation, Concordia University.

Qu, G., & Zaheeruddin, M. (2004). Real-time tuning of PI controllers in HVAC systems. *International Journal of Energy Research, 28*, 1313-1327.

Rentel-Gomez, C., & Velez-Reyes, M. (2001). Decoupled control of temperature and relative humidity using a variable-air-volume HVAC system and non-interacting control. *Proceedings of the 2001 IEEE International Conference on Control Applications, Mexico*, 1147-1151.

Salsbury, T. I. (2002). A new pulse modulation adaptive controller (PMAC) applied to HVAC systems. *Control Engineering Practice, 10*, 1357-1370.

Seem, J. E. (1997). Implementation of a new pattern recognition adaptive controller developed through optimization. *ASHRAE Transactions, 103* (1), 494-506.

Semsar, E., Yazdanpanah, M. J., & Lucas, C. (2003). Nonlinear Control and Disturbance Decoupling of an HVAC System via Feedback Linearization and Back-Stepping. *Proceedings of 2003 IEEE conference on control applications, Turkey, 1*, 646-650.

Shavit, G. (1994). Tuning of PID DDC controllers. *American control conference, 3*, 3065-3069.

Shavit, G., & Brandt, S. G. (1982). The dynamic performance of a discharge air-temperature system with a P-I controller. *ASHRAE Transactions, 88* (2), 826-838.

Singh, G., Zaheer-uddin, M., & Patel, R. V. (2000). Adaptive control of multivariable thermal processes in HVAC systems. *Energy Conversion & Management, 41*, 1671-1685.

Stoecker, W. F., Rosario, L. A., Heidenreich, M. E., & Phelan, T. R. (1978). Stability of an air-temperature control loop. *ASHRAE Transactions, 84* (1), 35-53.

Sun, J., & Reddy, A. (2005). Optimal control of building HVAC&R systems using complete simulation-based sequential quadratic programming (CSB-SQP). *Building and Environment, 40*, 657-669.

Tan, W., Liu, L., & Tam, P. K. (1998). PID tuning based on loop-shaping H_∞ control. *IEE Proceedings on Control Theory Applications, 145* (6), 485-490.

Tashtoush, B., Molhim, M., & Al-Rousan, M. (2005). Dynamic model of an HVAC system for control analysis. *Energy, 30*, 1729-1745.

Wallenborg, A. O. (1991). A New Self-tuning Controller for HVAC Systems. *ASHRAE Transactions, 97* (1), 19-25.

Wang, J. J., Jing, Y. Y., & An, D. W. (2006). Study of Neuron Adaptive PID Controller in a Single-zone HVAC System. *Proceedings of the First International Conference on Innovative Computing, Information and Control, China, 2*, 142 - 145.

Wang, J., Wang, Y., & Shao, H. H. (2005). Performance improvement of VAV air conditioning control system through diagonal matrix decoupling and Lonworks technology. *Energy and Buildings, 37*, 911–919.

Wang, Q. G., Lee, T. H., Fung, H. W., Bi, Q., & Zhang, Y. (1999). PID Tuning for Improved Performance. *IEEE Transactions on Control Systems Technology, 7* (4), 457-465.

Wang, S. W., & Jin, X. Q. (2000). Model-based optimal control of VAV air-conditioning system using genetic algorithm. *Building and Environment, 35*, 471-487.

Wang, Y. G., Shi, Z. G., & Cai, W. J. (2001). PID autotuner and its application in HVAC systems. *Proceedings of the American Control Conference, Arlington*, 25-27.

Wang, Y. W., Cai, W. J., Soh, Y. C., Li, S. J., Lu, L., & Xie, L. H. (2004). A simplified modeling of cooling coils for control and optimization of HVAC systems. *Energy Conversion and Management, 45*, 2915-2930.

Yang, I. H., Yeo, M. S., & Kim, K. W. (2003). Application of artificial neural network to predict the optimal start time for heating system in building. *Energy Conversion and Management, 44*, 2791–2809.

Zaheer-uddin, M. (1993). Optimal, sub-optimal and adaptive control methods for the design of temperature controllers for intelligent buildings. *Building and Environment, 28* (3), 311-322.

Zaheer-uddin, M., & Tudoroiu, N. (2004). Neuro-PID tracking control of a discharge air temperature system. *Energy Conversion and Management, 45*, 2405–2415.

Zaheer-uddin, M., & Zheng, G. R. (2001). Multistage optimal operating strategies for HVAC systems. *ASHRAE Transactions, 107* (2), 346-352.

Zaheer-uddin, M., Al-Assadi, S. A., & Patel, R. V. (1994). Decentralized preview control for multiple disturbance rejection in HVAC systems. *Control Engineering Practice, 2* (6), 989-1000.

Zheng, G. R. (1997). *Dynamic modeling and global optimal operation of multizone variable air volume HVAC systems.* Montreal, Canada: Doctoral dissertation, Concordia University.

Zheng, G. R., & Zaheer-uddin, M. (1996). Optimization of thermal processes in a variable air volume HVAC system. *Energy, 21* (5), 407-420.

Appendix

Sensor type	Variable measured	Sensor range	Accuracy	Output signal
RTD	Temperature	55~95F (13~35°C)	±0.5F (±0.3°C) ±0.12%	Ohms (1k max)
RH	Relative humidity	0~99%	±2%	4~20 MA
Pressure transducer	Pressure	0~0.1" WG	±1%	4~20 MA
Water flow meter	Chilled water flow rate	0.5~6 gpm	±2%	4~20 MA

Table A.1 Specifications and accuracy of the sensors used